IMPACT DAMAGE RESPONSE OF GRAPHITE/EPOXY FABRIC STRUCTURES

by

Michael John Kraft

S.B., Massachusetts Institute of Technology
(1986)

SUBMITTED IN PARTIAL FULFILLMENT
OF THE REQUIREMENTS FOR THE
DEGREE OF

MASTER OF SCIENCE IN
AERONAUTICS AND ASTRONAUTICS

at the

MASSACHUSETTS INSTITUTE OF TECHNOLOGY
July 1988

Signature of Author _____
Department of Aeronautics and Astronautics
July 8, 1988

Certified by _____
Professor Paul A. Lagace
Thesis Supervisor

Accepted by _____
Professor Harold Y. Wachman
Chairman, Department Graduate Committee

IMPACT DAMAGE RESPONSE OF GRAPHITE/EPOXY FABRIC STRUCTURES

by

Michael John Kraft

Submitted to the Department of Aeronautics and Astronautics on July 8, 1988 in partial fulfillment of the requirements for the Degree of Master of Science

ABSTRACT

The impact damage resistance and tolerance of graphite/epoxy fabric plate and cylinder structures was investigated in an analytical and experimental study. The material system used was Hercules A370-5H/3501-6 five harness satin weave cloth in a quasi-isotropic laminate configuration of (0,45)s. All specimens were impacted with 12.7 mm diameter steel spheres. Damage resistance of the specimens was determined through the use of dye-penetrant enhanced x-ray, sectioning, epoxy burn-off, and visual methods. Damage tolerance of the flat plate structures was determined for tensile loaded 350 mm by 70 mm coupons. Damage tolerance of the cylindrical structures was determined for an internally pressurized tube 610 mm long with a radius of 152 mm. Tests were conducted monotonically to failure. Impacted fabric laminates exhibited fiber bundle disbonding, delamination, matrix yielding, and fiber breakage. Plate delamination and bundle disbonding was found to be more extensive around the central core area than the cylinder. Both geometries exhibited a threshold level of damage before residual strength was affected. Damage resistance and damage tolerance was predicted by first considering the impact event on a global level to determine the force-time and acceleration-time response of the structures, followed by a local analysis to determine the damage to the laminate. Failure was predicted by applying an averaged strain ratio criterion to an anisotropic inclusion model. Curvature effects were incorporated at the global level only. Analysis results provided good correlation to the fiber damage radius of the plate and cylinder structures. Plate coupon damage tolerance was predicted well by the analysis. Application of the plate residual strength analysis to the pressurized cylinder indicated that further study of bending at the impact damage edge, due to the internal pressurization, is necessary.

Thesis Supervisor: Paul A. Lagace

Title: Associate Professor, Department of Aeronautics and Astronautics, Massachusetts Institute of Technology

ACKNOWLEDGEMENTS

Many thanks are due to the people who have helped in this research. First and foremost is the UROP team of Michelle Perry, Stephanie Purrington, Kelly Savage, and Charles Whetsel who had to bear the brunt of my 'management' style and stuck with the project to the end. Development of the new cylinder testing system would not have been possible without their input at the many design reviews.

At the top level, thanks to Al Supple, Carl Varnerin, Don Weiner, Earl Wassmouth, Ping Lee, Victor (GTL) and Jeff Michaeli at Salerno Tool for their advice and support. Thanks to Paul Lagace for the 28+ thesis chapter units. This research may not make the Times bestseller list, but it is largely his review that rounded it in to shape.

Special thanks must be given to Kevin Saeger and Pierre Minguet. Kevin came up with the new function for the local model. Pierre bailed me out with the orthotropic cylinder analysis when the old approach hit the wastebasket. The cylinder global analysis program listed in the APPENDIX A is his creation.

Thanks to my friends in Massachusetts and Michigan for keeping me sane over the years.

This thesis is dedicated to my parents.

FOREWARD

This work was performed in the Technology Laboratory for Advanced Composites (TELAC) of the Department of Aeronautics and Astronautics at the Massachusetts Institute of Technology. This work was sponsored by a joint FAA/Navy endeavor under contract N00019-85-C-0090.

TABLE OF CONTENTS

TABLE OF CONTENTS (continued)

TABLE OF CONTENTS (continued)

TABLE OF CONTENTS (continued)

LIST OF FIGURES

LIST OF FIGURES (continued)

LIST OF FIGURES (continued)

LIST OF FIGURES (continued)

LIST OF FIGURES (continued)

LIST OF FIGURES (continued)

LIST OF TABLES

APPENDIX TABLES

NOMENCLATURE

a	cylinder length
a_o	characteristic length in Whitney-Nuismer average stress criterion
a_{ij}	engineering compliance
A	elastic mode shape parameter
$[A]$	terms of local model boundary conditions
A_{ij}	laminate stretching constants
B	elastic mode shape parameter
D	shell bending stiffness
D_{ij}	laminate bending constants
E	longitudinal modulus of shell
$f(x)$	generalized beam function shape
$f_m(z)$	z component of Fourier-Bessel series
$F_{mn}(t)$	applied Hertzian spring load
$g_m(r)$	r component of Fourier-Bessel series
h	plate / shell thickness
J_o	zero order Bessel function
K	Hertzian spring constant
K	Folias stress intensification factor for a flat plate containing a hole
K_{aa}	terms of global stiffness matrix
L	Lagrangian operator
N_{hoop}	cylinder loading in hoop direction
N_{long}	cylinder loading in axial direction
$p(r)$	local model loading distribution
P	load on plate

NOMENCLATURE (continued)

q_{mn}	eigenvector of mn mode
Q_{ij}	reduced ply stiffnesses
r	half slit length (hole radius)
R	cylinder / shell radius
R_i	forcing function vector
S.R.	strain ratio (far field to average)
V	kinetic energy
α	local indentation of plate
β_n	elastic mode shape parameter
ε_{ij}	strain
ε_x	small displacement extensional strain in x
ε_y	small displacement extensional strain in y
γ_{xy}	small displacement shear strain in xy plane
θ	elastic mode shape parameter
κ_x	cylinder curvature in x
κ_y	cylinder curvature in y
κ_{xy}	cylinder curvature in xy
λ	shell parameter for use in the Folias curvature correction term
μ_m	roots of zeroth order Bessel function
Π_p	potential energy
ψ	polar stress function
ρ	cylinder area density
σ_{ij}	stress
ω_{mn}	eigenvalue of mn mode

CHAPTER ONE

INTRODUCTION

The use of composite materials in structures has increased significantly in the past decade. This is particularly true in the aerospace industries where advanced composite materials offer several advantages. For example, in fighter aircraft, the benefit of using advanced composite materials is a mass efficient structure that can increase the thrust to weight ratio and maneuverability. Furthermore, the directional properties of composites provide the possibility of structurally tailoring a design to function more efficiently. The experimental X-29 aircraft uses aeroelastic tailoring of the wings to prevent divergence and flutter from occurring, while realizing the aerodynamic benefits associated with a forward swept wing configuration. These cases are examples of the benefits that may be realized by using advanced composites and justify the impetus to design structures using greater percentages of composites.

As the use of advanced composites extends from secondary to primary structural applications, the need to fully understand the material characteristics of composites becomes increasingly important. Of particular concern is the response of composites to the conditions of their design environment. Like any other structural material, composites are exposed to a variety of damage phenomena. These damage conditions may

arise from a variety of occurrences: from poorly drilled fastener holes to tool drops to ballistic projectile impacts. Since composites are largely a heterogeneous material composed of stiff fibers embedded in a brittle matrix, the induced damage from these phenomena is often complex and may involve fiber breakage, matrix crushing, and delamination. Thus, the motivation exists to understand the consequences of the design environment on a composite structure, which may induce a complex state of damage affecting the overall integrity of the structure. The damage tolerance of the advanced composite structure must be understood.

Consider the working environment of a commercial or transport aircraft. Aircraft taking off or landing on a runway are often exposed to impact from small stones, glass, etc. which are kicked up by turbulence from the aircraft and hit the fuselage, wings, and engines. This may result in damage to the fuselage, barely visible to the naked eye either because of its small size or lack of any front surface damage. As the aircraft takes off and reaches cruising altitude, the interior is pressurized for passenger comfort, thereby inducing a state of stress in the fuselage membrane. The question to answer is: how does undetected and unrepaired impact damage affect the overall integrity of the structure?

This type of impact is referred to as runway kickup. It is a specific example of many impact phenomena. Other examples include the low velocity tool drop from a few meters and the high velocity ballistic projectile impact. A high

velocity impact generally requires that the inertial and structural dynamic properties of the target be included in an analysis of the impact event. The ballistic projectile punch through of a target, however, can actually result in a lesser damage state by producing a clean hole. Approaching the impact problem by a study of the higher damage state regime that exists before punch through and where the inertial loading effect of the impactor is important thereby yields the greatest information.

The first step in fully understanding the effects of impact on advanced composite materials is to determine the nature of the damage. This is the concept of impact damage resistance; the capability of a structure to withstand damage from an impact phenomenon. As stated before, damage to fibers and matrix as well as delamination may be found in impacted composite laminates. Work on the characterization of impact damage in composites has been investigated extensively for graphite/epoxy and Kevlar/epoxy laminates composed of unidirectional tape. However, very little work has been done on the determination of the characteristics of impact damage in composite laminates composed of graphite/epoxy woven fabric.

The next step is to develop an analytical method to predict the effects of impact damage on the integrity of the composite structure. This is the concept of impact damage tolerance; the capability of a structure to maintain its design integrity after an impact event. A particular goal

would be to develop the ability to predict the residual strength of any structure given a minimum of information about the impact event. A cost efficient approach to this goal could be found in the use of smaller sample structures (i.e. coupons) to develop a database for the effects of impact. The effects of impact could then be projected to a more complex structure. This could be accomplished by the use of a structural stress correction factor or a degraded property impact element in a larger finite element model of a complex structure.

The investigation of the impact response of fabric graphite/epoxy structures, therefore, involves the following steps. The first step is to determine the characteristics of impact damage on graphite/epoxy laminates composed of woven fabric plies with flat plate geometries. The second is to develop and experimentally confirm an analytical method of predicting the effects of the damage on unflawed flat plate laminates. The next steps involve the extension of the understanding of impact damage and the developed analytical methods for the flat composite plate to the more complex geometry of a cylinder.

The extension of the investigation of the impact event to the cylinder geometry was chosen for several reasons. The runway kickup damaged aircraft with a pressurized fuselage is essentially a cylinder under pressure load. Similar examples could include rocket motor cases or space habitat modules. The cylinder form is a relatively easy structure to

manufacture from composite materials, flat plates being the simplest. Cylinders are, therefore, a logical first step in the investigation of a structural effect on the impact event. At a minimum, the curvature of the cylinder geometry is expected to change the impact by introducing a membrane loading during the event, which is a condition not present in the plate geometry.

Concluding, the objectives of this research may be summarized as follows:

1) to determine the damage resistance of fabric graphite/epoxy flat plates and cylinders;
2) to develop and experimentally verify analytical models of the impact event for use as engineering tools in the determination of the impact damage tolerance of flat plate and cylindrical structures;
3) to relate information gathered on the effects of impact on flat plate structures to the cylinder case.

The following paragraphs describe in more detail the approach used and the corresponding work done in the attempt to attain these goals.

Chapter Two is a discussion of the previous work conducted on the impact damage response of composite structures. Experimental work on the characterization of impact damage to fabric graphite/epoxy plates is reviewed. Also included is an overview of a general analytical approach to the analysis of the impact event for composite plates and existing work on the analysis of impacted orthotropic cylinders.

In Chapter Three, the analytical approach used to predict impact damage and residual strength of laminated composite structures is detailed. The analysis philosophy follows the procedure implemented by Cairns [1]. The first step is to model the global impact event and generate a time history of the force on the structure. Next, a local model is used to predict the damage to the structure. Finally, the degraded portion is transformed into an equivalent inclusion in the structure to determine the post impact properties. The modifications to the existing analysis necessary for the treatment of impacted orthotropic cylinders are developed. In addition, a scheme for the use of a stress correction factor for pressurized, impacted cylinders is given.

The experimental portion of the investigation is outlined in Chapter Four. The test program for the characterization of impact damage and residual strength of plate and cylinder structures is detailed. Nondestructive and destructive examination techniques for the damage characterization study are discussed in detail as well as specimen manufacture and testing preparation. A detailed description of the design and analysis of the pressure test system developed for the cylinder study is included in this chapter.

Chapter Five contains the results of the experimental and analytical studies. Experimental and analytical data on damage characterization and residual strength for the considered geometries are presented. Comparisons are drawn between experimental and analytical results for the impact event effects

and residual strengths of the plate and cylinder specimens.

Chapter Six is a discussion of the primary observations of the study on the impact damage response of graphite/epoxy fabric structures. Impact damage and specimen failure modes of the two geometries are examined. The effectiveness of the extension of the impact analysis for plates to the cylinder case is discussed. Observations on the validity of the testing methods and analytical procedures are also made in this chapter.

Chapter Seven includes several conclusions about the experimental and analytical results of the impact study on fabric plates and cylinders. Recommendations for further experimental study and analytical enhancements may also be found in this chapter. In addition, several comments on possible refinements to the pressure vessel test system are included.

Finally, the Appendix contains a complete listing of the FORTRAN source codes used for the analysis of the impact event for plates and cylinders. This listing includes a step by step procedure for using the codes, the input required for each step, and a summary of the output generated from each program. A complete breakdown of the experimental data is also given.

CHAPTER TWO

PREVIOUS WORK

To understand the damage resistance and damage tolerance of composite laminates subjected to impact, it is necessary to comprehend all aspects of the impact event. The major areas of concern are the dynamic behavior of a laminate subjected to impact, the resulting damage because of the impact, and the post impact properties of the damaged laminate. An extensive amount of research has been conducted on these aspects of the impact event for a variety of laminate configurations. This chapter is an outline of some of the important results found in previous investigations of the impact of composite laminate materials.

2.1 Impact Damage Resistance and Tolerance of Fabric Laminates

A key in understanding the effect of impact on any material is knowing the damage that results from impact phenomena. Correct physical information is an invaluable aid in determining the parameters that govern the total impact response of a composite laminate. Characterization of the impact damage, therefore, is a primary step in developing a thorough analytical method.

Damage characterization has been extensively investigated

for tape laminates subjected to impact. Research done by a number of investigators [2-6] on the impact damage of graphite/epoxy and Kevlar/epoxy tape laminates has shown that a few common types of damage are extant in impacted composites. The damage states were found to be fiber breakage, angle ply splits parallel to fibers, and delaminations.

It has been found that composite laminates manufactured from graphite/epoxy fabric are able to suppress some damage states [7]. Specifically, it was observed that the weave of the fabric suppresses splitting of the plies. The hypothesis follows that the weave may be able to suppress the angle ply splitting of the laminate that is normally found in tape laminates subjected to impact. However, a lack of information exists on the effect of the fabric weave on the damage resistance of composite laminates subjected to impact.

Teti, et al., [8] made a few empirical observations of the effects of impact on graphite/epoxy cloth composites. Visual observations made of the damaged specimens revealed that the impact produced a rhomboidal damage site with the major axis of the rhomboid along the warp axis of the back surface of the laminate. The material damage developed by (a) first fiber failure probably preceeded by delamination, (b) extended fiber breakage, and (c) material penetration by the impactor. They also found that the damage proceeded from the lower tensile-loaded sample surface to the higher compression loaded surface.

Teti et al., and Winkel [9] also monitored the force versus time impact response curves for graphite cloth/epoxy. Winkel found that no significant difference existed between the curves for cloth and cross-ply laminates. Teti et al., was able to correlate some damage states to the force versus time impact curve for low velocity drop weight impacts.

Little work has been done to determine the impact damage resistance of fabric laminates. Of the work that was done, no investigation of the impact of graphite/epoxy fabric utilized a thorough nondestructive and destructive examination approach. Therefore, it is necessary that an extensive experimental evaluation of the impact damage resistance of graphite/epoxy fabric be undertaken to identify the damage mechanisms important in the impact event. This experimental work becomes the basis for analytic models of the effects of impact on graphite/epoxy fabric laminates.

2.2 Models of the Global Impact Event for Composite Plates

The study of the dynamic behavior of composite plates subjected to impact has received considerable attention. The models developed in these studies are used to predict the dynamic response and resulting global deflections of the impacted plate. Usually these models do not go beyond determining the dynamic response to predict the damage state at a local level.

A number of considerations specific to composites must be

made in the development of a global time history of the impact event. Shear deformation of the laminate is significant because of the high through the thickness shear compliance of composites [10]. A large length to thickness ratio is required composites before the influence of shearing deformation may be ignored. Consequently, laterally loaded models of composite laminates which do not account for this shearing deformation are unrealistically stiff.

Models also have been developed for determining the global time history of the impact event for composites. Tan and Sun [11] used a two dimensional finite element plate model subjected to low velocity impact. Their results correlated very well to experimental results. Sun and Chen [12] used essentially the same model to conduct a study of the influence of the local indentation law, impactor mass, laminate prestress, and impactor velocity on the impact event.

A larger three-dimensional finite element model modeling each ply of the laminate was developed by Wu and Springer [13]. This model was extended to predict the damage state on a local level. The three dimensional model incorporates through the thickness effects, but the accuracy of the model is governed by the degree of refinement of the mesh used. Obviously, the coarser the mesh, the less expensive the computational costs. If the damage state occurs on a very local level, a high degree of refinement is required, and the solution cost increases correspondingly.

Cairns and Lagace [14] utilized a Reissner-Mindlin plate

with shear deformation to predict the global force, acceleration, and displacement time histories of the impact event. This model was used to extract a peak force and acceleration during the event. These were used in a local static model to determine the damage state (Cairns [1]). This model was supposed to bridge the gap between the aforementioned analyses. The two-dimensional models require less computational time than the three-dimensional finite element models but often do not include enough detail or computational refinement to be used to predict damage. The three-dimensional finite element model pays a high computational cost outside the local region of damage, especially if the analysis is being conducted on a larger structure. Cairns hoped to produce a model that was computationally efficient enough to solve the impact event in a realistic time and still provide sufficient detail in the local region of impact.

Teti and Winkel [8,9] observed that the experimentally determined force versus time response curves were not affected by the ply material. The same impact response was found for equivalent layups of cross-ply tape laminates and fabric laminates. This observation allows the the analysis developed for tape laminates to be applied directly to fabric laminates.

2.3 Models of the Global Impact Event for Composite Cylinders

The global model for the determination of the time history of the impact event for a composite cylinder must consider three important items. Shearing deformation should be considered for the same reason previously discussed, unless the cylinder wall thickness is very small compared to the radius of the cylinder. Second, the in-plane displacement terms which give rise to membrane loading of the cylinder must be included. These terms may be likened to an initial prestress of a plate laminate. These terms may affect the maximum contact force during the impact event. Third, the true equations of motion of a cylinder must be used, as opposed to using the shallow shell constitutive relations, to accurately detail the boundary conditions of the cylinder during the impact event.

Little attention has been paid to the problem of impact of cylindrical structures. Razi et al., [15] developed an analysis for simply-supported orthotropic cylinders subjected to low velocity impact. This model was used to determine the global time history of the impact event only. The model included shear deformation of the shell and utilized the equations for an impactor induced pressure developed by Greszcuk [16]. The results for a low velocity impact were compared to an analysis utilizing finite-elements and the NASTRAN code. Correlation of the displacement results between the two analyses was good. This model was based on the

constitutive relations for a shallow shell, however, and did not utilize the constitutive relations for a cylinder.

No previous work has been found that utilizes the full cylinder equations of motion. Since it is a primary objective of this research to observe the structural effects of the cylinder curvature on the impact event, the proper model needs to be incorporated into the analysis.

2.4 Determination of Impact Induced Damage

Greszcuk [17] conducted some of the first work for predicting impact damage in composites exposed to low velocity impact. He utilized a theory of elasticity approach that neglected all dynamic effects and was essentially a static contact problem. This model was used to calculate the stresses and strains through the laminate on a local basis in order to predict damage. The model did not account for global bending of the target or inertial forces. For low velocity impact, this method was moderately successful.

Cairns and Lagace [18] also based their analysis on a theory of elasticity approach. In addition to Greszcuk's assumptions, Cairns attempted to include global bending effects and inertial loading effects. The stresses in the plate were computed by statically loading the plate with a point load at the center to represent the impactor and a distribution of point loads to represent the inertial acceleration loading. Damage to the plate was predicted by

applying the maximum strain criterion on a ply by ply basis to calculate the extent of delamination, angle ply splitting, and fiber breakage. This model has been shown to agree fairly well with experimental results (Cairns [1]).

This model was used solely on tape laminates. The extension of Cairns analysis to fabric laminates is complicated by the ability of the weave to suppress angle ply splitting. However, the fabric plies are much closer to an isotropic material than the unidirectional plies so the model may actually predict the stresses and strains on a ply by ply basis more accurately for the fabric laminate.

2.5 Post Impact Residual Strength of Composites

The impact damage tolerance of a structure is determined by its residual strength after impact. The initial approaches to the study of damage tolerance were experimental investigations on a specific structure and therefore limited in usefulness for general applications (Gustafson et al., [19], Click [20], Williams [21]). Overall, initial work on the impact damage tolerance of composite laminates lacked any analytical efforts.

An extensive study of the compressive residual strength of impacted composites was conducted by Starnes, Williams and others [21-23]. They developed a general empirical base for impacted composites under compression, where the behavior was governed by delamination. Less work has been done on the

tensile strength of composite laminates subjected to impact.

Two types of behavior have been observed in the tensile residual strength studies. Caprino [24] and Dorey et al., [25] found the existence of a threshold level of energy at which the impact event degraded the properties of the composite laminate. The difference between the two investigations exists in the leveling off of the reduction in residual strength for increasing impactor energy. Caprino's observations suggest a flat reduction past some given energy while Dorey emphasizes that the residual strength may actually increase beyond some high energy level. This increase in residual strength is attributed to the fact that the impact damage becomes a cleaner hole at higher punch through velocities. It must be noted that these studies made no attempt to discern between the ability of a structure to resist impact damage and the ability of a structure to retain its design strength after impact. The concepts of damage resistance and damage tolerance were not separated.

Cairns [1] duplicated most of these trends for graphite/epoxy laminates. However, the levels of impact were not high enough to show the trend suggested by Dorey. Cairns and Lagace [26] furthermore emphasized that the most important concept in the damage tolerance of a structure is that strength is dependent solely on the damage present, not on how the damage is introduced. An identical damage state produced by different events in a given structure will result in the same strength reduction for that structure.

As part of the development of an integrated analysis approach to the the impact problem (Cairns [1]) a model was constructed to determine the residual strength of composite laminates (Cairns and Lagace [26]). The method involved the construction of a degraded elliptical inclusion to model the impact area. A plate with an elliptical inclusion as developed by Leknitski [27] was used to determine the stress field around the damage area and thereby predict the residual strength of the impacted specimen.

The basis for the construction lies in observations of idealized damage in composite materials. As previously stated, typical impact damage in composites includes fiber breakage, angle ply splits, and delamination. Modeling all of these phenomena is a monumental task. Therefore, the problem was broken down into smearing the effects of impact damage.

It has been shown by Lagace and Cairns [28] that delaminations in tensile specimens had no observable effect on the residual strength of laminates under tensile load, as a result, the governing factor was approximated by the core fiber damage from the impact event. Regions of fiber damage were assumed to contribute nothing to the integrity of the laminate. The inclusion properties were calculated using laminated plate theory for the reduced laminate. The reduced strength properties were calculated by application of an averaged strain criterion. This analysis yielded good results.

2.6 Damage Tolerance of Composite Cylinders

Experimental work on the damage tolerance of composite cylinders has focused primarily on idealized damage. This damage was often geometrically simple cutouts in a structure, modelled such items as a window in a fuselage or an inspection port in a pressurized pipeline.

Lagace and Saeger [29] provided a review of work on the damage tolerance of pressurized composite cylinders. They found that experimental data from simple plate test specimens could be used to predict the damage tolerance of composite cylinders, thereby avoiding the expensive process of testing cylinders. For a variety of flaw types, correction factors were used to correlate coupon data with cylinder data. These correction factors accounted for the stress intensification arising from localized bending at the flaw in the pressurized cylinder.

The damage to the pressurized cylinders in these investigations was manufactured into the specimens. This work, therefore, did not address how the curvature of the cylinder affected the damage resistance of the structure.

CHAPTER THREE

ANALYSIS

This chapter is a description of the analytical approach used for the investigation of the impact damage resistance and tolerance of advanced composite laminate flat plate and cylindrical structures.

3.1 General Approach to Impact Analysis

The method used to predict the impact response of composite laminates consists of several separable analytical steps. The approach was developed by Cairns and this research essentially follows his method. The procedure is summarized in Figure 3.1. The first step is to generate the global time history of the impact event for the given geometry. The force versus time and acceleration versus time histories are used to examine the impact at the local level. The local model can be used to find the stress and strain state of the laminate under the impact load and to predict the damage to the laminate on a ply by ply basis. The damage state is used to determine the degraded properties of the laminate. Finally, the degraded properties of the laminate are used to describe an equivalent inclusion model from which the residual strength may be determined.

As stated in Chapter Two, all of these models are based

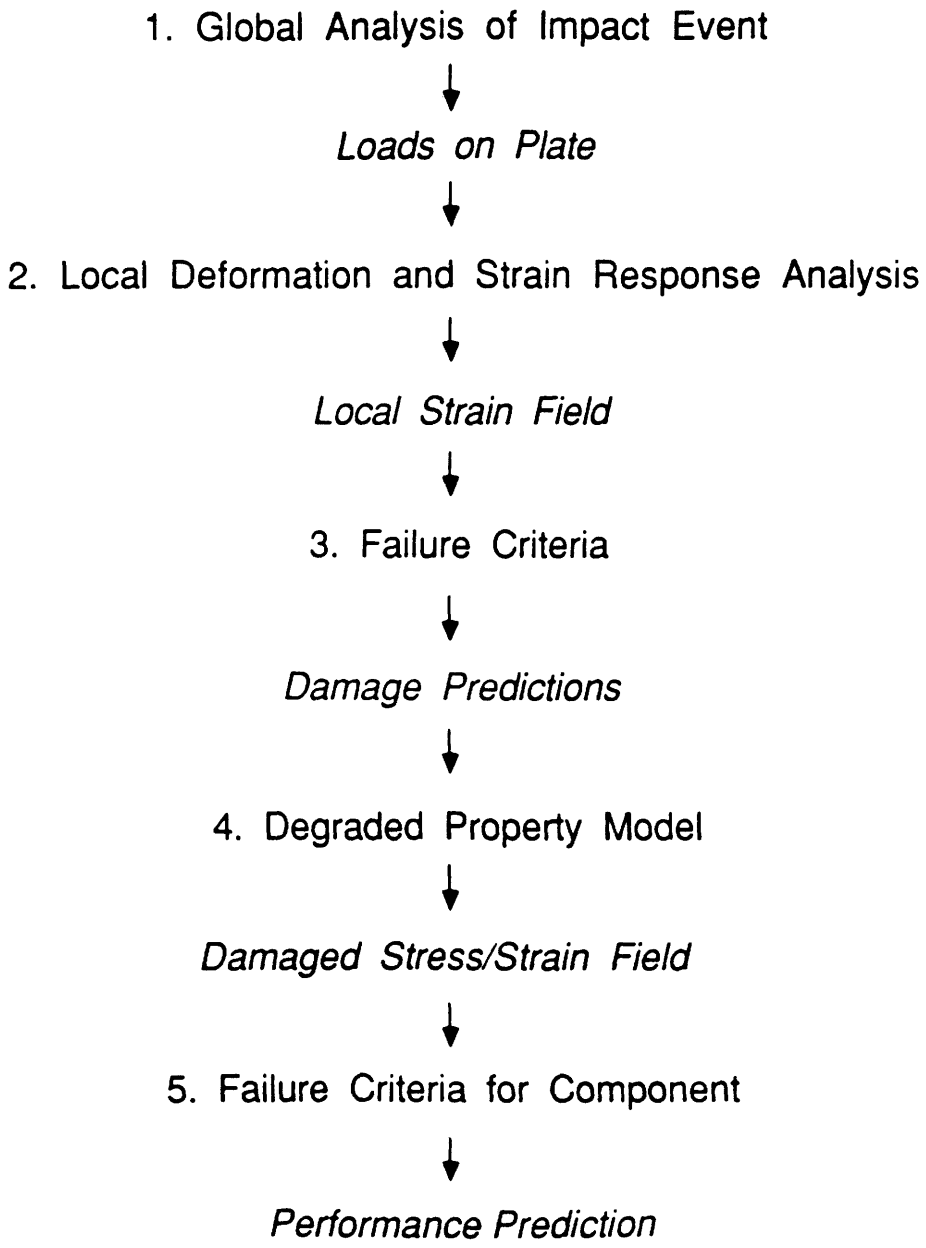

Figure 3.1 Flow Diagram for Analytical Approach Philosophy

on work by Cairns [1]. This chapter presents the modifications to Cairns's analysis for the global and local models.

3.2 Global Model

The global model is used to develop the impact event loading history. The outline of the analysis can be applied to other geometries as well, provided that the equations of motion and boundary conditions of the problem are known. This model is independent of the other analyses used and may be substituted by any other analysis that develops the loading history of an impact event.

The global model includes the influences of external variables on the impact event. These variables are the physical boundary conditions of the structure and the material constitutive properties. The impactor is treated as a Hertzian contact spring. Any local nonlinear behavior that may occur during the impact event is not accounted for in the analysis. Note that this challenges the validity of the analysis for high damage impacts, where the behavior of the structure is generally not linear because of the catastrophic effects of the event.

The dynamic model for flat rectangular plates incorporates bending-twisting coupling and shear deformation of the laminate. The cylinder analysis is a simplified isotropic model that includes the curvature terms but does not

include shear deformation. The method utilized for both cases is an assumed modes analysis.

3.2.1 Global Model for Flat Plate

The method utilized to generate the time loading history of the impact loading event follows closely the one developed by Cairns [14]. The only difference between the analysis used for this study and that of Cairns's was the implementation of generalized beam functions for the plate boundary conditions in the computer code. Unlike the traditional sine, hyperbolic sine, cosine, and hyperbolic cosine expressions, the generalized beam functions may be evaluated without numerical integration. Since the generalized beam functions may be integrated exactly, the run time efficiency of the code is increased.

These functions were developed by Dugundgi [30] and do not sacrifice any accuracy in the solution beyond the first mode. The generalized beam function is given by

$$\phi_n(x) = \sqrt{2}\ \sin(\beta_n x + \theta) + Ae^{-\beta_n x} + Be^{-\beta_n (1-x)} \qquad (3.1)$$

where the constants are given in Table 3.1.

TABLE 3.1

EULER BEAM ELASTIC MODE SHAPE PARAMETERS

Boundary Condition	β_n	θ	A	B
SS - SS	$n\pi$	0	0	0
CL - FR	$(n-1/2)\pi$	$-\pi/4$	1	$(-1)^{n+1}$
CL - CL	$(n+1/2)\pi$	$-\pi/4$	1	$(-1)^{n+1}$
FR - FR	$(n+1/2)\pi$	$-\pi/4$	1	$(-1)^{n+1}$
SS - CL	$(n+1/4)\pi$	0	0	$(-1)^{n+1}$
SS - FR	$(n+1/4)\pi$	0	0	$(-1)^{n}$

SS - Simply Supported

CL - Clamped

FR - Free

3.2.2 Global Model for Orthotropic Cylinder

The original objective of the cylinder analysis was to duplicate the approach used by Cairns for the global plate analysis. Lack of computer equipment powerful enough to provide a convergent solution for a cylinder with the D_{16}, D_{26}, A_{16}, and A_{26} terms included with shear rotation necessitated the use of a simplified model. The final analysis used an orthotropic cylinder with a Hertzian spring load.

The cylinder shell utilizes three displacements, u, v, and w, defined in the tangent plane of the cylinder as shown in Figure 3.2. The radius to thickness ratio is approximately 100 for the cylinders in this investigation. Consequently, the cylinder wall is thin compared to the overall geometry. Jones [31] shows that as the width of a plate becomes much larger than the thickness the effects of shearing deformation become less important. If the same conclusion can be drawn for the cylinder, the shear deformation of the cylinder may be neglected without sacrificing the accuracy of the model. Thus, the Kirchoff thin plate assumptions are used in this model.

The strains and curvatures are given by the equations:

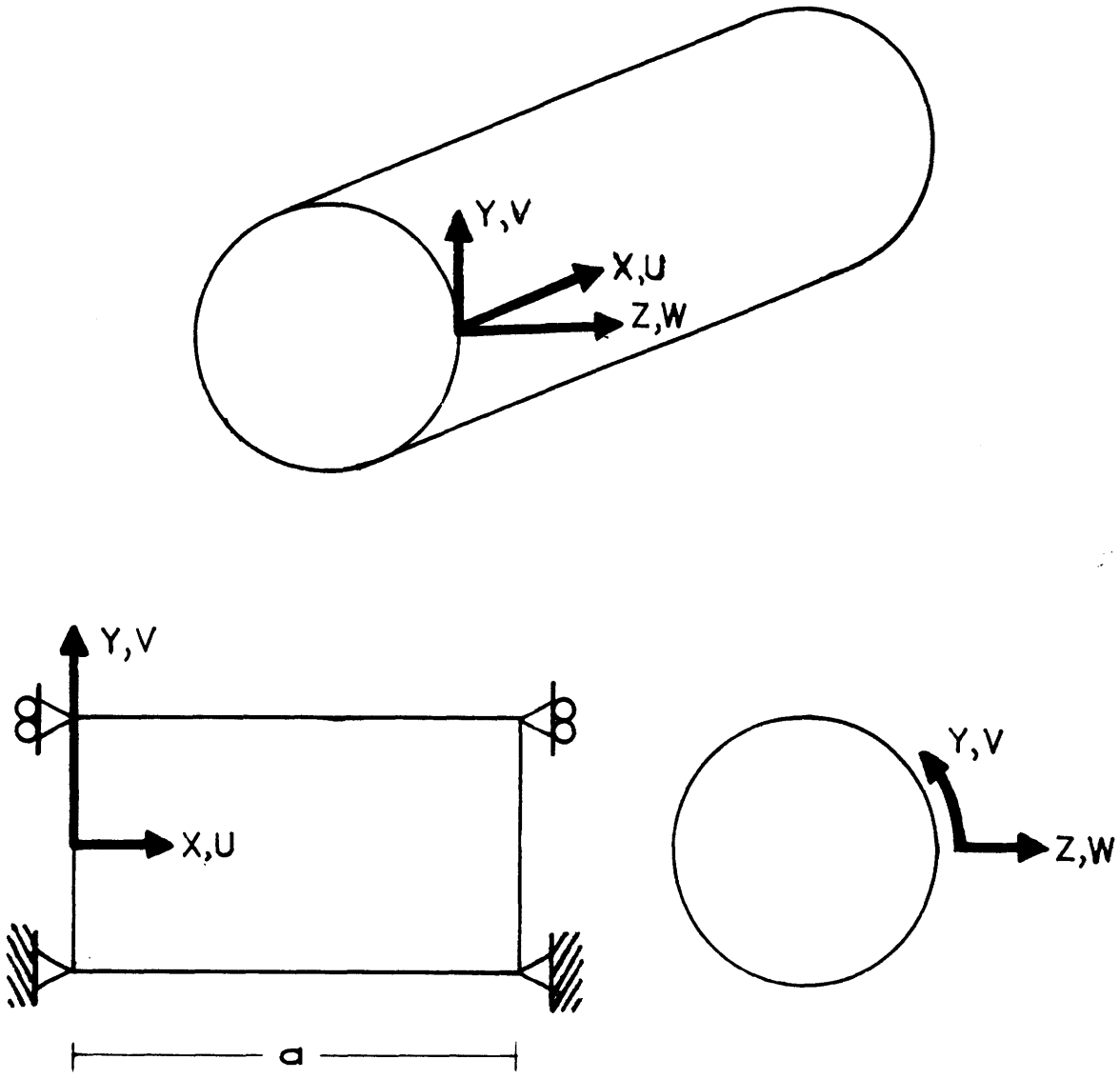

Figure 3.2 Cylinder Coordinate System for Global Model

$$\varepsilon_x = \frac{\delta u}{\delta x} \qquad \varepsilon_y = \frac{\delta v}{\delta y} + \frac{W}{R} \qquad \gamma_{xy} = \frac{\delta u}{\delta y} + \frac{\delta v}{\delta x}$$

$$\kappa_x = \frac{-\delta^2 w}{\delta x^2} \qquad \kappa_y = \frac{-\delta^2 w}{\delta y^2} + \frac{1}{R}\frac{\delta v}{\delta y} \qquad \kappa_{xy} = -2\,\frac{\delta^2 w}{\delta x\,\delta y} \tag{3.2}$$

The following four assumptions are made for this model (a) the edges of the cylinder at x equal to 0 and a are simply supported, (b) the solution for w is symmetric about x equal to a/2 and y equal to 0, (c) the solution for v is symmetric about x equal to a/2 and antisymmetric about y equal to 0, and (d) the solution for u is antisymmetric about x equal to a/2 and symmetric about y equal to 0. From these assumptions the assumed displacements are

$$u = \sum u_{mn} \cos\left(\frac{m\pi x}{a}\right) \cos\left(\frac{ny}{R}\right)$$

$$v = \sum v_{mn} \sin\left(\frac{m\pi x}{a}\right) \sin\left(\frac{ny}{R}\right) \tag{3.3}$$

$$w = \sum w_{mn} \sin\left(\frac{m\pi x}{a}\right) \cos\left(\frac{ny}{R}\right)$$

where

$$0 \leq x \leq a \qquad -\pi R \leq y \leq +\pi R$$

The analysis follows Cairns's [1] development. The assumed

displacements are substituted in for u, v, and w in equation (3.2). The strains and curvatures are given by equations (3.4) and (3.5).

$$\varepsilon_x = -u_{mn} \sin\left(\frac{m\pi x}{a}\right) \cos\left(\frac{ny}{R}\right)$$

$$\varepsilon_y = \left[v_{mn} \left(\frac{n}{R}\right) + w_{mn} \left(\frac{1}{R}\right) \right] \sin\left(\frac{m\pi x}{a}\right) \cos\left(\frac{ny}{R}\right) \qquad (3.4)$$

$$\gamma_{xy} = \left[-u_{mn} \left(\frac{n}{R}\right) + v_{mn} \left(\frac{m\pi}{a}\right) \right] \cos\left(\frac{m\pi x}{a}\right) \sin\left(\frac{ny}{R}\right)$$

$$\kappa_x = w_{mn} \left(\frac{m\pi}{a}\right)^2 \sin\left(\frac{m\pi x}{a}\right) \cos\left(\frac{ny}{R}\right)$$

$$\kappa_y = \left[w_{mn} \left(\frac{n}{R}\right)^2 + v_{mn} \left(\frac{n}{R^2}\right) \right] \sin\left(\frac{m\pi x}{a}\right) \cos\left(\frac{ny}{R}\right) \qquad (3.5)$$

$$\kappa_{xy} = 2\, w_{mn} \left(\frac{m\pi}{a}\right) \left(\frac{n}{R}\right) \cos\left(\frac{m\pi x}{a}\right) \sin\left(\frac{ny}{R}\right)$$

The next step is to form the potential energy Π_p given in equation (3.6):

$$\Pi_p = \frac{1}{2} \int_0^a \int_{-\pi R}^{+\pi R} \left[A_{11}\, \varepsilon_x^{\,2} + 2\, A_{12}\, \varepsilon_x \varepsilon_y + A_{22}\, \varepsilon_y^{\,2} + A_{66}\, \gamma_{xy}^{\,2} \right. \tag{3.6}$$

$$\left. + D_{11}\, \kappa_x^{\,2} + 2\, D_{12}\, \kappa_x \kappa_y + D_{22}\, \kappa_y^{\,2} + D_{66}\, \kappa_{xy}^{\,2} \right] dx\, dy$$

D_{ij} and A_{ij} are the laminate bending and stretching matrices:

$$\left[A_{ij} , D_{ij} \right] = \int_{-h/2}^{+h/2} \bar{Q}_{ij} \left[1 , z^2 \right] dz \tag{3.7}$$

where h is the plate thickness and Q_{ij} are the reduced lamina stiffnesses resulting from rotating the ply constitutive properties into the plate coordinate system. No inplane preloads are considered for this analysis; as the impact of the cylinder is considered to be conducted without internal pressure or longitudinal loading.

Since the material is orthotropic the kinetic energy is given by:

$$V = \frac{1}{2} \int_0^a \int_{-\pi R}^{+\pi R} \rho t \left[\dot{u}^{\,2} + \dot{v}^{\,2} + \dot{w}^{\,2} \right] dx\, dy \tag{3.8}$$

After integration, the Lagrangian is formed:

$$\frac{d}{dt}\left[\frac{\delta L}{\delta \dot{x}}\right] - \frac{\delta L}{\delta x_i} = R_i \tag{3.9}$$

where L is the Lagrangian or action integral

$$L = \sum \Pi_p - \sum V_i$$

and R_i is the forcing function vector.

Note that since all modes are orthogonal, each harmonic in (m,n) is uncoupled. This reduces the computation to a three by three eigenvalue problem.

The governing equations of motion are given by:

$$\frac{a\pi R}{2}\begin{bmatrix} K \end{bmatrix}\begin{Bmatrix} u_{mn} \\ v_{mn} \\ w_{mn} \end{Bmatrix} + \frac{a\pi R}{2}\begin{bmatrix} M \end{bmatrix}\begin{Bmatrix} \ddot{u}_{mn} \\ \ddot{v}_{mn} \\ \ddot{w}_{mn} \end{Bmatrix} = \begin{Bmatrix} 0 \\ 0 \\ F_{mn}(t) \end{Bmatrix} \tag{3.10}$$

The right hand side of the equation contains the loading terms. The load on the cylinder is assumed to be Hertzian in nature as used for the plate global analysis by Cairns [1]. The stiffness and mass matrices are given in equations (3.11) and (3.12) respectively:

$$K = \begin{bmatrix} K_{aa} & K_{ab} & K_{ac} \\ K_{ab} & K_{bb} & K_{bc} \\ K_{ac} & K_{bc} & K_{cc} \end{bmatrix} \tag{3.11}$$

The terms of the stiffness matrix are

$$K_{aa} = A_{11} \left(\frac{m\pi}{a} \right)^2 + A_{66} \left(\frac{n}{R} \right)^2$$

$$K_{ab} = -2\, A_{12} \left(\frac{m\pi}{a} \right)\left(\frac{n}{R} \right) - 2\, A_{66} \left(\frac{m\pi}{a} \right)\left(\frac{n}{R} \right)$$

$$K_{ac} = - A_{12} \left(\frac{m\pi}{a} \right) \frac{1}{R}$$

$$K_{bb} = A_{22} \left(\frac{n}{R} \right)^2 + A_{66} \left(\frac{m\pi}{a} \right)^2 + D_{22} \left(\frac{n}{R} \right)^2$$

$$K_{bc} = A_{22} \left(\frac{n}{R^2} \right) + D_{22} \left(\frac{n^3}{R^4} \right) + D_{12} \left(\frac{m\pi}{a} \right)^2 \left(\frac{n}{R^2} \right)$$

$$K_{cc} = D_{11} \left(\frac{m\pi}{a} \right)^4 + \left(2\, D_{12} + 4\, D_{66} \right) \left(\frac{m\pi}{a} \right)^2 \left(\frac{n}{R} \right)^2$$

$$+ D_{22} \left(\frac{n}{R} \right)^2 + A_{22} \left(\frac{1}{R} \right)^2$$

$$M = \begin{bmatrix} \rho t & 0 & 0 \\ 0 & \rho t & 0 \\ 0 & 0 & \rho t \end{bmatrix} \tag{3.12}$$

This sets up the eigenvalue problem:

$$\frac{1}{\rho t} \begin{bmatrix} K \end{bmatrix} q_{mn} = \omega_{mn}^2 \, q_{mn} \tag{3.13}$$

The solution procedure is composed of the following four steps. First, solve for all harmonics and get three eigenvalues and corresponding eigenvectors for (m,n). Of those three solutions, the lowest frequency corresponds to the flexural waves and the other two frequencies correspond to extensional waves. Second, retain only the flexural wave solution. This is possible because the magnitude of the eigenvectors associated with the extensional waves are very small compared to those for the flexural wave. Third, reduce this solution to the equations of (3.14):

$$\ddot{q}_{mn} + \omega_{mn}^2 \, q_{mn} = \frac{w_{mn}}{\left(\frac{a\pi R\rho t}{2} \right)} \, F_{mn}(t) \sin \left(\frac{m\pi}{2} \right) \tag{3.14}$$

where F(t) is the applied Hertzian spring point load at x equal to a/2, y equal to 0 and w_{mn} is the eigenvector

component. Finally, these equations are integrated in time to generate the displacement, force, and acceleration time histories of the impact event for the cylinder.

3.2.3 Hertzian Contact Spring

The contact loading for the impact event for both the plate and cylinder geometries is assumed to be Hertzian in nature. The value of the Hertzian spring constant is calculated using the local model for the plate and cylinder. No curvature of the cylinder is taken into account because the constant is computed for a very localized region of the total problem. The procedure is identical to that described by Cairns and Lagace [18].

The spring constant is computed from a static indentation of the laminate. A geometric approach, α, is assumed and a unit load with no acceleration is applied. The local model is used to compute the displacement of the top and bottom surfaces. This displacement is identical to the approach α_{unit} for a unit load. Since the load scales linearly with α, the load required to recover the assumed geometric α is simply the ratio

$$P_{required} = \frac{\alpha_{geometric}}{\alpha_{unit}} \qquad (3.15)$$

The spring constant, K, was computed from the formula:

$$P = K \alpha^{1.5} \tag{3.16}$$

For this analysis, an average K was used based on ten different values of the approach α from 0.00 to 0.20 mm.

3.3 Local Model for Flat Plate and Cylinder Geometries

For this analysis, the consideration of the effects of the impact event at the local level was the same for both flat plate and cylinder structures. The model developed by Cairns cannot be modified to include curvature of the cylinder. The small radius of damage to radius of cylinder ratio considered for this investigation should allow use of the flat plate model if damage is localized.

One modification is made to the analysis utilized by Cairns. In Cairns's analysis, the stress function ψ is given by:

$$\Psi = \sum_{m=1}^{\infty} f_m(z)\, g_m(r) \tag{3.17}$$

The separable function in r and z utilizes the Bessel function J_o in r and an exponential f(z) of the form:

$$f_m(z) = A_m\, e^{(s_1\omega_m z)} + B_m\, e^{(s_2\omega_m z)} + C_m\, e^{-(s_1\omega_m z)} + D_m\, e^{-(s_2\omega_m z)} \tag{3.18}$$

The resulting matrix equation to find the modal amplitudes A_m, B_m, C_m, and D_m is numerically ill conditioned for the high number of modes required to obtain solution convergence. A new series in z, therefore, is chosen to alleviate the numerical problem. This series is a sum of hyperbolic sines and cosines of the form:

$$f_m(z) = A_m \sinh(s_1\omega_m z) + B_m \cosh(s_1\omega_m z) + C_m \sinh(s_2\omega_m z) + D_m \cosh(s_2\omega_m z) \tag{3.19}$$

After using the prescribed boundary conditions pictured in Figure 3.3 and stated here:

$$\sigma_{zz}(r, -h/2) = -p(r) \qquad \sigma_{rz}(r, -h/2) = 0$$
$$\sigma_{zz}(r, +h/2) = 0 \qquad \sigma_{rz}(r, +h/2) = 0 \tag{3.20}$$

the following set of equations needs to be solved to find the modal amplitudes for the assumed series f(z):

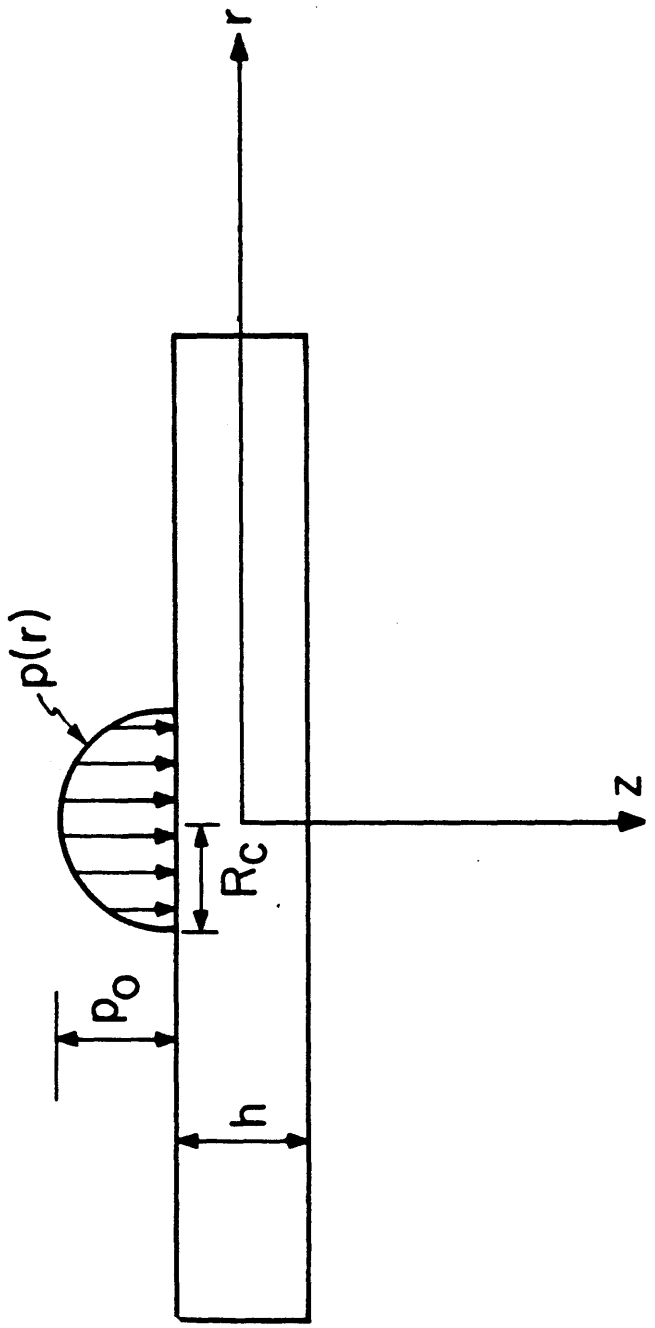

Figure 3.3 Sketch of Problem for Local Model

$$\begin{bmatrix} A_{11} & A_{12} & A_{13} & A_{14} \\ A_{21} & A_{22} & A_{23} & A_{24} \\ A_{31} & A_{32} & A_{33} & A_{34} \\ A_{41} & A_{42} & A_{43} & A_{44} \end{bmatrix} \begin{Bmatrix} A_m \\ B_m \\ C_m \\ D_m \end{Bmatrix} = \begin{Bmatrix} -p(r) \\ 0 \\ 0 \\ 0 \end{Bmatrix} \qquad (3.21)$$

The components of the A matrix are listed in APPENDIX E. Implementation of this new series into the existing local model code yields favorable results. Numerical stability and solution convergence within five percent of steady state is achieved.

The new results are compared to experimental work done by Tan and Sun [11] for a $[0/+45/0/-45/0]_{2s}$ graphite/epoxy laminate. Properties of the material used in their study are included in Table 3.2. Figures 3.4 and 3.5 are plots of the normalized indentation and pressure distribution versus number of modes respectively. The solutions are for plate radius/plate thickness ratio of 20. The static indentation requires approximately 60 harmonics for convergence. The Hertzian force distribution on the plate exhibits very slow convergence and requires nearly 200 harmonics. Figure 3.6 is a comparison of the force versus indentation results for the experimental work by Tan and Sun and the present analysis. Since the model is axisymmetric, the analysis must be run for two cases to account for the different E_L and E_T of the

TABLE 3.2

TAN AND SUN GRAPHITE/EPOXY PLY PROPERTIES

$E_1 = 120.0$ GPa
$E_2 = 7.9$ GPa
$G_{12} = 5.5$ GPa $= G_{13} = G_{13}$
$\nu_{12} = 0.30$
$\rho = 1582.0$ kg/m^2

All data from reference [11]

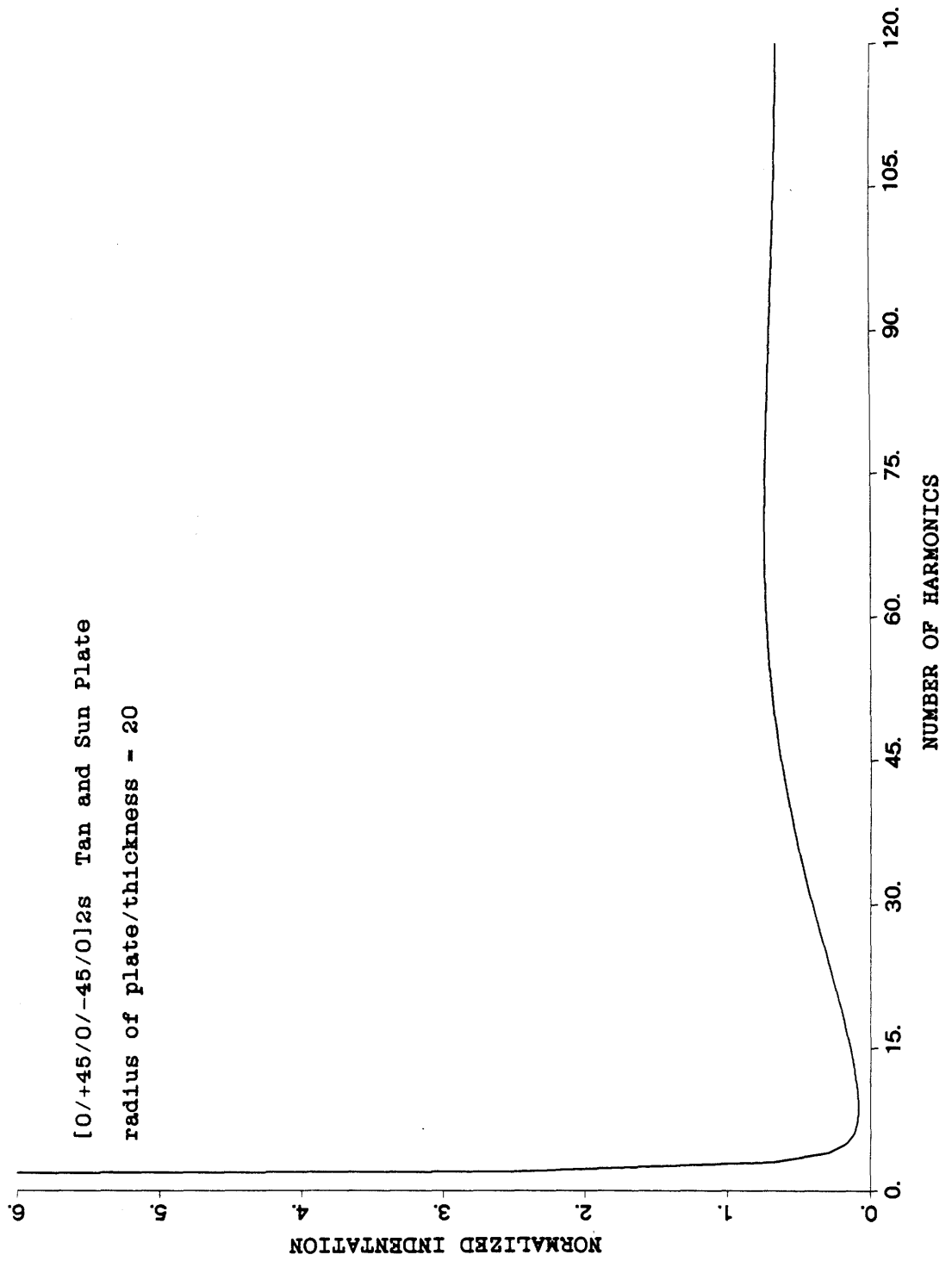

Figure 3.4 Convergence of Indentation α for $[0/+45/0/-45/0]_{2s}$ Tan and Sun Plate

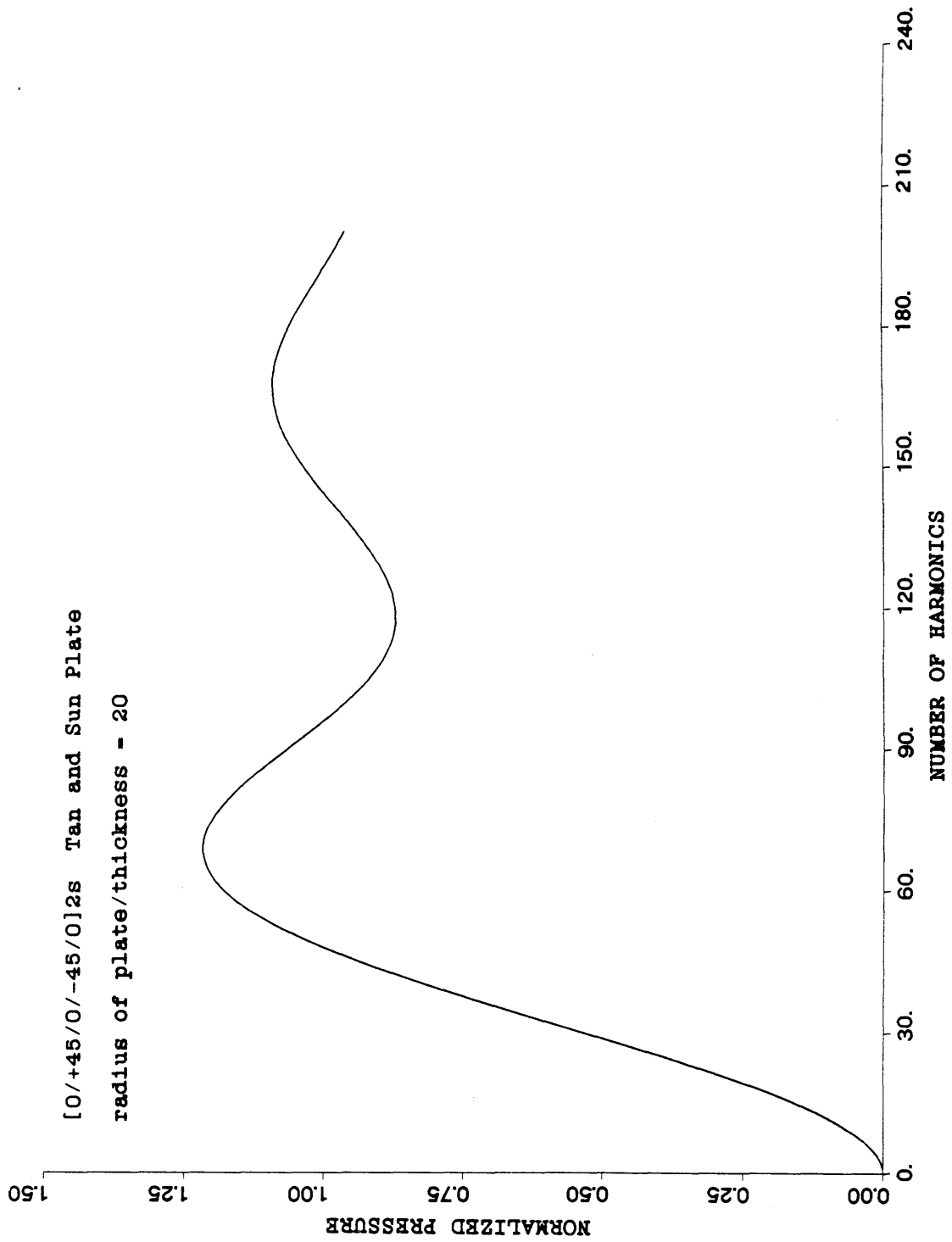

Figure 3.5 Convergence of Hertzian Loading Distribution p(r) for $[0/+45/0/-45/0]_{2s}$ Tan and Sun Plate

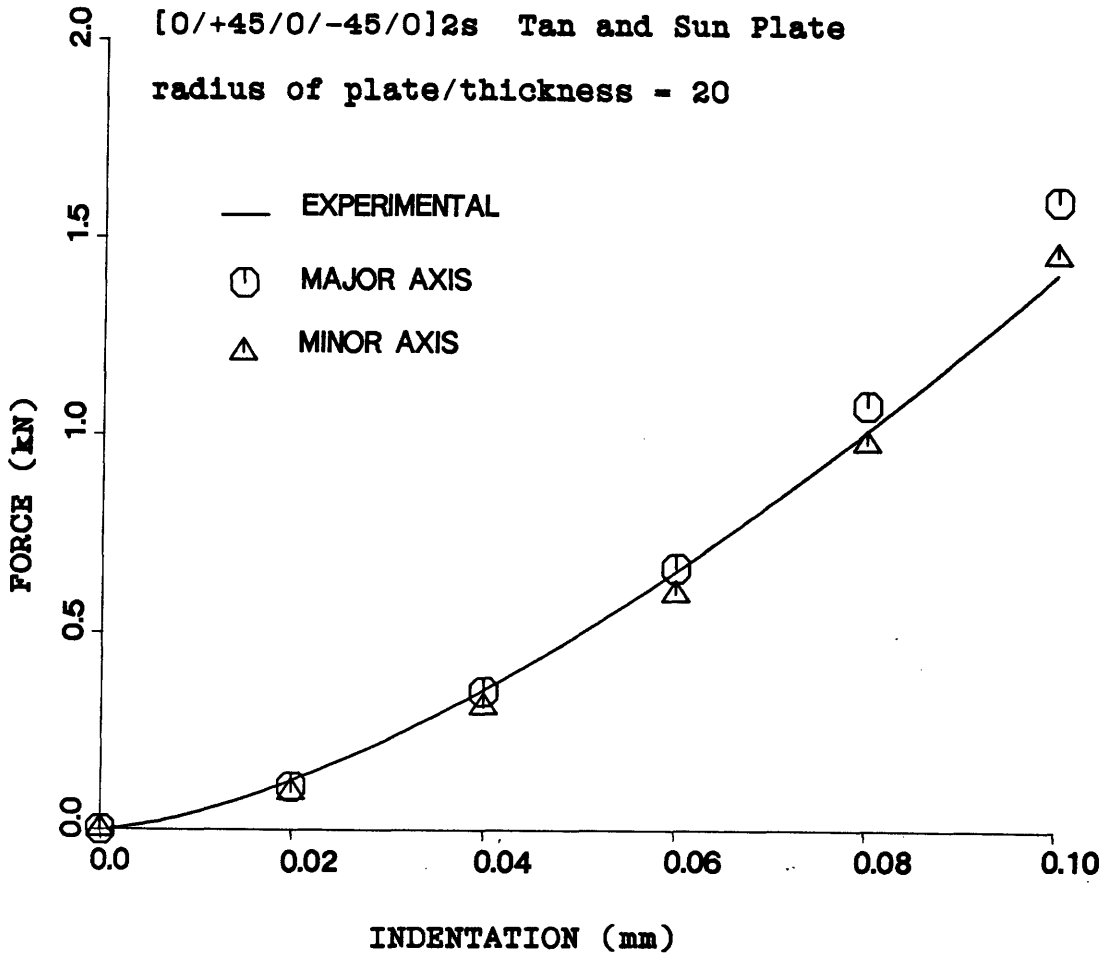

Figure 3.6 Indentation Force versus Static Indentation α for $[0/+45/0/-45/0]_{2s}$ Tan and Sun Plate

laminate. The E_L analysis corresponds to the major axis. The E_T analysis corresponds to the minor axis. Agreement between the analytical and experimental work is excellent.

3.4 Degraded Property Model

The stress and strain field predicted by the local Fourier-Bessel model is used to determine the damage state of the laminate. The maximum strain criterion is applied to the laminate on a ply by ply basis. Based on the assumption that the fabric is linear to failure the maximum strain values used for fiber breakage of the A370-5H/3501-6 are:

$$\varepsilon_{11t} = 11269\mu s \qquad \varepsilon_{11c} = 10745\mu s$$
$$\varepsilon_{22t} = 10028\mu s \qquad \varepsilon_{11c} = 9807\mu s$$

Fiber failure is assumed to be the governing factor in the degradation of properties and therefore in the reduction of tensile residual strength of a laminate. This is the only damage state predicted. If the predicted strain in the fiber exceeds the maximum strain envelope, the fiber is considered to be incapable of carrying any load. The damage region is predicted by determining the region over which fiber failure occurs. The properties for that region are based on the remaining undamaged laminate. For example, if it is predicted that the 0° fibers in the top and bottom ply of a $(0,45)_s$ laminate exceed the maximum values for an area 10 mm in

diameter, the remaining laminate is modeled as a $(0,45)_s$ laminate with a 10 mm inclusion having the properties of a $(45)_s$ laminate.

The degraded property model is a planar model of an anisotropic, elliptic inclusion. It is the same as that employed by Cairns and Lagace [26] and originally developed by Lekhnitski [27]. Note that the total laminate used for this study is quasi-isotropic and the solution reduces to the biharmonic equation for a planar, isotropic, elasticity problem. This analysis is directly applied using the code developed by Cairns [1]. The stress and strain field in the inclusion model is computed and the residual strength is predicted by application of the average strain criterion.

An important concept used in Cairns's model for the prediction of post impact residual strength of composite laminates is the average strain criterion. This criterion is based on Whitney and Nuismer's [32] analysis, in which the dominant stresses are averaged over a region a_o which is determined experimentally. The averaging dimension used in this investigation is based on experimental data obtained for circular holes.

Composites have been shown not to be perfectly notch sensitive [32]. Whitney and Nuismer took this into account by using a region over which damage could develop prior to fracture. Failure was assumed to occur if the average stress or strain exceed that of an unflawed laminate in this region. Cairns [1] applied this averaging concept on the basis of

strain.

The application of the average strain criterion is particularly convenient since it allows the use of the strain ratio directly. The strain ratio is defined as:

$$S.R. = \frac{\bar{\varepsilon}_x^o}{\frac{1}{a_o}\int_0^{a_o} \bar{\varepsilon}_x\,(x,y)\,dr} \qquad (3.22)$$

where $\bar{\varepsilon}_x^o$ is the far field laminate strain along the x-direction (parallel to applied load);

$\bar{\varepsilon}_x\,(x,y)$ is the x strain distribution along a radius; and

a_o is the averaging distance (material parameter)

The undamaged experimental strength is simply multiplied by this ratio to find the degraded strength. This may only be applied with the assumption that ultimate failure is governed by fracture of the 0° plies and that the applied load is unidirectional and parallel to the 0° fibers.

The averaging distance, a_o, is calculated from experimental data for circular holes in fabric graphite/epoxy in a $(0,45)_s$ layup. The value of the averaging distance for this material is 4.7 mm. It is based on experimental data obtained in this research and by Kageyama [33].

3.5 Stress Correction Factor for a Pressurized Cylinder

The goal of the use of a correction factor is to relate the impact damage residual strength data from the plate geometries to the impact damage tolerance of composite cylinders exposed to similar impact conditions.

The pressurized cylinder with impact damage presents the following problem. In reference to Figure 3.7, the cylinder damage area is equivalently a membrane of damaged material spanning a region in the undamaged cylinder surface. If this membrane has a very low bending stiffness compared to the undamaged material, the impact damage may be modelled as a hole covered by a diaphragm that allows the flaw edge to deflect and rotate but transmits the pressure force to the shell in the form of a uniform transverse shear stress at the flaw edge. This interaction creates the presence of higher stress levels because of the internal pressure loading than those found in a similarly loaded flat plate.

The cylinder material is assumed to be quasi-isotropic. Consequently, the prediction for the damage area from the local model is circular. If the laminate A_{ij} and D_{ij} stiffnesses of the flawed area are small compared to the unflawed properties, it may be possible to model the damage area as a circular hole. Lagace and Saeger [29] cite a stress correction factor [34] to account for the interaction between stretching and bending for the circular hole. The correction parameter for this case is given by:

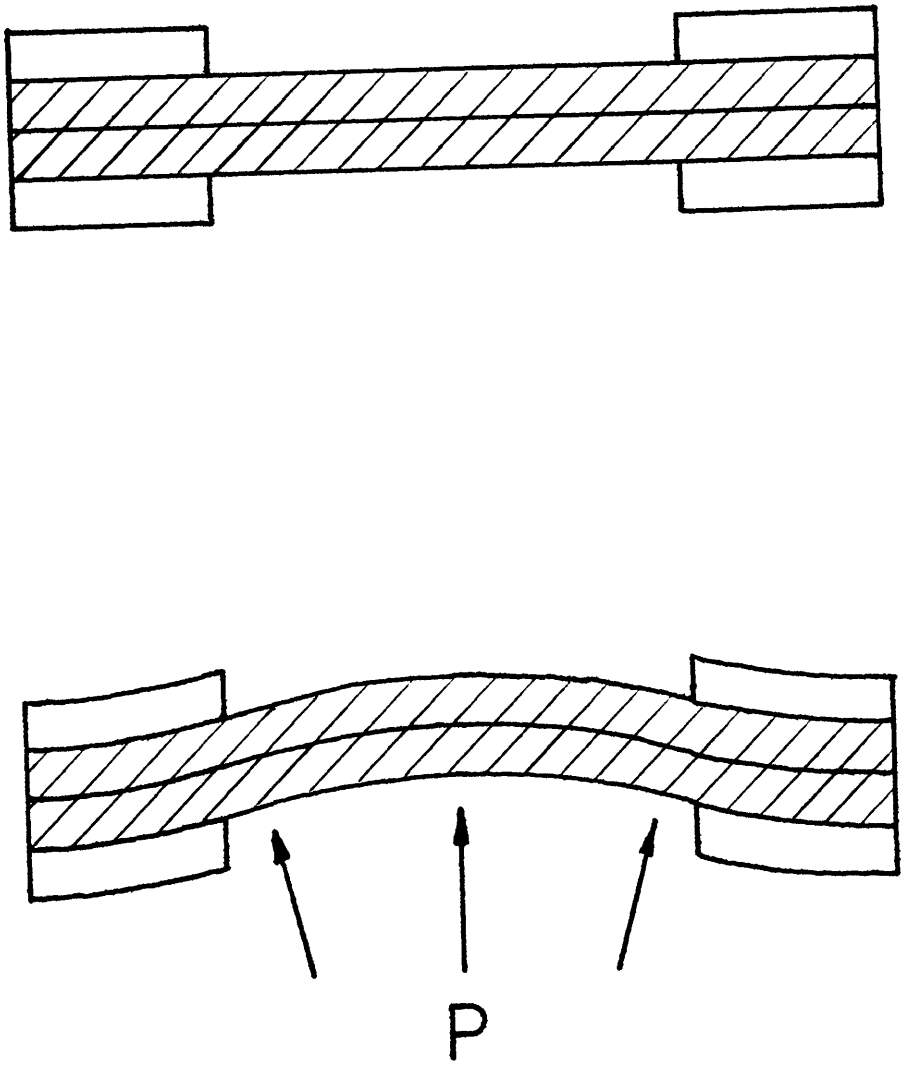

Figure 3.7 Illustration of Localized Bending at Impact Damage Location for Pressurized Cylinder

$$K = 0.532 + 0.696\lambda - 0.0586\lambda^2$$

$$\lambda = \frac{Eh^2}{RD} r^4 \qquad (3.23)$$

where: E - longitudinal modulus
h - shell wall thickness
R - shell radius
D - bending siffness
r - half slit length

The correction factor is derived for the case of a circular hole in a pressurized cylinder. It is a correction for the stress at the hole edge only. The degraded property area predicted by the local damage model is circular but obviously not a hole. Hence a direct application may not be valid.

The residual strength of the cylinders is calculated on the basis of failure of the cylinder in the hoop direction. The inclusion model is utilized with a 2 to 1 loading ratio of N_{hoop} to N_{long}. This loading condition simulates the internal pressure load of the cylinder. The average strain criterion is invoked to find the hoop strain along a line through the inclusion which is parallel to the longitudinal axis of the tube.

3.6 Implementation

All analysis is implemented in a FORTRAN computer code and run on a Digital Equipment Corporation Microvax II Minicomputer. A complete listing of the source code, input data, and output data is included in APPENDIX A. Run times are listed in Table 3.3. These times are dependent on the amount of information required.

TABLE 3.3

SOLUTION RUN TIMES FOR IMPACT ANALYSIS PROGRAMS[a]

Solution Procedure	Modes	CPU Time
Hertzian Spring Constant	100	1 minute
Global Plate Response	17(x) by 17(y)	8 hours
Global Cylinder Response	100(x) by 100(y)	10 minutes
Local Stress Analysis	200	5 minutes
Inclusion Model	EXACT	1 minute

a - Run times stated for DEC Microvax II Minicomputer

a - Solution times are for convergent cases

CHAPTER FOUR

EXPERIMENT

This chapter is a presentation of the experimental methodology for the study of impact response of fabric graphite/epoxy structures. A summary of the test program for plate coupon and cylindrical pressure vessel specimens is given. The manufacturing process for both specimen geometries is described. Test preparations of the specimens, particularly the cylindrical pressure vessels, are explained in detail. This includes the testing fixtures developed for this research. Damage examination techniques and testing procedures are also described in this chapter. The final section is a summary of the methods used for data reduction.

4.1 Experimental Test Program

The experimental test program may be divided into two phases. The first phase is the investigation of the characteristics of impact damage in flat plate and cylindrical graphite/epoxy fabric laminates. Phase two is the determination of the residual strength of impacted flat plate and cylindrical shell structures. Included in this research is a study of the effect of implanted delaminations on the strength of fabric coupon structures.

The material used for this investigation is Hercules

A370/5H-3501-6 graphite/epoxy. This material is a five-harness satin weave fabric prepreg system as illustrated in Figure 4.1. The elastic constants and failure stresses for this system are listed in Table 4.1.

The layup used for all specimens in this experimental work is (0,45)s. Parenthesis and commas indicate the use of fabric plies. The ply angles are measured with respect to the warp direction of the fabric. This layup enables comparison with previous pressure cylinder investigations conducted at TELAC [33,35]. The total laminate is quasi-isotropic and specially orthotropic, providing a specimen well-suited to the analysis developed for the impact of an orthotropic cylinder.

4.1.1 Impact Damage Characterization

The impact damage characterization of flat plate structures was conducted with 200 mm by 72 mm rectangular specimens. This size corresponds to the minimum size of the specimen restraints in the impact fixture. It also maximizes the number of test articles obtained from a standard 350 mm by 300 mm cure plate.

The specimen and its boundary conditions are shown in Figure 4.2. The specimens were impacted over a range of velocities. Cairns [14] concluded that the effect of specimen boundary conditions on the impact was negligible. Consequently, the only boundary condition used was clamped(X)-free(Y).

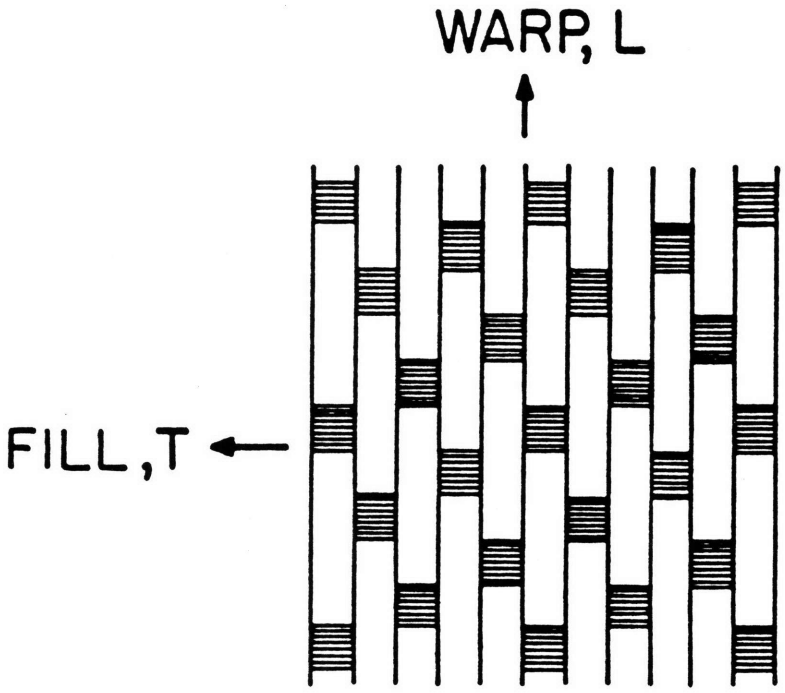

Figure 4.1 Illustration of Five Harness Satin Weave

TABLE 4.1

HERCULES A370-5H/3501-6 PLY PROPERTIES

$E_{11} = 72.5$ GPa	$E_{22} = 72.6$ GPa
$E_{33} = 10.0$ GPa	
$G_{12} = 4.43$ GPa	$G_{13} = 6.0$ GPa
$G_{23} = 6.0$ GPa	
$\nu_{12} = 0.059$	$\nu_{13} = 0.30$
$\nu_{23} = 0.30$	
$t_{ply} = 0.35$ mm	$\rho = 1540.0$ kg/m^2
$X^t = 817$ MPa	$X^C = 779$ MPa
$Y^t = 728$ MPa	$Y^C = 712$ MPa
$S = 105$ MPa	

All data from reference [40]

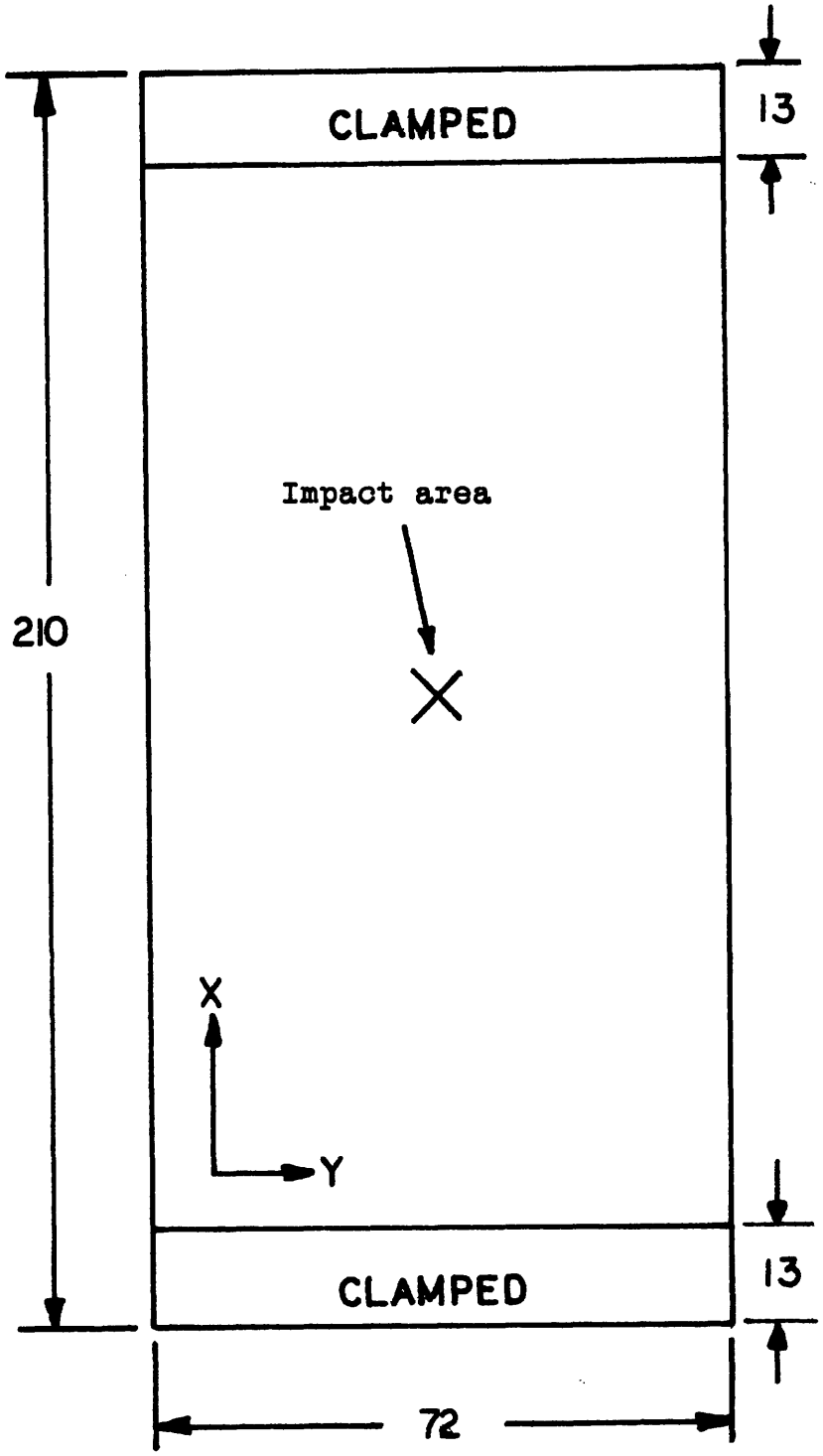

Figure 4.2 Characteristics of Impact Damage Characterization Plate Specimen

Damage investigation for the cylinder geometry was conducted using a specimen impacted at multiple sites. The manufactured tube was marked off into three longitudinal sections of 203 mm and six radial sections of 160 mm. After each section was impacted, the cylinder was sectioned using a hand-held jigsaw and a carbide blade to facilitate further examination.

The test matrix for the impact damage characterization phase of the experimental program is given in Table 4.2. The objectives of the plate and cylinder damage characterization study were to utilize several forms of destructive and nondestructive examination to provide data on the types of impact damage found in fabric laminates and to observe the structural effect of the cylinder curvature on impact damage. This matrix provides a base for the damage characterization data. In addition, it enables correlation between x-ray examination and sectioning or epoxy burn-off. The examination of the structural effect of curvature is accomplished by using the same procedures on the cylinder specimens.

4.1.2 Residual Strength Studies

The residual strength coupons were 70 mm by 350 mm. 3M glass/epoxy loading tabs were bonded to each end of the coupon with American Cyanamid FM-123-2 film adhesive as illustrated in Figure 4.3. The width of 70 mm was chosen to minimize any finite width effects without exceeding the geometric

TABLE 4.2

IMPACT[a] DAMAGE CHARACTERIZATION TEST PROGRAM

Specimen Geometry	Specimens Tested	Destructive Examination	Nondestructive Examination
Plate			
	14	sectioned	DiB x-ray
	17	burn-off	DiB x-ray
	8		DiB x-ray
Cylinder			
	6	sectioned	DiB x-ray
	12	burn-off	DiB x-ray
	18		visual

[a]All specimens impacted with 12.7mm diameter steel ball

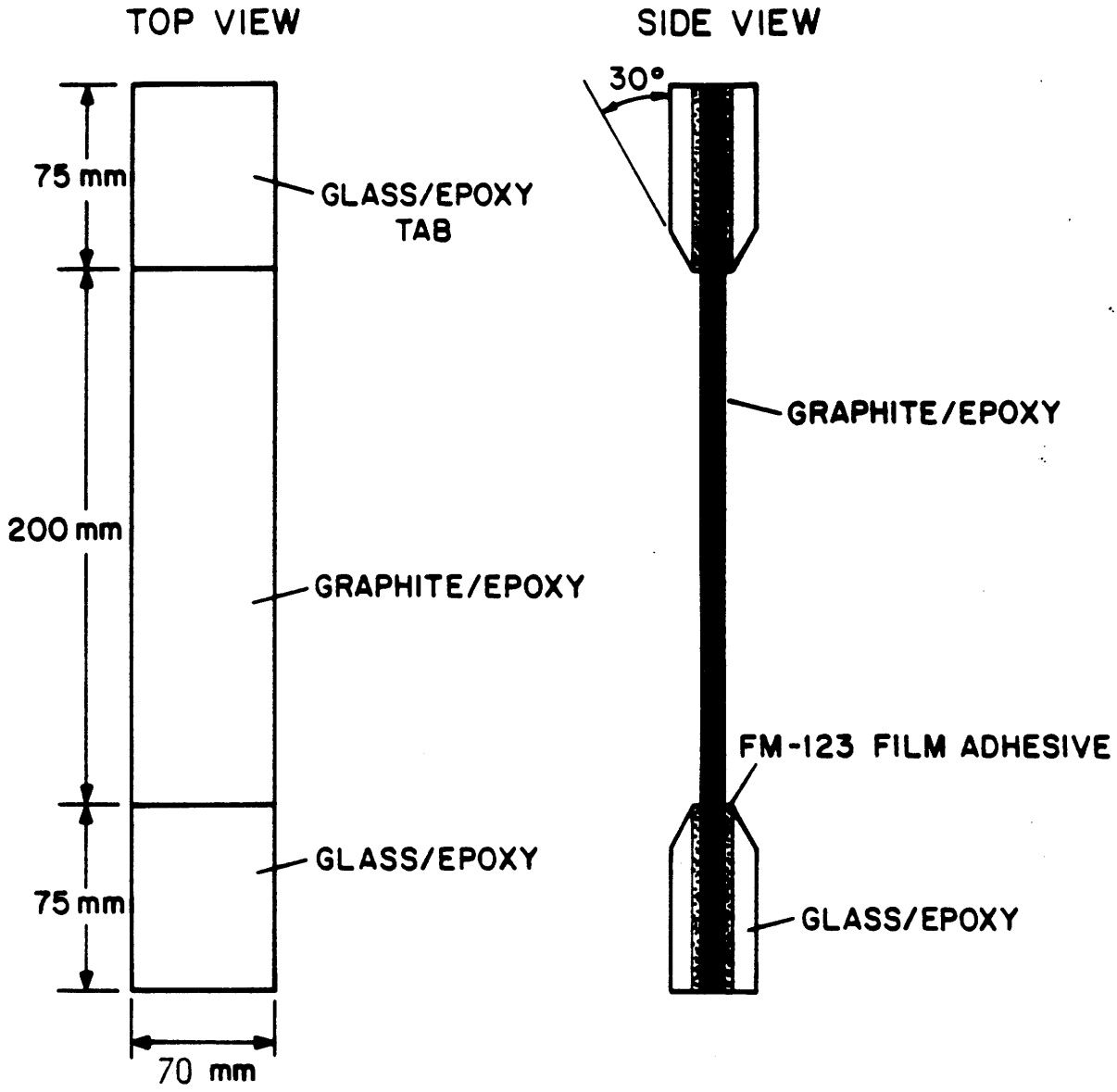

Figure 4.3 Characteristics of Standard 70 mm Wide Coupon Specimen

limitations of the testing equipment. The size was also wide enough to prevent the impact damage from propagating to the edges of the specimen during impact. The specimen gage length was approximately 200 mm.

Each plate residual strength specimen was inspected using nondestructive x-ray examination. The tests were conducted using a MTS 810 hydraulic testing machine. The specimens were loaded in tension using stroke control at a constant ramp rate.

For the pressure vessel residual strength study, cylindrical tubes with a diameter of 305 mm and a length of 610 mm, as shown in Figure 4.4. were used. The cylinders were impacted over a range of velocities. The impact boundary condition used for these tests was simply-supported. Examination of the cylinder residual specimens was visual only. The cylinders were tested using an internal pressure load until catastrophic failure occured.

The test matrix for the residual strength investigation of the plate and cylinder geometries is given in Table 4.3.

4.1.3 Delamination Implant Study

The objective of the study is to isolate the effects of delamination on the tensile residual strength of fabric plate specimens. This study is similar to work done by previous investigators on tape laminates with delaminations [29]. The test matrix for this study is shown in Table 4.4.

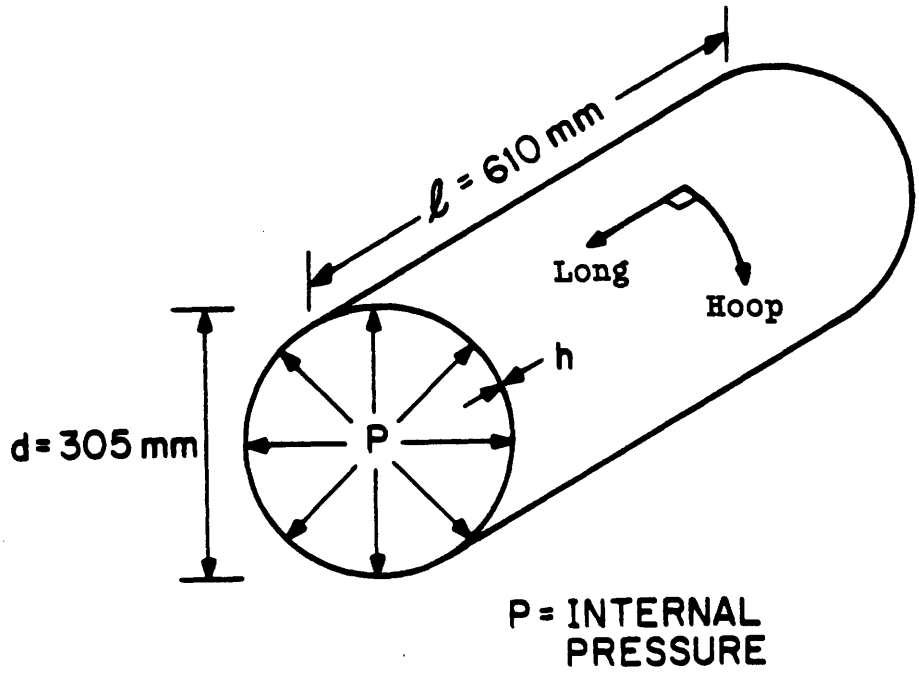

Figure 4.4 Characteristics of Cylinder Specimen

TABLE 4.3

RESIDUAL STRENGTH TEST PROGRAM

Specimen Geometry	Specimens Tested	Flaw Type	Nondestructive Examination
Plate			
	5	unflawed	
	5	12.7 mm hole	
	27[a]	impacted	DiB x-ray
Cylinder			
	4	unflawed	
	8	impacted	visual

a - two specimens received photoelastic coatings

TABLE 4.4

DELAMINATION STUDY TEST MATRIX

Specimens Tested	Delamination[a] Location and Size (mm) (ply interface)		
	0/45	45/45	45/0
1	-	-	-
3	10	10	10
3	30	30	30
3	50	50	50
1	10	-	-
2	20	-	-
1	30	-	-
1	40	-	-
1	50	-	-
1	-	10	-
1	-	20	-
1	-	30	-
1	-	40	-
1	-	50	-
1	30	20	-
1	40	30	20
1	50	40	30

[a] Delamination implanted via 0.03 mm thick teflon

The delamination implant coupons were 70 mm by 350 mm. The configuration was the same as for the residual strength specimens. The width of 70 mm allowed the use of delamination implants as large as 50 mm in diameter. The delamination sizes were chosen to approximate the NDE x-ray observations of delamination damage found in the impacted plate study. The unsymmetric implants were models of the delamination pattern normally found in the sections of impacted fabric laminates.

All tests of the implanted specimens were conducted in tension at a constant ramp rate to failure. All implants were circular and made of Dupont Teflon film with a thickness of 0.03 mm. This thickness produced no observable change in the laminate thickness. The implants were located at the center of the specimen test section. The specimen gage length was approximately 200 mm.

4.2 Specimen Manufacture and Preparation

4.2.1 Plate/Coupon Specimens

All plies were cut using a 300 mm by 350 mm rectangular template. The resulting laminate, therefore, had no individual plies with seams. The template was aligned to the desired angle on the raw fabric roll and a straight edge razor knife was used to cut the ply. The individual plies were then stacked in a $(0,45)_s$ layup sequence.

For those specimens with circular delaminations, the

implants were placed between the plies of the uncured laminate using a plexiglass template. The procedure is identical to that used by Robichaux [36].

Peel ply was placed on the top and bottom plies to protect the laminate surfaces during the manufacturing cycle. The prepared laminates were placed on an aluminum cure plate covered with non-porous teflon. The laminates were covered by one layer of porous teflon, five layers of paper bleeder, and an aluminum plate wrapped in non-porous teflon. Aluminum and cork dams were used to hold the assembly in place during the cure. The entire cure plate was then covered with a plastic vacuum bagging material and sealed with vacuum tape. A schematic of the setup is shown in Figure 4.5.

The cure cycle for the coupons followed the manufacturers recommended procedure. The cure cycle was conducted under vacuum. The first phase consists of one hour at 116°C and 0.55-0.59 MPa autoclave gauge pressure. The second phase was conducted at the same pressure with the temperature at 177°C for two hours. Both heating and cooling rates were maintained at 3°C per minute. An eight hour postcure at 177°C, 0 MPa gauge was used. A time history of the cycle is shown in Figure 4.6.

Four coupons of width 70 mm were cut from each panel using a water cooled diamond cutting wheel. The width and thickness of the specimens was measured with a caliper and micrometer, respectively. Three width measurements and nine thickness measurements were taken. The average thickness of

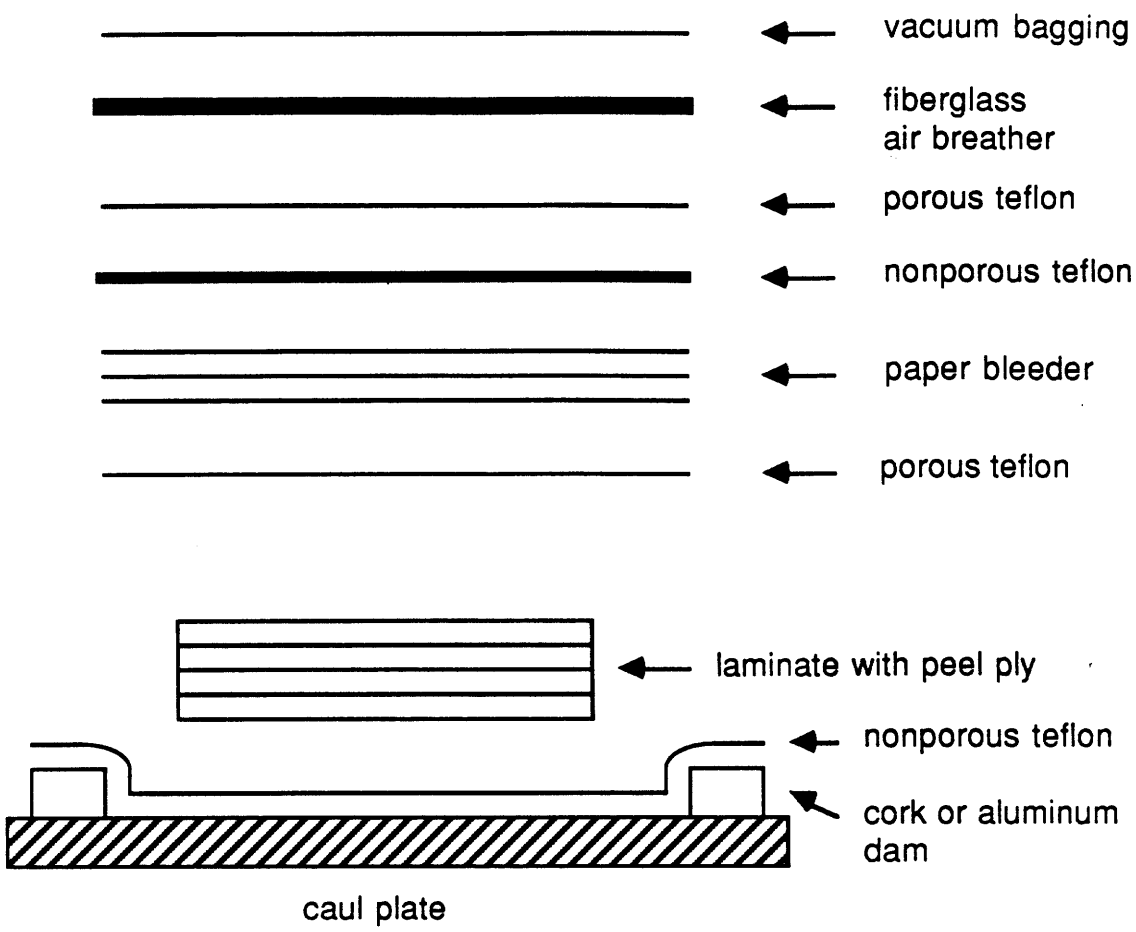

Figure 4.5 Cross-Section of Cure Assembly

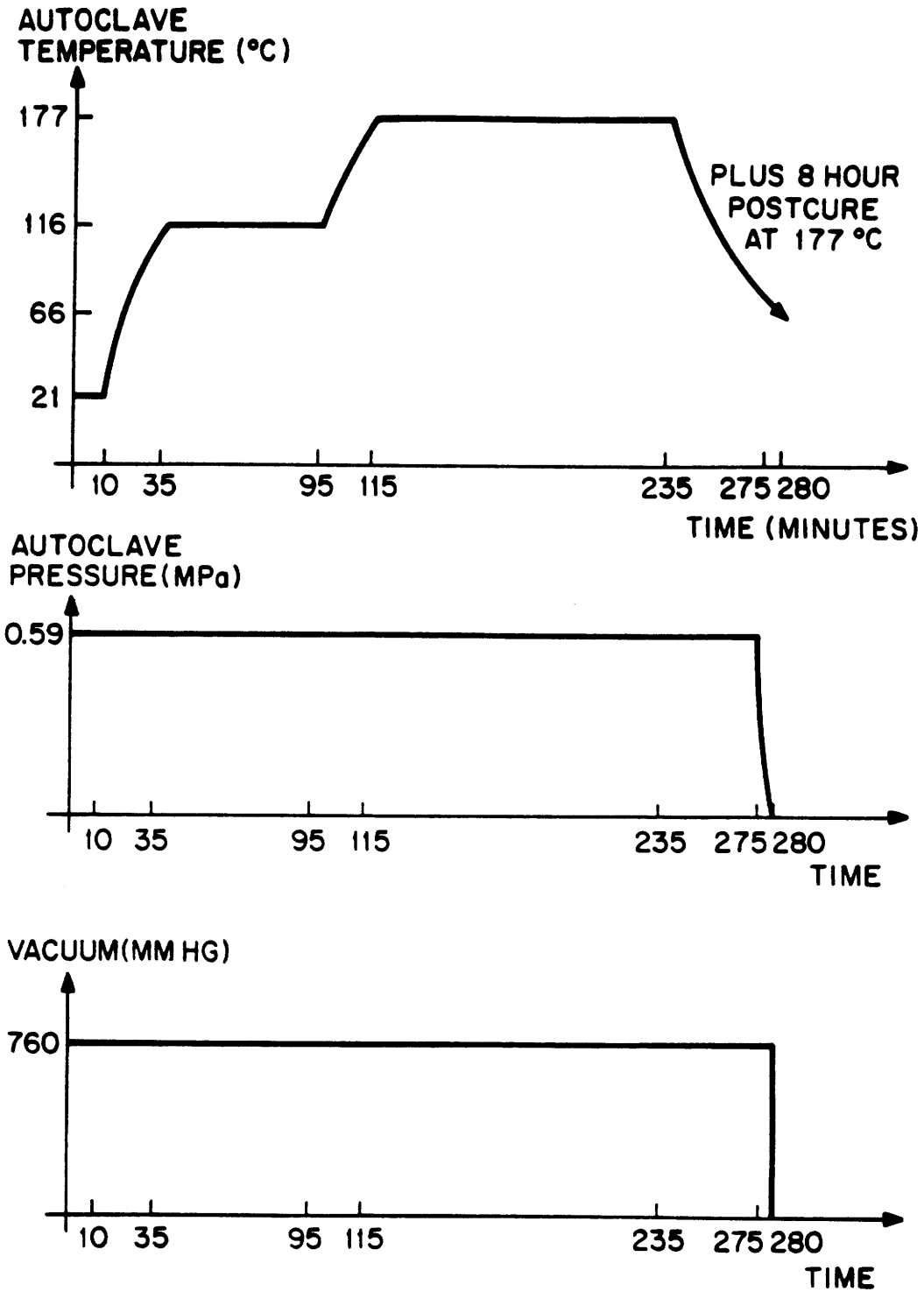

Figure 4.6 Hercules A370-5H/3501-6 Graphite/Epoxy Curing Cycle

the coupons is found to be 1.33 mm with a coefficient of variation of 1.09%. The measured thickness was used in the stress calculations. Nominal thickness of the fabric laminate is 1.4 mm. A measurement summary may be found in APPENDIX B.

4.2.2 Cylinder Specimens

The cylinder specimens were also of the (0,45)s configuration. The plies were cut from the raw fabric roll using a long straightedge. The dimensions of the plies are shown in Figure 4.7.

The cylinders were manufactured on an aluminum mandrel wrapped with non-porous teflon. The fabric graphite/epoxy plies were wrapped over the teflon. After the first zero degree ply was wrapped around the mandrel, the first 45 degree ply was applied so that its seam intersected the 0 degree seam at its midpoint. The second 45 degree ply was applied so that the tip of its seam was aligned with the first zero degree ply. The last ply was wrapped with the midpoint of the zero degree seam intersecting the second 45 degree ply seam. This scheme was chosen to provide the greatest impact test section area with a minimum amount of seam intersection and is depicted in Figure 4.8.

All other aspects of the manufacture of the cylinders were similar to the processes used by previous researchers at TELAC (Kageyama [33], Graves [35],..). After the layup of the plies was complete, a layer of peel ply was wrapped around the

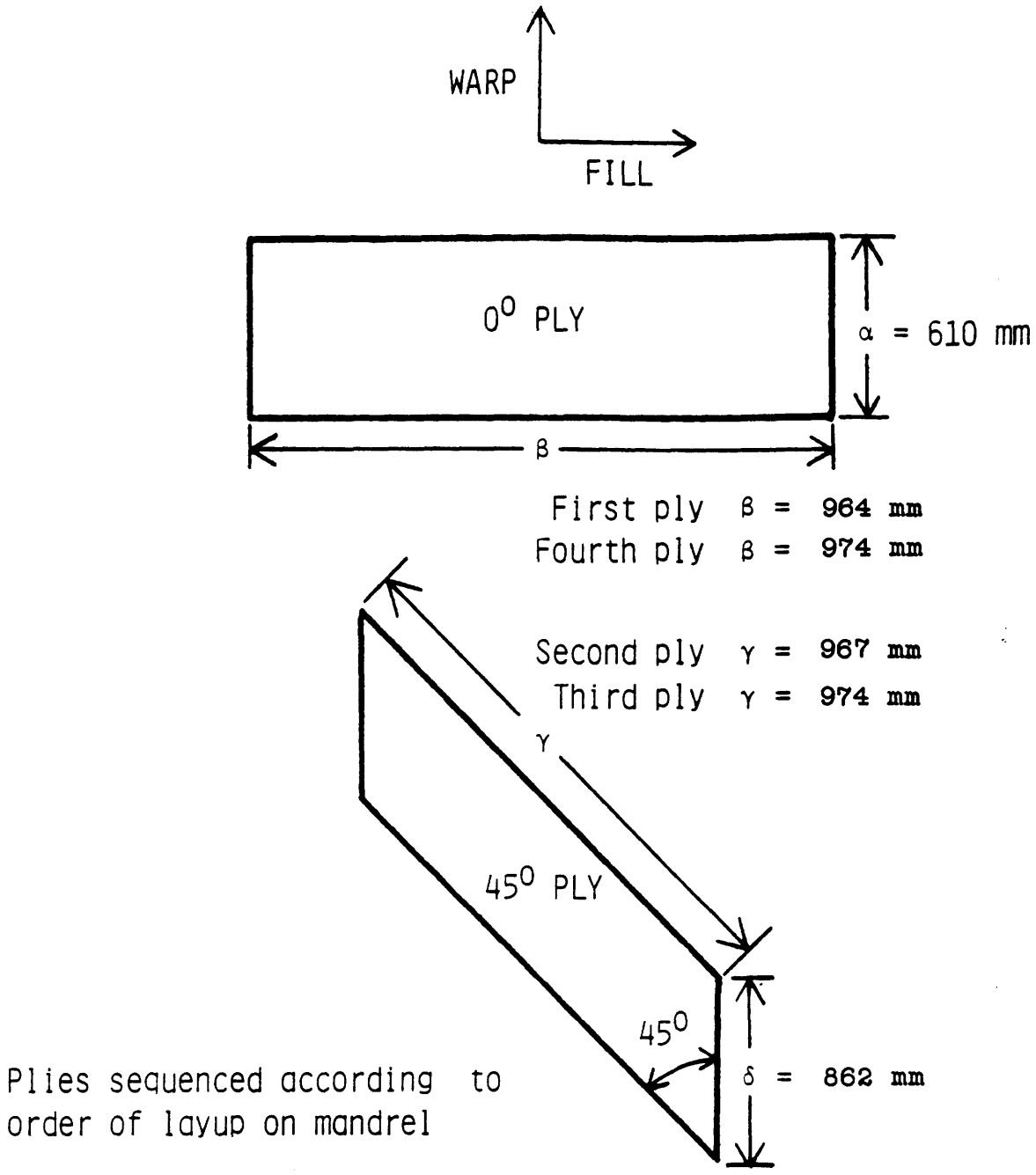

Plies sequenced according to order of layup on mandrel

Figure 4.7 Cylinder Ply Dimensions

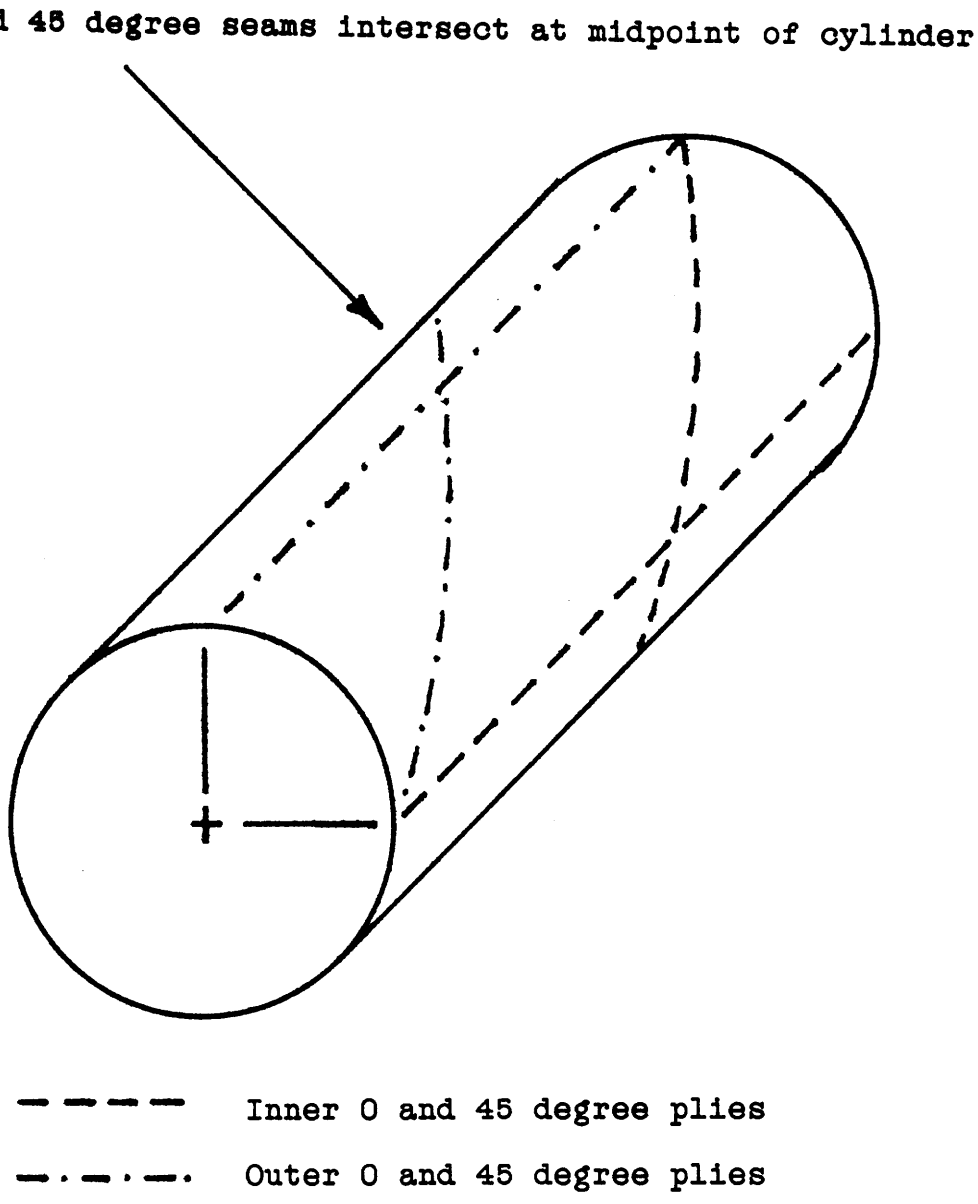

Figure 4.8 Illustration of Cylinder Seam Intersection

cylinder. The cylinder was then tightly wrapped with one layer of porous teflon and five layers of paper bleeder. The paper bleeder was a continuous sheet wrapped under tension to prevent wrinkling of the cylinder. The entire assembly was covered with a plastic vacuum bag and sealed with vacuum tape.

Special emphasis was placed on making certain that all layers of the assembly were tightly wrapped, including the fabric. Note, however, that the fabric sheared easily, so any tension applied had to be uniform and in the warp direction of the fabric. Any slack in the assembly produced a wrinkle in the cured product once vacuum was drawn.

The cure cycle was nearly identical to the procedure used for the coupons. The only modification to the cycle was an increase of 0.069 MPa in the internal pressure of the autoclave. This accounted for the weight of the aluminum top plates used in the plate cure assembly. No thickness measurements of the cylinder were made.

An unresolved problem prevented the manufacture of a totally wrinkle free tube. The inner zero degree seam always precipitated a longitudinal ridge across the cylinder. Previous investigations were not hampered by this flaw because of the relatively low pressures used. In order to prevent seam failure at this wrinkle for unflawed and barely damaged specimens, the seam had to be reinforced. This was accomplished with the use of two 102 mm wide strips of wet layup fiberglass on the inner and outer surfaces of the cured

cylinder. This is shown in Figure 4.9. The fiberglass plies were offset by 26 mm. The fiberglass cloth was placed on the cylinder with the zero degree cloth direction aligned with the longitudinal tube direction. The material used was Boatex 7781 Fiberglass VOLAN finish plain weave with a matrix system of Shell Epon V40 resin/815 hardener. Both surfaces were sanded with 400 grit emery paper and cleaned with alcohol to aid in adhesion. The reinforcement was placed under vacuum to remove air bubbles and cured for one hour at 100°C. Figure 4.10 is a photograph of the completed seam reinforcement.

4.3 Description of Test Fixtures

4.3.1 Impact Test Equipment and Procedures

The impact test equipment used for this investigation was a modified pressurized air gun designed and used by NASA-Langley [21,22,23]. Pressurized nitrogen was fed into a plenum with the same volume as a smooth bore 50 caliber machine gun barrel. The gas was expanded through the barrel to accelerate a 12.7 mm diameter projectile. Variations in plenum pressure and orifice size allowed the control of the impactor velocity. A schematic of the impact device is shown in Figure 4.11.

The impact gun was mounted on a movable cart. The impact specimen was contained in a protective chamber to prevent injuries to personnel from rebounding projectiles. The

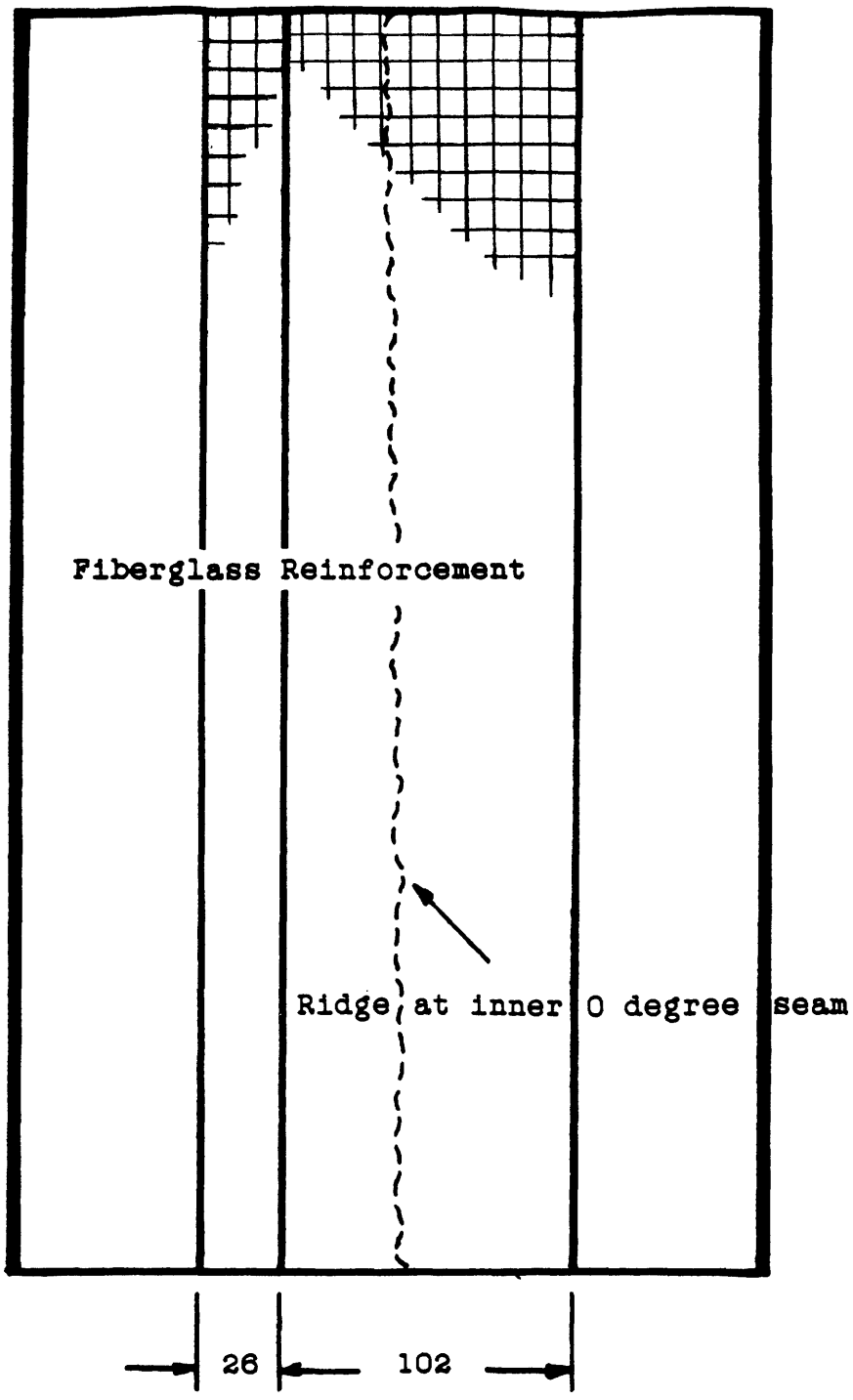

All dimensions in millimeters

Figure 4.9 Sketch of Cylinder Ridge Reinforcement

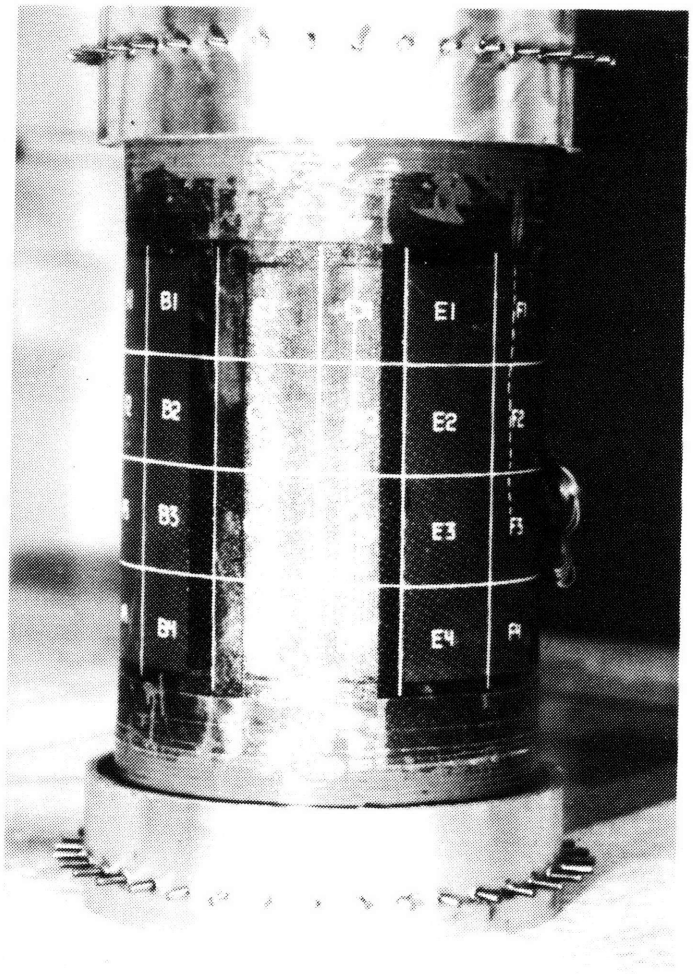

Figure 4.10 Photograph of Cylinder Ridge Reinforcement

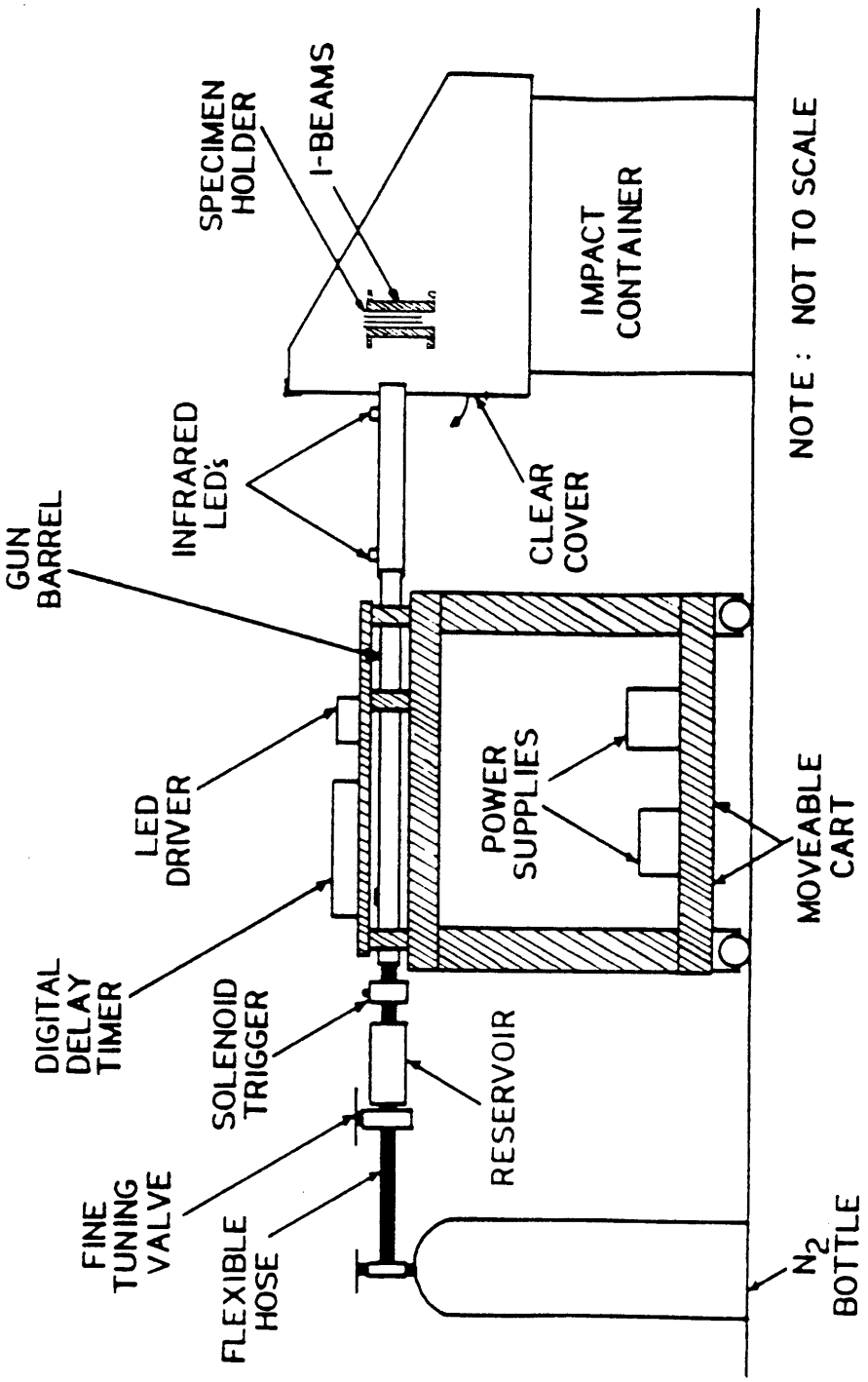

Figure 4.11 Schematic of Impact Test Facility Setup

specimen was held in the protective chamber by a large drill stand which allowed easy replacement of the test article.

The velocity of the projectile was measured using high intensity infrared diodes and a Schmidt-Trigger connected to a timer. Because of machining variations in the barrel, a large scatter in projectile velocity for a given orifice size and plenum pressure was encountered. The repeatability of the impactor velocity at a given plenum pressure was always an uncertainty and variations of ± 5 m/s were not uncommon. In addition, the degradation of the quality of the bore resulted in untracked impactor velocities at times. When the impactor was not tracked by the infrared LED's, the velocity of the ball was determined by the average of four tracked shots at the same plenum pressures. The tracking failure rate during the cylinder tests was approximately 90%.

The coupons were held in a special fixture made for the impacting of flat laminates under various boundary conditions. A sketch of this fixture is shown in Figure 4.12. Clamped-free boundary conditions were used for all specimens. The clamped boundary condition spacers and the laminates were coated with teflon tape to minimize membrane loading during the impact event. The complete assembly was mounted on a stiff drill stand fixture and swung into place.

The cylinder specimens were held in a fixture manufactured from steel channel as shown in Figure 4.13. The simply-supported boundary conditions, shown in Figure 4.14 , were simulated using two endcaps with a small groove. The

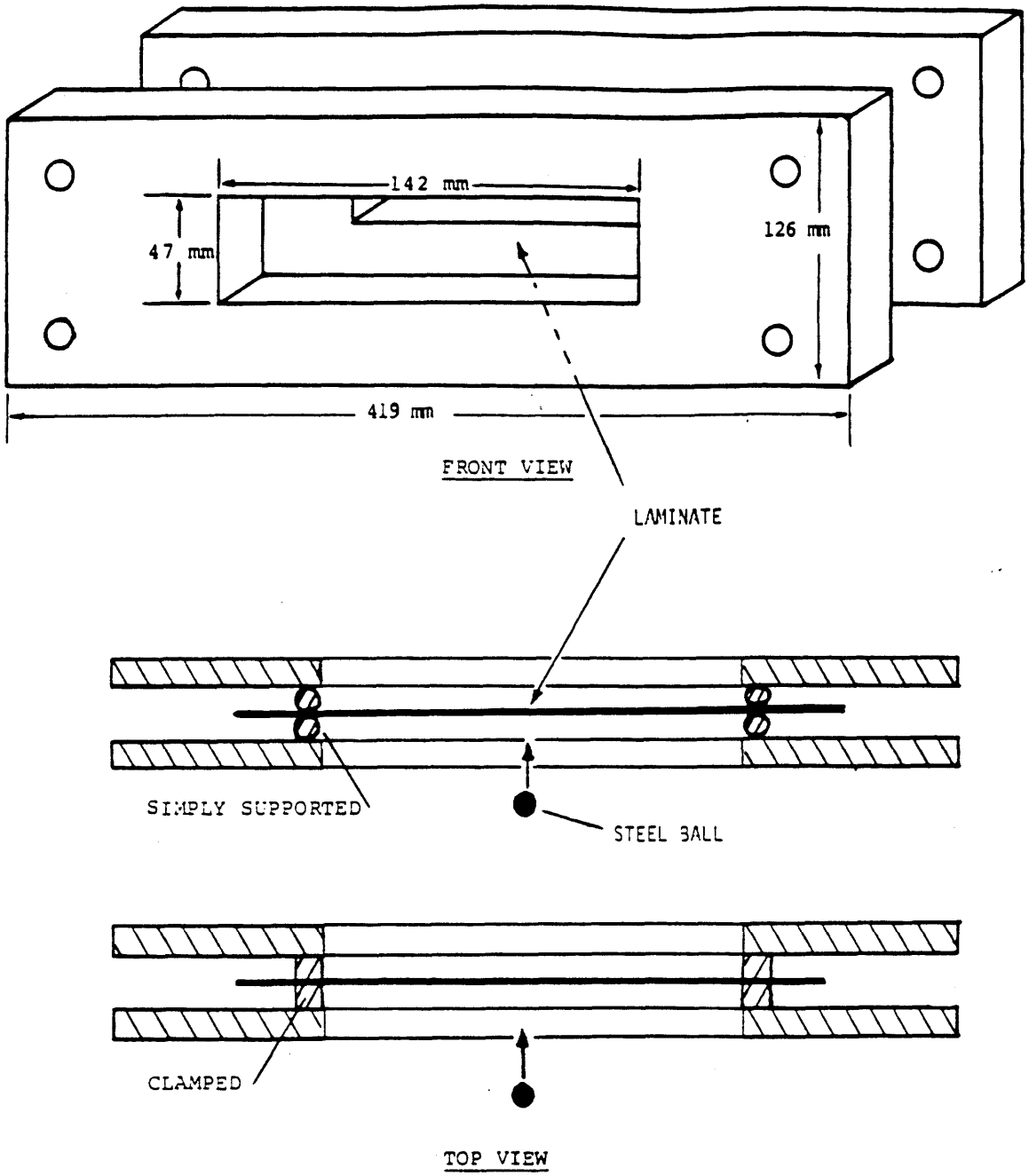

Figure 4.12 Schematic of Specimen Holder Showing Various Boundary Conditions

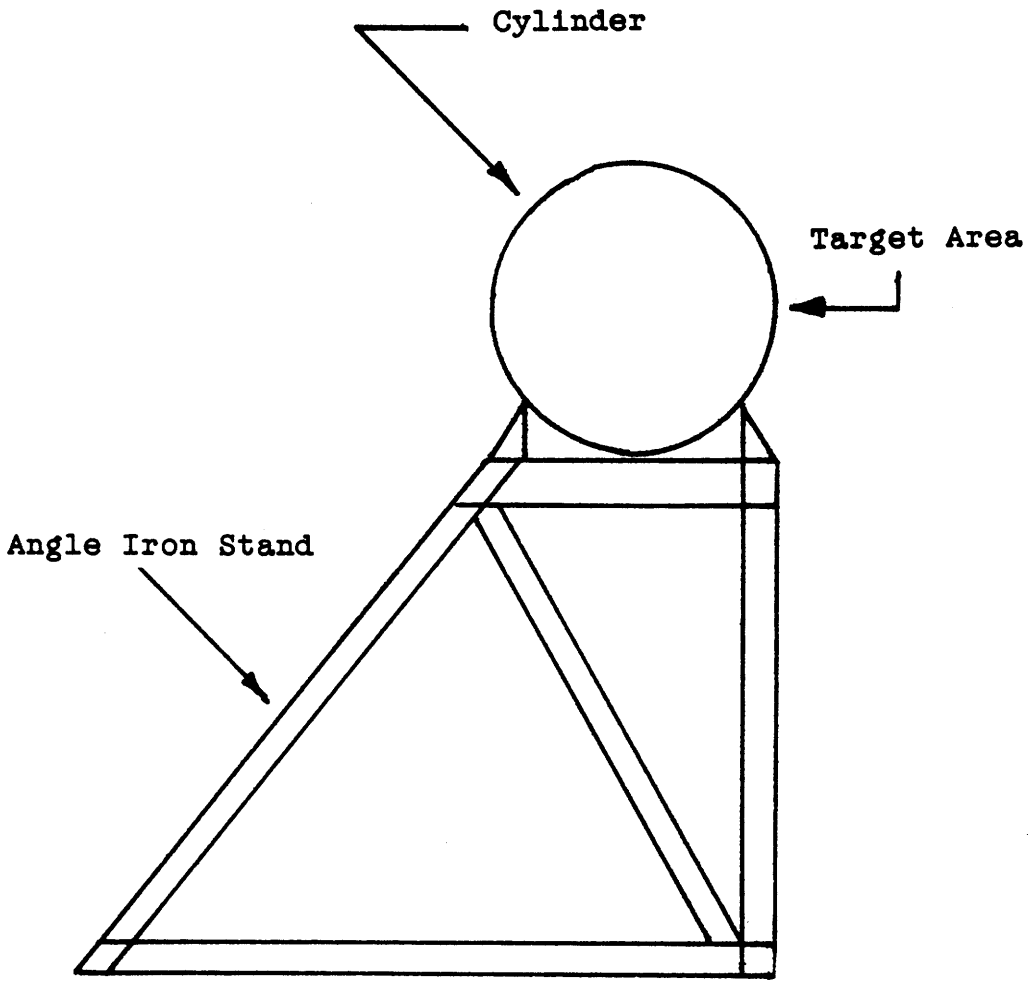

Figure 4.13 Sketch of Cylinder Impact Fixture

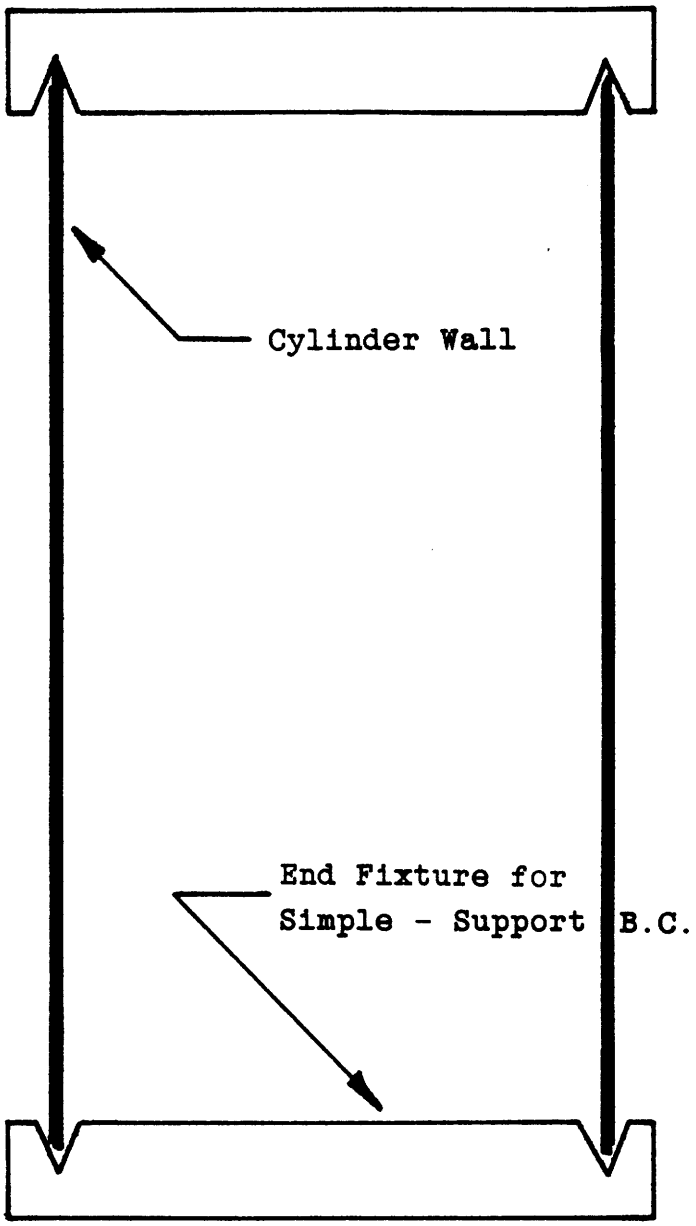

Figure 4.14 Sketch of Cylinder Impact Boundary Conditions

groove allowed for rotation of the cylinder ends without deformation from the cylindrical shape. A wood block coated with plasticine clay was mounted on the inside of the cylinder directly behind the impact target area to trap penetrating projectiles and prevent further damage. The tube and endcap assembly was tightly strapped to the steel channel support fixture. Since the size of the assembly precluded the use of the impact containment chamber, clay was wrapped around the barrel to catch a rebounding projectile.

Once the test article was placed into the proper fixture, the procedure for impact was as follows. First, the gun was rolled into place and aligned with the target area. A 12.7 mm stainless steel sphere was loaded into the breach of the gun. The plenum was then charged to the desired pressure to attain the required velocity for a given orifice size. The Schmidt-Triggers were adjusted for maximum sensitivity and a solenoid valve was activated to release the gas in the plenum and accelerate the projectile through the barrel.

4.3.2 Cylindrical Pressure Vessel Test System

A major problem was encountered in the testing of unflawed and barely damaged cylinders. No previous pressure vessel test had been successfully conducted at TELAC for small flaws without endcap failure. This limited all previous work to pressures less than 1.4 MPa. A new system had to be designed to test cylinders with impact damage often less than

12 mm in diameter. The design goals were set by the failures encountered both by previous investigators at TELAC and baseline research done for this study.

Four major considerations in the development of the pressure test system governed the final design:

1) relaxing the end clamping condition to prevent failure of the test article at the endcaps from a bending concentration;
2) retaining endcaps under the longitudinal load exerted on the endcaps by the internal pressure;
3) maintaining seal integrity under maximum pressure;
4) providing the ability to inspect and replace the sealing mechanism.

The pressure vessel test system is shown schematically in Figure 4.15 and in the photograph of Figure 4.16. It consists of the fabric graphite/epoxy test article reinforced with fiberglass and fixed in an aluminum endcap by 36 hardened pins. A highly flexible epoxy fills in the gaps between the test article and the endcaps. The inside of the assembly is lined with a rubber bladder attached to the two inspection port covers and is inserted after the endcaps are completely attached.

To relax the endcap clamping condition, nine layers of wet layup fiberglass cloth were wrapped around the ends of the cylinder. The feathering scheme is shown in Figure 4.17. Plain weave Boatex 7781 Fiberglass with a VOLAN finish was used for the reinforcement. The matrix system was Shell Epon

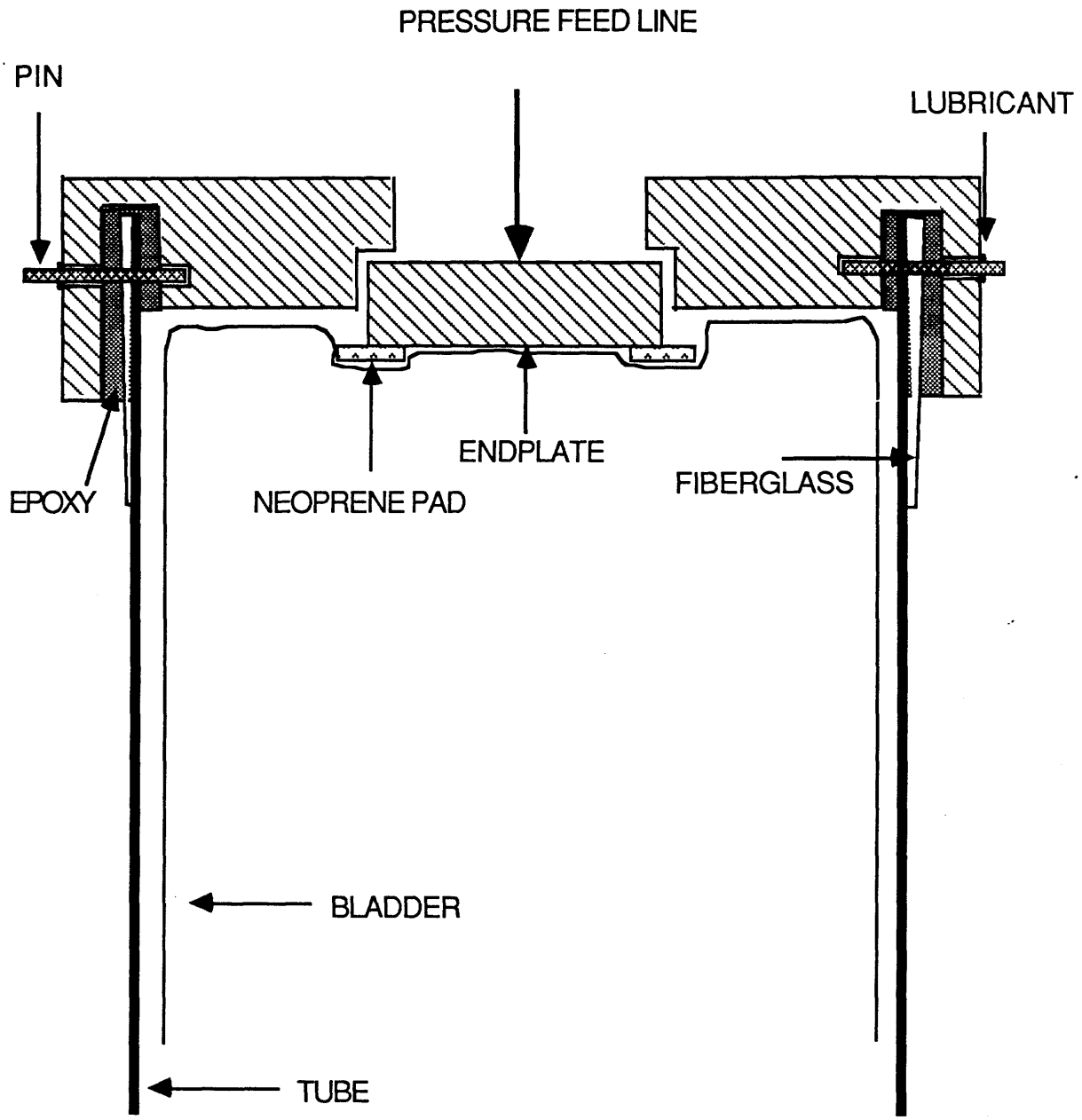

Figure 4.15 Schematic of Pressure Vessel Test System

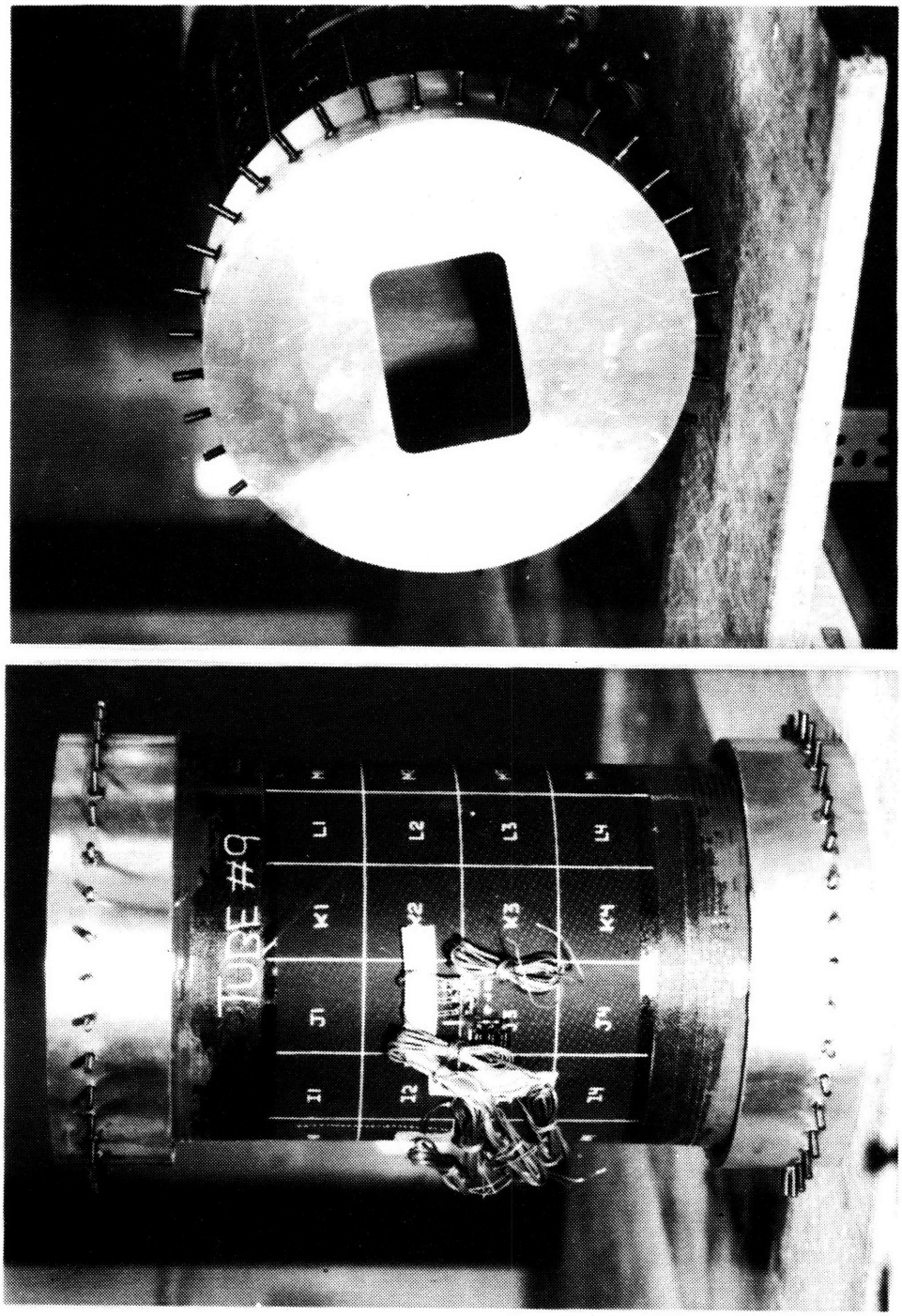

Figure 4.16 Photograph of Completed Cylinder Test Assembly - (a) Side View (b) End View

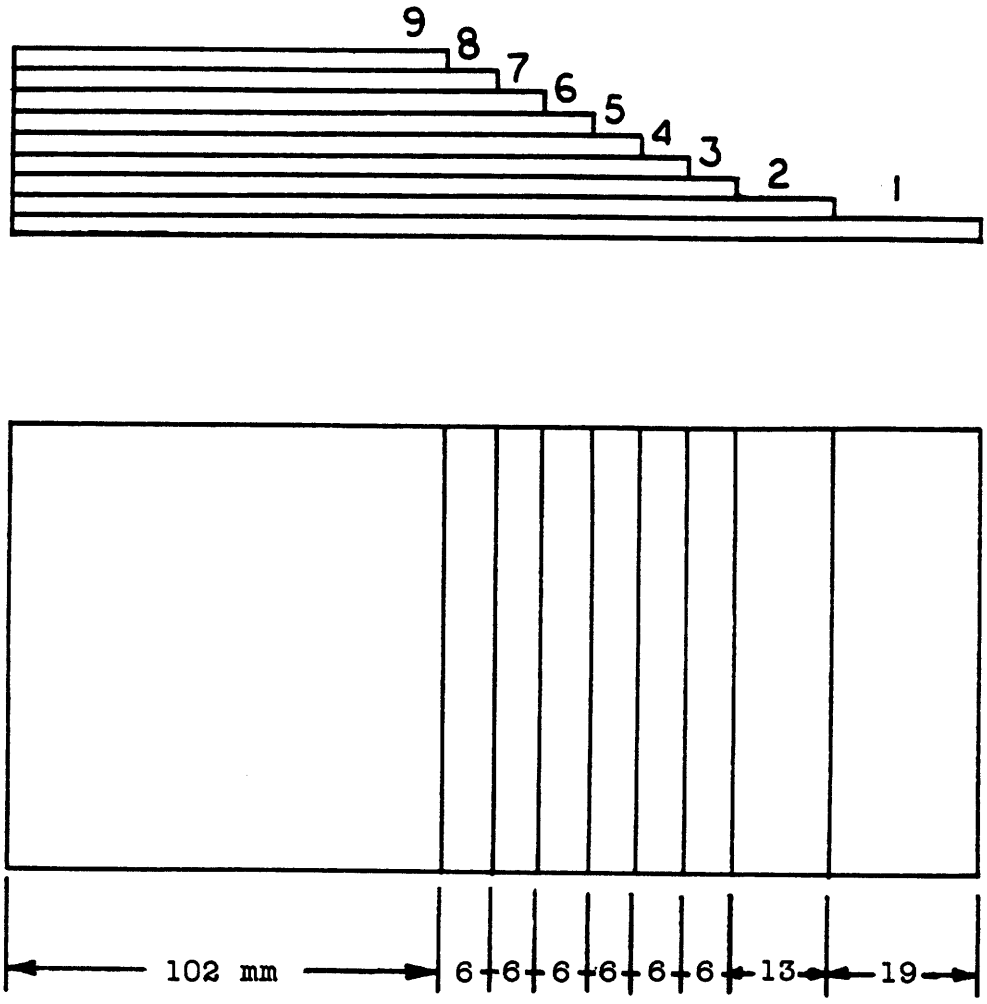

All dimensions in millimeters

Figure 4.17 Illustration of Feathering Scheme for Tube End Reinforcement

V40 resin with 815 hardener cured for two hours at 100°C. The layers of fiberglass also served to prevent shear-out of the graphite/epoxy tube from the pins. The flexible epoxy filler chosen was 3M Scotch-Weld 2216 B/A Gray Epoxy Adhesive cured for one hour at 80°C.

The design analysis predicted that the epoxy alone would not be sufficient to retain the endcaps under limit pressure. Hardened straight dowel pins were used to carry the load instead of epoxy. All dowel pins were coated with Fel-Pro Hi-Temp C5-A Anti-Seize Lubricant to allow easy removal for cleanup.

Seal integrity was maintained through the use of a rubber bladder manufactured from three pieces of 0.8 mm (1/32 inch) dental dam rubber sheet. The pattern used for the bladder material is shown in Figure 4.18. Assembly is straightforward. The ends of the bladder were attached to the two inspection port covers. A neoprene boot surrounded the inside edge of the port covers to prevent pinching of the bladder. Globe Rubber Works Utility Industrial Adhesive No. 503 was used for all bonding.

The rectangular inspection ports of the endcaps facilitated the inspection of the inner epoxy seal and the replacement of faulty bladder liners. The port covers served as the connections for the nitrogen feed and pressure transducer lines.

Manufacture of the endcaps was contracted to Salerno Tool Inc. of Warren, MI [37]. The endcaps and inspection ports

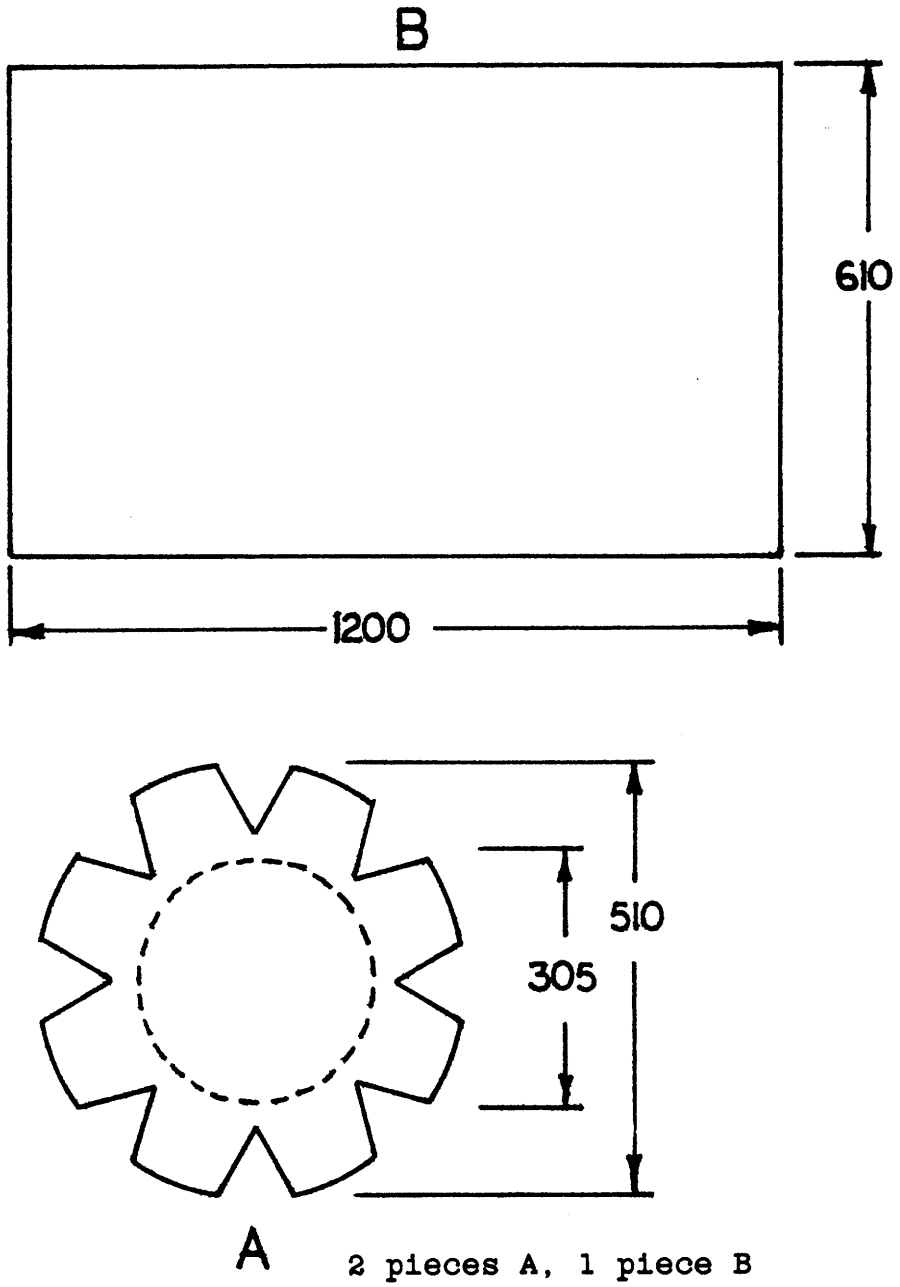

All dimensions in millimeters

Figure 4.18 Bladder Material Pattern

were made of 7075-T6 aluminum, chosen for its dimensional stability during machining processes. The equipment used was a computer controlled MHP CNC B18 Machining Center.

The optimization of the pressure vessel test system was accomplished through the use of a parametric finite element study. Four node axisymmetric finite elements were used in the system model. The dimensions of the test article were the only fixed constraints. A picture of the finite element mesh for the undeformed assembly is shown in Figure 4.19.

The dimensions of the fiberglass reinforcement, epoxy filler, and aluminum endcap were varied to find the optimum configuration for the assembly which resulted in a minimum bending concentration at the ends of the cylinder and a constant test section stress state. Figure 4.20 is a plot of the deformed shape of the assembly at 5.0 MPa. The top and section views of the endcap, with dimensions, are shown in Figures 4.21 and 4.22 respectively.

Construction of the pressure vessel test assembly consists of the following steps: (a) inserting the reinforced cylinder into the endcap; (b) fixing the cylinder in place using wood wedges, leaving approximately 10 mm of space between the cylinder and endcap wall; (c) drilling a hole through the cylinder with a letter E high speed twist drill, using the endcap pin hole for alignment; (d) coating the dowel with lubricant and tapping it into the hole, leaving 20 mm of the dowel outside the endcap; (e) repeating the pin insertion by quarters, then eighths, and so on; (f) vacuuming all debris

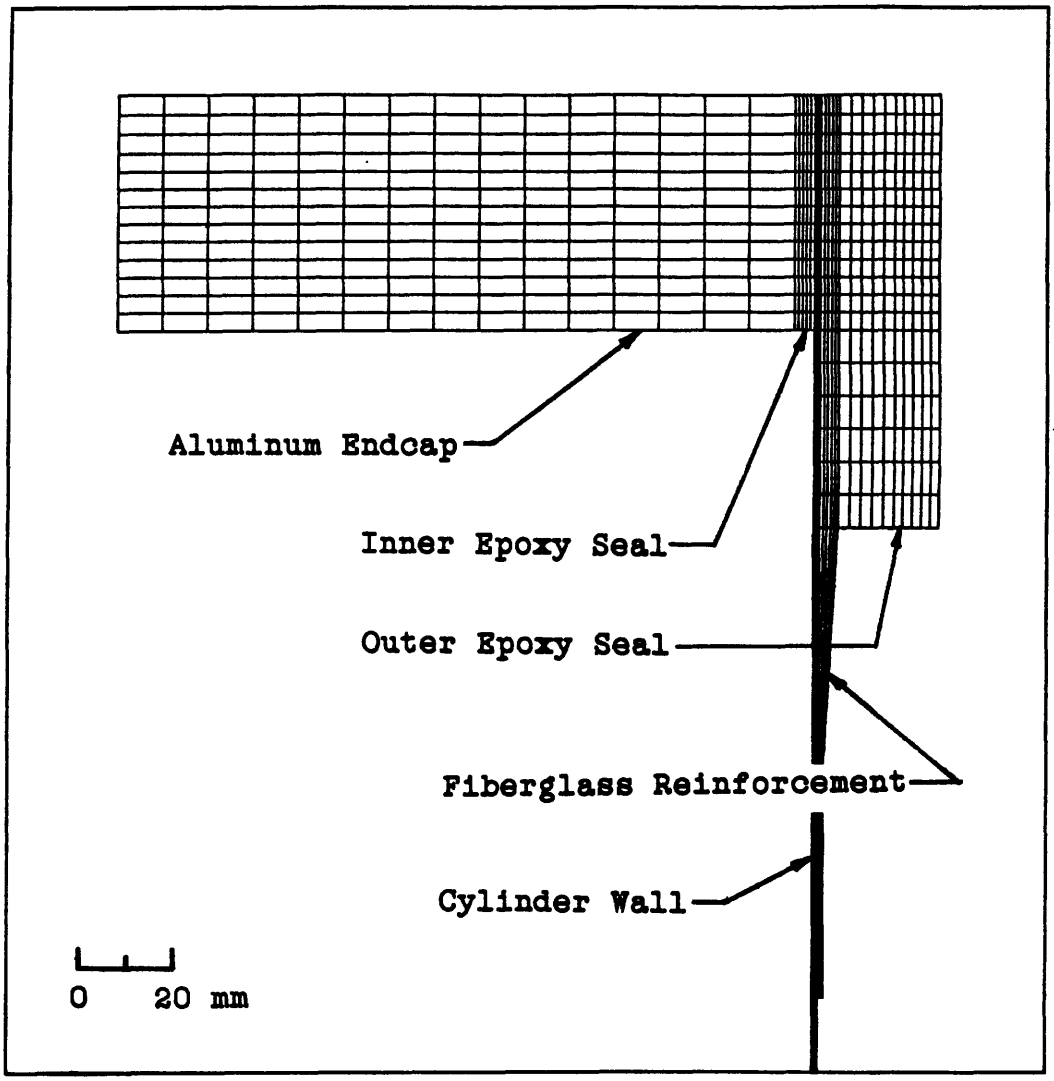

Figure 4.19 Undeformed Finite Element Mesh of Endcap System

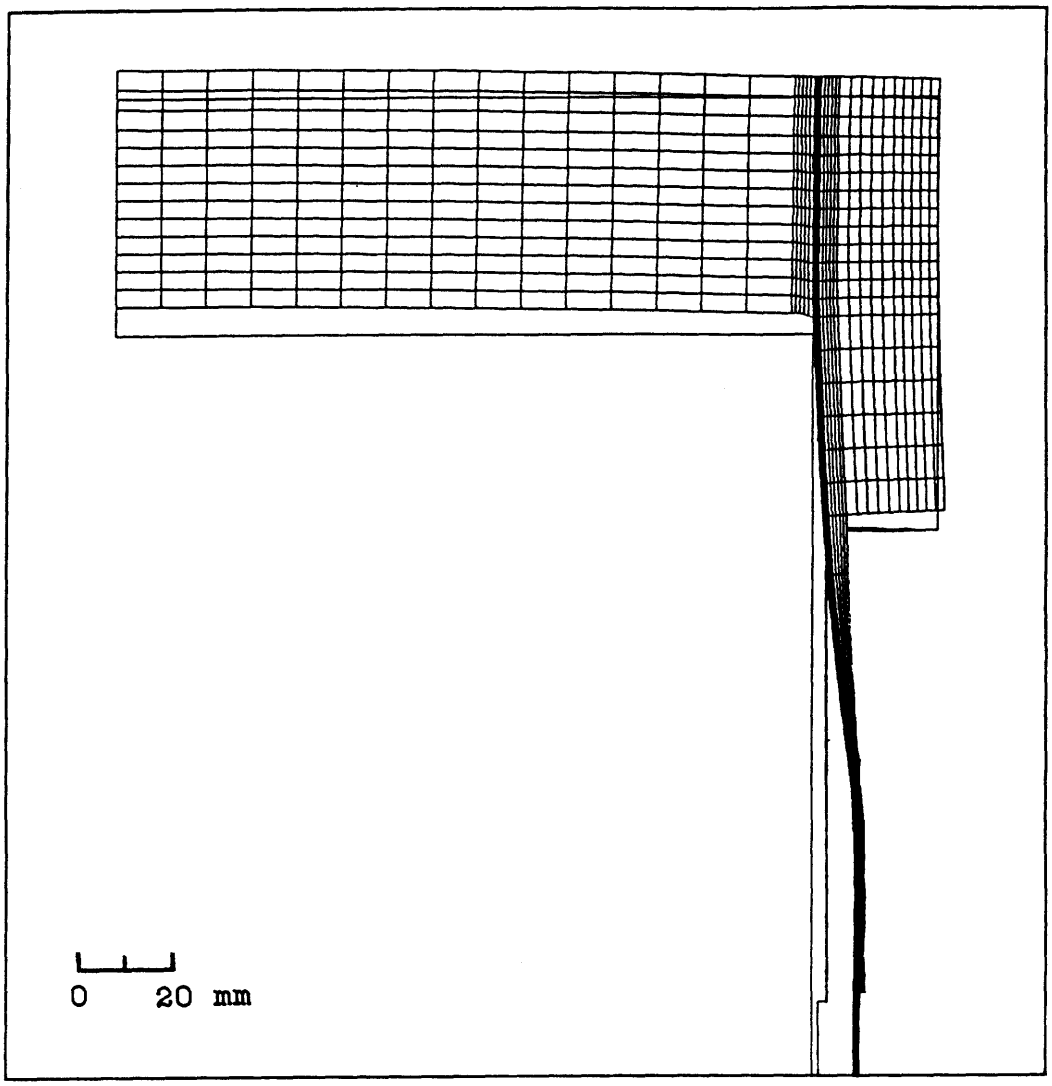

Figure 4.20 Deformed Finite Element Mesh of Endcap System at 5.0 MPa Internal Pressure

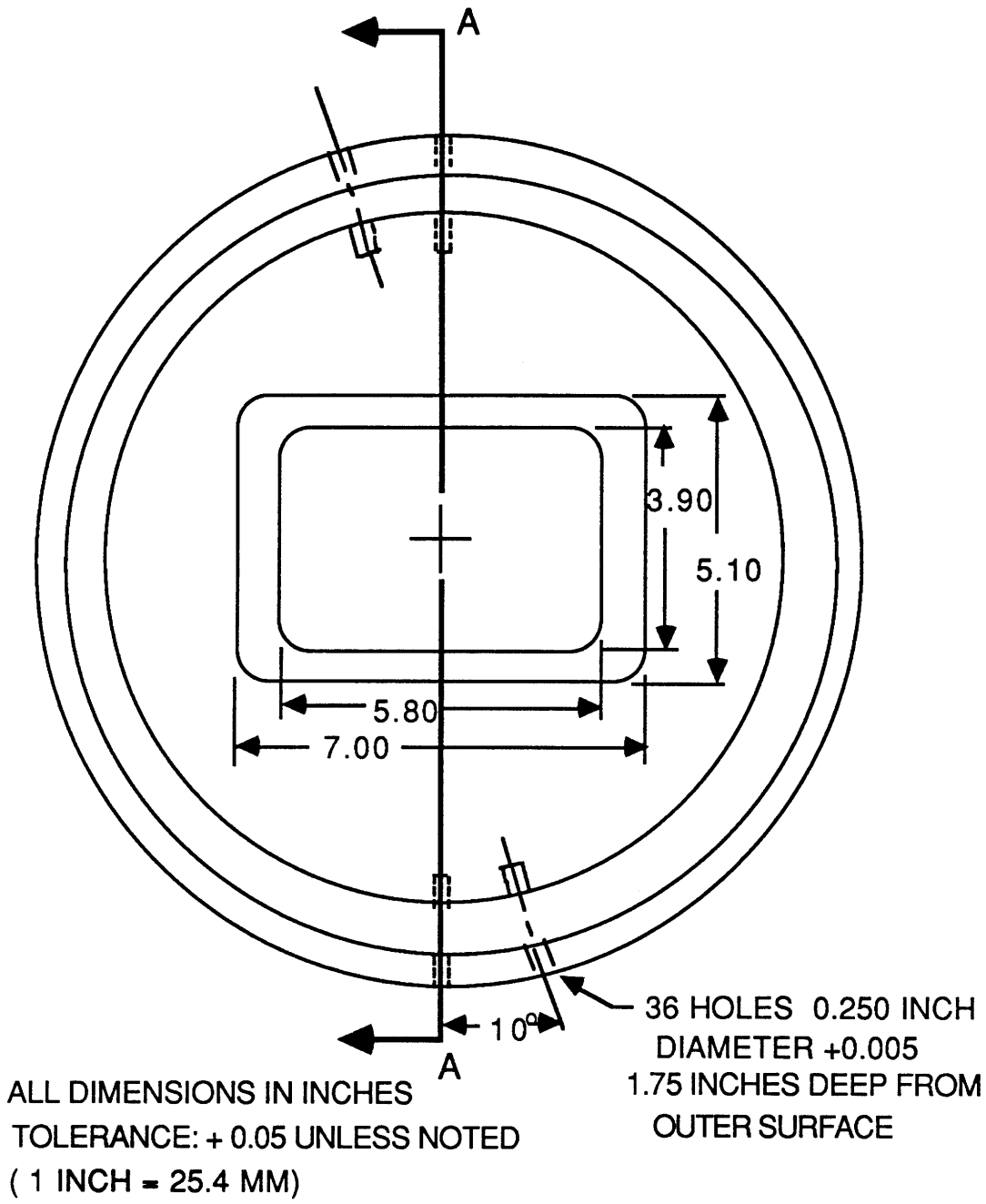

Figure 4.21 Endcap Dimensions - Top View

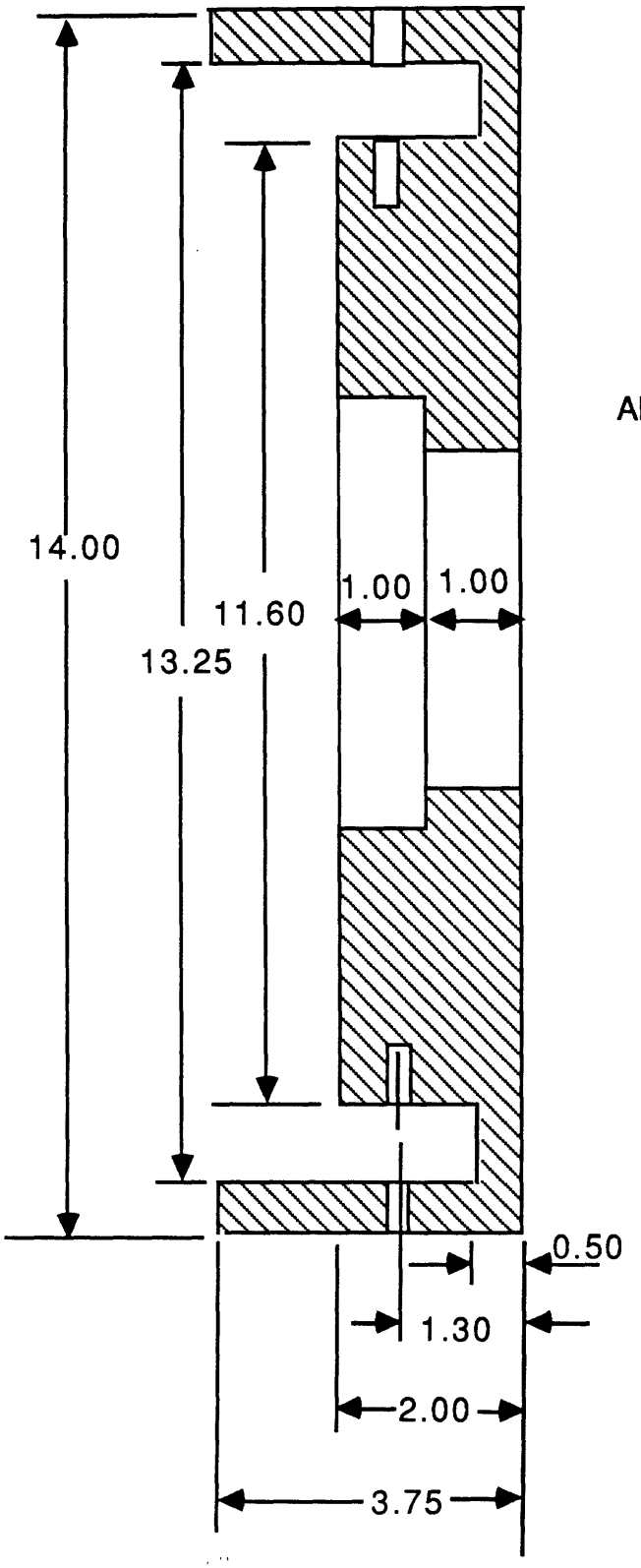

MATERIAL 7075-T6 AL

ALL DIMENSIONS IN INCHES

TOLERANCE + 0.05

(1 INCH = 25.4 MM)

Figure 4.22 Endcap Dimensions - Section View

out of the groove; (g) sealing the inner groove with masking tape to prevent leakage of the epoxy; (h) pouring the mixed epoxy filler into the outer groove from one side for proper flow; (i) curing the epoxy; (j) repeating this procedure for the other endcap. A few points require special attention. Care must be taken to align the cylinder wall properly so that it is perpendicular to the endcap bottom. Also, the inner groove must be filled with epoxy or the bladder will be cut when the tube is pressurized. Overall, assembly is complicated and time consuming, and the previous description is not intended to be used as a construction procedure.

Cleanup of the test assembly involves: (a) sawing off all excess tube material, (b) removing all pins by gripping with vise-grips and then prying out with a crowbar while simultaneously rotating the pin, (c) heating the endcap to 177 C, (d) immediately drilling out epoxy while endcap is hot, (e) sectioning the tube ring into a minimum of four sections with a cold chisel, and (f) extracting the tube remains with a prybar. A breakdown of the assembly and disassembly time is given in Table 4.5.

4.4 Specimen Instrumentation

Coupon and cylinder specimens were instrumented with Micro Measurements type EA-09-125AD-120 strain gages. Gages were mounted on specimens after non-destructive evaluation was complete.

TABLE 4.5

PRESSURE TEST ASSEMBLY TIME BREAKDOWN

Manufacturing Task	Time Required (hours)
Seam Reinforcement	2
End Feather / Reinforce	5
Pin Insertion (one end)	1
Epoxy Fill (one end)	3
Disassembly / Clean-up	4
Bladder Assembly	3

4.4.1 Coupon/Plate Specimens

All coupons were fitted with a far-field strain gage oriented in the longitudinal direction of the coupon. Unflawed specimens were fitted with a transverse gage as well. Figure 4.23 is an illustration of the location of the strain gages on the unflawed specimens. Impacted coupon specimens were also fitted with longitudinal strain gages near the impact site on the front and back surface of the laminate. The near impact gages were placed as close to the damage area as possible without covering any part of the surface damage. The front and back gages were used to detect any bending that might occur as a result of unsymmetric damage through the thickness of the laminate. This allowed observation of the effect of the impact on the strain field around the damage area. The impact site was masked off during strain gaging to prevent adhesive from entering the damage area. The location of the strain gages on the damaged coupon specimens is illustrated in Figure 4.24.

4.4.2 Cylindrical Pressure Vessel Specimens

The cylinder specimens were instrumented after assembly of the test system was complete. A 100 mm by 100 mm grid was painted on the cylinder test section and the sections were numbered to facilitate reconstruction after failure. The test section was approximately 305 mm long. Eight strain gages

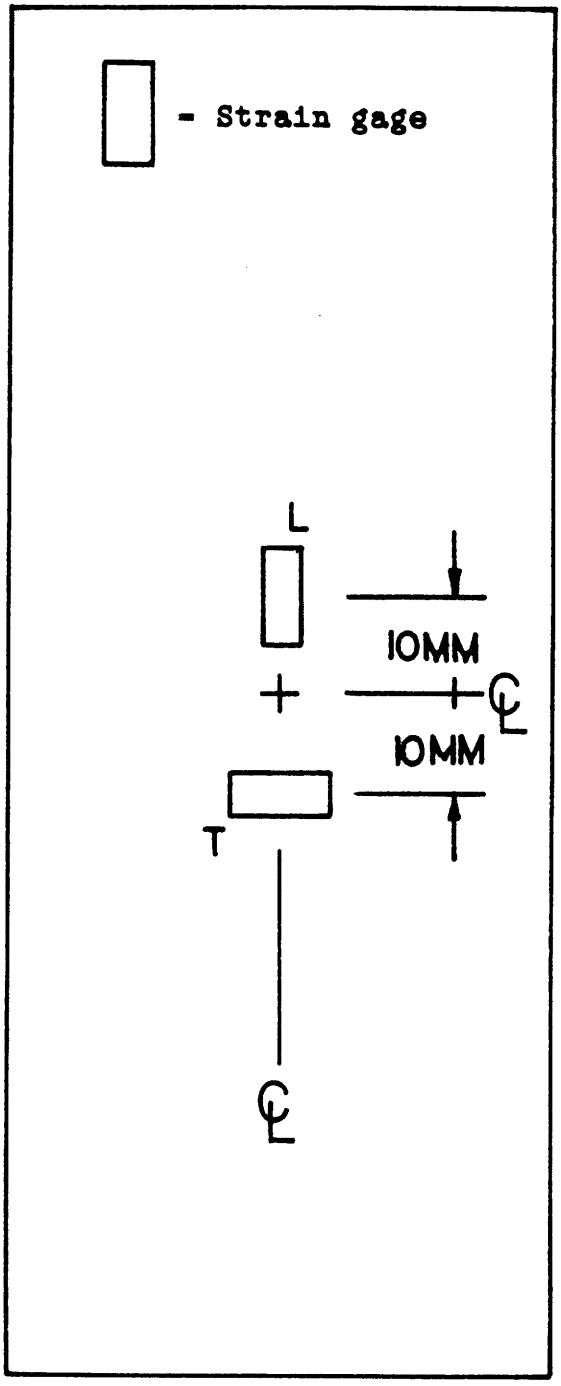

Figure 4.23 Unflawed Coupon Strain Gage Locations

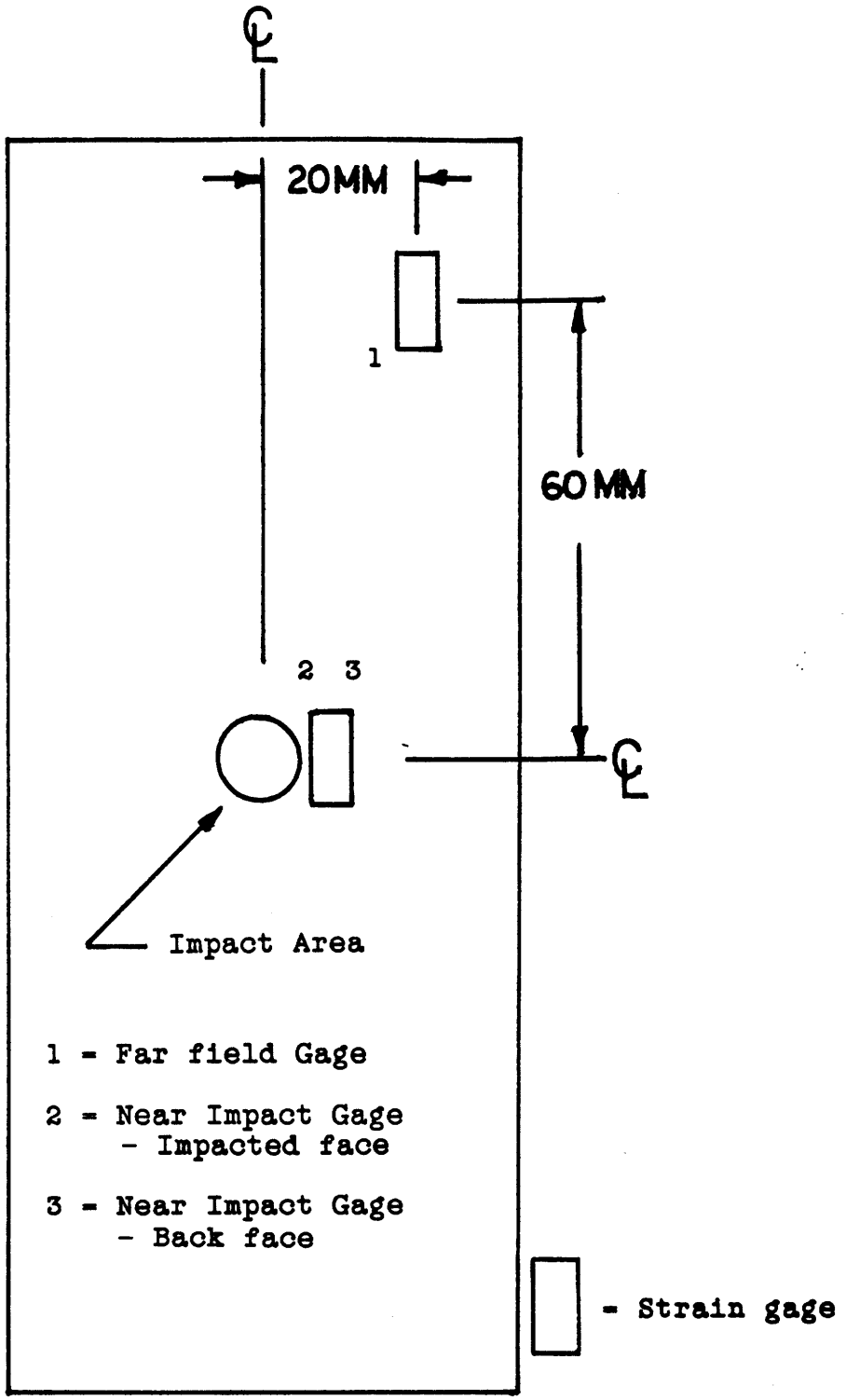

Impact Gage Placed Close as Possible to Impact Area

Figure 4.24 Damaged Coupon Strain Gage Locations

were mounted on the tube.

Unflawed tubes were fitted with five hoop gages and three longitudinal gages. Figure 4.25 is a schematic of the gage locations for the unflawed specimens. These locations were chosen to provide data on the stress distribution in the test section area of the cylinder.

Impacted tubes were fitted with far-field gages in the longitudinal and hoop directions. Near-impact gages were also mounted in the tube longitudinal and hoop directions. As with the plate specimens, these gages were placed as close as possible to the impact area without covering any surface damage. Figure 4.26 is a schematic of the locations of these gages. These gage locations were chosen to enable observations of the strain field near the impact area. As with the plate coupons, the impact site was masked off to prevent adhesive from entering the damaged area.

4.5 Description of Examination Techniques

The examination techniques used for the damage characterization and residual strength studies may be divided into two groups, non-destructive and destructive examination.

4.5.1 Destructive Examination Techniques

The two destructive examination techniques used were epoxy burn-off and specimen sectioning. These methods were

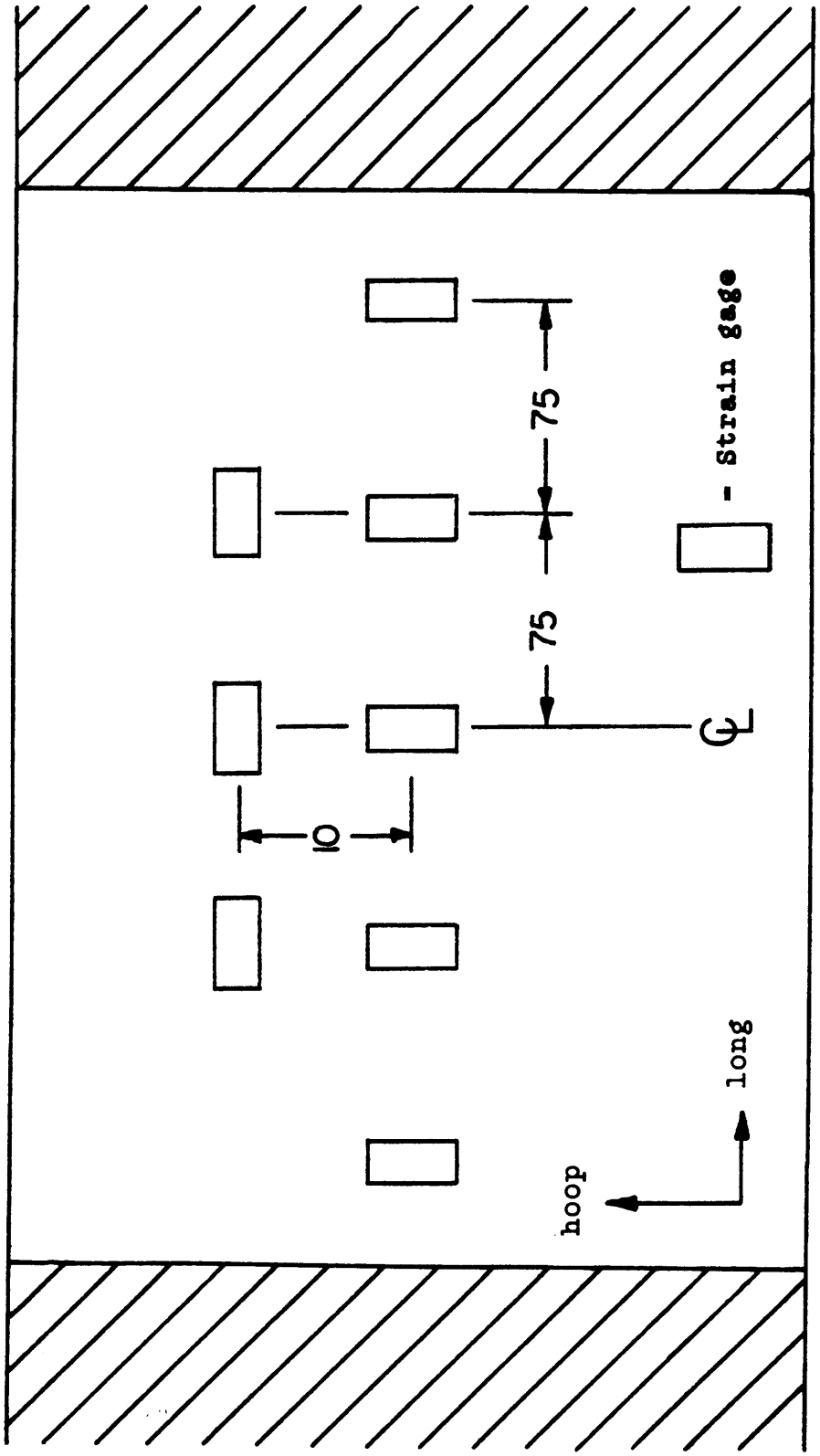

Figure 4.25 Unflawed Cylinder Strain Gage Locations

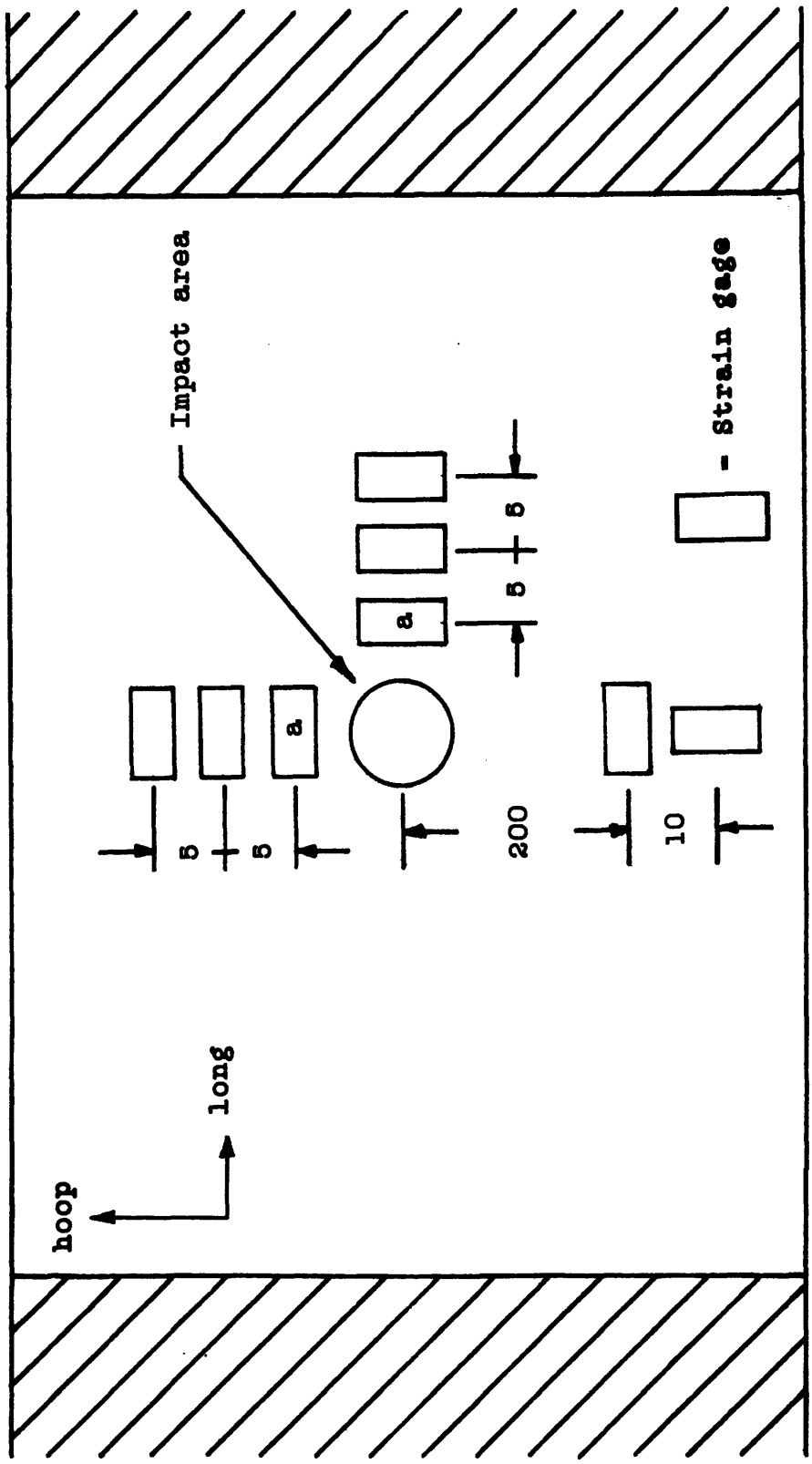

a Impact Gage Placed Close as Possible to Impact Area

All dimensions in millimeters

Figure 4.26 Damaged Cylinder Strain Gage Locations

used for the damage characterization studies and for correlation of the nondestructive inspections.

The epoxy burn-off procedure for impacted specimens required the use of an oven capable of reaching 550°C and a small amount of stainless steel mesh or suitable substitute. This technique was easier to implement with fabric than with tape, because the weave of the fabric plies prevented any breakup of the specimen. Unidirectional tape laminates require more effort. This procedure is detailed by Freeman [38].

The first step in the burn-off method was to pre-cut the specimens to the maximum horizontal dimensions of the oven. The oven was then pre-heated to 430°C. The specimen was placed on a stainless steel wire mesh and inserted into the oven. After approximately five minutes, the epoxy burned off, and the specimen was carefully removed (some smoking of the epoxy occurred). The deplyed specimen was allowed to cool and the individual plies of the specimen were separated.

Once the plies were separated, the impact damage to the fibers was determined on a ply by ply basis. This was accomplished by pulling out the broken fiber bundles of the woven cloth from the edge of the specimen with tweezers. Information was recorded in terms of the number of fiber bundles (tows) broken.

A water cooled high speed diamond grit blade was used to section the specimens through the centerline of the impact area. The cut surface was polished using a cotton bob soaked

in a mild abrasive (KALOPOLITE). The sections were examined and photographed with a optical microscope using magnifications from 49X to 240X.

4.5.2 Nondestructive Examination Techniques

Attempts to use ultrasonic pulse-echo equipment were unsuccessful because of the thinness of the specimen and the refractory nature of the weave in the fabric. The only nondestructive examination method successfully utilized was dye-penetrant enhanced x-ray. This technique was used on all of the damage characterization specimens for the flat plate and cylindrical geometries.

1,4-Diiodobutane dye penetrant was chosen for its low viscosity and relative low health risk. The dye was sparingly injected into the damage area with a needle and syringe. A 200 millirad exposure of the specimen was taken using a Scan-Ray Corporation Torrex 150D x-ray inspection system and Polaroid 52 film.

X-ray examination was also used on the residual strength flat plate coupons. No cylindrical residual strength specimens were x-rayed because of the size limitations of the equipment. The impact damage on these specimens was measured visually. The dimension documented was the maximum diameter of the footprint, or mark, left on the cylinder by the impactor.

4.6 Testing Methods

4.6.1 Coupon Tests

All coupon tests were conducted using an MTS 810 hydraulic testing machine. Strain gage and load data was sampled every 0.5 seconds and stored on a PDP 11/34 data acquisition computer. The tests were conducted monotonically to failure using stroke control with a ramp rate of 1.5 mm per second. This gave a strain rate of approximately 7000 microstrain per minute in the test section.

The coupons were first gripped at the upper loading tabs and checked for proper alignment with the loading axis. This was accomplished through the use of a right triangle placed between the testing machine head and the specimen edge. Because of the larger than normal width of the test article, the upper grip and test specimen had to be lowered into position so that the bottom tab could be gripped. The strain gages were calibrated in this position at zero load before the lower loading tab was gripped.

Most coupons were tested directly to failure. Several tests were stopped at audible or visible damage indications. For these tests, the coupon was removed and x-rayed before being placed back into the testing machine for further loading. This was done in an attempt to monitor any damage growth during the loading process.

4.6.2 Pressure Vessel Tests

The cylinders were tested in a blast chamber with a maximum energy release level rating equivalent to two pounds of TNT. Pressurization of the cylinders was accomplished using bottled nitrogen.

The high energy release of the cylinder failures required a number of added safety measures. A minimum of a single layer of sandbags was placed completely around the cylinder except for the top. A minimum of three feet of sandbags was used behind the endcaps. Note that longitudinal expansion of the cylinder was not restricted. The entire assembly was then covered with cardboard or any other suitable energy absorbing material. The strain gage/pressure transducer hookup box, constructed of 37 mm (1.5 in) marine plywood and ballasted with sandbags, was protected from projectiles by a steel plate. The strain gages were connected to the main hookup box through the use of tear-away terminal strips.

The cylinder tests were conducted using a manual pressurization rate of approximately 0.69 MPa/min (100 psi/min). All tests were conducted to catastrophic failure. Strain gage and transducer data was sampled every 0.4 seconds and fed to a PDP 11/34 data acquisition computer. Transducer data was also fed to a X-Y plotter to monitor the nitrogen feed rate during pressurization. A schematic of the cylinder test setup is given in Figure 4.27.

Upon completion of the cylinder test, the blast chamber

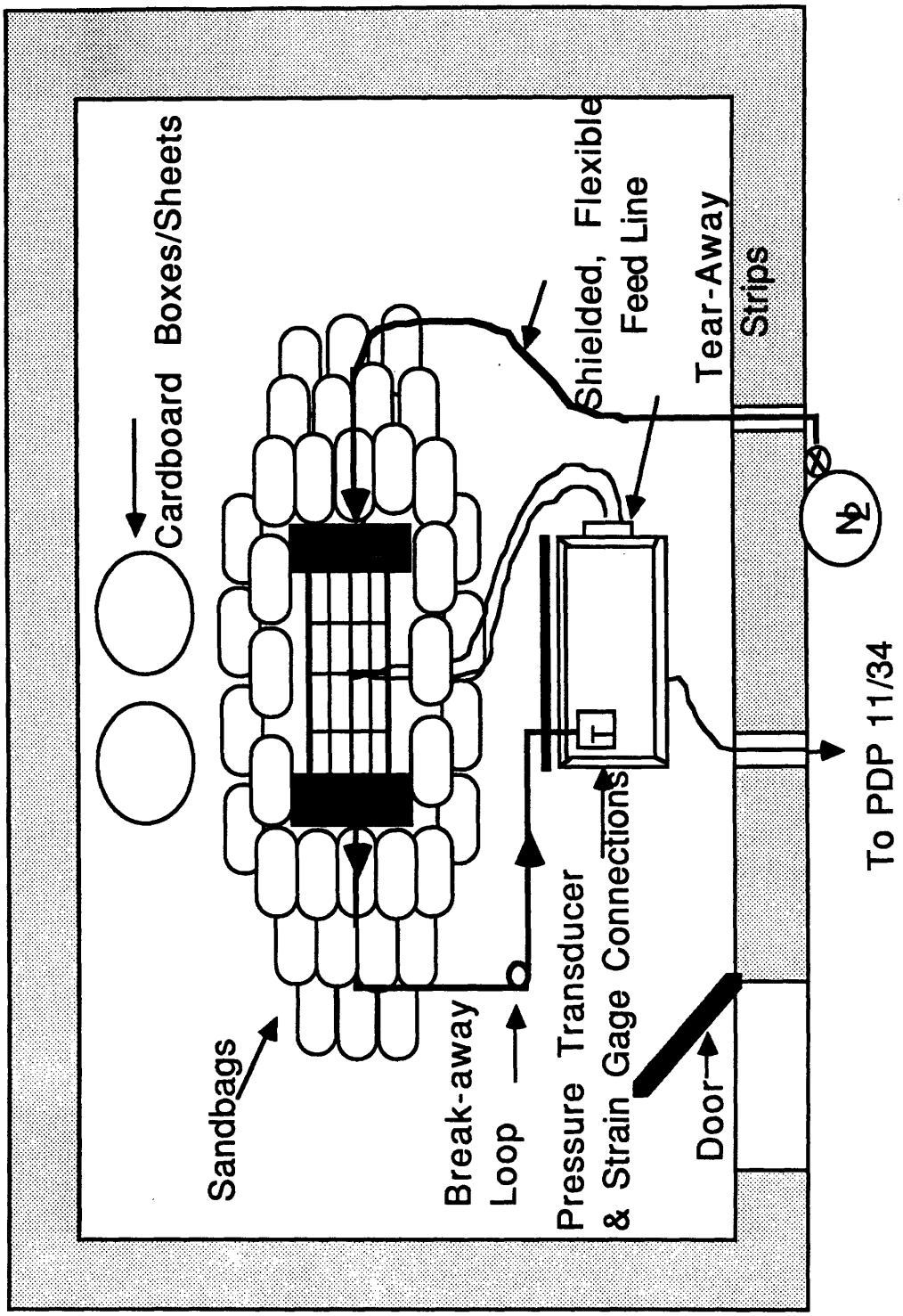

Figure 4.27 Illustration of Cylinder Test Set-up in Blast Chamber

was ventilated for 30 minutes. Particle masks and gloves were used when entering the chamber after the test because of floating debris. Recoverable tube components were then pieced together to determine the cause of failure.

4.7 Data Reduction Methods

All experimental data acquisition was done on a PDP 11/34 computer. Using the data processing software developed at TELAC [39], raw data was processed according to the flow chart in Figure 4.28. Data was first edited to include only points taken during the loading sequence. LIN6 data analysis was used to determine linear regions of the load and strain gage data obtained for the far-field gages only.

Analytical data was processed and stored on a Digital Equipment Corporation Microvax II minicomputer. Data obtained from measurements of the x-ray photographs and epoxy burn-offs was also processed on this system.

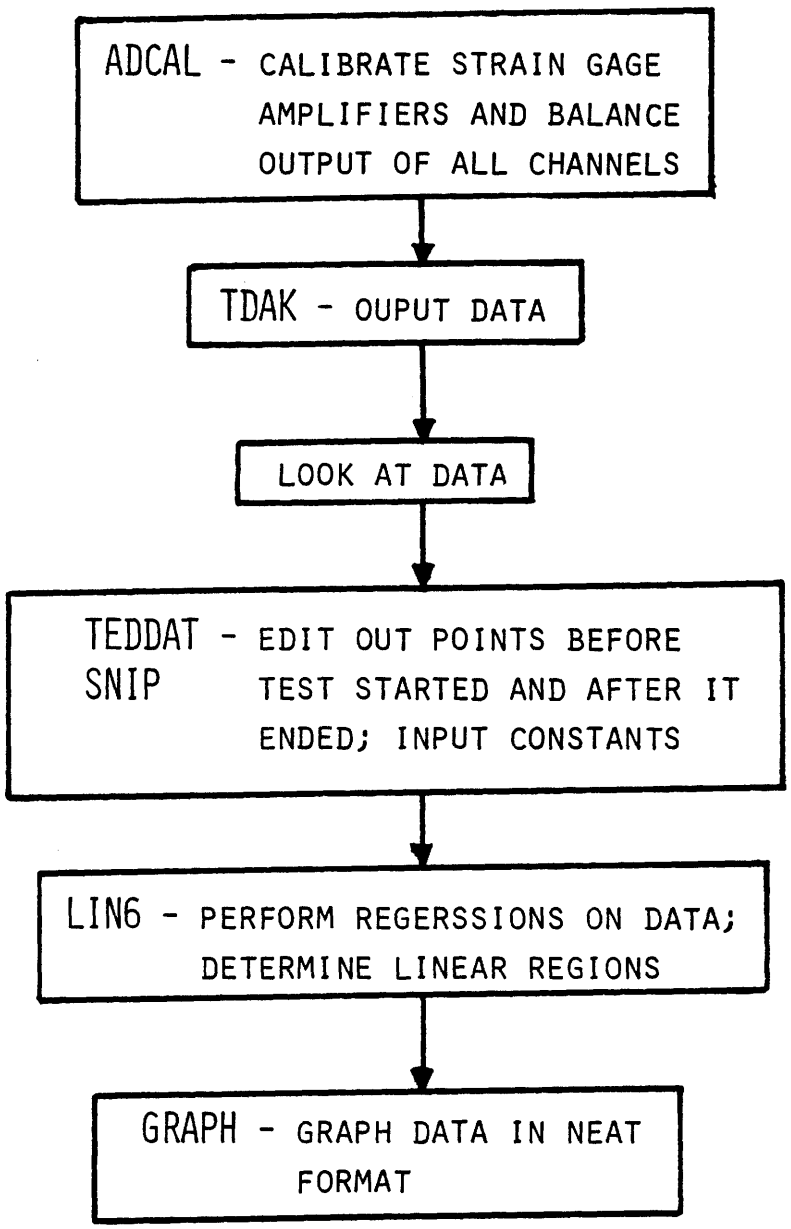

Figure 4.28 Flow Chart of Test Data Reduction

CHAPTER FIVE

EXPERIMENTAL RESULTS

5.1 Impact Damage Characterization of Fabric Gr/Ep

5.1.1 Plate Structures

Impact damage of the $(0,45)_s$ fabric graphite/epoxy plate laminates is characterized by several modes. Matrix yielding, fiber breakage, delamination, and fiber bundle disbonds were found to occur as a result of impact.

Matrix yielding is defined as the permanent deformation or change in thickness of the laminate under the impact area. The indentation of the impactor causes the matrix material directly beneath it to yield and thus creates a damage state. A photograph and sketch of a $(0,45)_s$ laminate cross-section exhibiting the first signs of matrix yielding damage is shown in Figure 5.1. The extent of the damage is dependent on the impactor velocity.

For low velocities, the matrix exhibits a permanent deformation on the impacted surface without visible damage to the matrix through the thickness of the laminate. This agrees with the observations made by Sun and Tan [11] on the static indentation of composite laminates. In their work, the spring constant associated with the unloading of the material was found to be different than the constant found during the

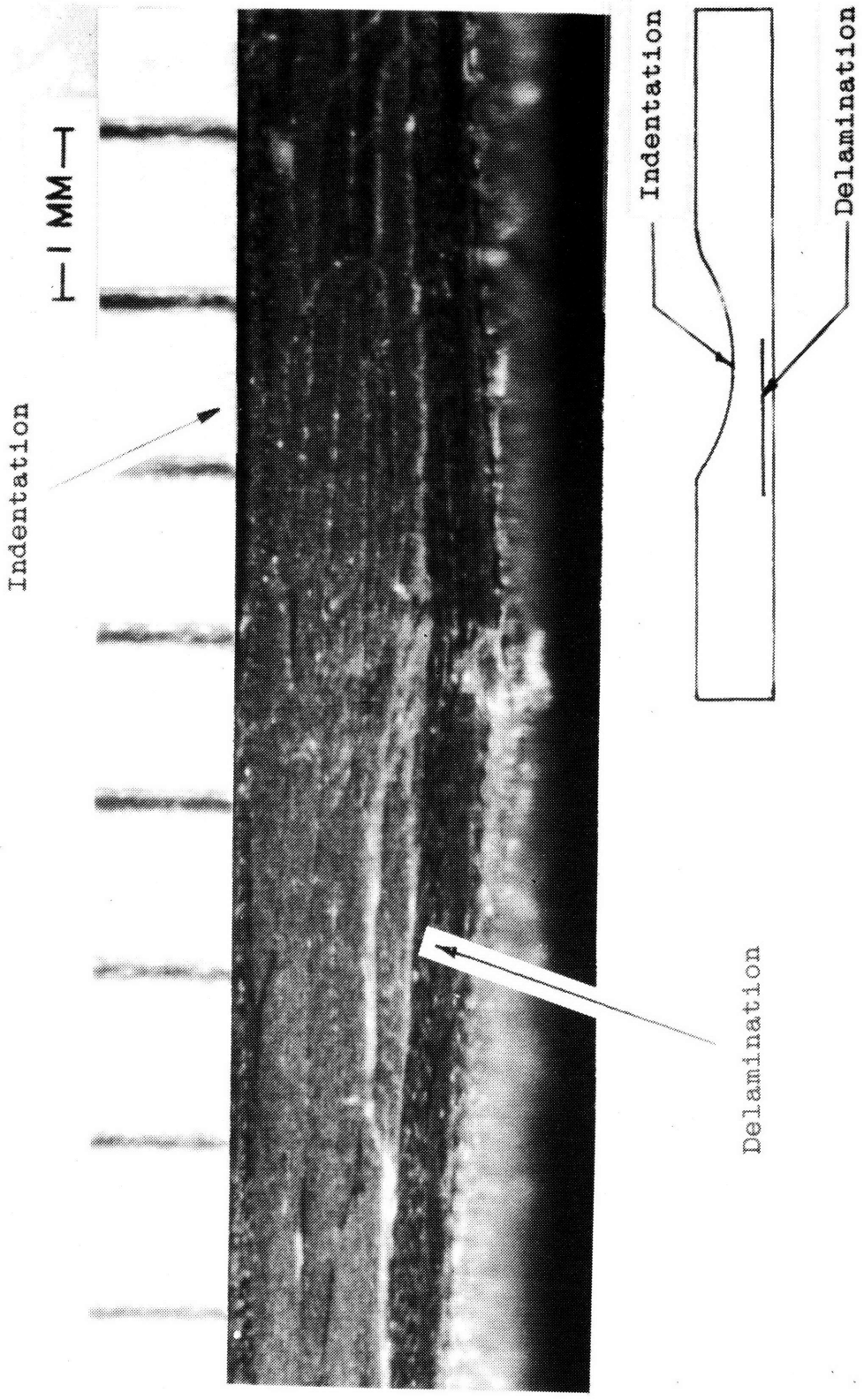

Figure 5.1 Photograph and Sketch of Fabric Plate Cross Section with Matrix Yielding Damage

loading process. This phenomenon was attributed to the permanent deformation of the laminate.

As the velocity of the impactor increases, the permanent deformation progresses to a complex state of micro-cracking through the thickness of the laminate. Some cross-sections reveal evidence of different amounts of matrix yielding dependent on whether the impactor initially hit a fill fiber tow or a warp fiber tow. Because of inaccuracies in predicting the aim of the impact gun, further consistent observations were not possible.

Fiber breakage is defined as the clear breaking of graphite fibers under the impact area. Epoxy burn-off was used to determine the extent of fiber breakage in a given laminate. The damage to the fibers was a single cut at the impact area. Figure 5.2 is a plot of the maximum number of fiber bundles (tows) broken in a ply versus impact velocity. The largest number of broken fiber bundles typically occured in the ply opposite the impact surface. The amount of broken fibers per ply increased through the thickness from the impacted surface. Figure 5.3 is a plot of the number of fiber bundles broken per ply versus velocity. The number of data points in this plot has been reduced to emphasize the increase in fiber damage away from the impact surface through the thickness of the laminate. The number of fibers broken in the warp direction was approximately the same as the number of fibers broken in the fill direction. No damage to the fibers was detected by the epoxy burn-offs until the impactor

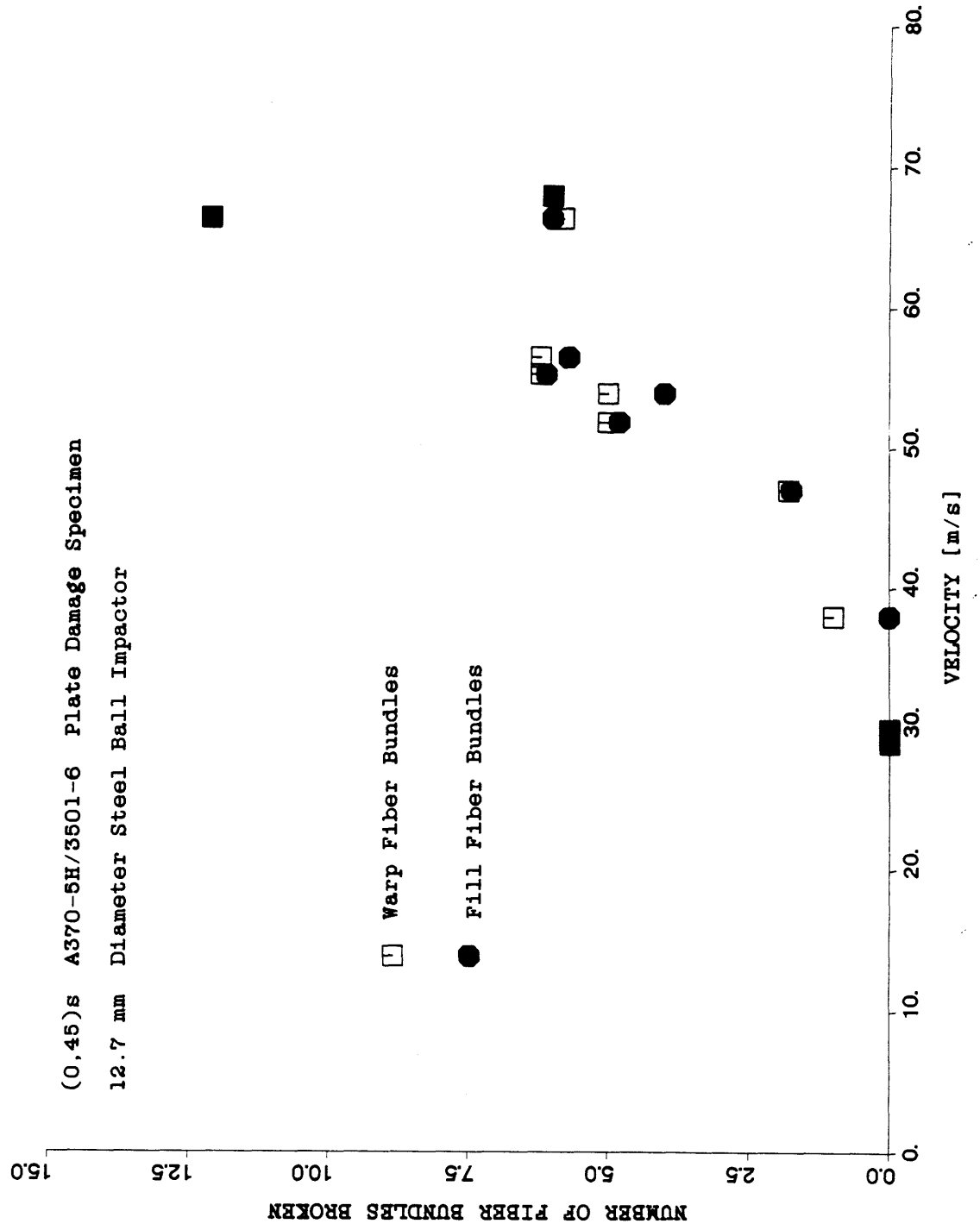

Figure 5.2 Maximum Number of Fiber Bundles Broken in Laminate Plies versus Impactor Velocity for Fabric Plate Damage Characterization Specimens

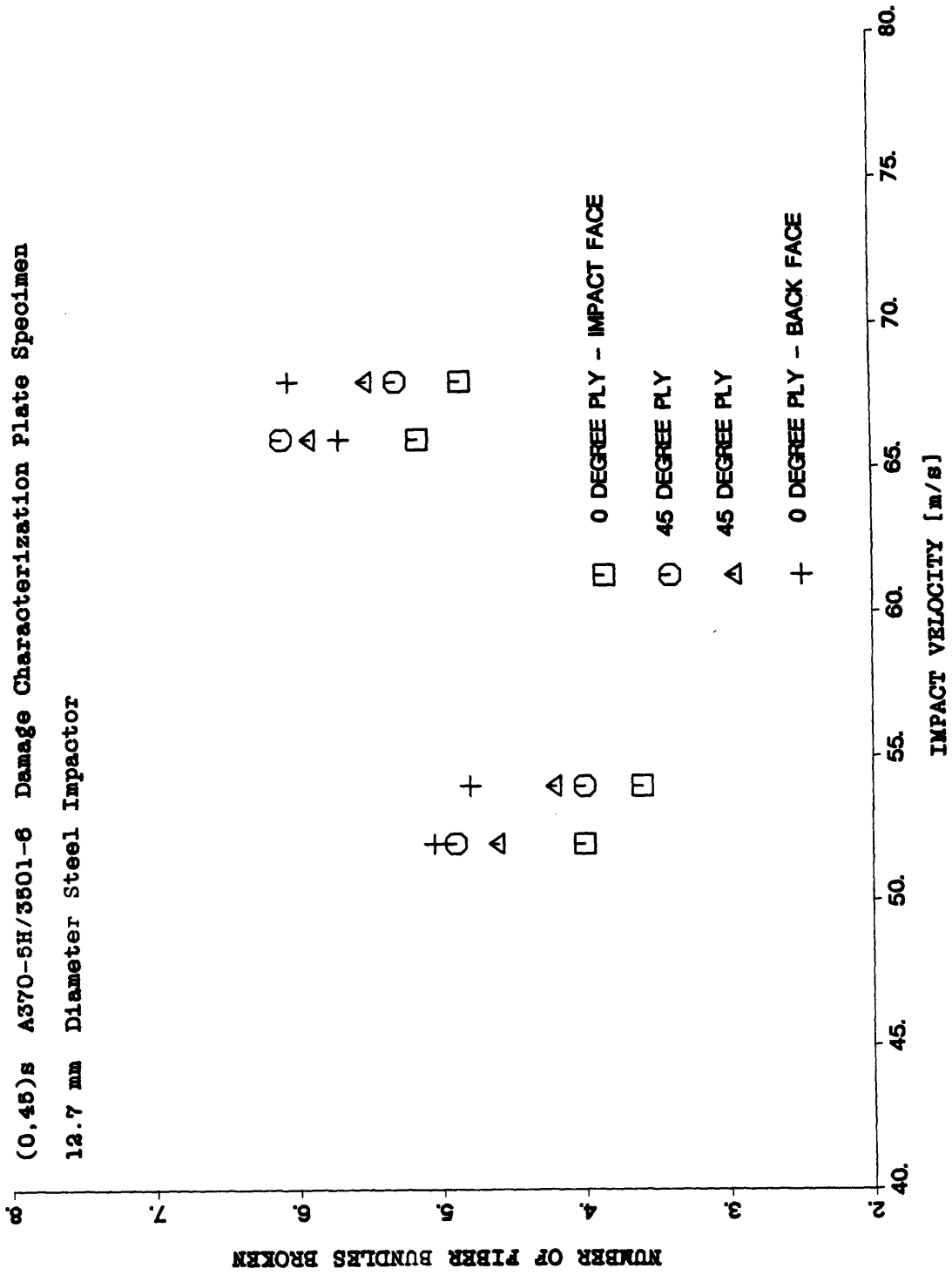

Figure 5.3 Number of Fiber Bundles Broken Per Ply versus Impactor Velocity

velocity reached approximately 30 m/s. The broken fiber damage was a cross-hair shape, aligned with the local 0° and 90° directions of the ply in which the damage occured.

Delamination is defined as the out of plane failure of the matrix between two consecutive plies. Unlike tape laminates, the delaminations are not as easily observed in the fabric laminate, as the woven nature of the material obscures the ply interfaces. Figure 5.4 is a photograph of the cross-section of a fabric specimen with a large amount of delamination. The maximum amount of delamination was found at the 45/0 ply interface opposite the impact surface. The delamination size was determined by two measurements taken in the zero and ninety degree laminate directions. Figure 5.5 is a sketch of the delamination area as it appears on the x-ray photographs. The x-ray is the integral of the delaminations through-the-thickness of the specimen. Figure 5.6 is a plot of the delamination axes versus impactor velocity. The delamination length increased with velocity and the largest axis of the delamination corresponded to the direction of the visually dominant fiber tows on the face opposite the impact. For the $(0,45)_s$ layup, the zero degree laminate direction corresponds to the warp fiber direction of the top and bottom plies. Thus, a specimen impacted on the front warp fiber dominant face has the largest amount of delamination propagating ninety degrees away in the fill fiber direction on the back surface of the specimen.

The aspect ratio of the delamination area is plotted in

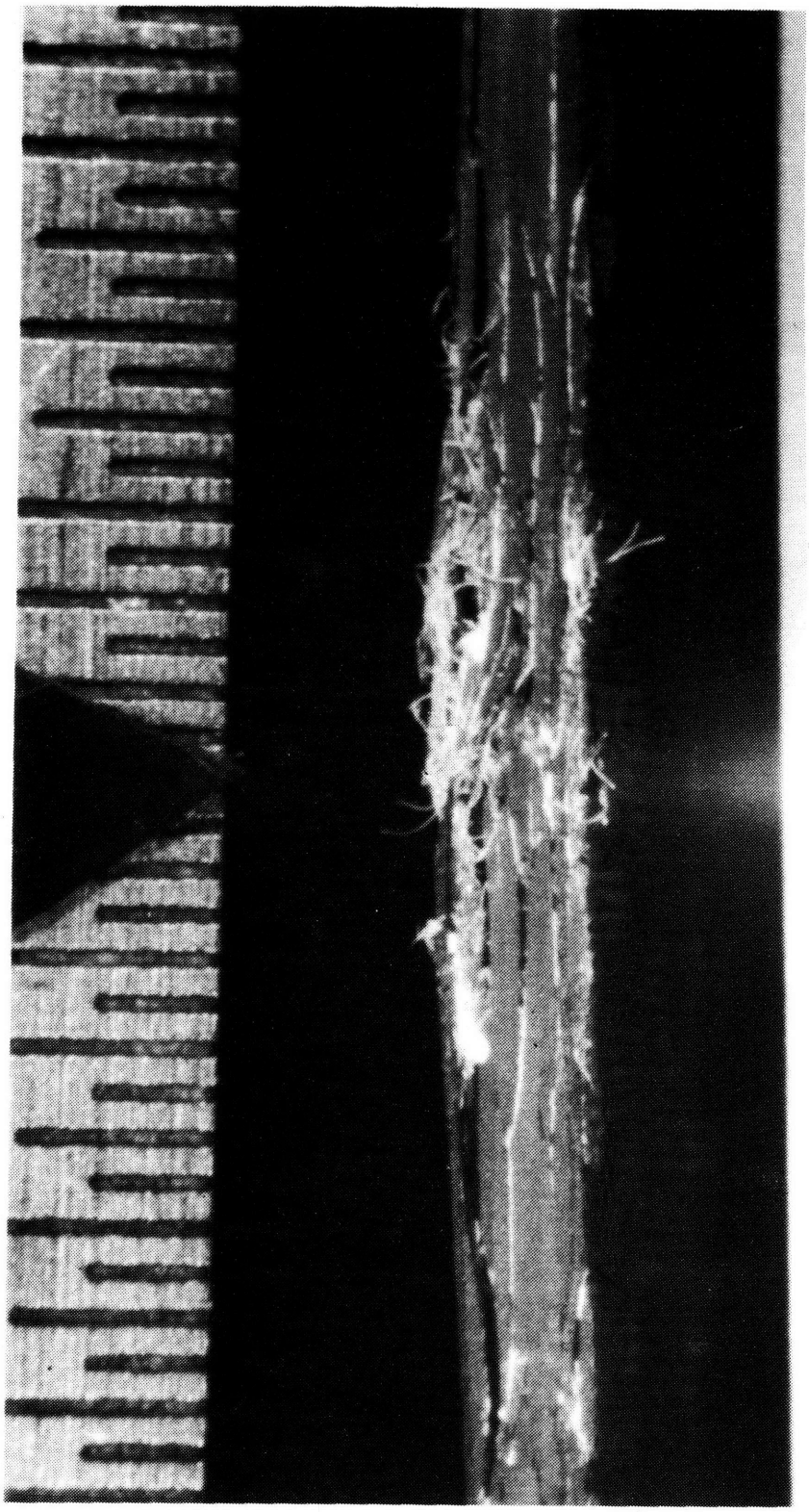

Figure 5.4 Photograph of Fabric Plate Cross Section with Extensive Delamination

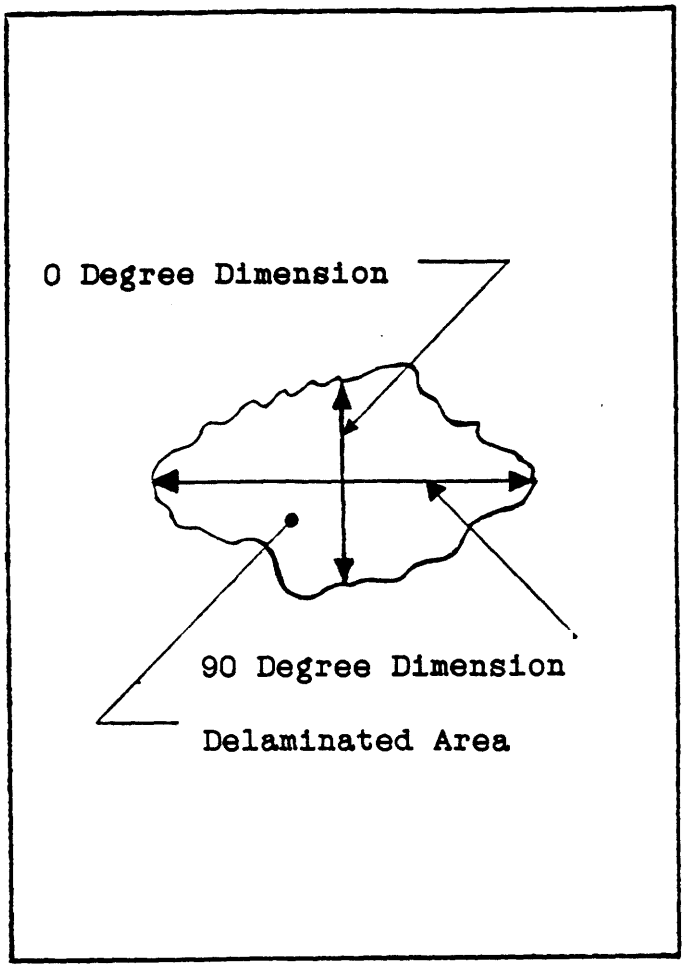

Figure 5.5 Sketch of Typical Delaminated Area

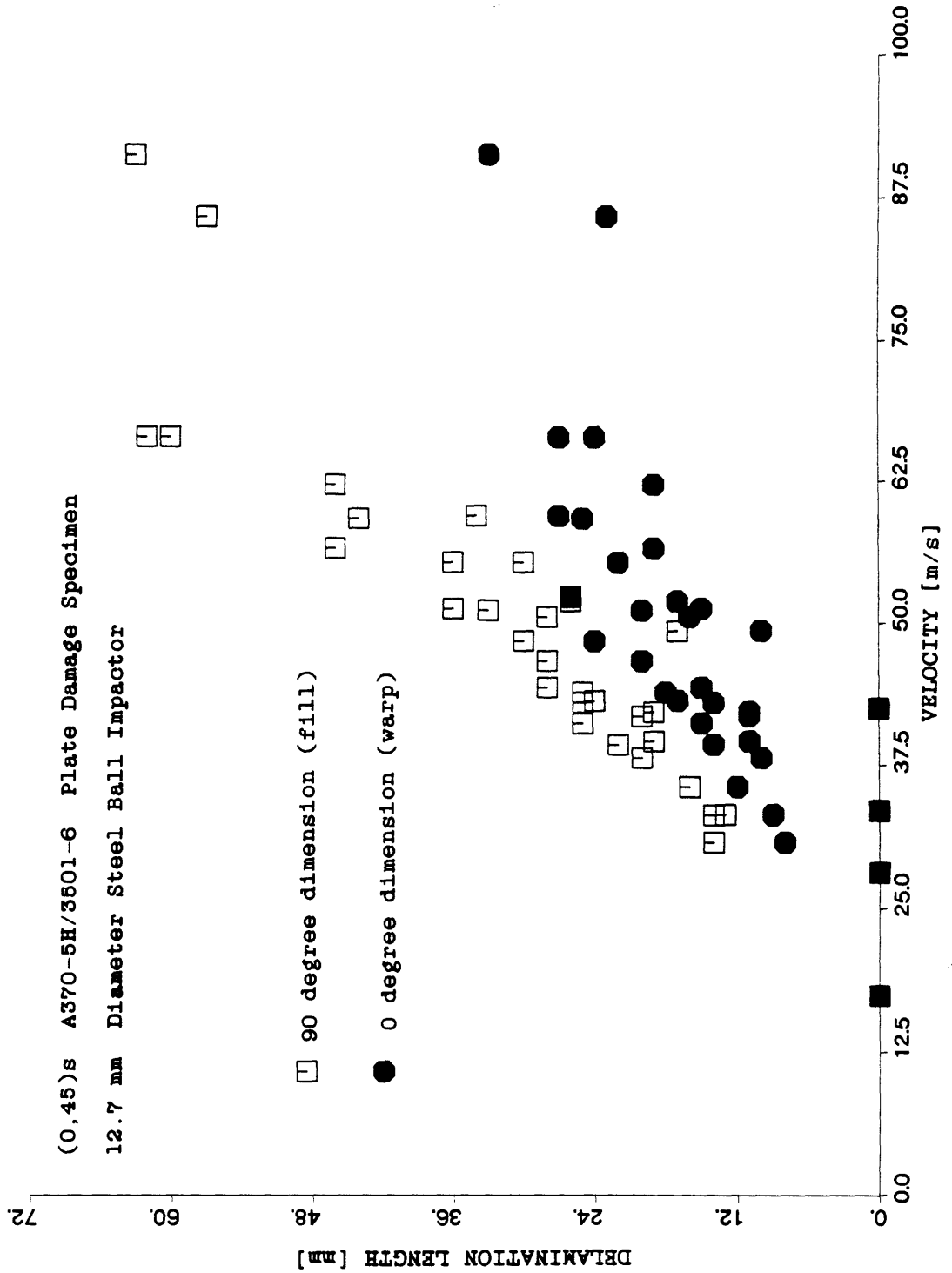

Figure 5.6 Delamination Length versus Impactor Velocity for Fabric Plate Damage Characterization Specimens

Figure 5.7. The aspect ratio is defined as the ratio of 90° length to 0° length. The aspect ratio increased with increasing velocity.

Fiber bundle disbonds are defined as the separation of a single fiber bundle or tow from its associated lamina. Figure 5.8 is a sketch of a fiber bundle disbond. The disbonds occur on the face of the laminate opposite the impact surface. The direction of the bundle disbond is governed by the visually dominant bundle direction on that face. In reference to Figure 5.9, if a $(0,45)_s$ laminate is impacted on a warp bundle dominated face, the fiber bundle disbond occurs on the rear surface in the tow dominated direction. The specimen in the x-ray of Figure 5.10 was impacted on the warp-dominated face; thus, the bundle disbond propagation is 90 degrees away in the fill direction.

It was not possible to detect any trends in the size of the disbonds versus impactor velocity. The disbonds often propagated from random locations around the impact area. Furthermore, the disbonds were not always symmetric about the center of the impact. The fiber bundle disbonds, however, were found at all damage levels and appeared first in the sequence of damage propagation in the fabric laminate. Fiber bundle disbonds were a precursor to fiber breakage. This was shown by the fact that fiber bundle disbonds were found to occur for impacts of approximately 25 m/s while fiber breakages were not detected for impact velocities less than approximately 30 m/s. The fiber bundle disbond allowed the

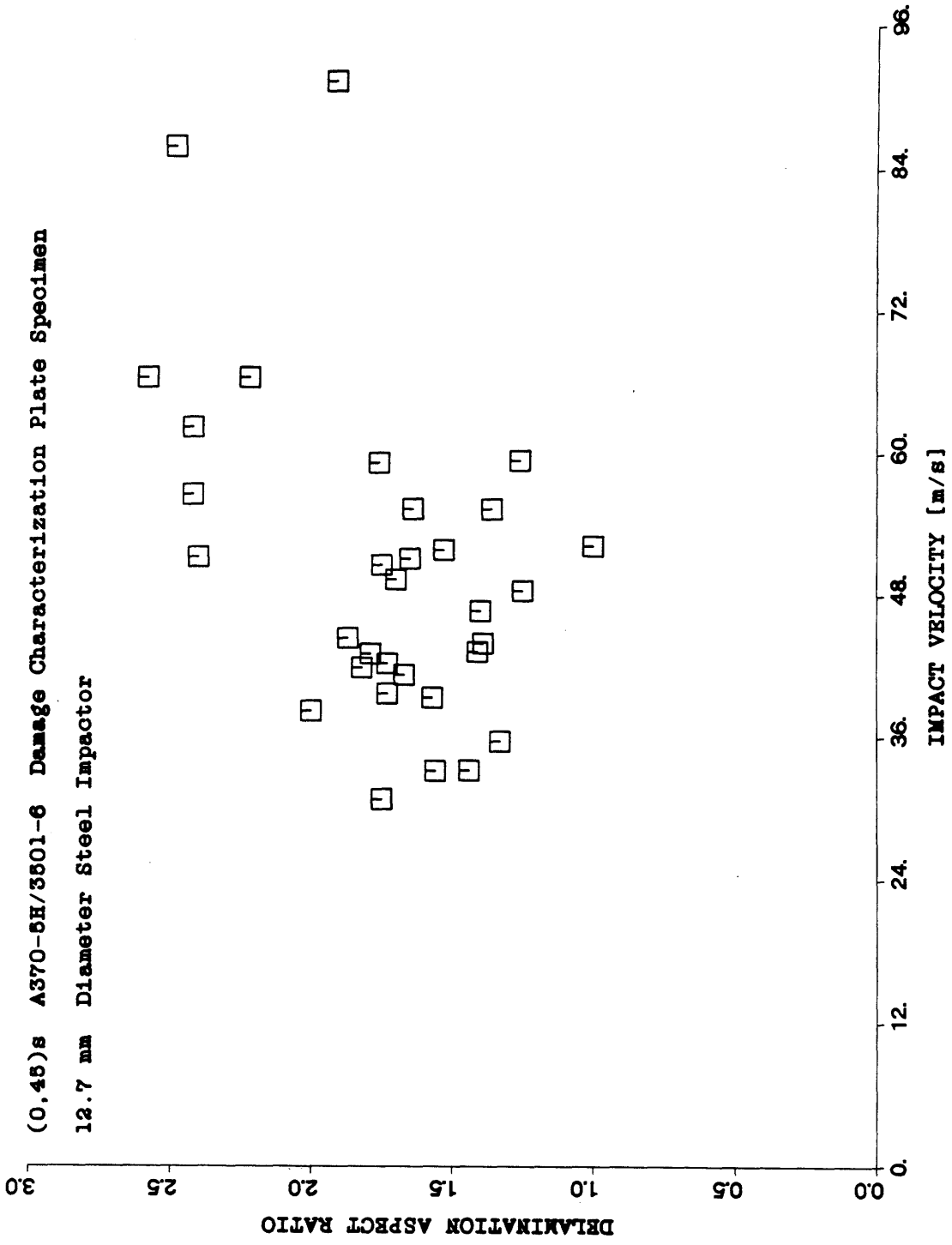

Figure 5.7 Aspect Ratio of Delamination Length versus Impactor Velocity for Fabric Plate Damage Characterization Specimens

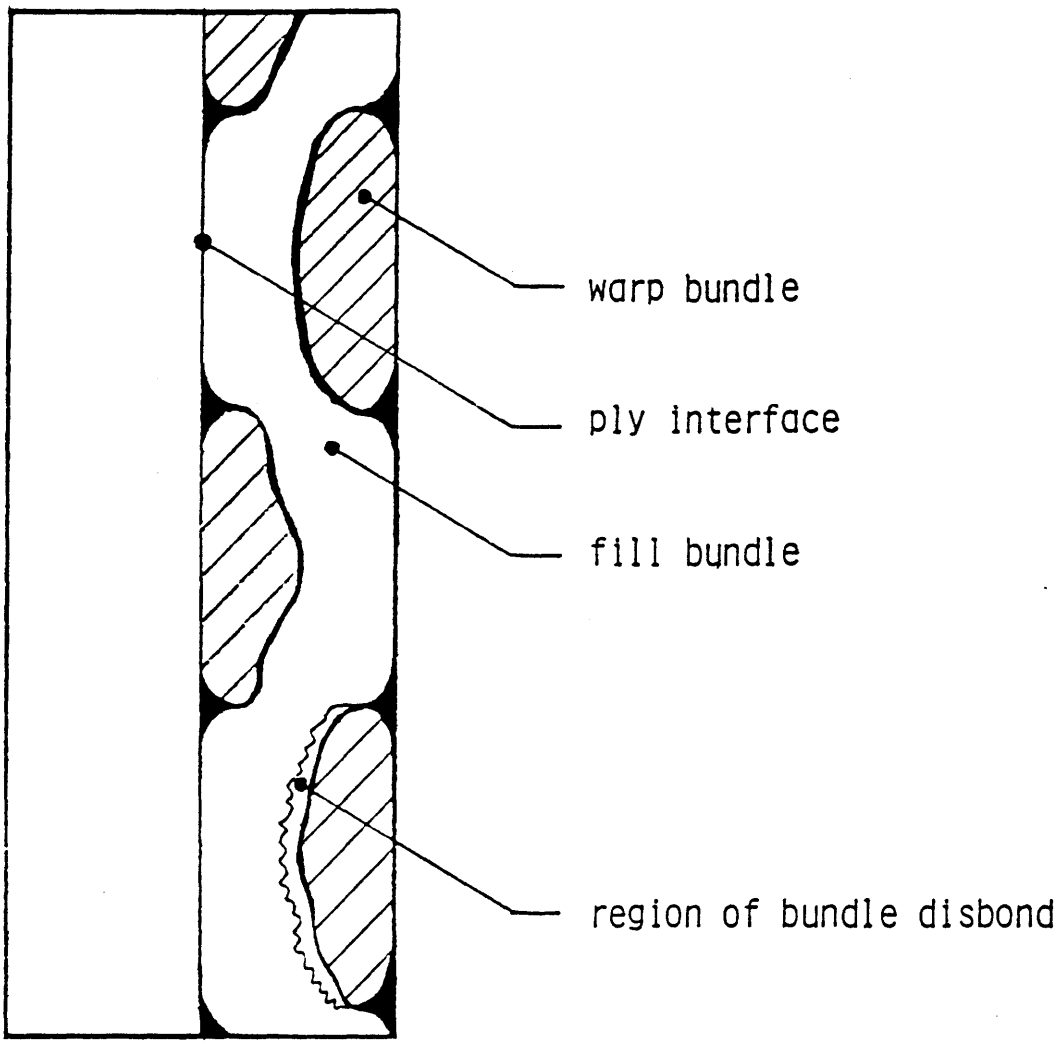

Figure 5.8 Sketch of Section View Showing Fiber Bundle Disbond

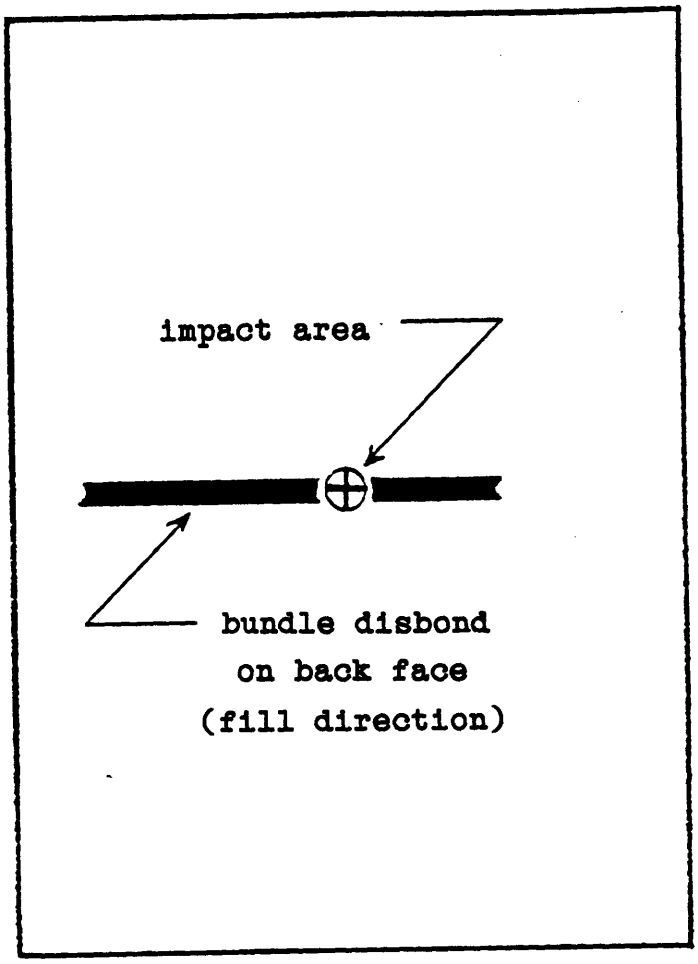

Figure 5.9 Sketch of X-ray Showing Fiber Bundle Disbond

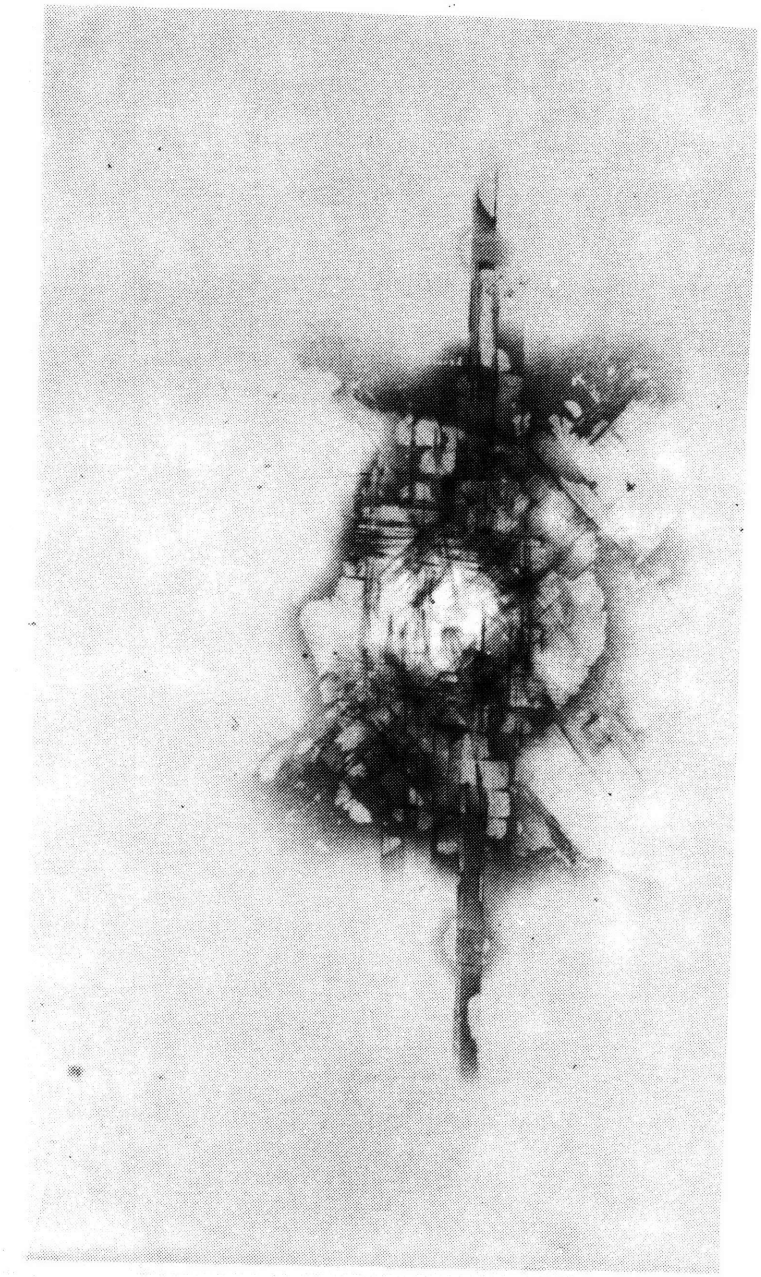

Figure 5.10 X-ray Picture of Fabric Plate Specimen Impacted at 91 m/s Exhibiting Fiber Bundle Disbond Propagation

dye penetrant to be injected into the laminate to assess the core area diameter.

The epoxy burn-offs reveal that a bundle disbond may pass through a weave without disturbing the crossed bundle. Fiber bundle disbonds are the fabric ply equivalent of angle ply splits. The weave of the fabric, however, prevents a total split from developing in the ply. This split suppression quality of the fabric material is a key to the success of the epoxy burn-off technique. For any amount of damage, the weave always held the laminate plies together.

On the basis of these observations and excellent correlations between sectioning and x-ray examinations the x-ray photographs are interpreted as follows in reference to the x-ray of Figure 5.11. The gray shaded area surrounding the center of the impact corresponds to the delamination of the plies. The gray ligaments propagating out from the center of the impact are fiber bundle disbonds. Finally, the dark central core region represents an area of matrix yielding, fiber damage and delamination. The darkness of this area is attributed to the large amount of damaged surface area available for the dye penetrant to wet.

This core area containing all types of damage was considered to be the key factor in assessing the damage tolerance for tension loading. The core area was a region of highly-damaged material considered to be useless for carrying load. Damage tolerance was thus governed by the size of the core damage area as was determined by Cairns [1] for tape

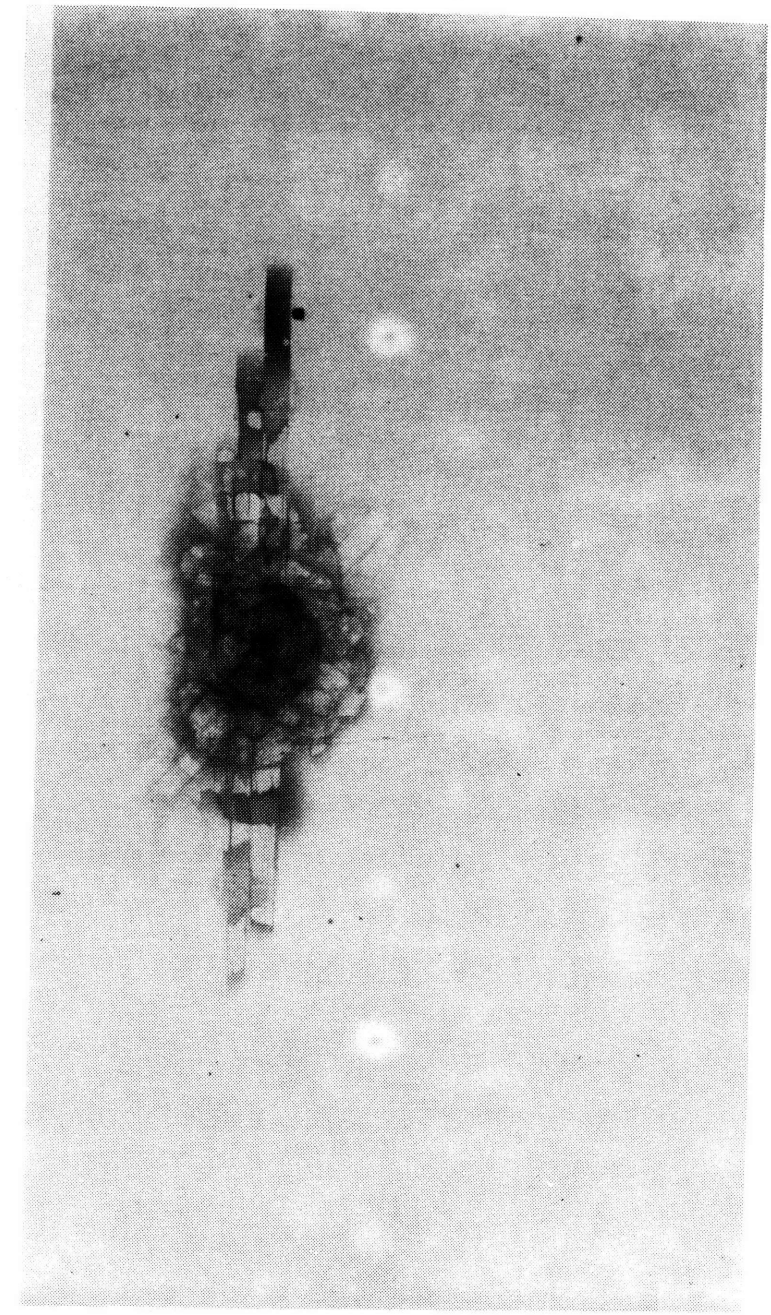

Figure 5.11 X-ray Picture of Fabric Plate Specimen Impacted at 43 m/s Showing Typical Damage Characteristics

laminates. The shape of the core area was approximately circular in all of the x-ray observations. The core area diameter, as stated in Chapter 4, was measured by fitting a circular template to the largest dimension of the core in the x-ray picture. The measurement was taken to the nearest 0.5 mm. Figure 5.12 is a plot of this central core damage area diameter versus impact velocity for all specimens in the damage resistance part of the study.

The first detectable signs of damage occured at approximately 25 m/s. Punch-through occured at approximately 55 m/s. Punch-through is defined as the passing of the ball through the laminate and is detected by penetration of a thin paper sheet taped to the back surface of the specimen.

5.1.2 Cylinder Structures

The damage state in the circular cylinder specimens consists of the same phenomena found in the flat plate specimens: matrix yielding, fiber breakage, delamination, and fiber bundle disbonds. The curvature of the cylinder, however, has the effect of containing the damage in a more local area than the plate specimens.

Figure 5.13 is a dye penetrant enhanced x-ray of a cylinder impacted at 66.8 m/s. This specimen was impacted on a 45° ply seam. The damage shown in the x-ray for the cylinder sections was more contained around the core region than the plate specimens. The fiber bundle disbonds that were

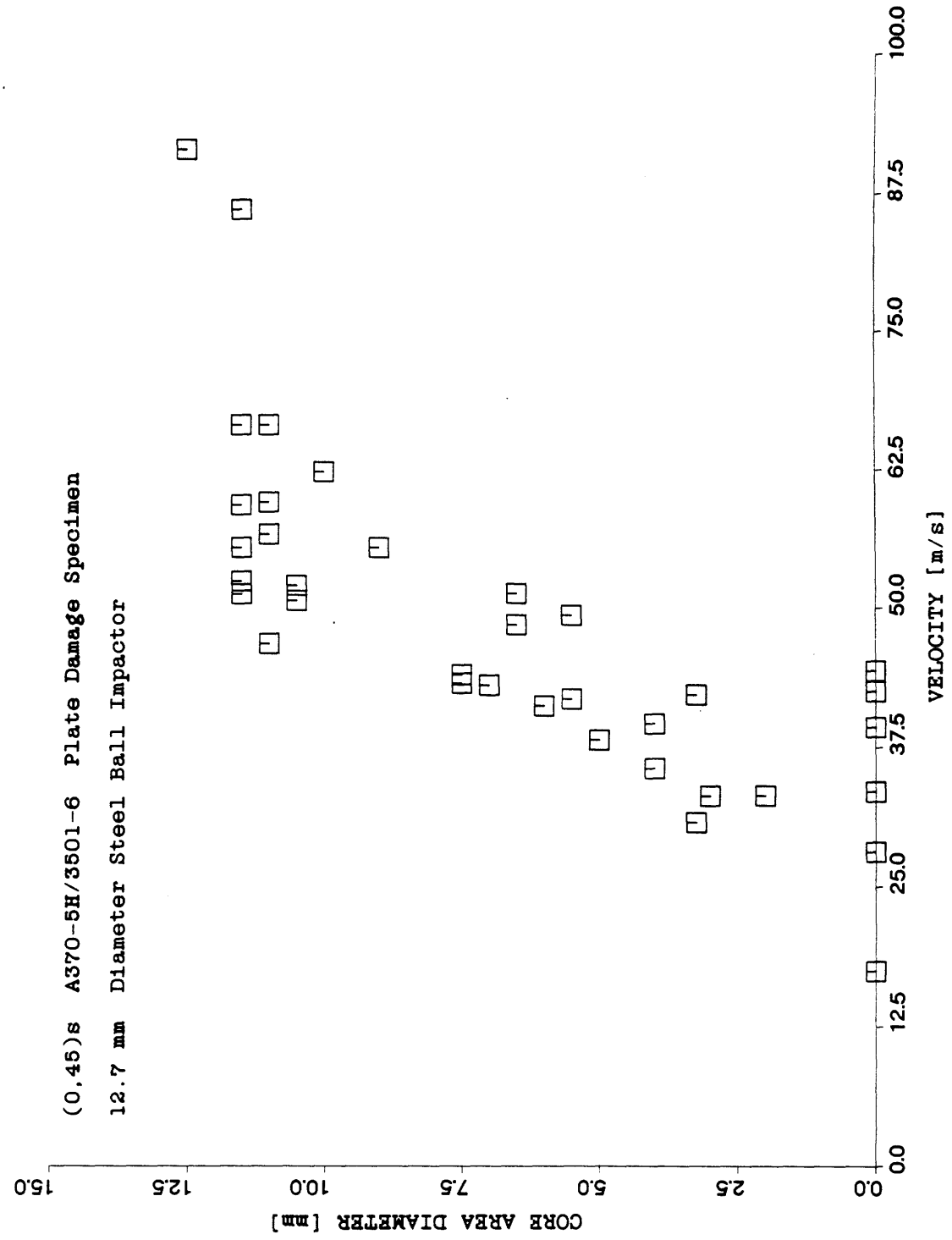

Figure 5.12 Core Damage Diameter versus Impact Velocity for Fabric Plate Damage Characterization Specimens

Figure 5.13 X-ray Picture of Cylinder Section Specimen Impacted at 66.8 m/s

prominent in the plate specimens no longer were a significant part of the damage area. Delamination was not as evident as it was for the plate geometry.

The results from the epoxy burn-offs reveal that for low impact velocities, fibers in a single ply can be broken in the hoop direction without damaging fibers in the longitudinal direction. Figure 5.14 is a plot of fiber breakage versus impact velocity for the cylinder specimens. No damage to the fibers is found until the velocity of the impactor is greater than approximately 40 m/s.

Another observation made for the cylinder geometry was that the damage that existed at very high punch-through velocities was cleaner than that observed for a plate impact at the same velocities. The delamination and fiber bundle disbonds became less prominent in the overall damage assessment after punch through. This is shown in the x-ray of Figure 5.15 where the core damage area dominates the damage, as opposed to Figure 5.16, where delamination and fiber bundle disbonding around the impact area comprises a greater part of the total damage state than the core damage area. Thus the impact damage became cleaner and was dominated by the core damage for high punch through velocities.

As with the plate specimens, the dark region in the center of the impact area on the x-ray photographs was defined as the core area. The x-ray information showed that the shape of the core area was circular. The cylinder core area was measured using the technique outlined for the plate

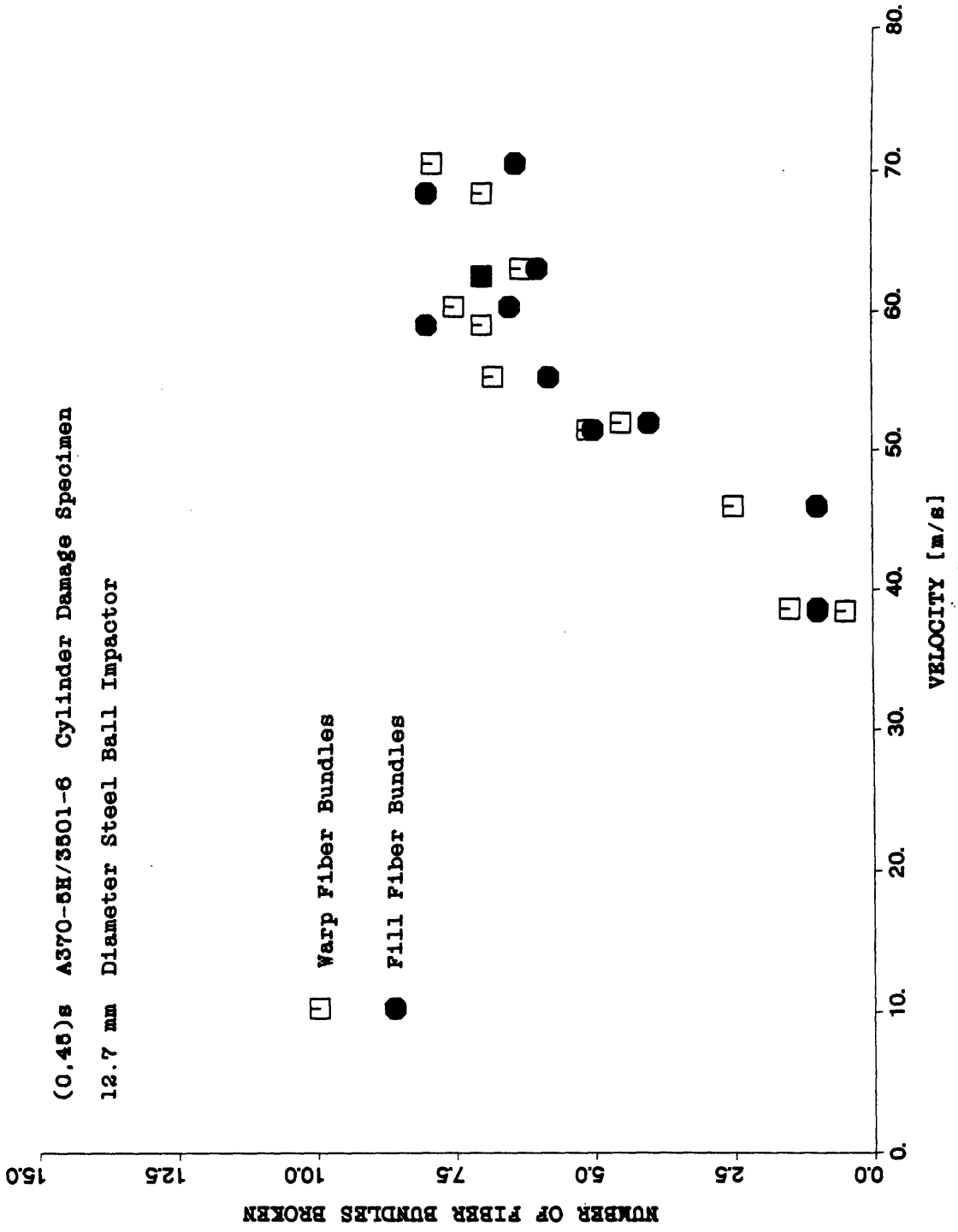

Figure 5.14 Fiber Breakage versus Impactor Velocity for Fabric Cylinder Damage Characterization Specimens

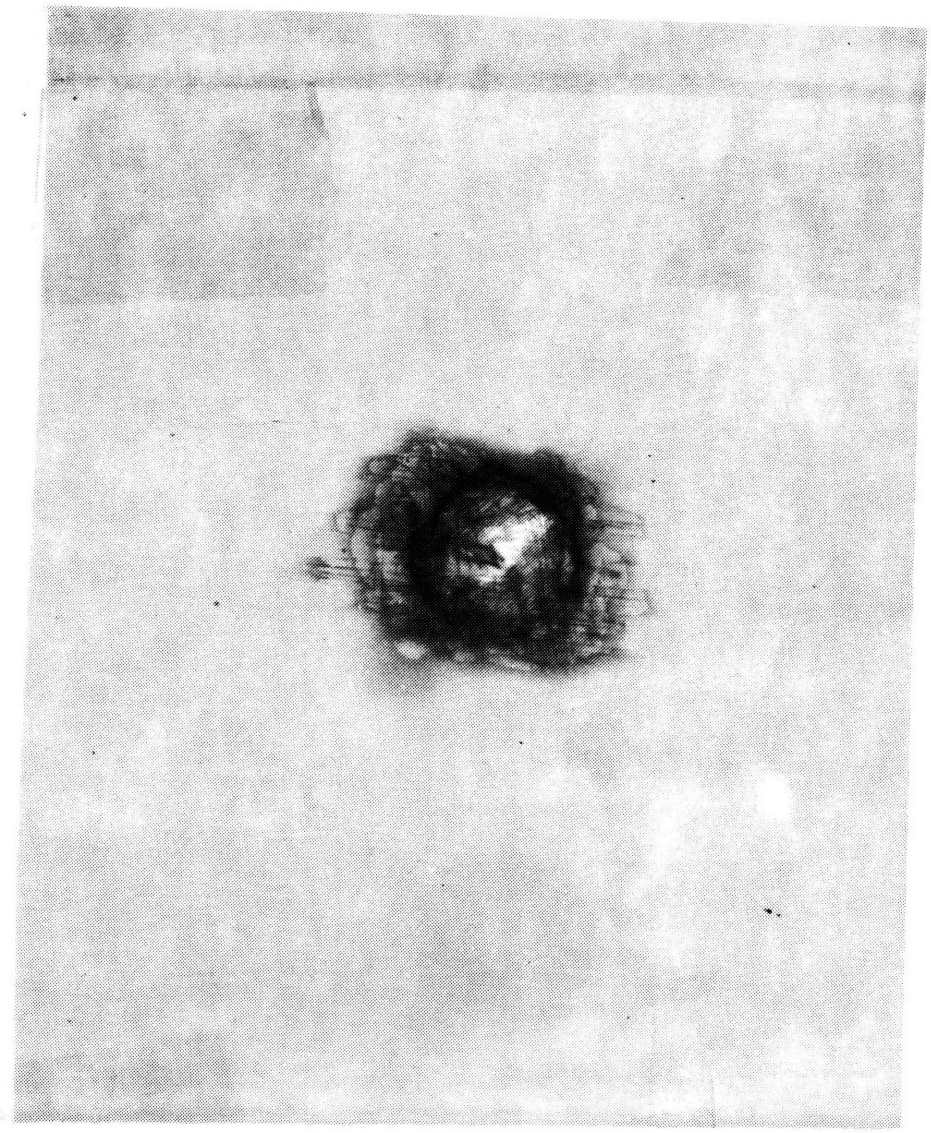

Figure 5.15 X-ray Picture of Fabric Cylinder Section Impacted at 63 m/s Showing Contained Punch-through Damage

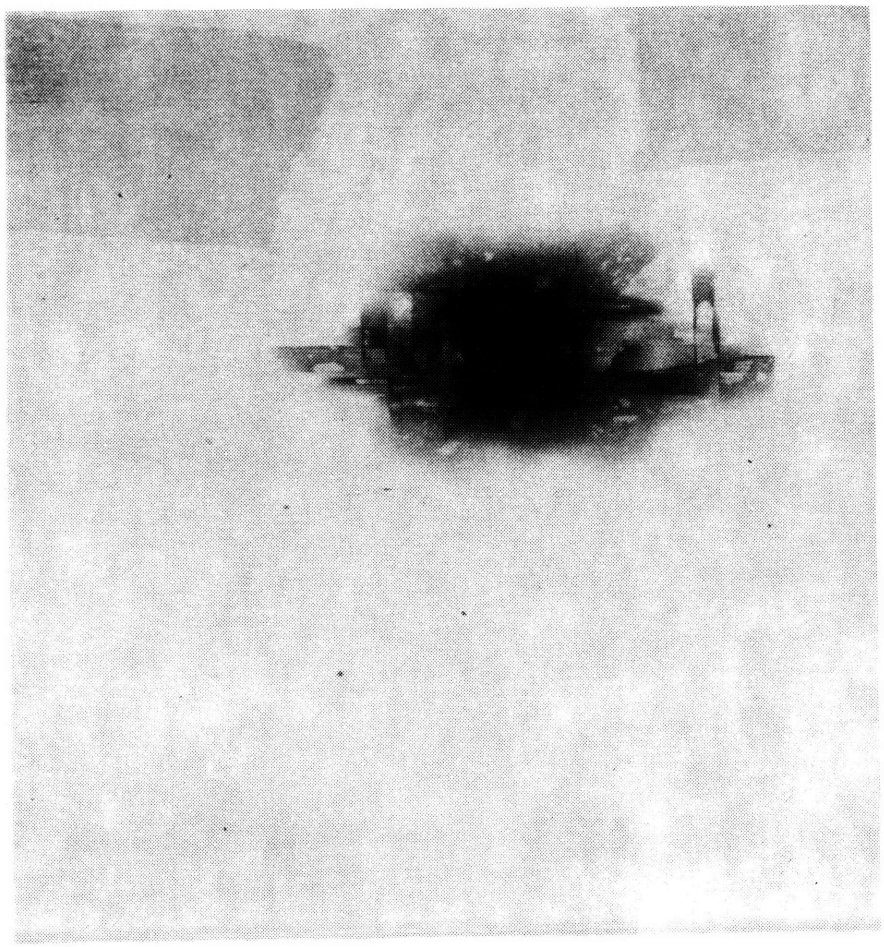

Figure 5.16 X-ray Picture of Fabric Cylinder Section Impacted at 55 m/s Showing Pre-punch-through Damage

specimens. Figure 5.17 is a plot of the core area diameter versus impact velocity for the cylinder specimens. No damage is detected until the impactor velocity reaches approximately 40 m/s. Punch through of the cylinder occurs at approximately 70 m/s.

5.2 Failure of Specimens with Implanted Delaminations

The purpose of the delamination implant study was to determine the effects of delamination on the tensile strength of fabric laminates. The implants were models of the delamination that was found to exist in the impacted specimens. These tests isolated one aspect of impact damage in an effort to pinpoint the important mechanisms involved in the reduction of the unflawed strength of impacted laminates in tension.

The delamination implant sizes and locations had no observable affect, within experimental scatter, on the tensile strength of the laminates. The failure stress versus delamination size for all of the implanted specimens is shown in Figure 5.18. The average failure stress of these specimens was 540 MPa with a coefficient of variation of 6.6 %. The average failure stress of the all $(0,45)_s$ unflawed specimens was 583 MPa with a coefficient of variation of 6.2%. The measured thickness of the specimens was used for stress calculations. APPENDIX D contains a listing of the data obtained for the delamination implant study.

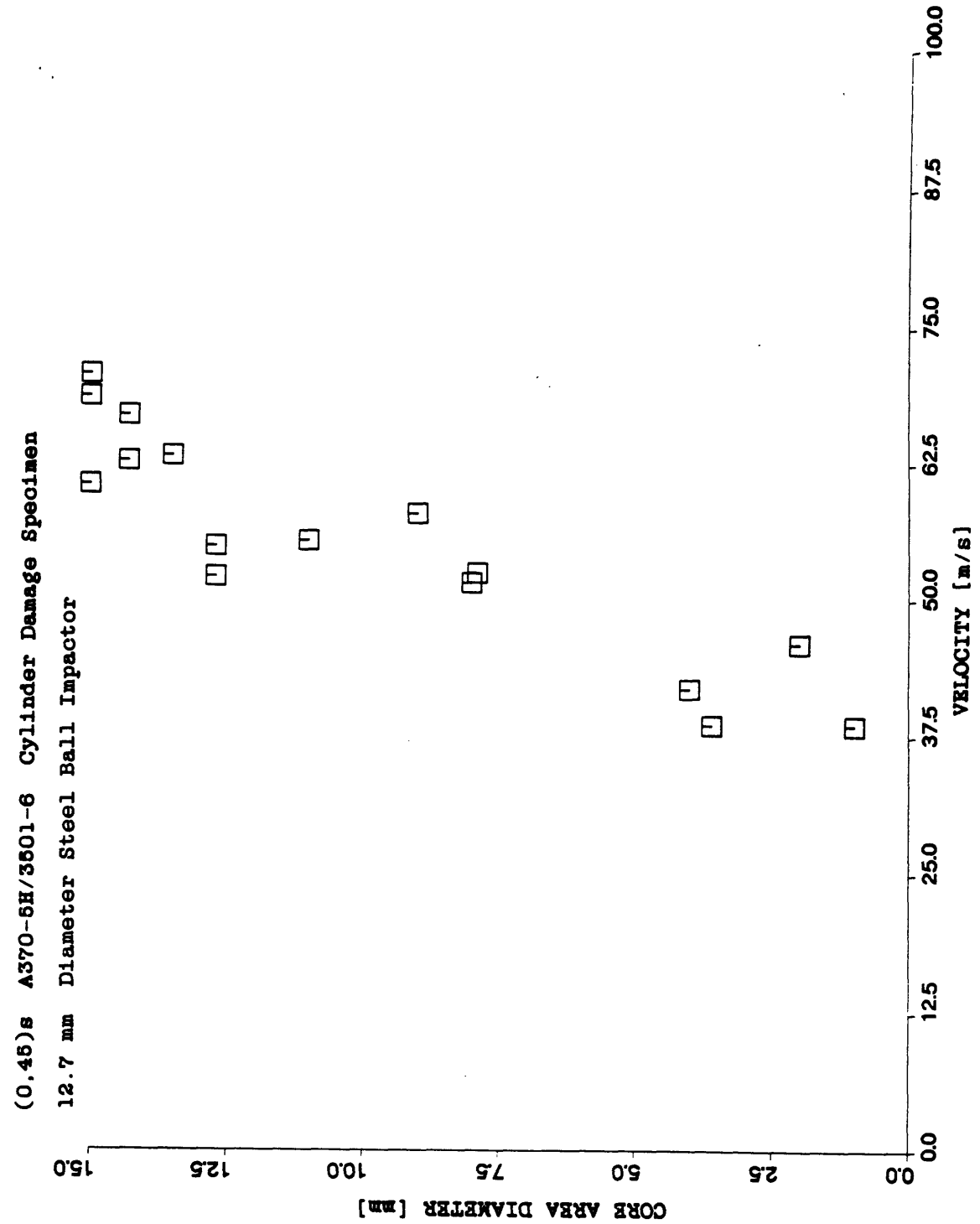

Figure 5.17 Core Damage Area Diameter versus Impact Velocity for Fabric Cylinder Damage Characterization Specimens

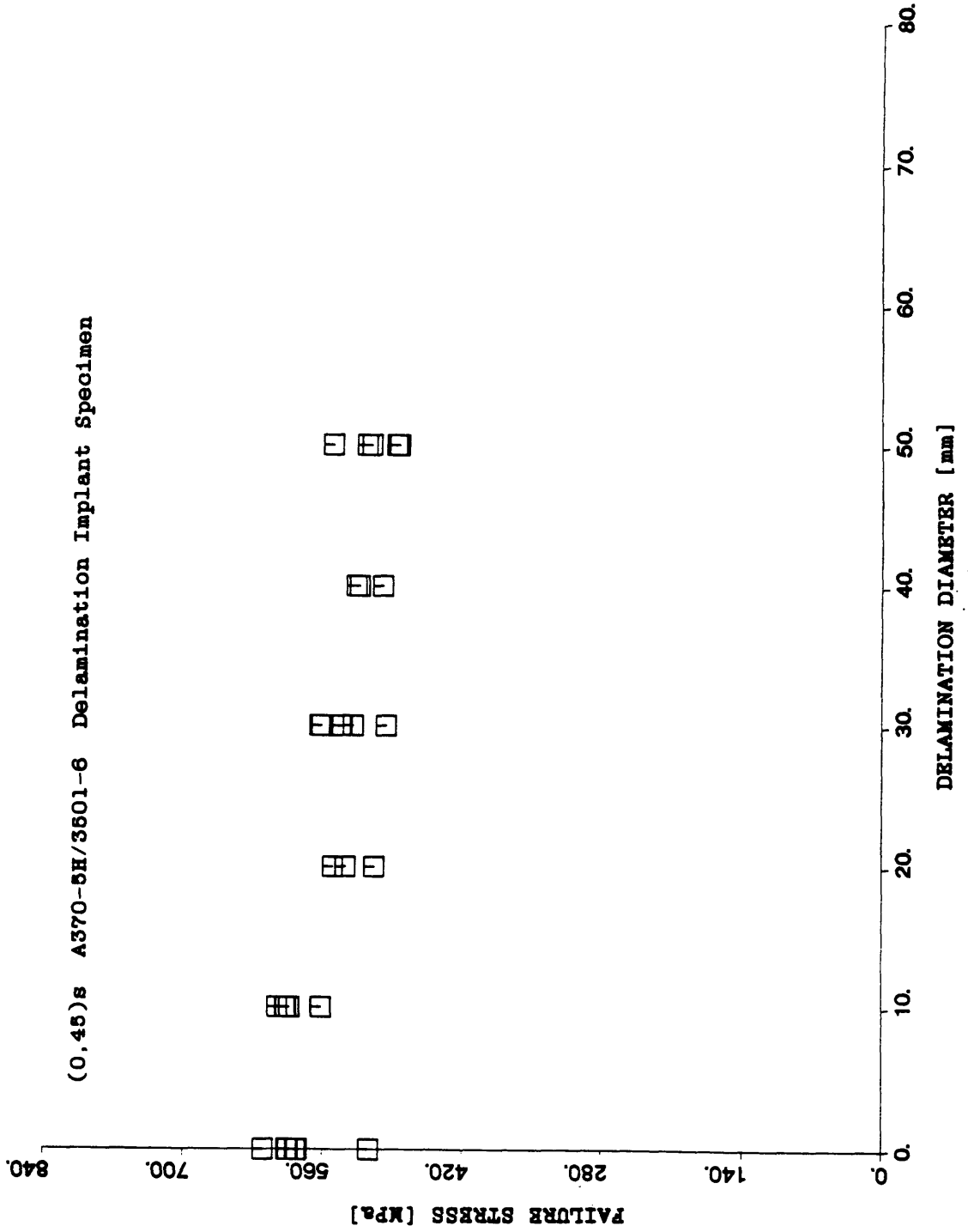

Figure 5.18 Failure Stress versus Delamination Size for Implant Study Specimens

The implanted delamination specimens failed by in-plane fracture of the outer zero degree plies. A typical failure is shown in the photograph of Figure 5.19. Failure of the implanted specimens is essentially the same as the unflawed specimens. Failure did not typically occur at the delamination implant area except for the specimens with 50 mm delaminations at all ply interfaces. Growth of the delamination could not be detected during tensile loading of the specimens.

The information obtained by this study showed that delamination had little effect on the strength of the laminates and could be neglected in modeling the impact damage for tensile loaded specimens. Predictions of the residual strength of tensile loaded fabric laminates could therefore be based on fiber damage only.

5.3 Damage Tolerance of Impacted Fabric Plates

5.3.1 Strain Gage Data

The strain gage data obtained for the tensile test of a typical impacted specimen is shown in Figure 5.20. The impact damage did not have a consistent measurable effect on the strain field in comparison to the far-field data. The measured strain near the impact site was not significantly higher or lower than the far-field strain. Furthermore, no difference between the front and back surface strain readings

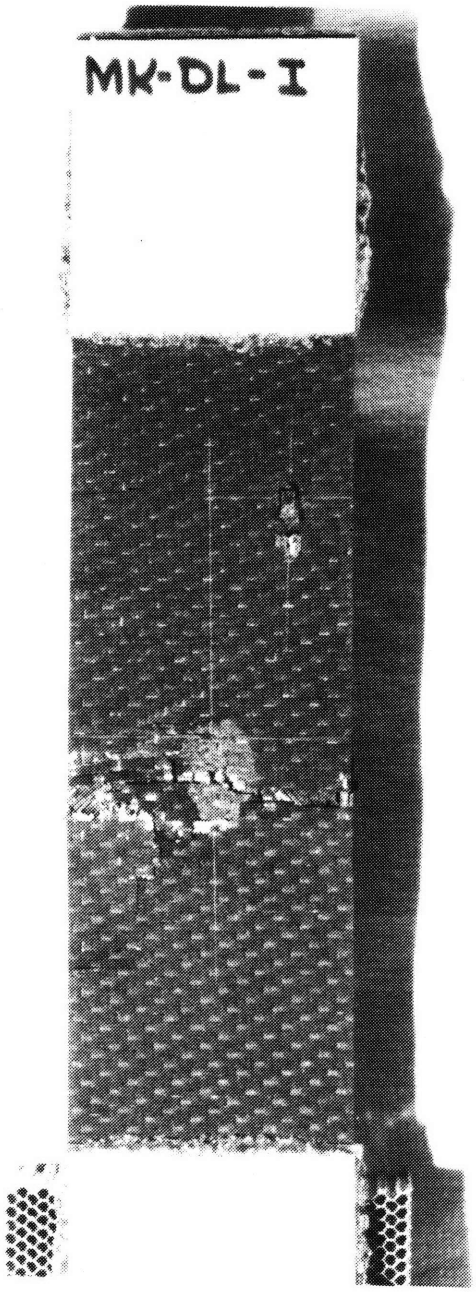

Figure 5.19 Photograph of Typical Implanted Delamination Specimen Failure

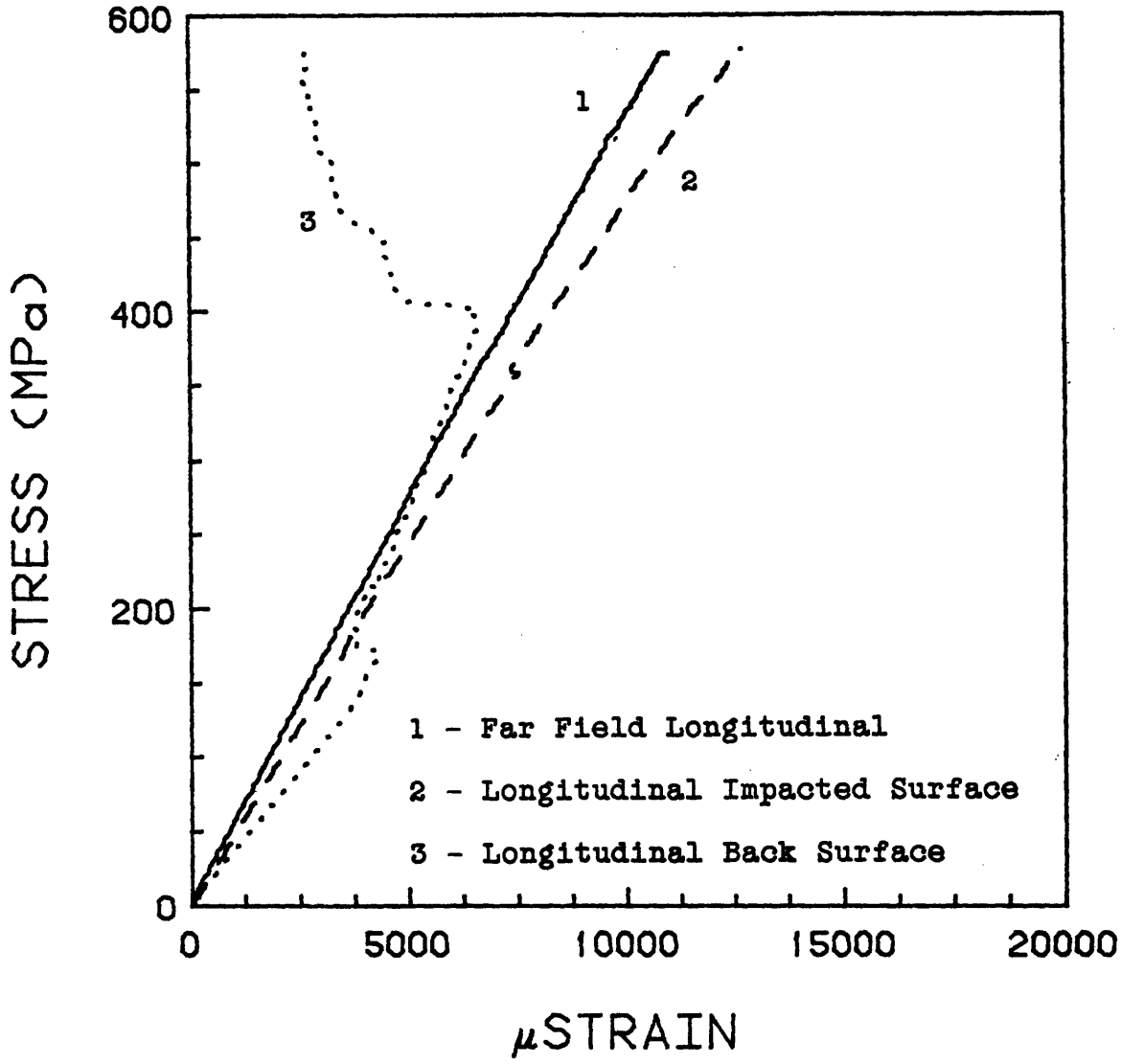

Figure 5.20 Typical Strain Gage Data for Impacted Plate Specimen

was observed that would indicate local bending around the impact area.

The possible explanation for the lack of any significant change in the strain field was the strain gage location. In the effort to prevent the strain gage adhesive from filling the impact damage area, the gage may have been placed too far from the impact area to detect any changes in the strain field. Also, the size of the gage element may have been too large, resulting in a strain reading averaged over too large an area. This is also evidence that the region where the impact damage affects the strain is small in that the impact effects on strain are negligible beyond 2 to 5 mm away from the impact damage area.

The average longitudinal modulus of the flat plates, as computed from the far-field strain gage linear region data, is 53.2 GPa. The coefficient of variation of the modulus is 8.7 %. The value of the longitudinal modulus calculated from basic ply properties is 51.2 GPa. Total specimen elongation was not monitored; therefore, no conclusions may be made on the effects of impact on the compliance of the full plate.

5.3.2 Failure Modes and Stresses

The residual strength, or damage tolerance, study of graphite/epoxy fabric laminates exhibited many of the same trends found by Cairns [1] for graphite/epoxy tape laminates. The common trends found were the existence of a threshold

impact level where degradation of the unflawed strength was first observed and a leveling off of the reduction in strength at higher damage levels.

Figure 5.21 is a plot of the post impact strength of the plate versus the core area diameter. This plot represents the measure of the damage tolerance of the fabric $(0,45)_s$ plate specimen. The residual strength decreases with increasing core damage. A threshold of strength reduction is evident at approximately 3 to 4 mm of core area damage. APPENDIX B contains a full listing of the information gathered from this study.

The failure modes of the impacted plate specimens were dependent on the amount and type of damage inflicted on the coupons. In all cases, final failure was governed by the in-plane fracture of the two outer zero degree plies.

The unflawed specimens failed exclusively by in-plane fracture of the zero degree outer plies with a fracture path perpendicular to the applied load, as seen in the sketch of Figure 5.22 and the photograph of Figure 5.23. The average failure stress for the unflawed specimens was 583 MPa with a coefficient of variation of 6.2 %. Failure stress calculations were based on measured thickness.

The specimens with 12.7 mm drilled holes failed by in-plane fracture of the outer zero degree plies with a fracture path along the 45°, direction as shown in the sketch of Figure 5.24 and the photograph in Figure 5.25. The failure stress for the drilled hole specimens was 329 MPa with a

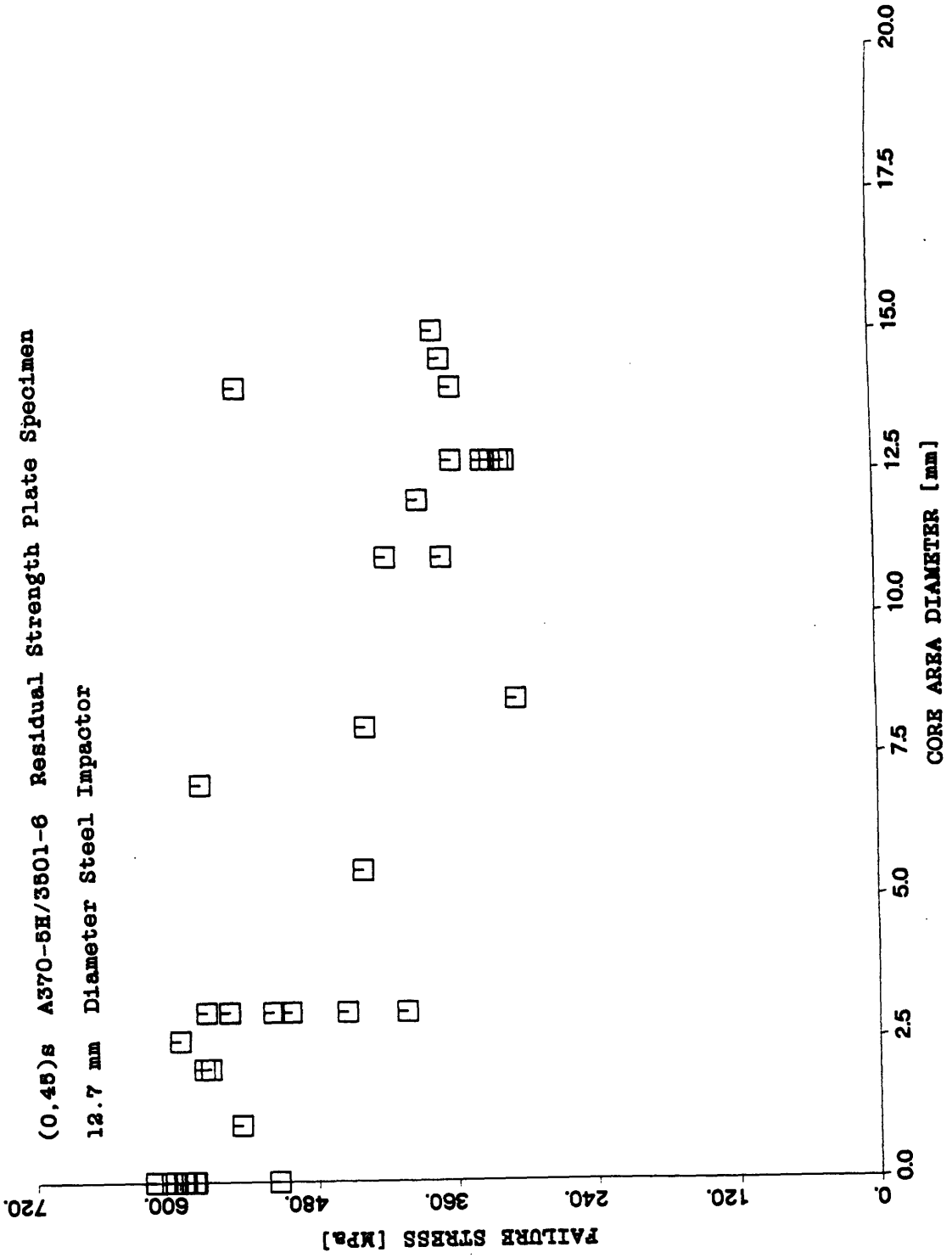

Figure 5.21 Plate Residual Strength versus Core Area Diameter

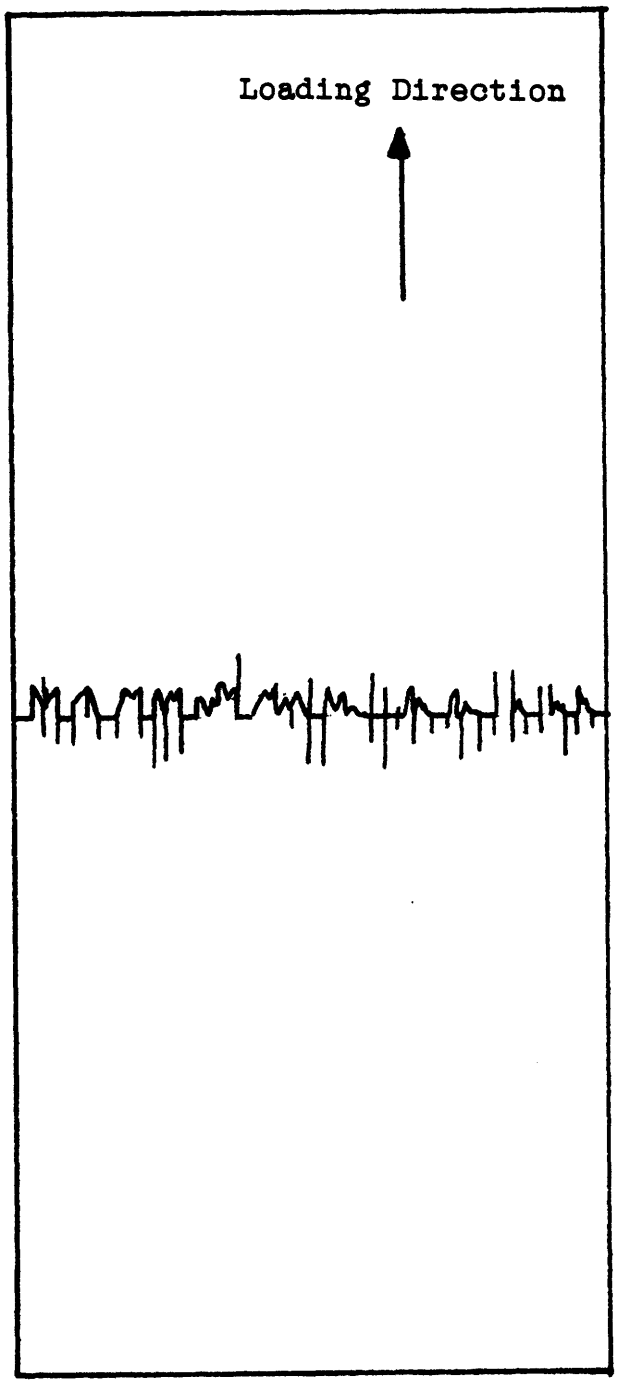

Figure 5.22 Sketch of Undamaged Plate Specimen Failure

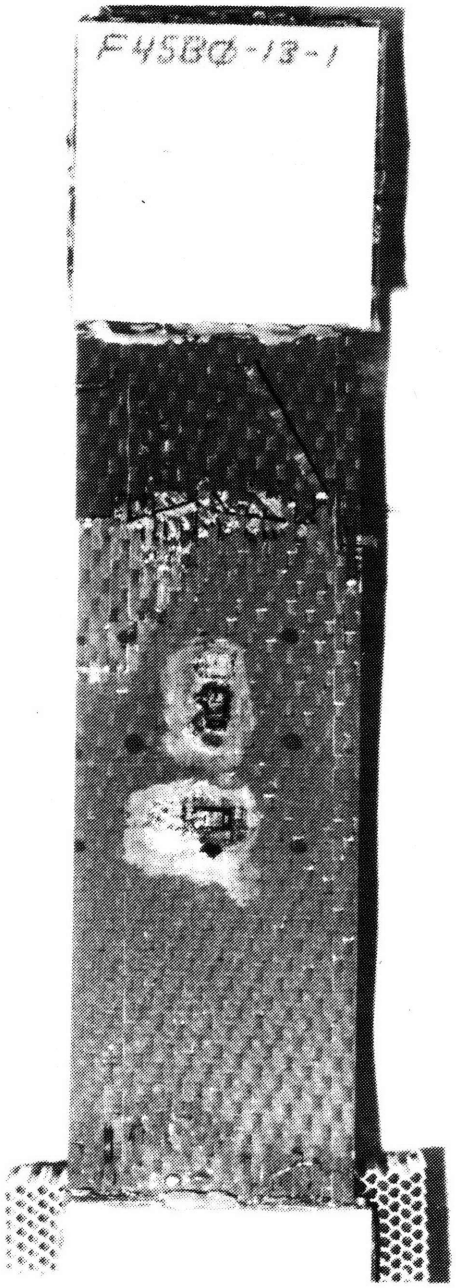

Figure 5.23 Photograph of Undamaged Plate Specimen Failure

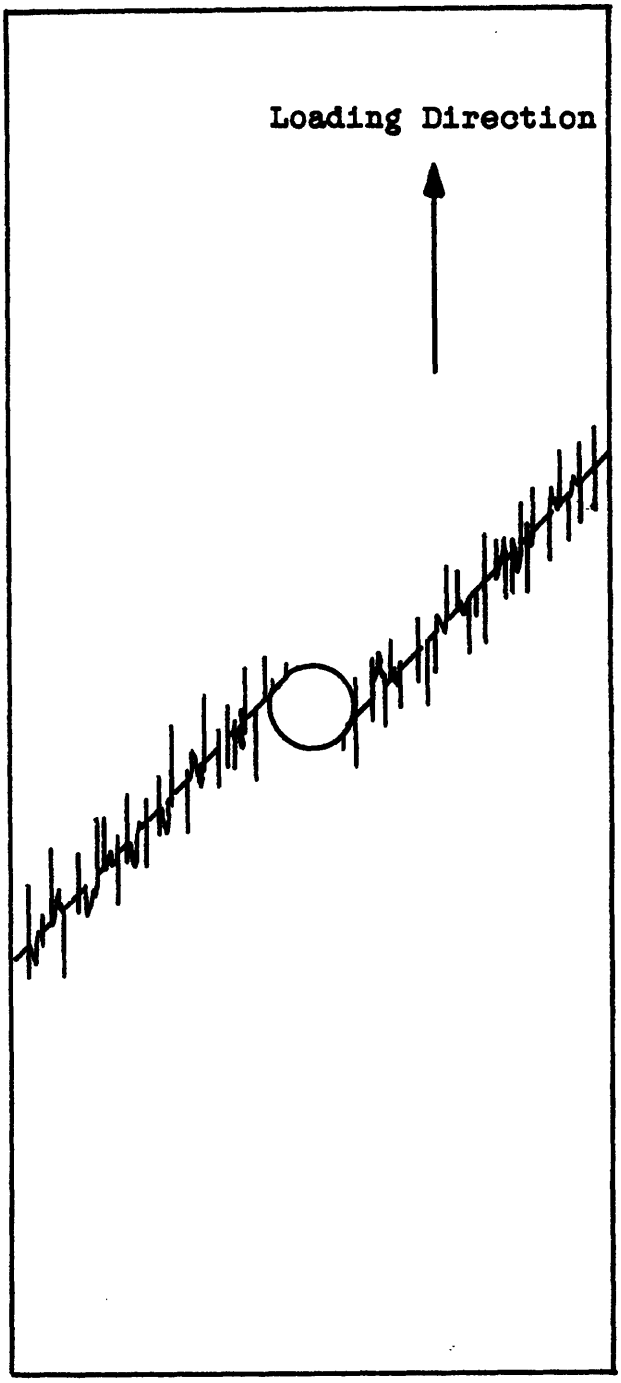

Figure 5.24 Sketch of Failure of Specimen with 12.7 mm Drilled Hole

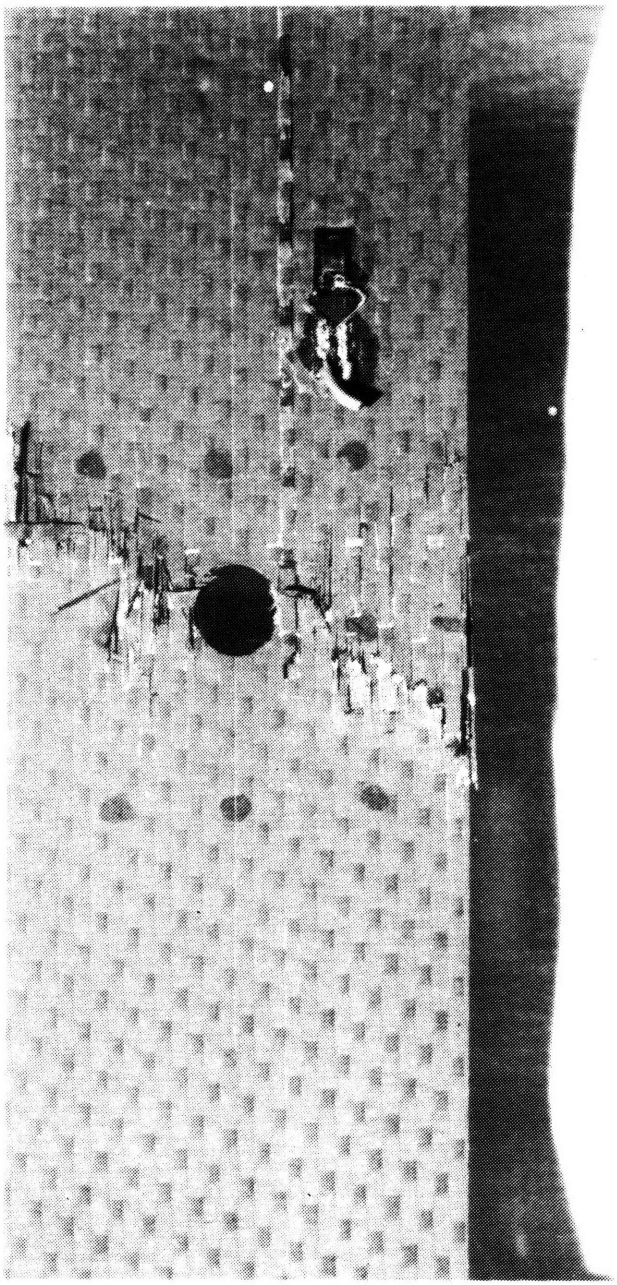

Figure 5.25 Photograph of Failure of Specimen with 12.7 mm Drilled Hole

coefficient of variation of 5.4 %. The drilled hole specimens did not exhibit any delamination growth around the hole area. Delamination was not associated with final failure of the drilled hole specimens to any measurable extent.

The impacted specimens provided the most interesting failures. When loaded in tension, the impacted specimens were found to exhibit visible propagation of the delamination caused by the original impact. This was evident as the specimen was loaded and the outer zero degree plies wrinkled and separated from the inner 45° plies. Figure 5.26 is a sketch of the wrinkling pattern observed on the face of the laminate. The wrinkling occured primarily on the face opposite the impact. The damage resistance studies determined that the greatest amount of delamination and fiber breakage existed on this face. Attempts to capture this phenomenon were performed by manually stopping the tests upon visual wrinkle growth. Figure 5.27 (a-c) is a series of x-rays taken of the same specimen at successive increasing loads. Note how the extent of delamination increased between the original x-ray of 5.26a and the x-ray of 5.26c.

Inspection of the failed impacted specimens revealed through the width delaminations of the specimen at all ply interfaces in the area of the impact accompanied by the failure of the zero degree plies. This failure mode is shown in the sketch of Figure 5.28 and the photograph of Figure 5.29.

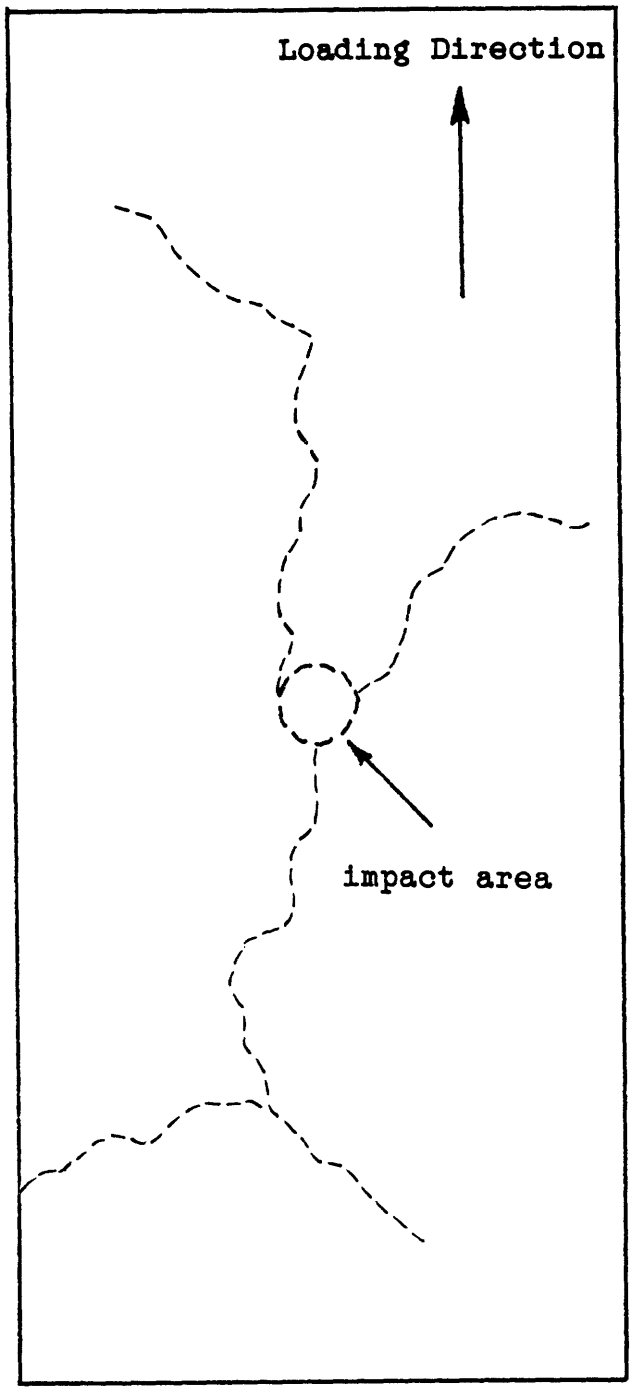

Figure 5.26 Sketch of Wrinkling Pattern on Plate Specimen Face

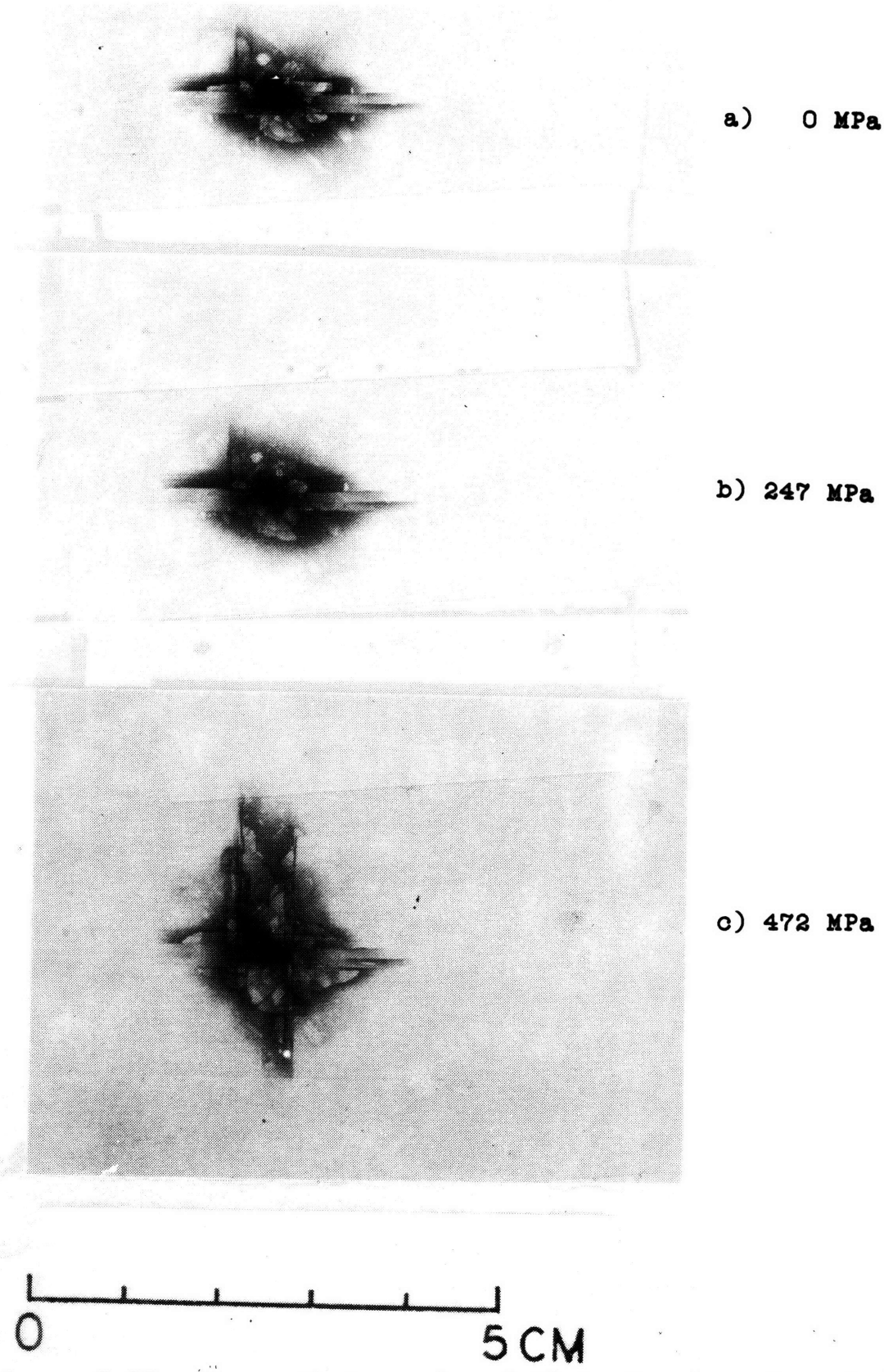

Figure 5.27 X-ray Photographs of Plate Specimen Impacted at 46 m/s at (a) zero stress, (b) 247 MPa, and (c) 472 MPa

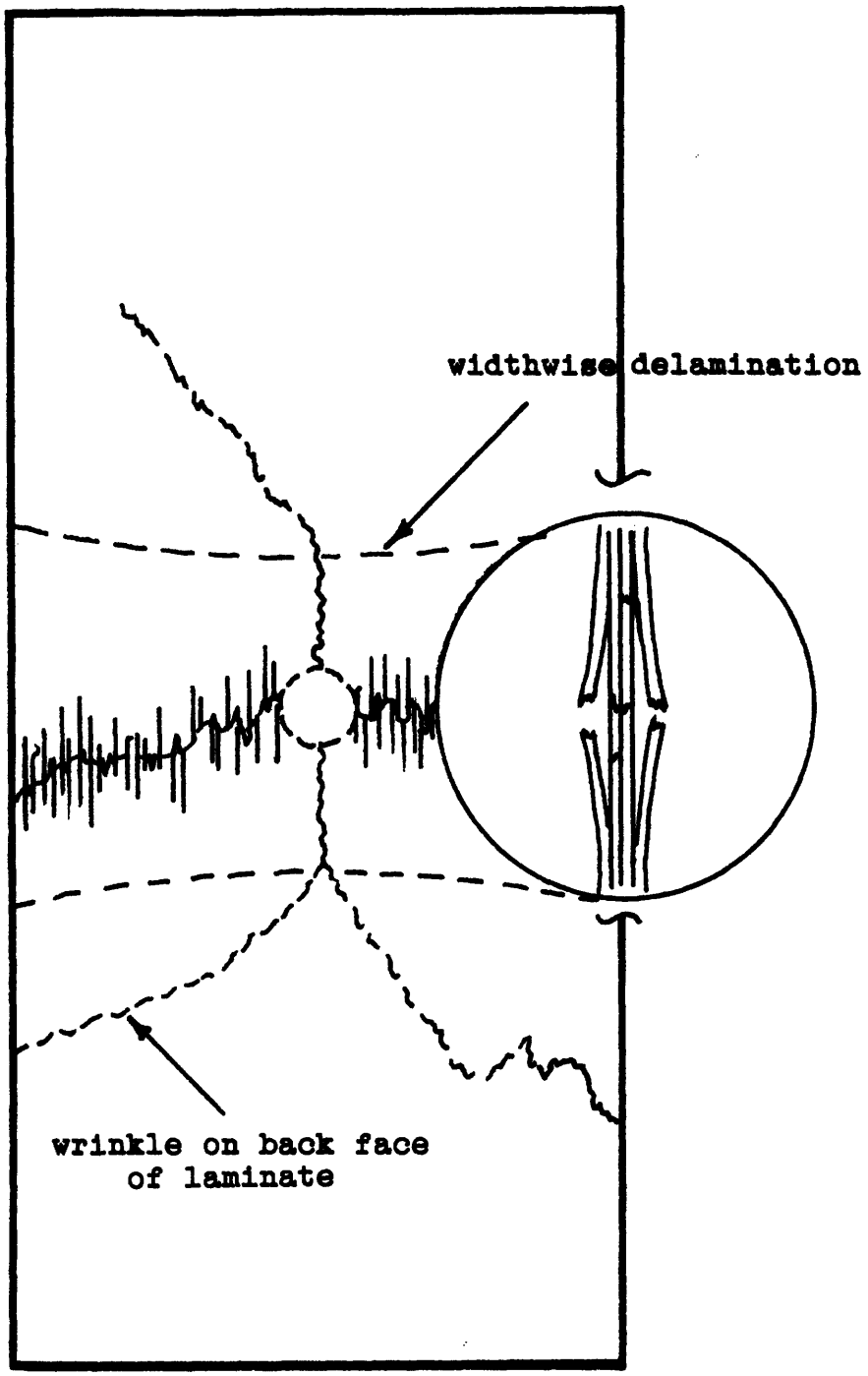

Figure 5.28 Sketch of Impacted Specimen Failure

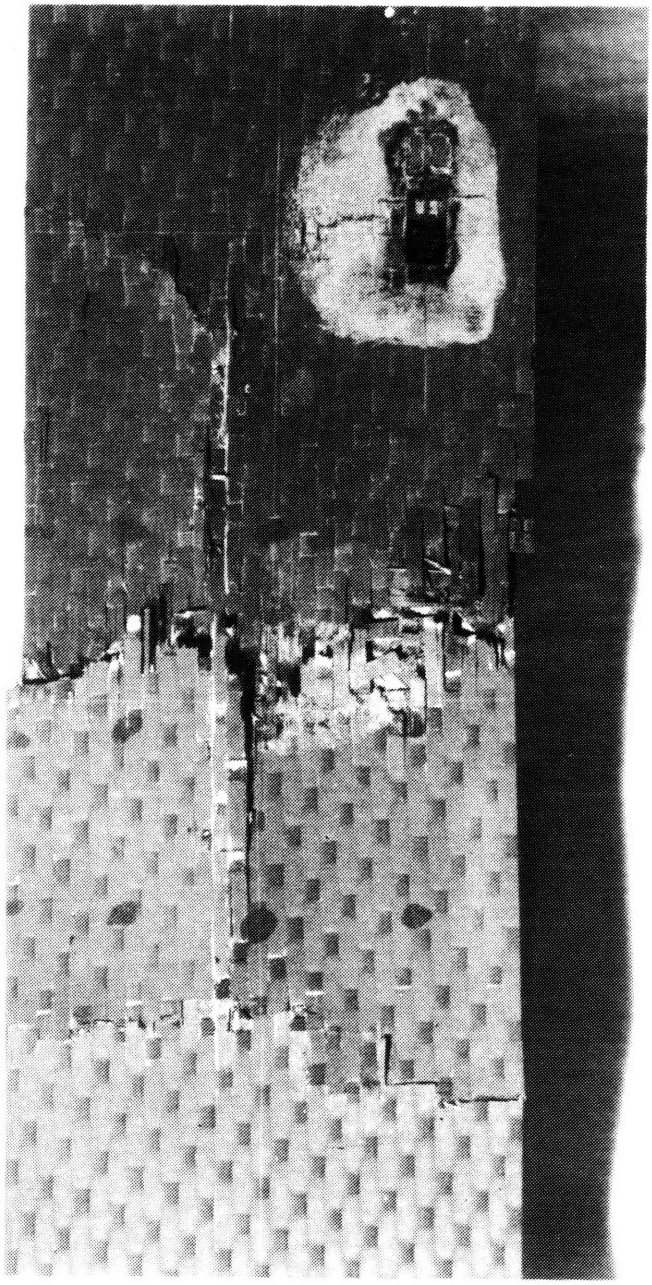

Figure 5.29 Photograph of Failed Specimen Impacted at 46 m/s

5.4 Damage Tolerance of Impacted Fabric Cylinders

The damage tolerance study of pressurized cylinders was subject to two difficulties. The first problem was cylinder seam failure in the unflawed and barely damaged cylinders. This was rectified by the reinforcement design detailed in Chapter 4. The second problem was in controlling the speed and direction of the steel sphere impactor. A degradation in the quality of the bore of the impact gun barrel at this phase of the research often prevented tracking the ball speed. The procedure for obtaining the impact speed of the untracked impacts is detailed in Chapter 4. The variation in the tracked speed of these shots casts considerable doubt on the validity of comparisons based on velocity for the cylinder tests.

5.4.1 Strain Gage Data

Examination of the strain gage data for the flawed cylinders clearly emphasized a difference from the gage data obtained for the tensile plate coupons. Figures 5.30 and 5.31 are typical strain gage plots from an impacted cylinder. The strain gage closest to the impact site indicated that the strain reading was substantially higher in this area. This was attributed to bending at the edge of the damage because of the internal pressure load. Unlike the flat plate, a noticeable difference in the strain field existed near the

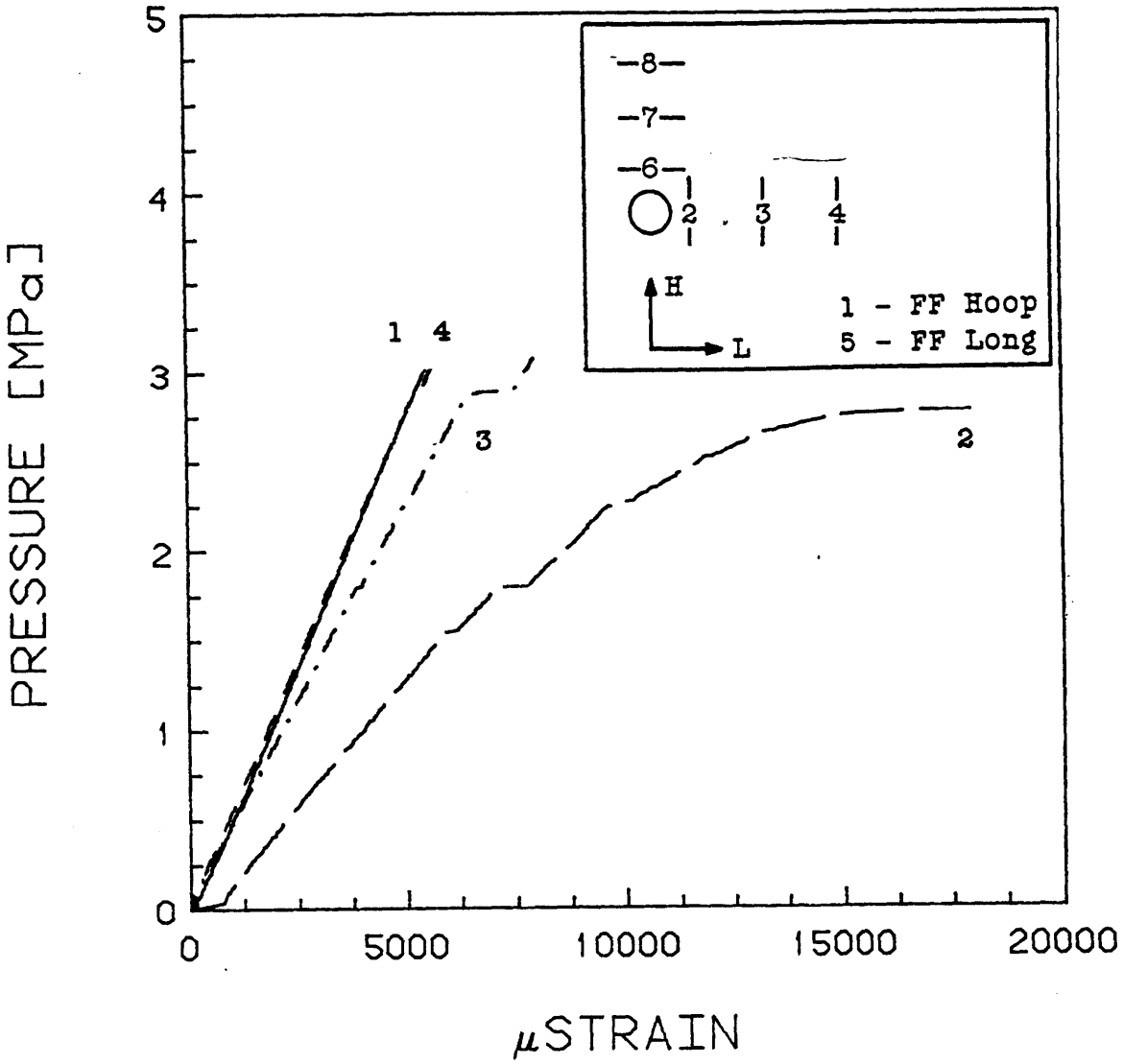

Figure 5.30 Hoop Strain Gage Data for Tube 5 Impacted at 61 m/s

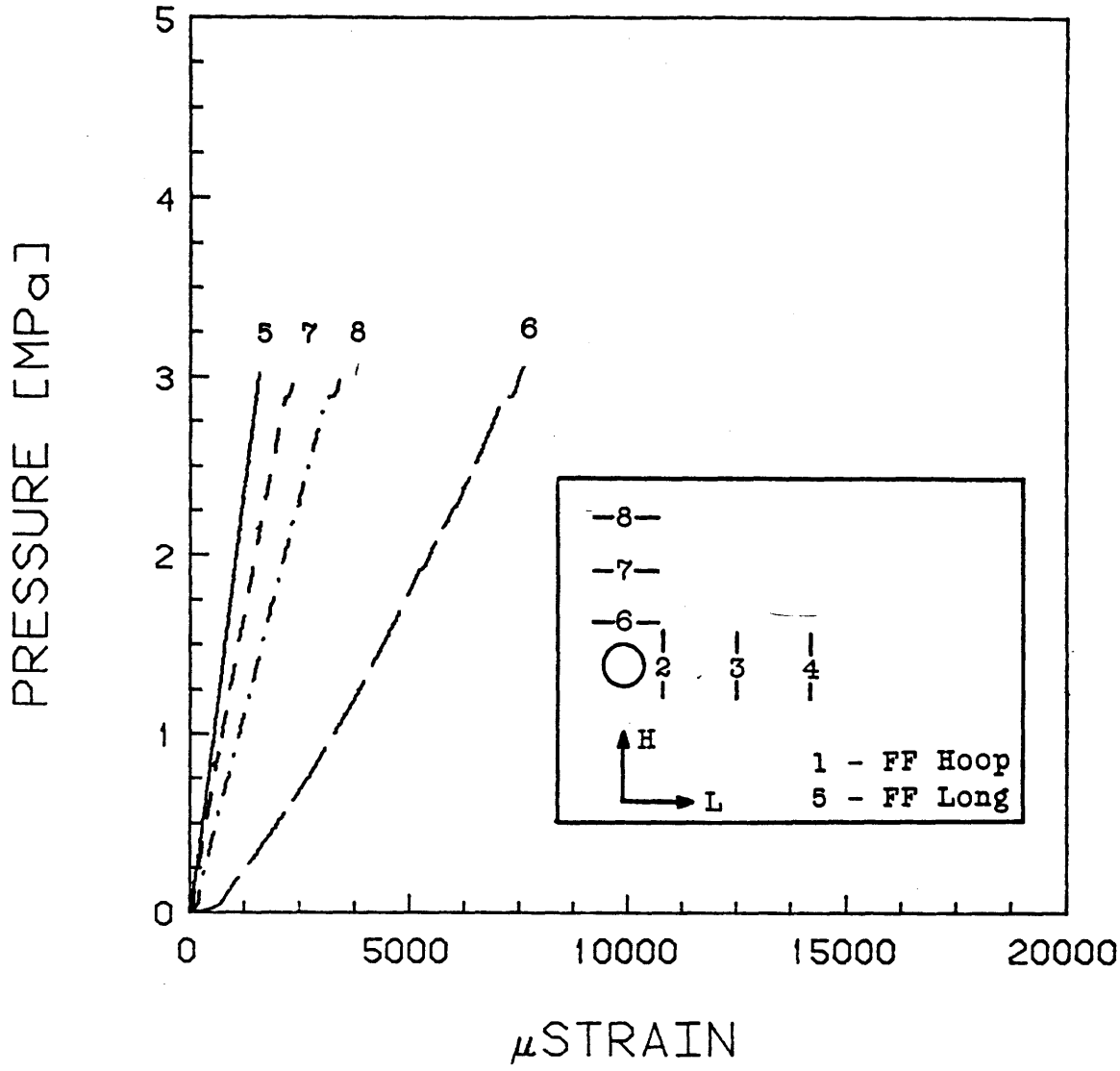

Figure 5.31 Longitudinal Strain Gage Data for Tube 5 Impacted at 61 m/s

impact area. This effect, however, died out within five millimeters of the near impact gage. This is shown by the curves corresponding to the gages located five millimeters away from the near impact gages.

5.4.2 Failure Modes and Pressures

None of the cylinders failed at the endcap attachment. This conclusion was drawn from two observations. One, after the explosion, the endcaps were not displaced from the original pre-test position. In previous tests with endcap failures, the tube assembly had acted as a rocket when one end had failed. Two, the cylinder and reinforcement unzipped from the endcap assembly at the same location on both endcaps. The explanation used for this is illustrated in Figure 5.32: (a) the cylinder fails at the center section; (b) the failure path propagates to the endcap; and (c) the remaining energy peels the cylinder away from the endcaps.

Figure 5.33 is a plot of the pressure cylinder post impact strength versus the visually determined core damage area diameter. As found in the plate specimens, the cylinder residual strength falls off with increasing damage, and a threshold level of residual strength reduction, evident at 5 to 6 mm of core damage. The unflawed cylinders failed at an average of 4.4 MPa internal pressure. APPENDIX C contains a listing of all data obtained for these tests.

The failure mode of the pressurized cylinders was

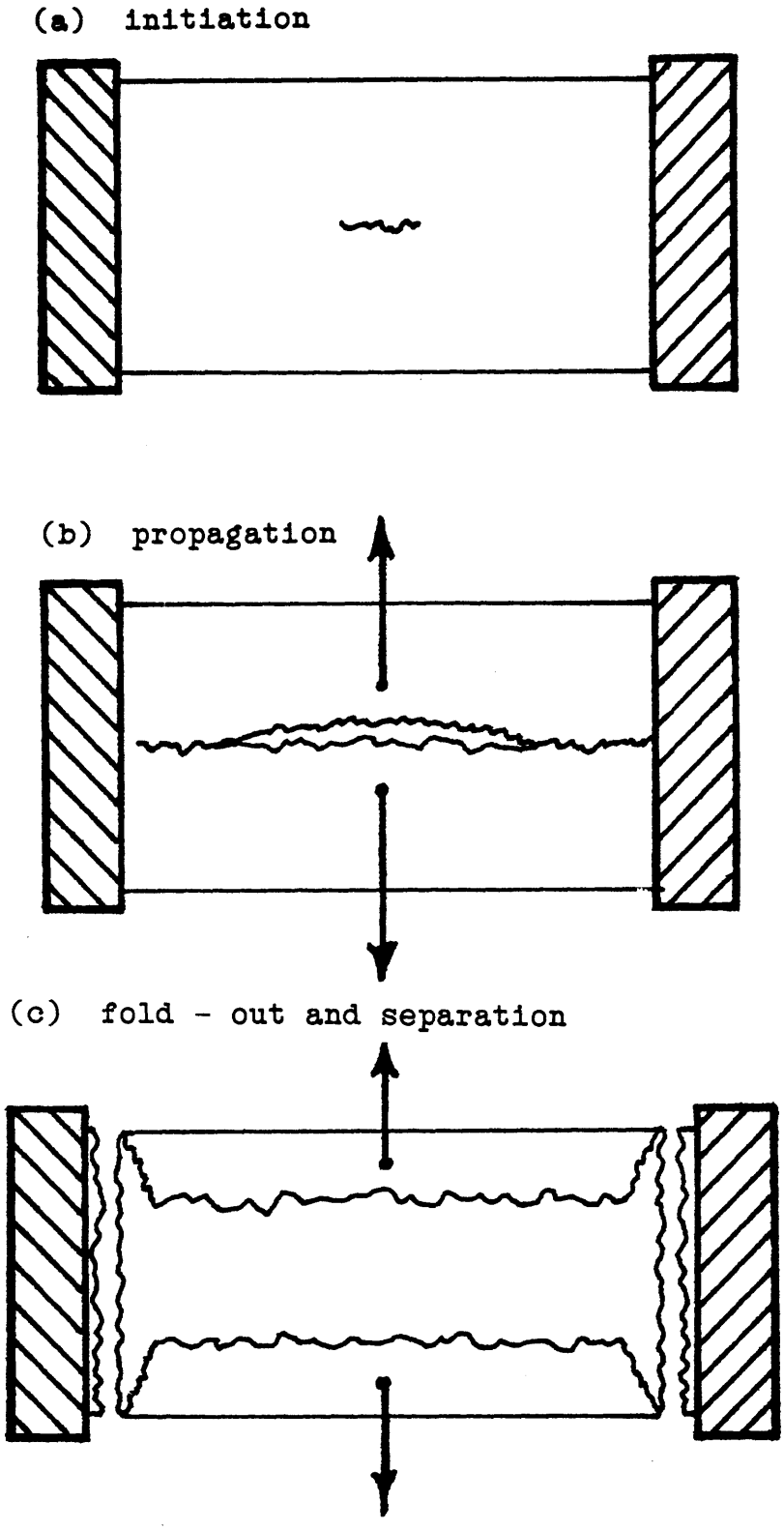

Figure 5.32 Sketch of Sequence of Events for Pressure Cylinder Failure

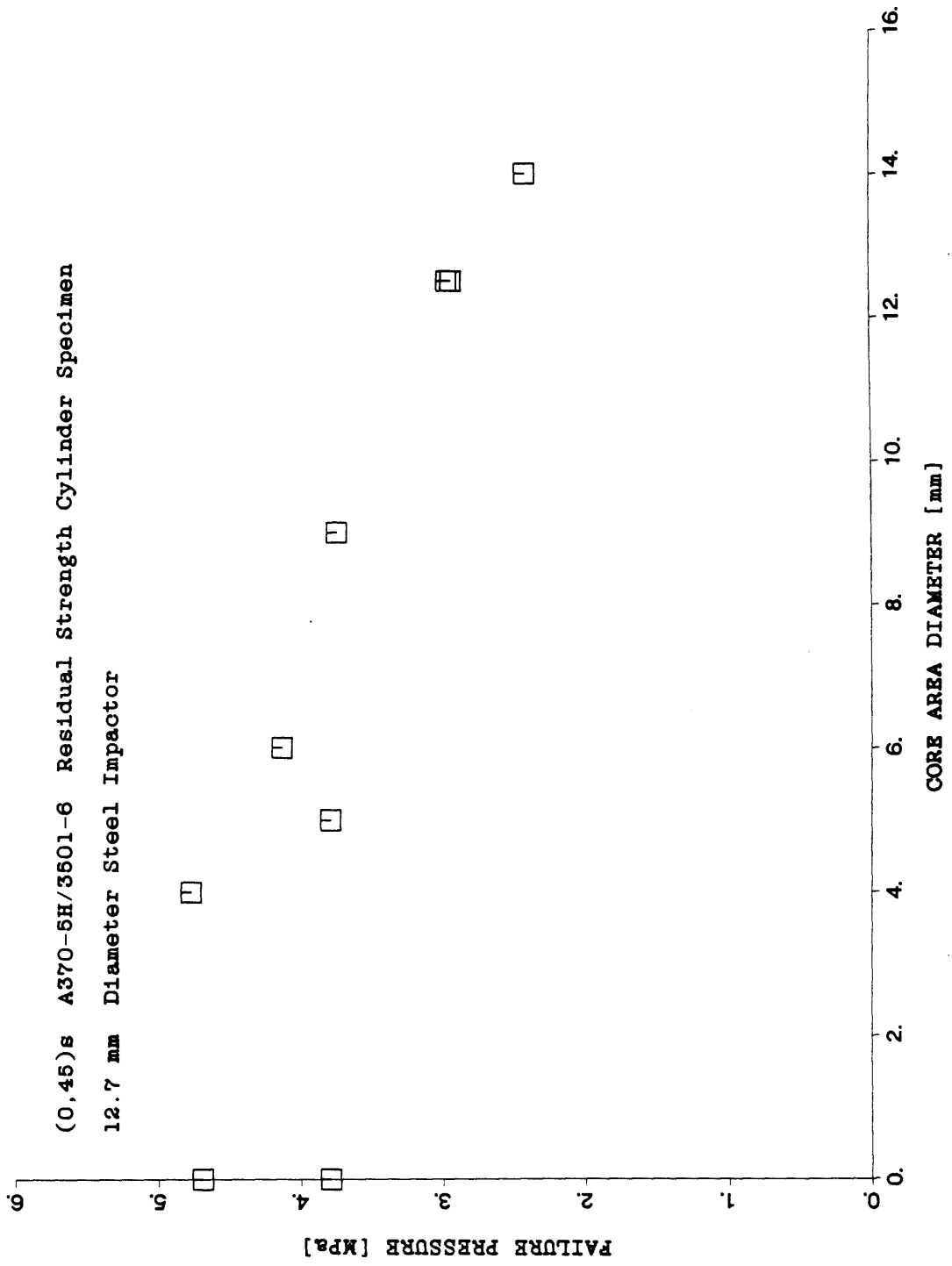

Figure 5.33 Cylinder Failure Pressure versus Core Damage Area Diameter

determined by reconstructing pieces of the failed tube. The large amount of energy released during the failure of the cylinders prevented the observation of clear fracture paths as found in previous studies [29,33,35]. Reassembly of the failed cylinders revealed three different types of failure dependent on the level of damage inflicted by the impact.

Reconstruction of the two unflawed cylinders with seam reinforcements indicated multiple fracture paths. The many broken sections of the cylinder prevented the determination of a single fracture path. In both failures, however, the pieces were broken parallel to the longitudinal direction and 45° seam direction of the cylinder. An idealized sketch of this failure is given in Figure 5.34.

In cylinders with barely visible impact damage on the inside surface, the failure was in-plane fracture parallel to the longitudinal direction of the cylinder. Barely visible damage was defined as (a) damage not being visible on the front surface of the laminate save for a small mark from the impactor and (b) damage that could just be felt by the fingers on the inside surface. This amount of damage corresponded to a core diameter of approximately 1 mm on the cylinder damage characterization specimens. A small crack was also found to propagate parallel to the hoop direction. The photographs of Figure 5.35 show the front and back views of the failed section of the tube containing the impact. Figure 5.36 is a sketch of this type of failure. In the two tubes exhibiting this state of impact damage, Tube 6 failed through the

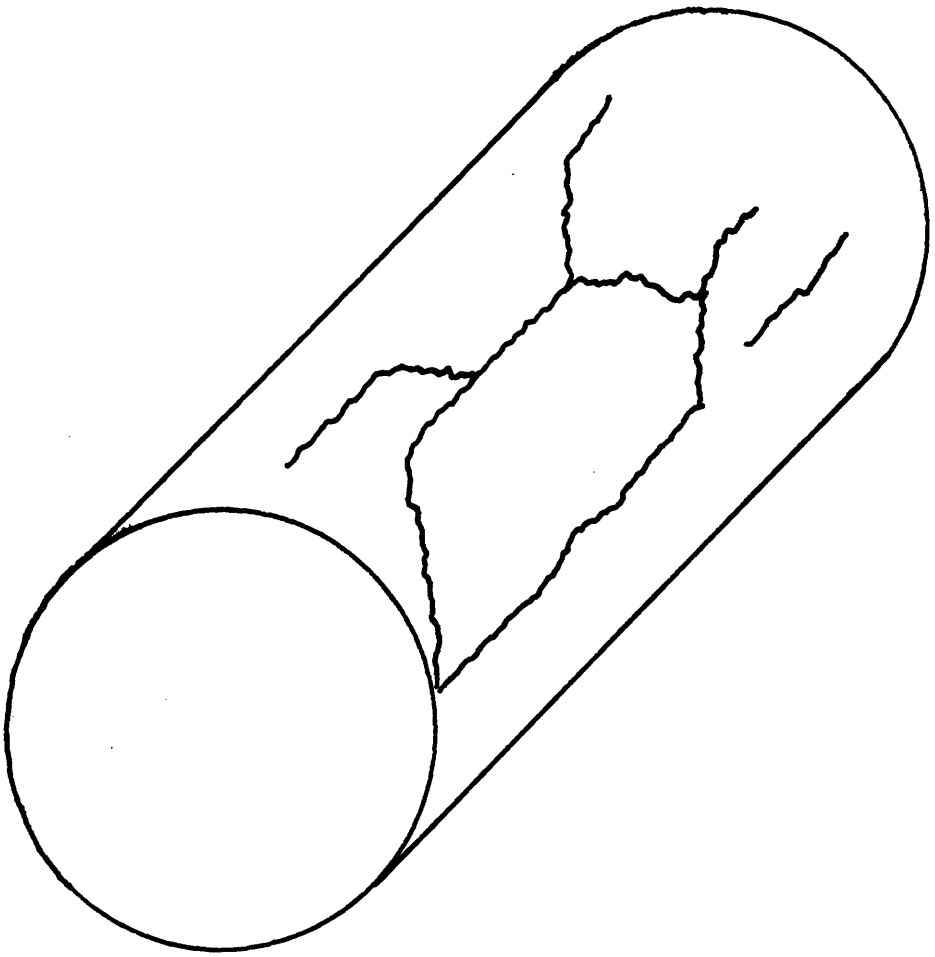

Figure 5.34 Sketch of Unflawed Cylinder Failure

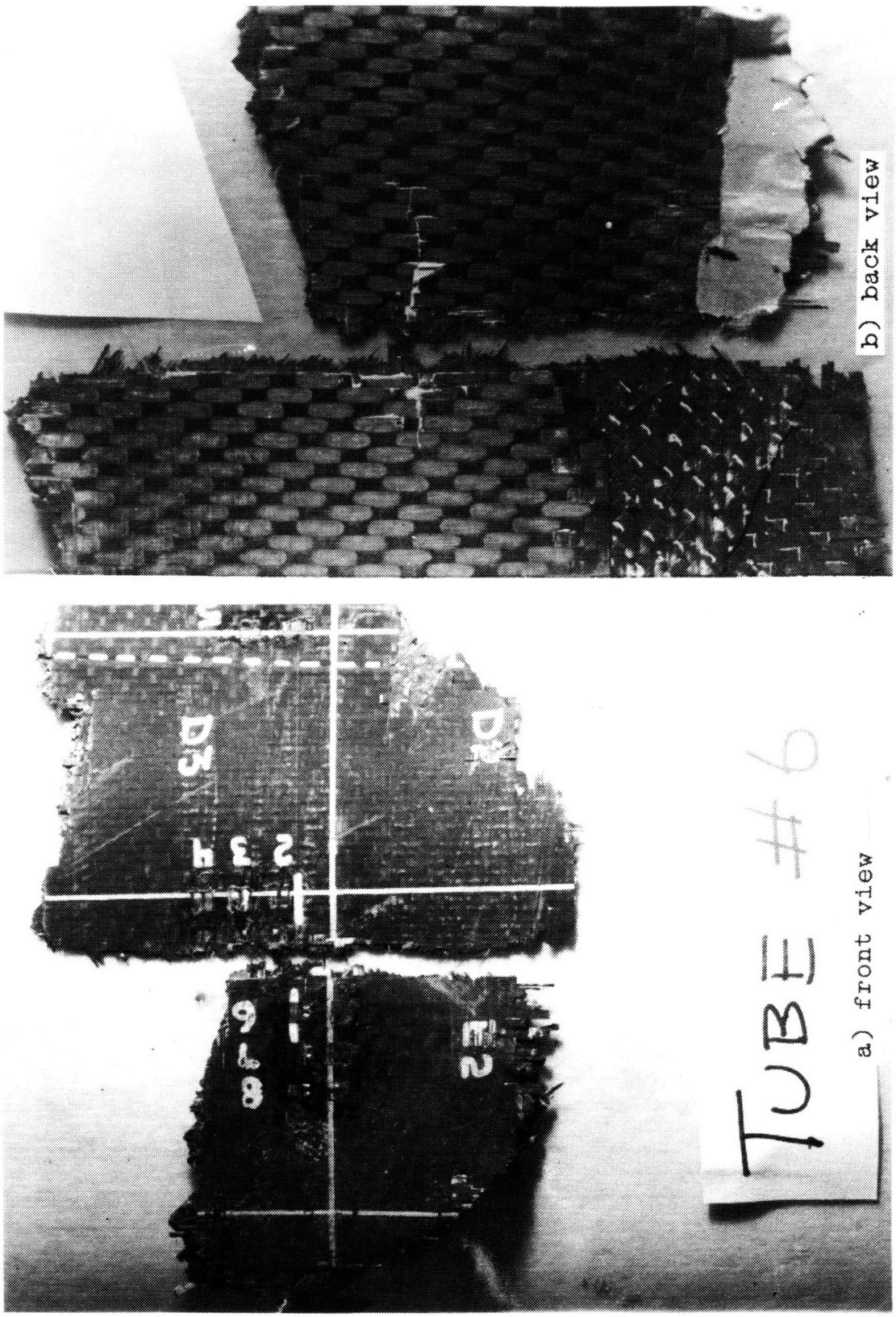

Figure 5.35 Photograph of Tube 6 Failure through Impact Section - a) Front View and b) Back View

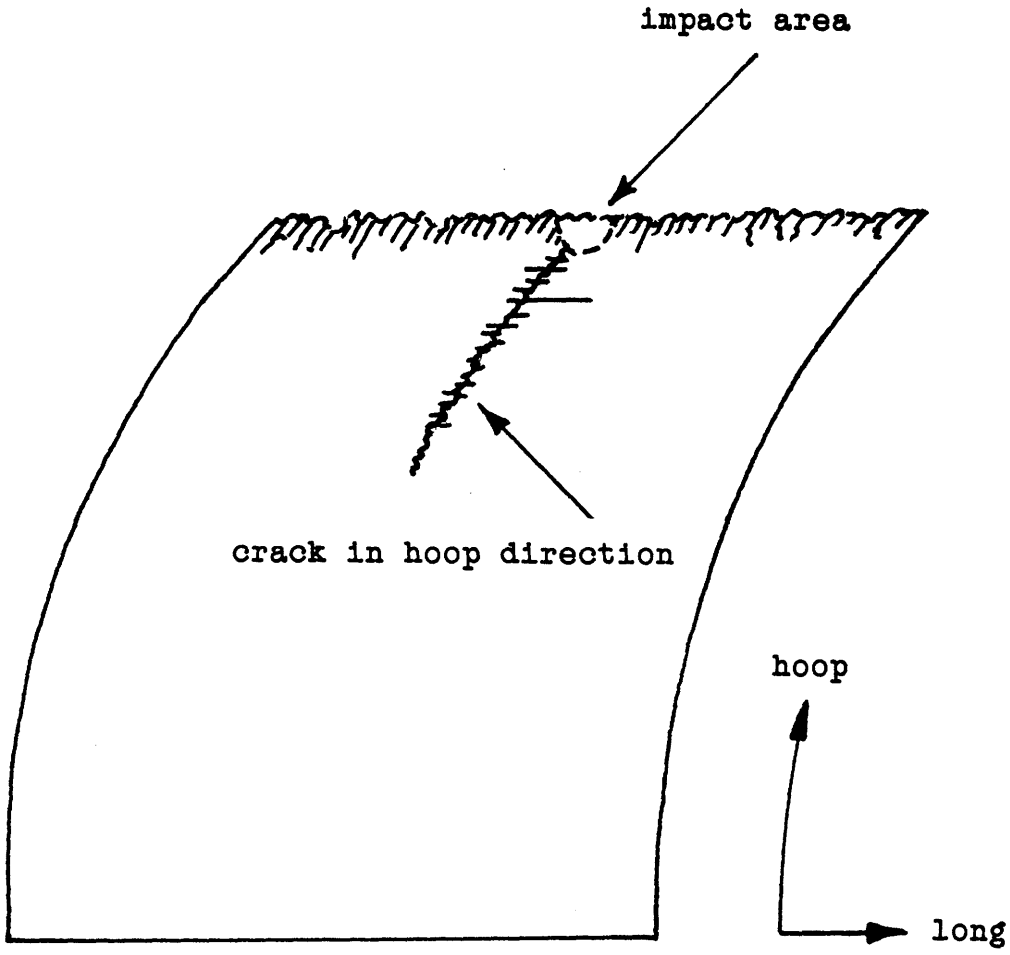

Figure 5.36 Sketch of Cylinder Failure with Small Impact Damage

original damage area while Tube 11 did not fail through the original damage area.

Cylinders with visible front and back surface damage were especially hard to reconstruct. The observation was made that the cylinder wall in the area of the impact had delaminated into four separate plys. In cases where reconstruction was possible, it was observed that the failure was fracture parallel to the longitudinal direction of the cylinder accompanied by large amounts of delamination near the impact area. Figure 5.37 is a sketch of this type of failure. The extended delamination at the edges of the failure (not shown in the sketch) may have been caused by the pressure release coupled with the propagating delamination similar to that which was found in the impacted coupon specimens. The photographs of Figure 5.38 show the full and close-up views of a reconstructed cylinder with visible front and back surface impact damage. The photographs of Figure 5.39 show the full and close-up views of a reconstructed cylinder with punch-through impact damage.

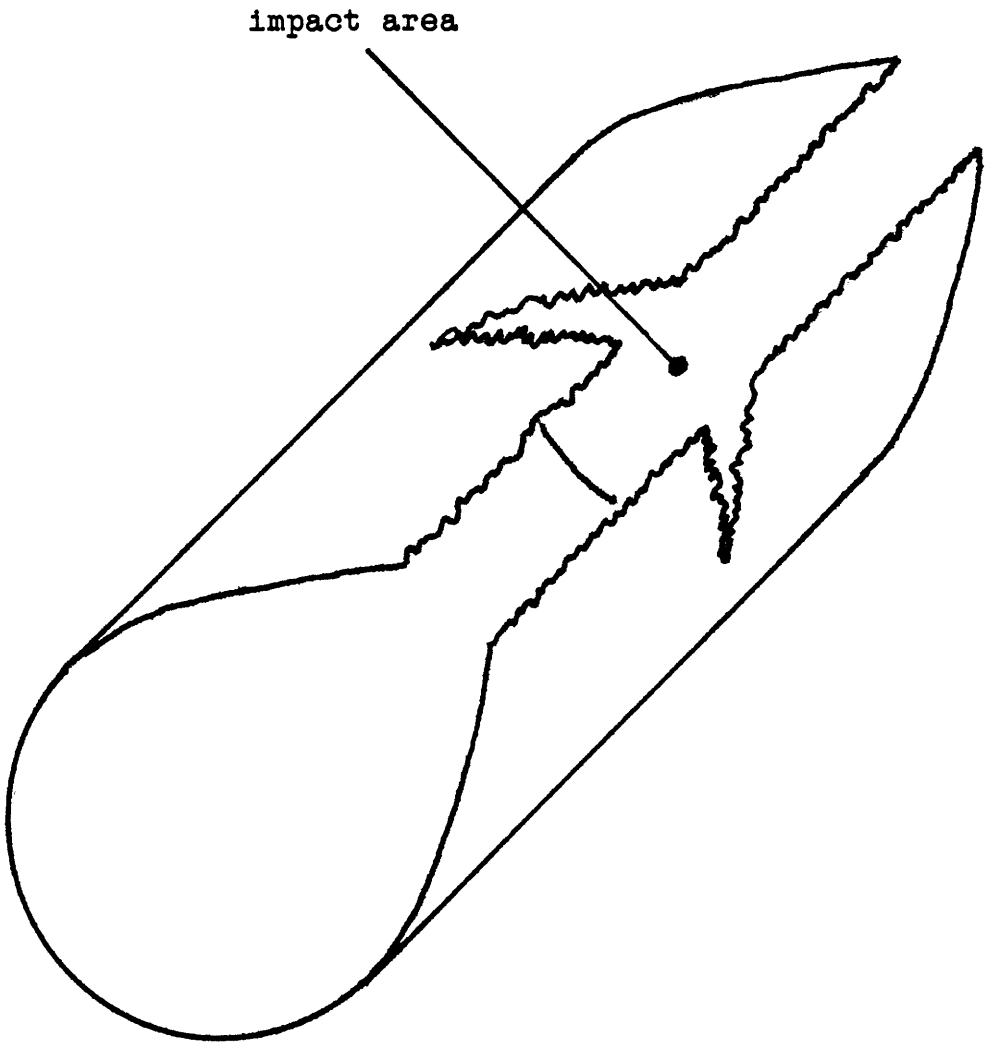

Figure 5.37 Sketch of Cylinder Failure with Punch-through Impact Damage

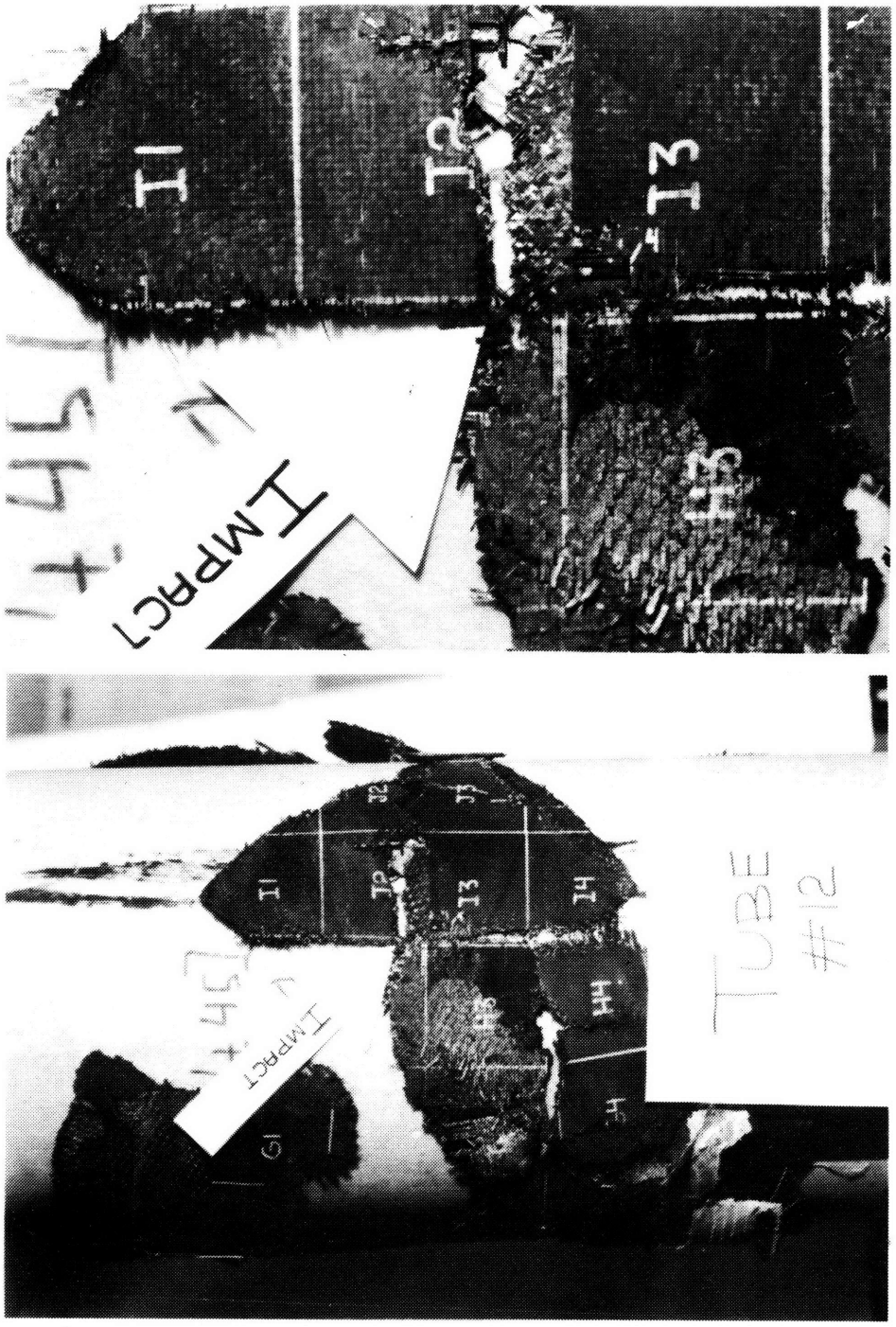

Figure 5.38 Photograph of Tube 12 Failure through Impact Section - a) Full View and b) Close-up View

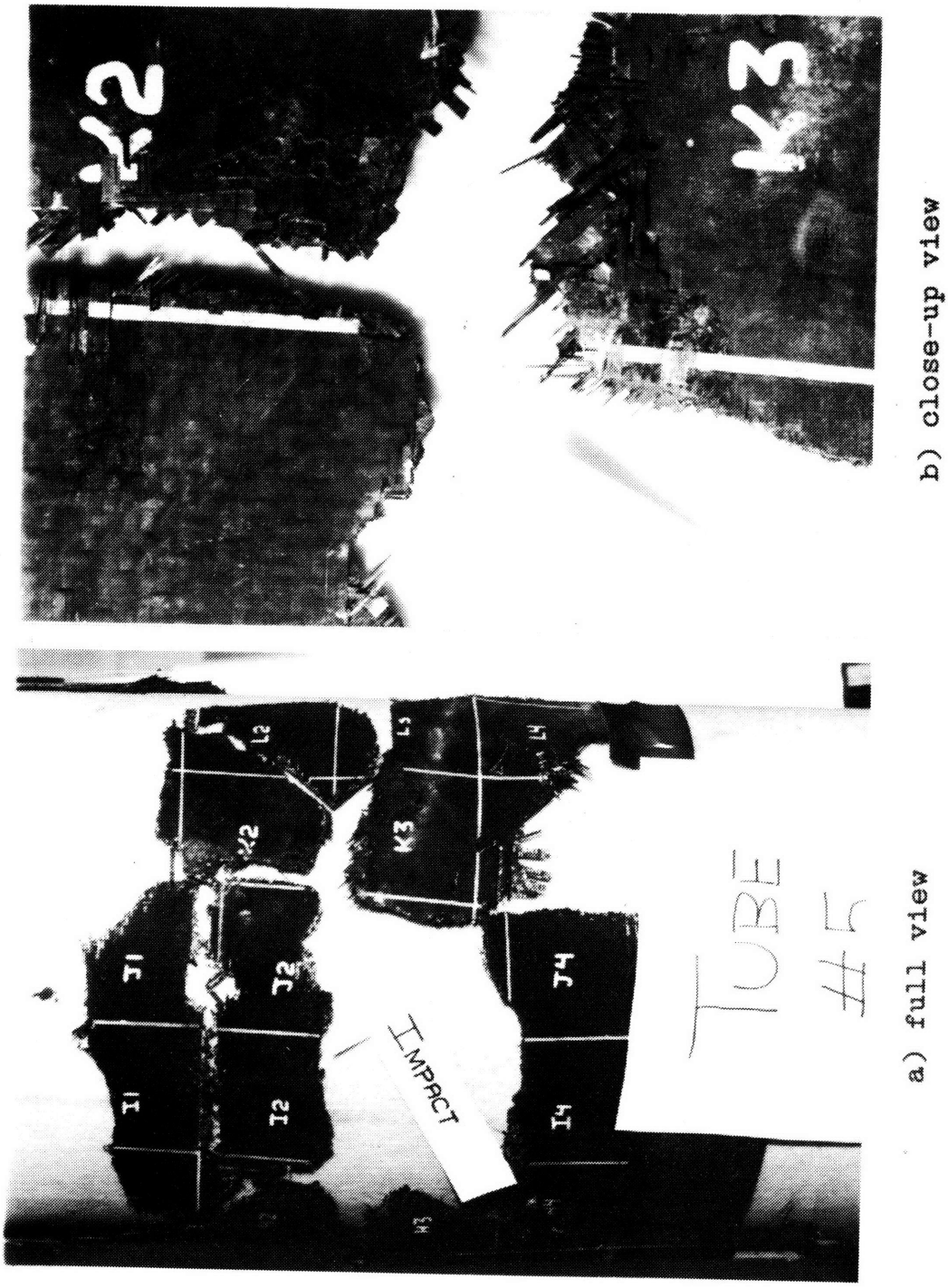

Figure 5.39 Photograph of Reconstructed Tube 5 with Punch-through Damage - a) Full View and b) Close-up View

CHAPTER SIX

DISCUSSION

This chapter is a discussion of the results of the investigation of the impact damage response of fabric graphite/epoxy plate and cylinder structures. The results for the analytical work are first presented with a discussion of general trends and convergence of the analysis. This discussion is followed by a comparison of the analytical and experimental results for the plate and cylinder studies. The damage resistance of the structure is addressed followed by the damage tolerance. Finally, the extension of the plate data to the coupon data is presented.

6.1 Analysis

6.1.1 Global Models for Plate and Cylinder

The global models for the plate and cylinder were used to obtain the peak force of the impact event. The peak load and acceleration corresponding to this peak were used in the local model to determine the strain field in the laminate which was then utilized to predict the damage resistance. For the plate model, a 17 modes in x by 17 modes in y solution was used with a time integration step of 0.25 microseconds. The simplified cylinder model for the global event was run using a 100 modes

in x and 100 modes in y solution and a 0.25 microsecond time integration step. This provided acceptable spatial and time convergence for the models. The value of the Hertzian spring constant for the $(0,45)_s$ fabric laminate was analytically determined to be 2.09×10^9 $N/m^{1.5}$. This is a laminate property and does not change for the cylinder configuration. The laminate engineering properties were determined using classical laminated plate theory and are listed in Table 6.1.

The force-time history of the impact event for a fabric plate impacted at 40 m/s is shown in Figure 6.1. Figure 6.2 is a plot of the acceleration-time history for the same case. A plot of the variation of the peak force versus impact velocity is given in Figure 6.3. As can be seen, the peak force curve is nearly linear with velocity. The same trend is observed for the acceleration versus impact velocity curve shown in Figure 6.4.

The linear behavior of these curves for this laminate configuration of $(0,45)_s$ suggest that the global analysis need only be run for a low and high velocity impact. For a given impact velocity, the peak force and acceleration could be interpolated from these curves for use in the local damage prediction model. The major implication of the linear response of the force and acceleration curves is a substantially reduced cost for the computation time associated with running the global model. Since the local model requires a very short time to generate the strain field, the total impact analysis scheme used in this work becomes much more

TABLE 6.1

$(0,45)_s$ A370-5H/3501-6 LAMINATE PROPERTIES

A_{11} = 81.0 GPa * mm		A_{22} = 81.0 GPa * mm	
A_{12} = 26.9 GPa * mm		A_{16} = 0.0 GPa * mm	
A_{66} = 27.1 GPa * mm		A_{26} = 0.0 GPa * mm	
D_{11} = 15.8 GPa * mm^3		D_{22} = 15.8 GPa * mm^3	
D_{12} = 1.8 GPa * mm^3		D_{16} = 0.0 GPa * mm^3	
D_{66} = 1.9 GPa * mm^3		D_{26} = 0.0 GPa * mm^3	

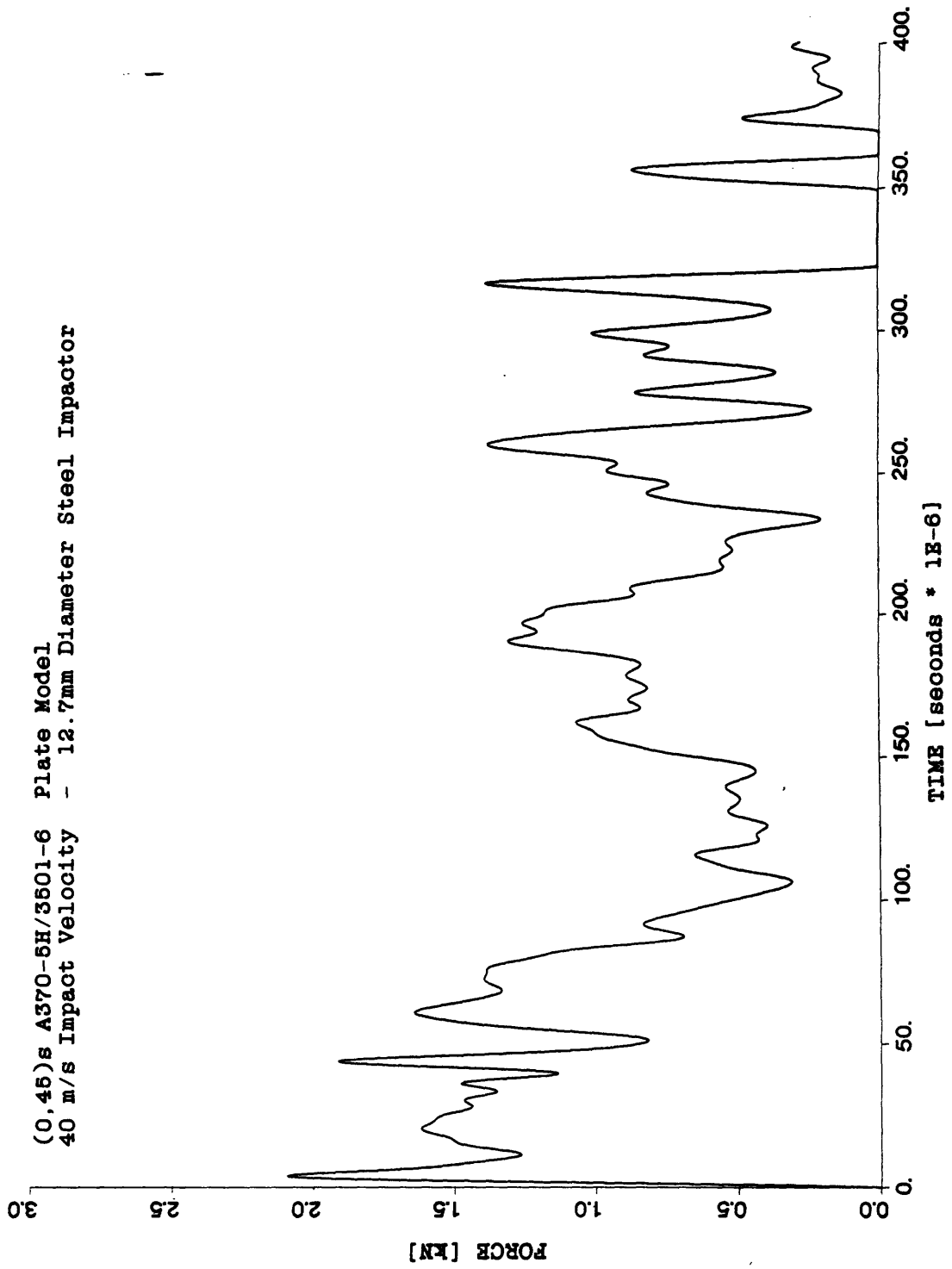

Figure 6.1 Force versus Time History of Plate Impacted at 40 m/s

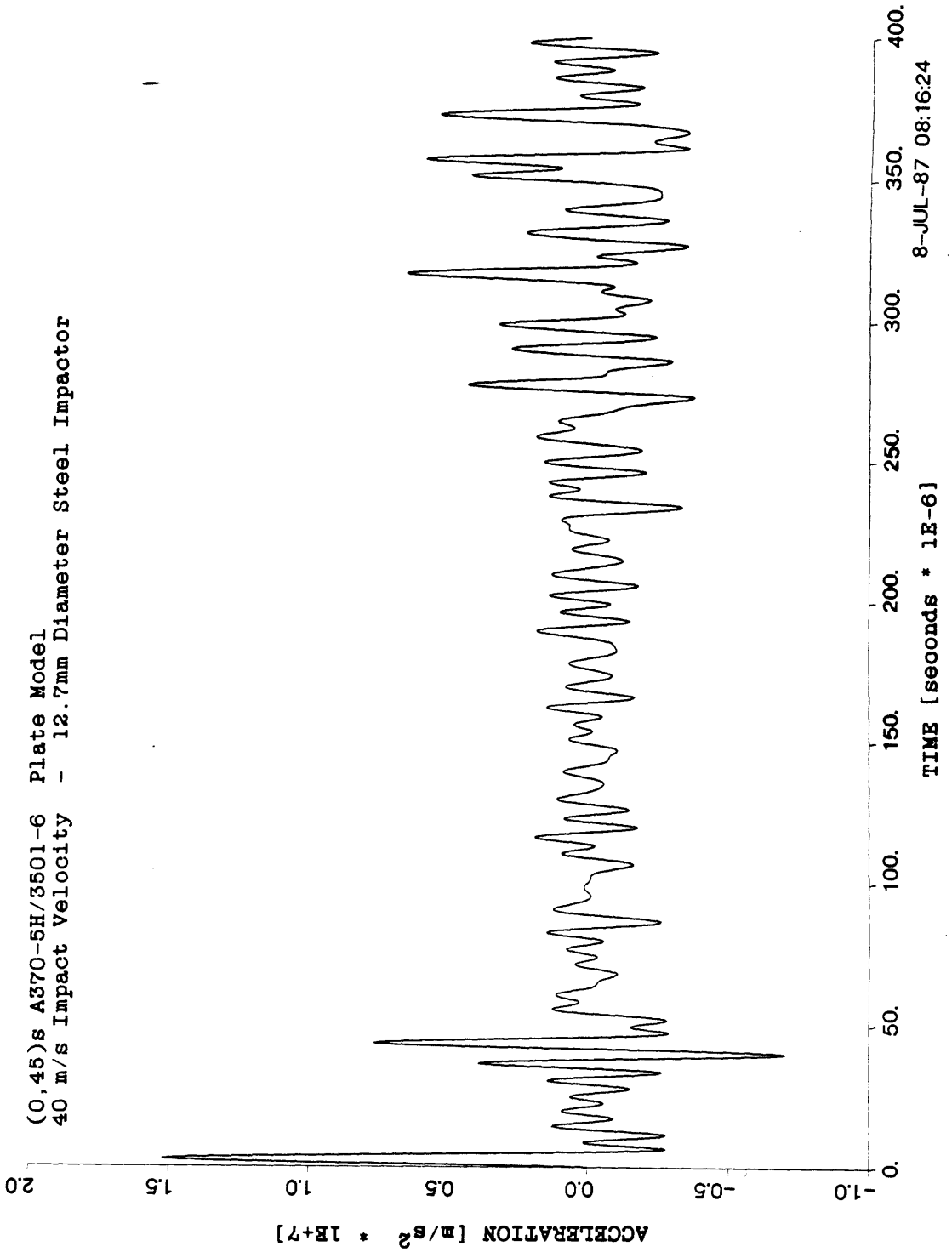

Figure 6.2 Acceleration versus Time History of Plate Impacted at 40 m/s

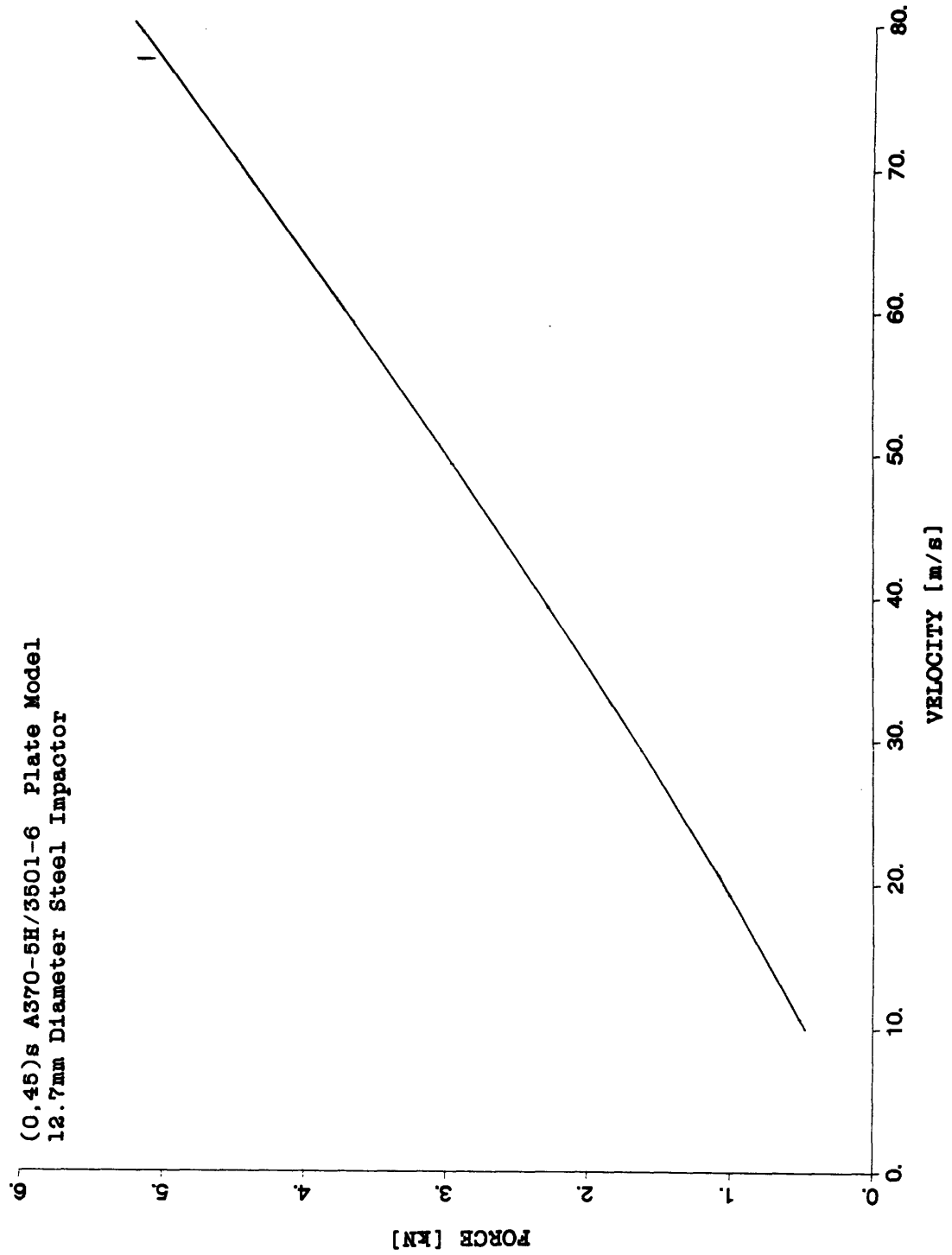

Figure 6.3 Peak Force versus Impact Velocity for Plate

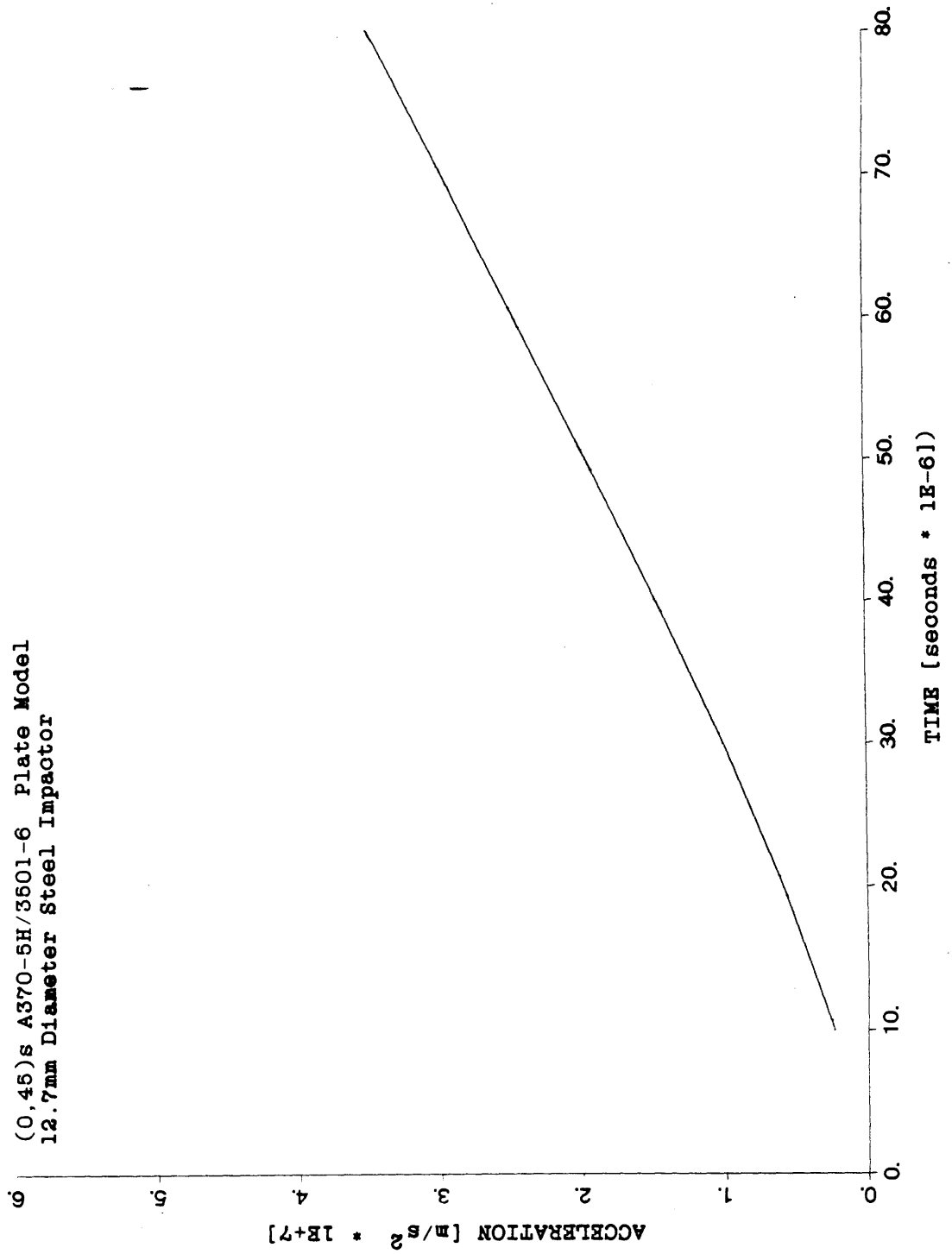

Figure 6.4 Peak Acceleration versus Impact Velocity for Plate

efficient than a three-dimensional finite element approach.

A plot of the force-time history of the impact event for a cylinder impacted at 40 m/s is given in Figure 6.5. The corresponding acceleration curve is shown in Figure 6.6. An interesting observation in the force response curve is the existence of two peaks with considerably different associated accelerations. In reference to the two figures, the first force peak is accompanied by a large acceleration. By the time the second peak occurs, the acceleration has become very small in comparison to the first peak acceleration. Since the inertial loading from the plate acceleration is used in the local model to assess damage, all cylinder analysis predictions were made utilizing both force peaks.

The force-time and acceleration-time impact histories of the plate and cylinder are very different. The force-time history of the plate shows a considerable amount of loading and unloading during the 400 microsecond period shown. The cylinder history is much smoother, with the only unloading periods after the first and second peaks. The acceleration-time response of the plate shows much more plate activity than the cylinder response, which shows an acceleration peak at approximately 10 microseconds and then dies out to zero. However, the magnitude of the peak forces and accelerations are approximately equal for the two geometries. Also, the slope of the force-time curves for the two geometries is approximately equal up to the first peak. The major differences in the impact event histories may or may

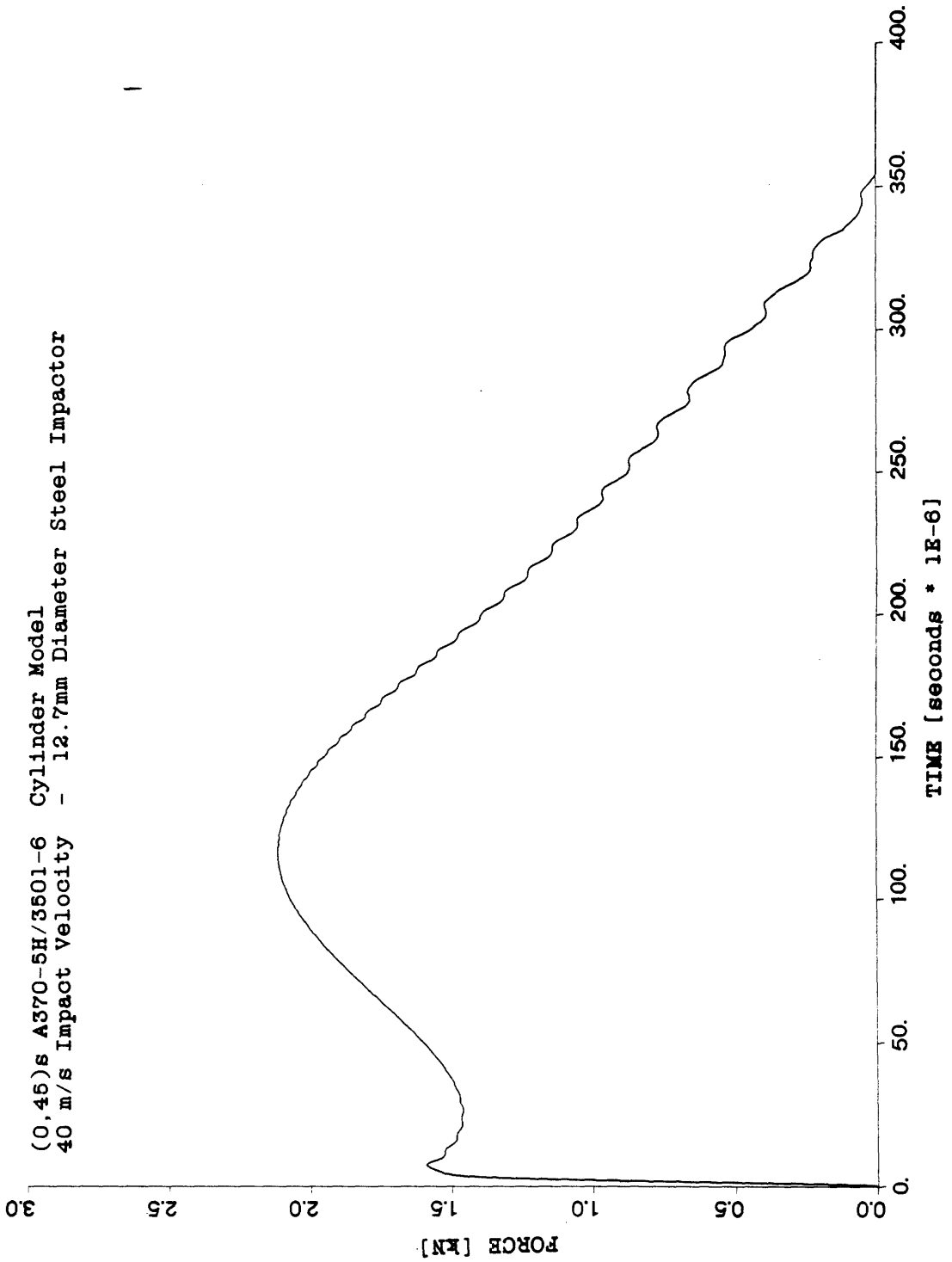

Figure 6.5 Force versus Time History of Cylinder Impacted at 40 m/s

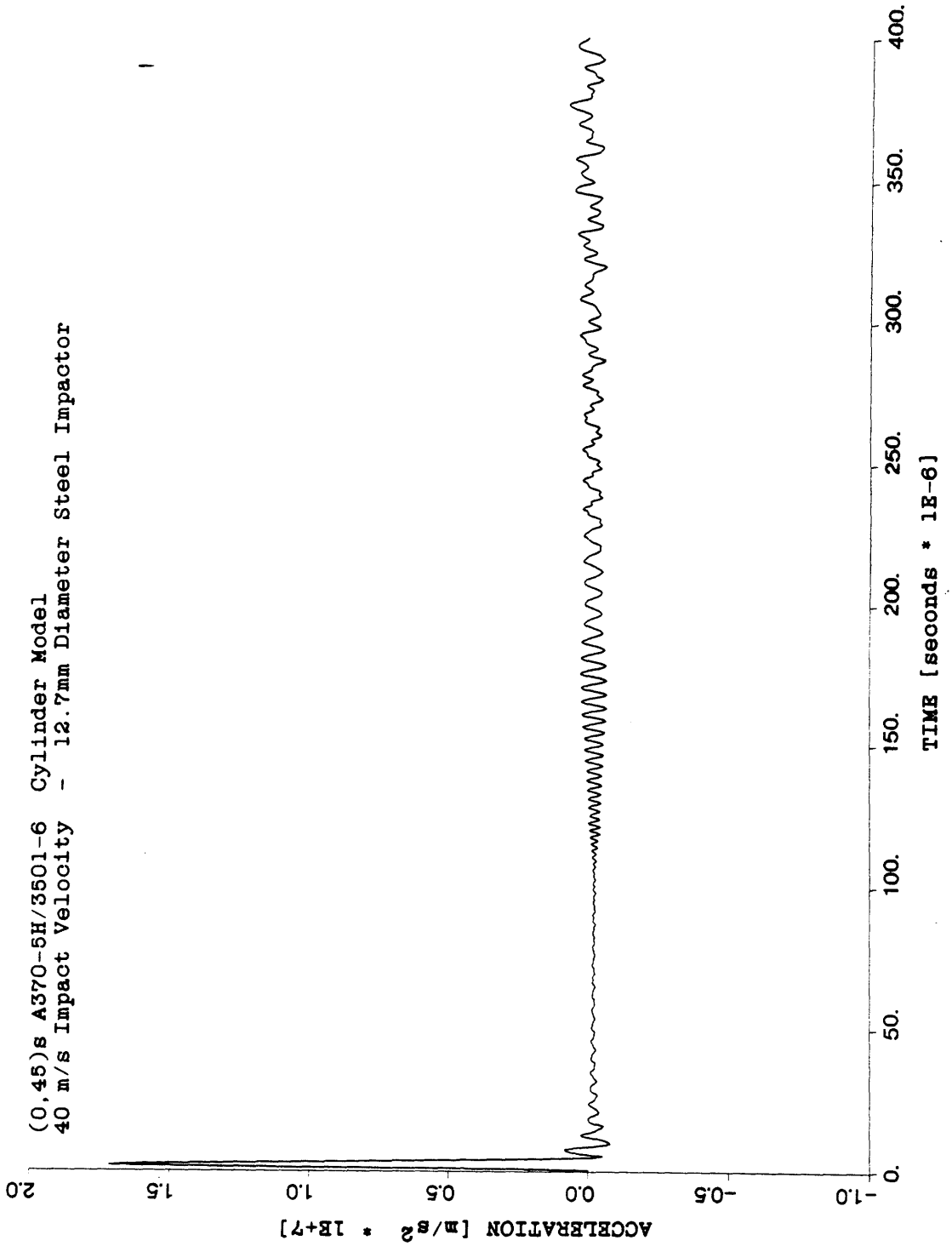

Figure 6.6 Acceleration versus Time History of Cylinder Impacted at 40 m/s

not be one of the causes of the different damage states found in the plates and cylinders. Experimental verification of the cylinder model is needed before any conclusions can be drawn.

6.1.2 Local Model for Damage Prediction

The local model for computation of the stresses and strains around the impact area was implemented only for Hertzian loading distribution of the impactor. The equivalent engineering properties used in this model for the $(0,45)_s$ laminate are listed in Table 6.2. Since the laminate was quasi-isotropic with E_L and E_T approximately equal, the local model was only used for one set of values. In Cairns's analysis [1], the material was not quasi-isotropic and the analysis had to be conducted for the different E_L and E_T cases.

The analysis to calculate the Hertzian spring constant required 100 modes of the Fourier-Bessel series to provide a convergent solution. Convergence for the spring constant was based on the static indentation (see Figure 3.4) and 100 modes provided a solution within $\pm 5\%$ of a steady state value. Convergence of the stress and strain calculations was based on how well the Hertzian loading distribution was modeled by the Fourier-Bessel expansion. The pressure at the center of the loaded area from the expansion was compared to the exact integral of the load evaluated at the plate center [1]. A 200 mode expansion of the series was required to achieve a $\pm 5\%$

TABLE 6.2

$(0,45)_s$_A370-5H/3501-6 EQUIVALENT ENGINEERING PROPERTIES

E_{xx}	=	51.5 GPa	E_{yy}	=	51.5 GPa
			E_{zz}	=	26.9 GPa
G_{xy}	=	19.3 GPa	G_{xz}	=	6.0 GPa
			G_{yz}	=	6.0 GPa
ν_{xy}	=	0.33	ν_{xz}	=	0.21
			ν_{yz}	=	0.21

convergence of the loading distribution. The higher number of modes required for this computation was dictated by the slow convergence of the Hertzian loading distribution (see Figure 3.5). The plate radius used for the local model analysis was 20 mm. Stresses and strains were calculated along lines in the laminate at 0°, 45°, and 90° directions. Calculations were made every 0.5 mm from the center of the plate.

Inertial loading from the acceleration of the plate was included in the analysis. The inertial load was applied as a uniform pressure over the total area of the plate model. These loads were implemented as outlined by Cairns and Lagace [18]. The inertial loads have little influence on the magnitude of the Hertzian loading distribution. For the extreme case of a 80 m/s velocity impact, the maximum value of the pressure load on the plate was reduced by approximately 3%. However, the damage resistance predictions were affected by including the d'Alembert force. For the 40 m/s impact, the predicted core area diameter was 2.0 mm for the analysis that included the acceleration of the plate. Neglecting the inertial loading increased the fiber damage prediction to 3.0 mm. In Figure 6.7, the predicted core area damage is superimposed on an x-ray photograph of a plate laminate impacted at approximately 40 m/s.

The predicted fiber damage area was circular. This was not a general characteristic of the local model prediction. The local model is axisymmetric, as is the Hertzian loading distribution. However, this does not mean that the stresses

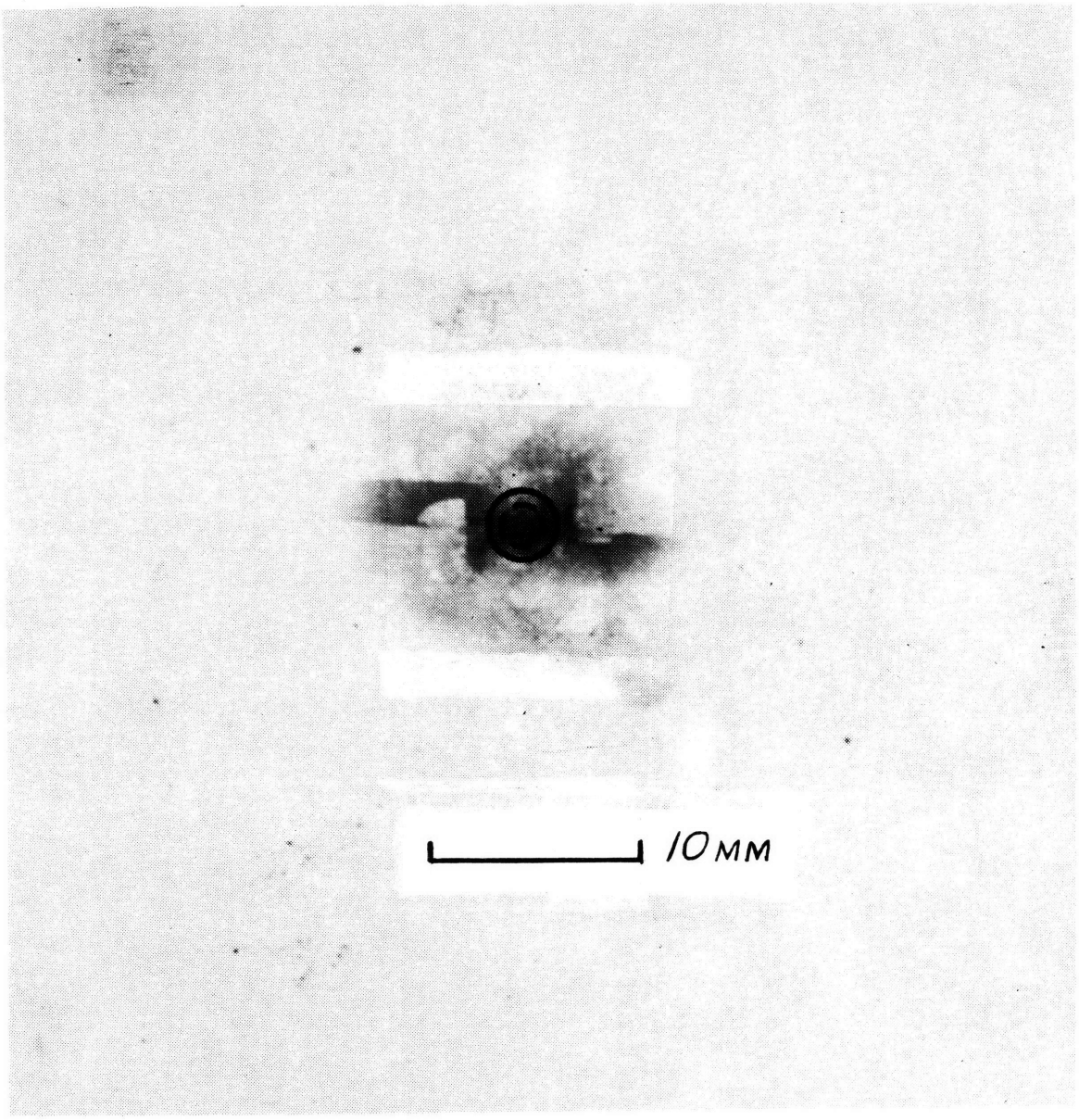

Figure 6.7 Predicted Core Area Diameter for Plate Specimen Impacted at approximately 40 m/s

and strains around a concentric circle in the laminate are equal after they are rotated into a common direction. Thus, the damage area cannot be stated to be any particular shape *a priori*. The fabric material is the factor that made the fiber damage area circular. Since the fabric is composed of warp and fill bundles, fibers can be damaged in both directions whereas in tape plies only one direction is affected. The maximum strain to failure of the warp and fill fibers is nearly equal and this results in the circular fiber damage area.

Fiber breakage was determined to occur when the fiber exceeded the maximum strain criterion limits. For the $(0,45)_s$ laminate, the only damaged plies were the top and bottom 0° plies. This was true for all impact velocities considered, up to 80 m/s. The local model predicted damage that was symmetric through the thickness of the laminate. This was a result of the values used for the maximum tensile and compressive laminate strain, 11269 and 10745 μstrain for the *in situ* ply respectively. Experimental data showed that the damage was not symmetric through the thickness, particularly fiber damage as shown in Figure 5.3. The local plate model was used to predict damage for both the plate and cylinder geometries. No correction was made to the model for the curvature of the cylinder.

6.1.3 Degraded Inclusion Model

The elliptical inclusion model was used to calculate the strain averaged over a distance a_o. The inclusion area was a model of the damaged area of the laminate as predicted using the local Fourier-Bessel series model. The implementation of the analysis followed Cairns's [1] method exactly.

Based on evidence from the delamination study and previous work done on tape laminates [1], fiber breakage was used as the governing factor in the reduction in tensile strength of impacted laminates. Therefore, the inclusion, or degraded area of the laminate, was based solely on fiber failure. The size of the degraded area was determined by the maximum radius of the predicted fiber breakage. Since the local model did not predict any fiber damage to the two inner 45° plies, the inclusion had the configuration $(45)_s$. The degraded area properties were calculated using classical laminated plate theory. The properties for this layup are listed in Table 6.3.

The maximum stress criterion was applied to predict first-ply failure for the $(0,45)_s$ laminate. First-ply failure for the tensile loaded laminate was predicted to occur in the outer 0° plies. The near-field averaged strain was calculated at the edge of the degraded area. All calculations were done along a line 90° to the laminate 0° axis. The strength reduction was based on the ratio of the near-field averaged strain to the far-field strain.

TABLE 6.3

$\dagger(45)_s$ A370-5H/3501-6 INCLUSION PROPERTIES

A_{11} =	30.1 GPa * mm	A_{22} =	30.1 GPa * mm
A_{12} =	23.9 GPa * mm	A_{16} =	0.0 GPa * mm
A_{66} =	24.0 GPa * mm	A_{26} =	0.0 GPa * mm

D_{11} =	1.2 GPa * mm^3	D_{22} =	1.2 GPa * mm^3
D_{12} =	1.0 GPa * mm^3	D_{16} =	0.0 GPa * mm^3
D_{66} =	1.0 GPa * mm^3	D_{26} =	0.0 GPa * mm^3

The averaging dimension a_o used for the fabric laminates was based on data obtained in this research and that by Kageyama [33]. The value for a_o was determined to be 4.7 mm.

6.2 Comparison of Plate Analysis and Experiment

6.2.1 Damage Resistance

The core area diameter versus impact velocity for the plate damage characterization specimens and the analytical predictions is plotted in Figure 6.8. The analysis correlates well with the data. The analysis predicted first fiber damage at an impact velocity of approximately 25 m/s for the 12.7 mm diameter steel ball. The first evidence of core damage from the x-ray photographs occurred at an impact velocity of approximately 30 m/s. The analytical curve matched the experimental data very well.

The analytical curve is based on the maximum radius of the predicted fiber damage. The analysis predicts a circular region of fiber damage. The experimental burn-off evidence shows that fiber damage occurs in a cross-hair pattern. The length of the cross-hair axes correspond to the length of the core area diameter. During the actual impact event, the fibers break and act as a stress relieving mechanism, which prevents damage to the fibers outside of this cross-hair pattern. Since the local model cannot update damage to the laminate as it occurs during the impact event, the cross-hair

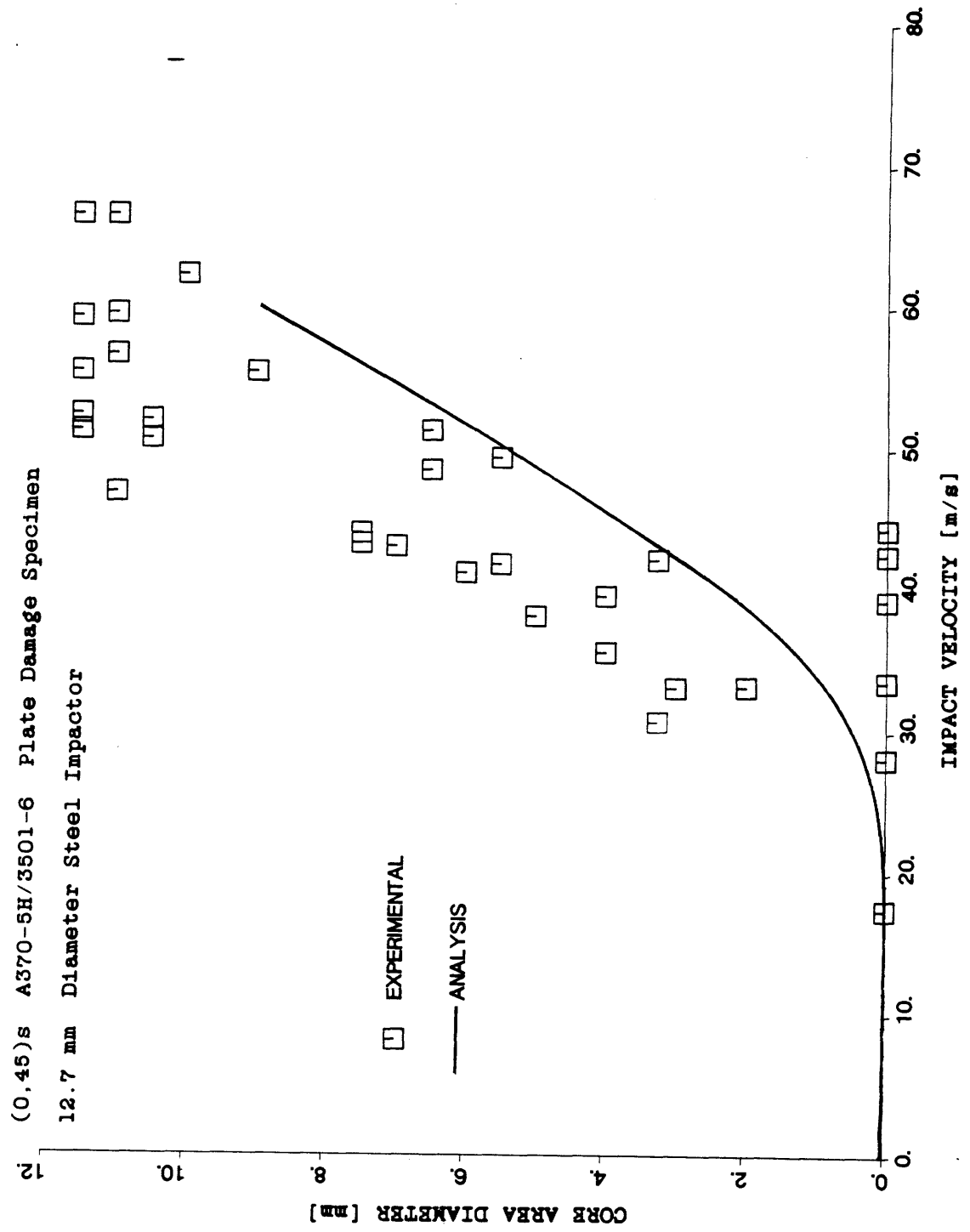

Figure 6.8 Core Area Diameter versus Impact Velocity for Plate Damage Characterization Specimens

cannot be accurately predicted. The plate loading is not severe enough for the analysis to predict fiber damage in the inner 45° plies. For a 80 m/s impact analysis including inertial loads, the maximum tensile strain in the 45° ply fibers was 90% of the failure value. The burn-offs however, clearly show evidence of fiber damage to the 45° plies at impact velocities greater than 40 m/s. The maximum radius of fiber damage, therefore, is accurately predicted by the analysis. However, the local model is incapable of duplicating the fiber damage pattern in the plane and through the thickness of the laminate.

6.2.2 Damage Tolerance

The predicted damage tolerance of the coupon laminate was found using the plate inclusion model. The strength reduction was found be dividing the average strain over a distance a_o at the edge of the inclusion by the far-field strain.

The failure stress of the flat plate specimens versus the core area diameter is plotted in Figure 6.9. A considerable amount of scatter is evident in the experimental data for this plot. This was attributed in part to the method of measurement of the core area diameter as described in Chapter Four. The analytical curve was generated by assuming (a) that the $(45)_s$ circular inclusion and experimental core damage area radii were equal and (b) that laminate failure was governed by the 0° outer plies. Overall, the inclusion analysis that is

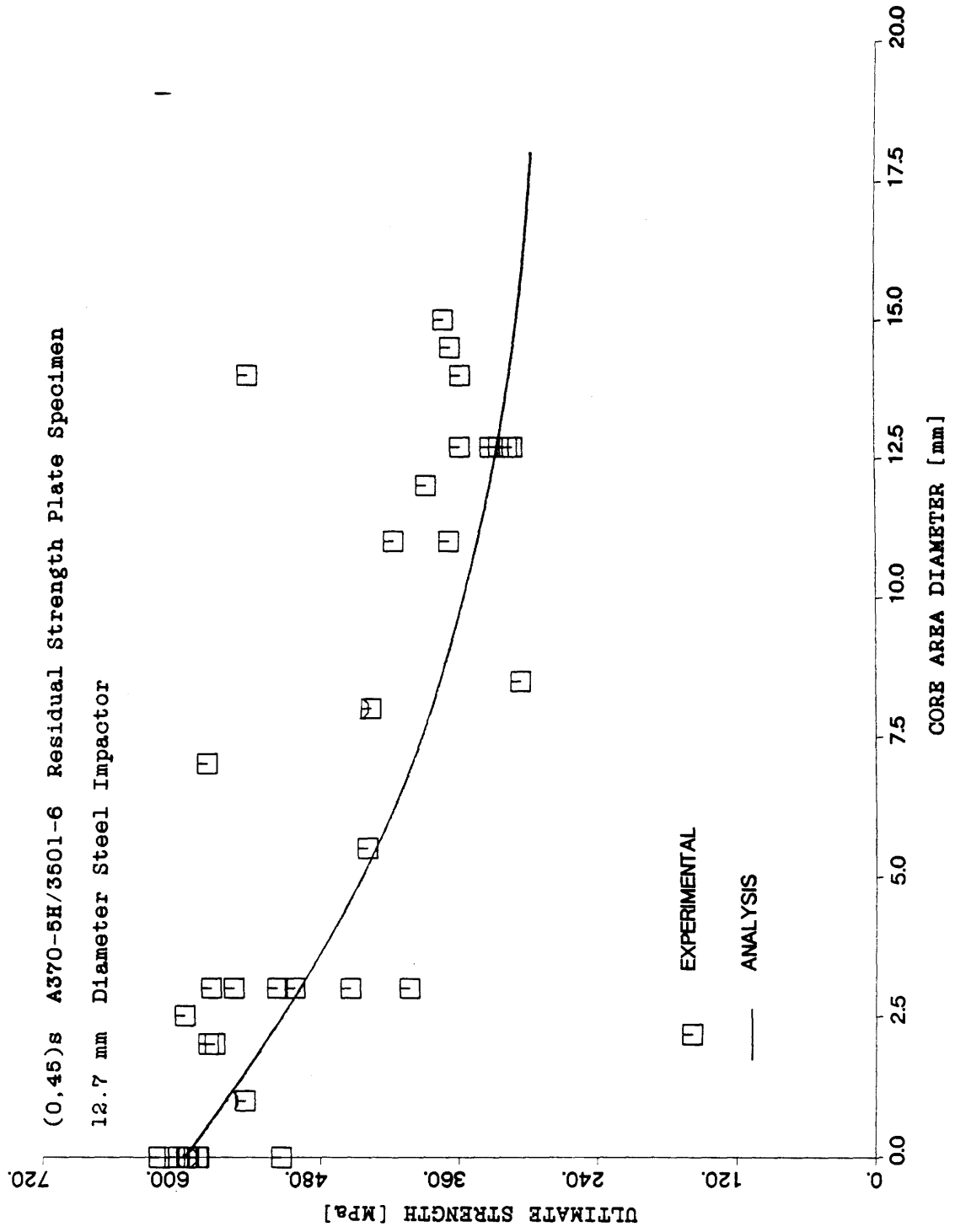

Figure 6.9 Failure Stress versus Core Area Diameter for Plate Residual Strength Specimens

used to generate the curve correlates the data well and provides a conservative bound for the residual strength of the laminate.

Combining the concepts of damage resistance and damage tolerance, the failure stress of the flat plate specimen versus impactor velocity is plotted in Figure 6.10. Predicted failure stress was computed by running a simulated impact event for a given velocity. The steps involved were: (a) finding the peak force and corresponding acceleration of the impact event from the global plate model, (b) computing the stress and strain field in the laminate from the local Fourier-Bessel model, (c) determining the radius of the fiber damage area from the stress and strain information, and (d) calculating the strength reduction for a $(45)_s$ circular inclusion with the same radius as the predicted fiber breakage area. The analysis provides a good conservative bound for the experimental data.

It is known that the inclusion area used for the strength reduction analysis does not accurately model the actual damage to the laminate. However, the size of the predicted inclusion area and the size of the core damage area are approximately the same (see Figure 6.7) for an impact at a given velocity. The experimental results indicated that the circular core damage area was a high-damage region essentially useless for carrying load. Coupled with the observation that the shape of the fiber damage was a cross-hair, it may be surmised that the crushed matrix in the core damage area prevented the fiber

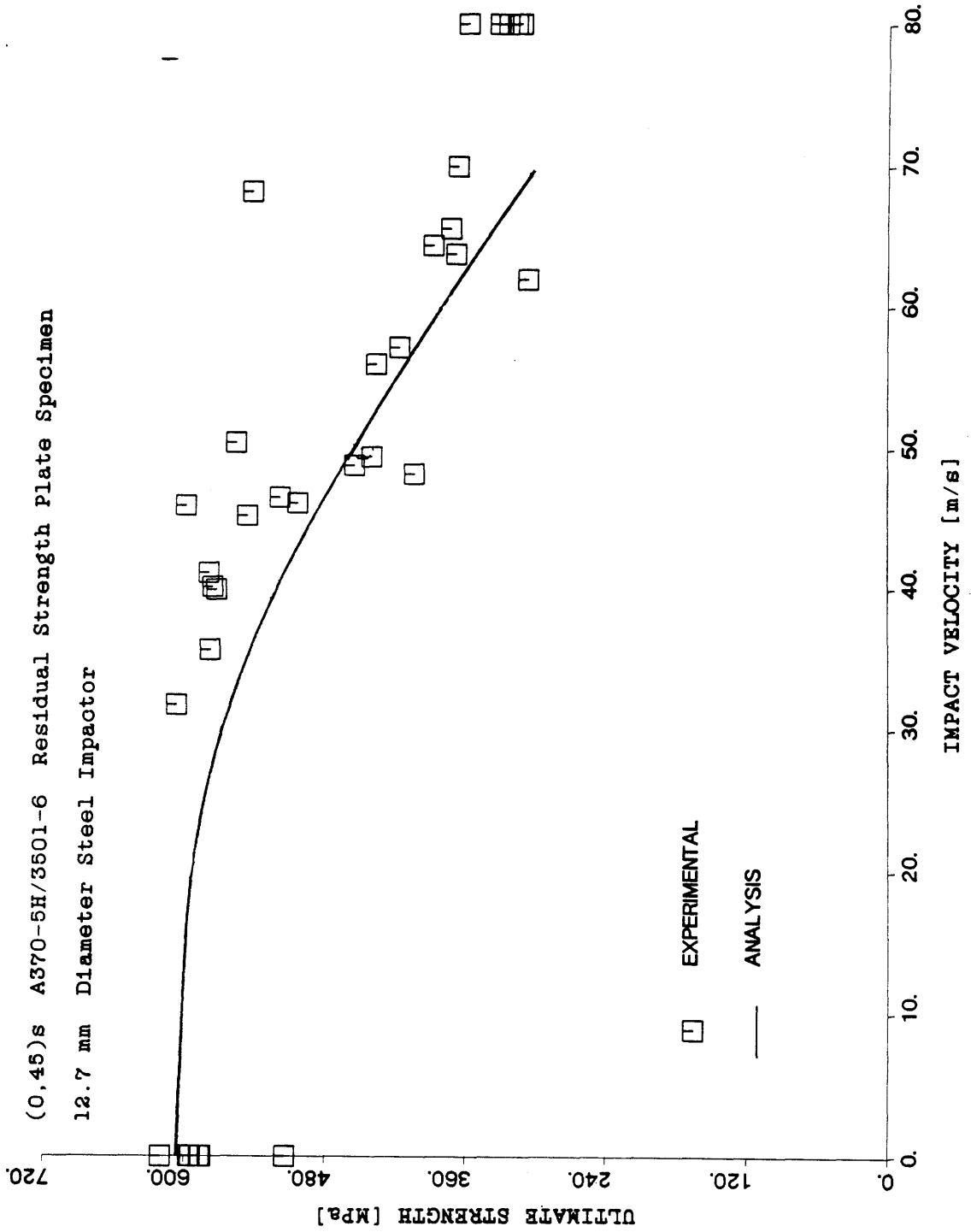

Figure 6.10 Failure Stress versus Impact Velocity for Plate Residual Strength Specimens

loading mechanism of shear lag to occur. Thus, the predicted fiber damage area matched the observed core damage area that is incapable of carrying load. The inaccurate prediction of fiber damage resistance was masked by the matrix crushing in the actual specimen, which provided good correlation between the experimental and analytical results.

6.3 Comparison of Cylinder Analysis and Experiment

6.3.1 Damage Resistance

The core area diameter versus impact velocity is plotted in Figure 6.11 for the cylinder damage characterization specimens and the cylinder analysis predictions. The two force peaks predicted by the global analysis were used to provide an envelope for the damage resistance predictions. The analytical curves are generated using the radius of the fiber breakage areas as previously described in section 6.2.1. The second peak analysis curve provides excellent correlation to the experimental data.

As found in the plate specimens, the fiber breakage area predicted by the local model analysis could not duplicate the cross-hair pattern of fiber damage found in the epoxy burn-off specimens. The maximum radius of fiber damage was adequately predicted. The dimensions of the other damage, however, could not be predicted. The global model peak loads on the plate and cylinder were approximately the same for a given impact

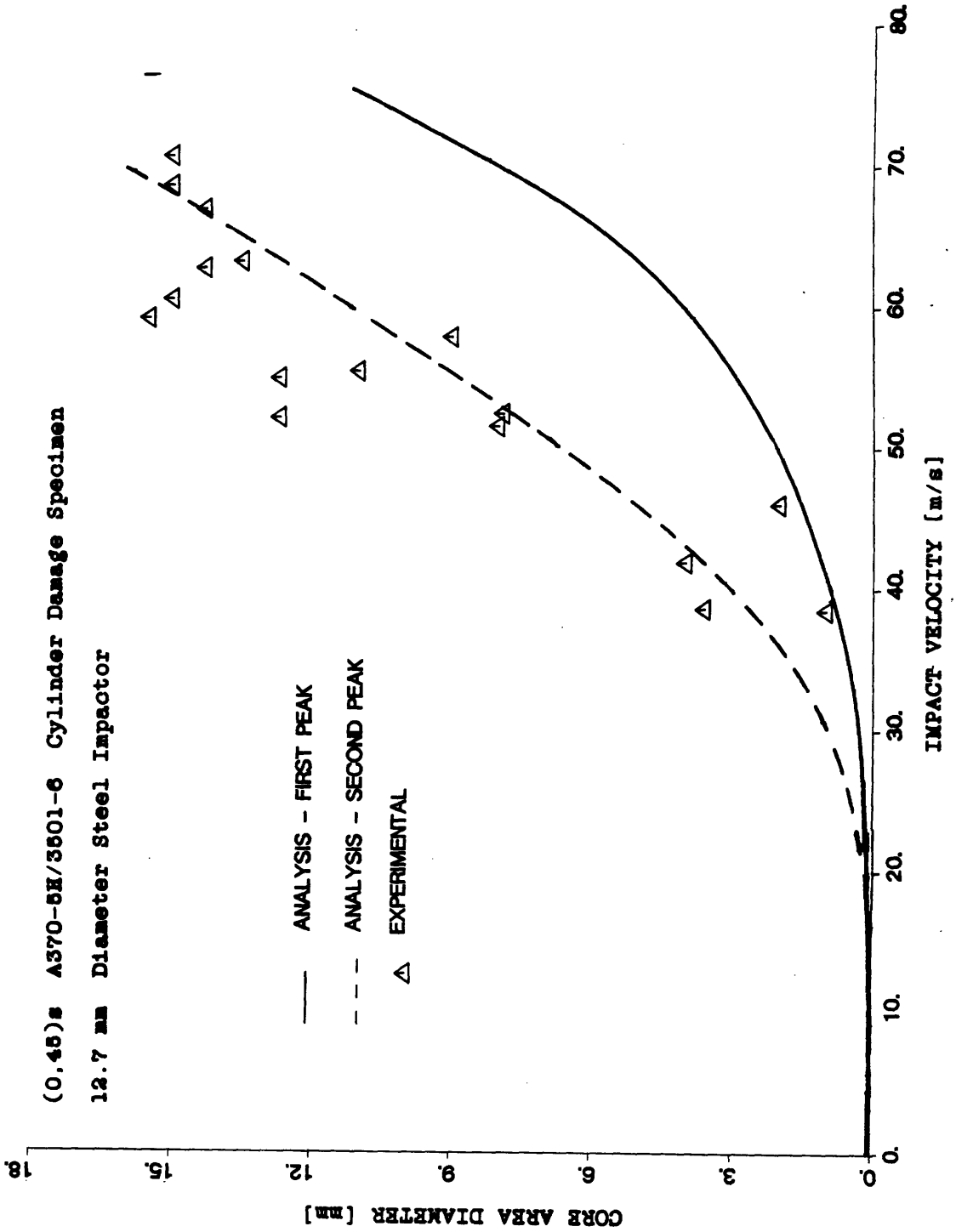

Figure 6.11 Core Area Diameter versus Impact Velocity for Cylinder Damage Characterization Specimens

velocity. Since the local model had no correction for the cylinder curvature, the predicted damage area around the impact site was no different than the plate prediction. This contradicted the experimental results showing the cylinder impact damage area to be very different than the plate damage area, especially for delamination and fiber bundle disbond damage.

6.3.2 Damage Tolerance

The failure pressure of the cylinder versus the core area diameter is plotted in Figure 6.12. This plot includes no correction for the bending at the impact damage area due to the internal pressure load. Measurements of the core area diameter are based on visual observation of the impact footprint as described in Chapter Four. The the analysis curve does not follow the experimental data when the strength reduction is based on the unflawed cylinder pressures. Furthermore, application of a correction factor as utilized by previous investigators [29] would only move the analysis curve further below the experimental data. The predicted strength reduction, however, does capture the boundaries of the experimentally observed failure pressures.

One possible explanation for the analysis discrepancy could be premature failure of the unflawed cylinder. Even with seam reinforcements, the cylinders were not completely free of defects. These defects, mentioned in Chapter Four,

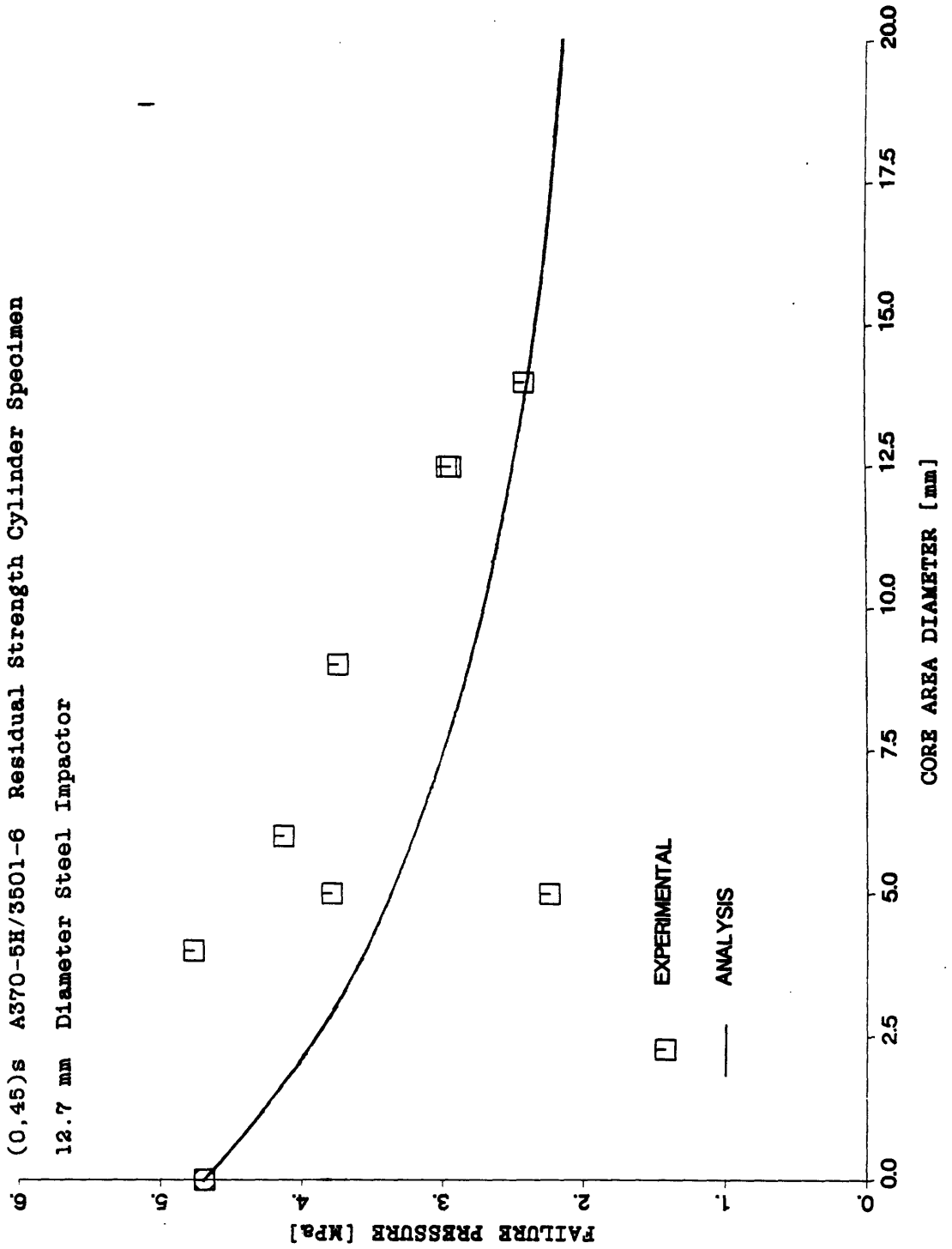

Figure 6.12 Failure Pressure versus Core Area Diameter for Cylinder Residual Strength Specimens

could not be avoided in the current manufacturing process. Unlike the flat plate coupons where the manufacturing process is much simpler, the cylinders almost always had small epoxy ridges on the inner and outer surfaces because of the paper bleeder or tape used to secure parts of the cure assembly. The predicted failure pressure of a unflawed cylinder, based on a maximum stress criterion analysis, is 6.2 MPa. The inherent flaws in the cylinder prevented obtaining this maximum failure pressure and resticted the value to 4.7 MPa. If the damage tolerance analysis was based on this predicted value of 6.2 MPa for the unflawed failure pressure, the curve in Figure 6.12 would match the failed cylinder data better, but the predicted failure pressures would lie well above experimental pressures.

The failure pressure of the cylinder versus the impactor velocity is plotted in Figure 6.13. This plot combines damage resistance and damage tolerance concepts for the cylinder geometry. Note that the experimental scatter in the velocity measurements for the impact event is very large because of the tracking problems detailed in Chapter 4. The experimental data for the impacted cylinders spans approximately a 20 m/s range in the impactor velocity and includes barely visible to punch-through damage levels. Although the amount of experimental data is limited, the second peak analysis provides a conservative lower bound for the experimental data.

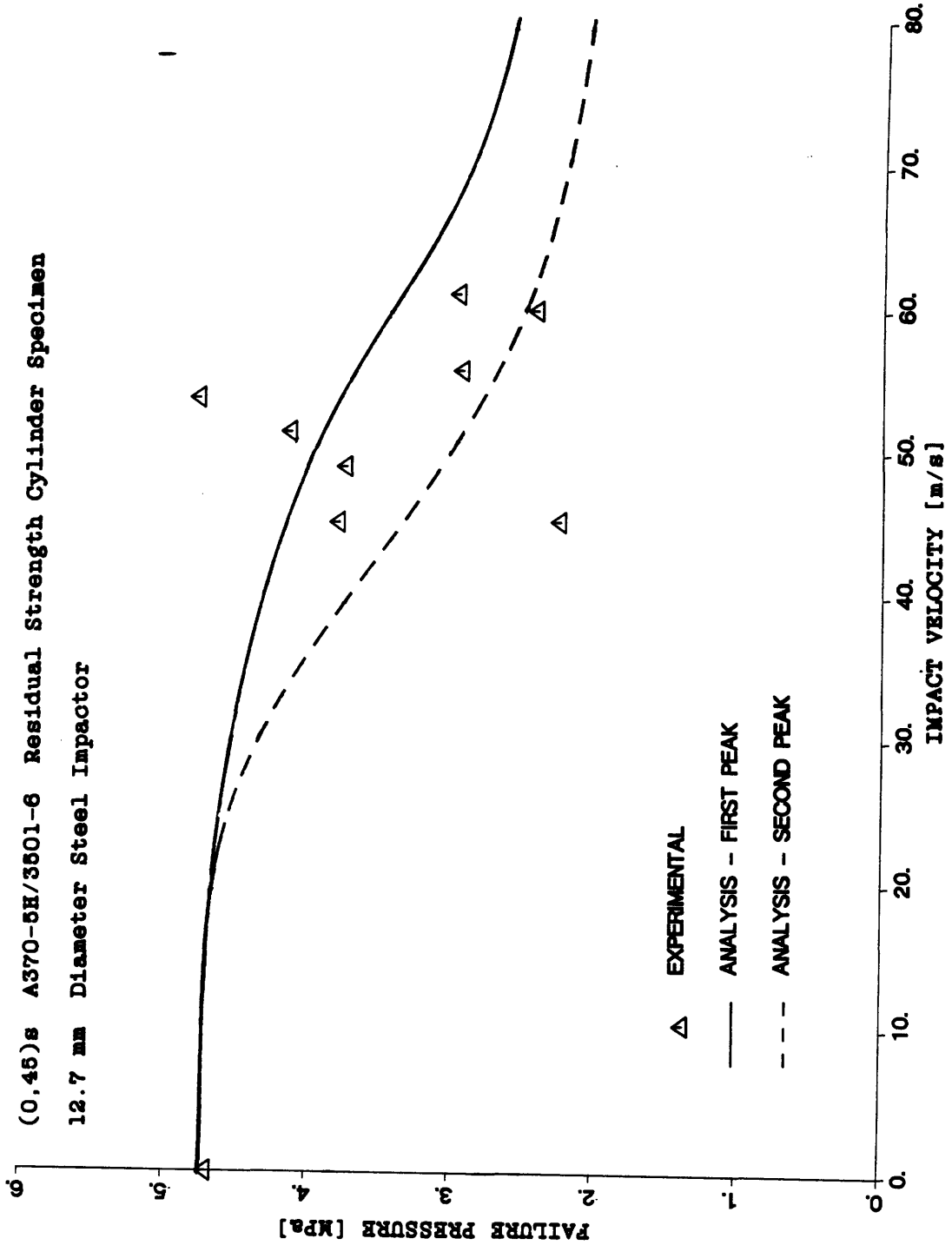

Figure 6.13 Failure Pressure versus Impact Velocity for Cylinder Residual Strength Specimens

6.4 Correlation of Plate and Cylinder Results

A primary goal of this research is to use the experimental data obtained for the plate specimen impact study as a basis for an analytical projection to a different structure, the cylinder. Acute observations of the damage resistance and damage tolerance characteristics of the two geometries may provide a basis for the adaptation of the proven impact analysis scheme for plate geometries to cylinder geometries.

6.4.1 Damage Resistance

The damage resistance characteristics of the plate and cylinder structures were different in shape and size as determined by the experimental work covered in Chapter Five. However, the damage types in the two structures; matrix yield, fiber bundle disbond, delamination, and fiber breakage, were observed to be common to both geometries.

The peak load versus impact velocity from the plate and cylinder global analysis is shown in Figure 6.14. The second peak load from the cylinder is used in this figure. Both peak force curves exhibit a nearly linear behavior with respect to impact velocity. The difference between the two forces is small, but does increase with velocity and the plate peak load becomes higher than the cylinder peak. Since the accelerations associated with the second peak of the cylinder

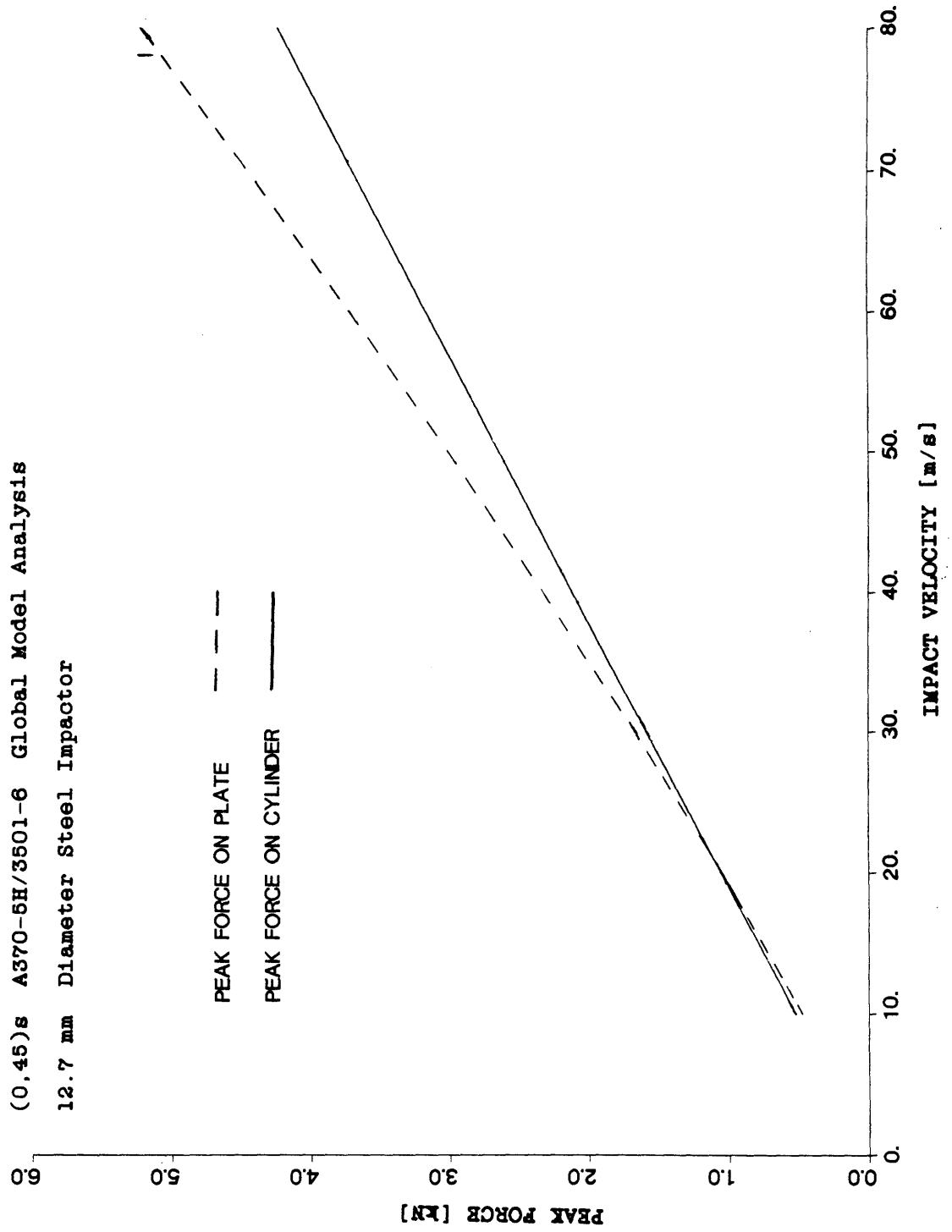

Figure 6.14 Comparison of Peak Load versus Impact Velocity for Plate and Cylinder Structures

global analysis are approximately zero, the inertial loading will not reduce the second peak cylinder damage predictions as was the case for the plate (see Figure 6.7). Consequently, the combined effects of the lower peak load and the negligible acceleration of the cylinder caused the damage predictions of the cylinder to be nearly the same as for the plate for the same impact event.

The damage area in the cylinder case was cleaner and more contained around the core area than the plate case. In reference to the x-rays in Figures 5.11 and 5.15, the delamination and bundle disbonding was less dominant than in the plate specimen. The difference is ultimately because of the curvature of the cylinder. One explanation could be the difference in contact area between a flat surface and a sphere and a curved surface and a sphere. Another might be the absorption of impact energy into the wall of the cylinder, which would appear in the force-time impact history. Teti et. al., [8] were able to associate variations in the force-time curve to certain types of damage for drop-weight impact tests. In reference to Figures 6.1 and 6.5, the loading on the cylinder is much smoother than the plate. Likewise, the acceleration histories in Figures 6.2 and 6.6 show a less severe case for the cylinder geometry. If it could be experimentally verified, the smoother loading of the cylinder might partially explain the contained damage.

The predicted core area diameter versus velocity for the plate and cylinder geometries is shown in Figure 6.15. As

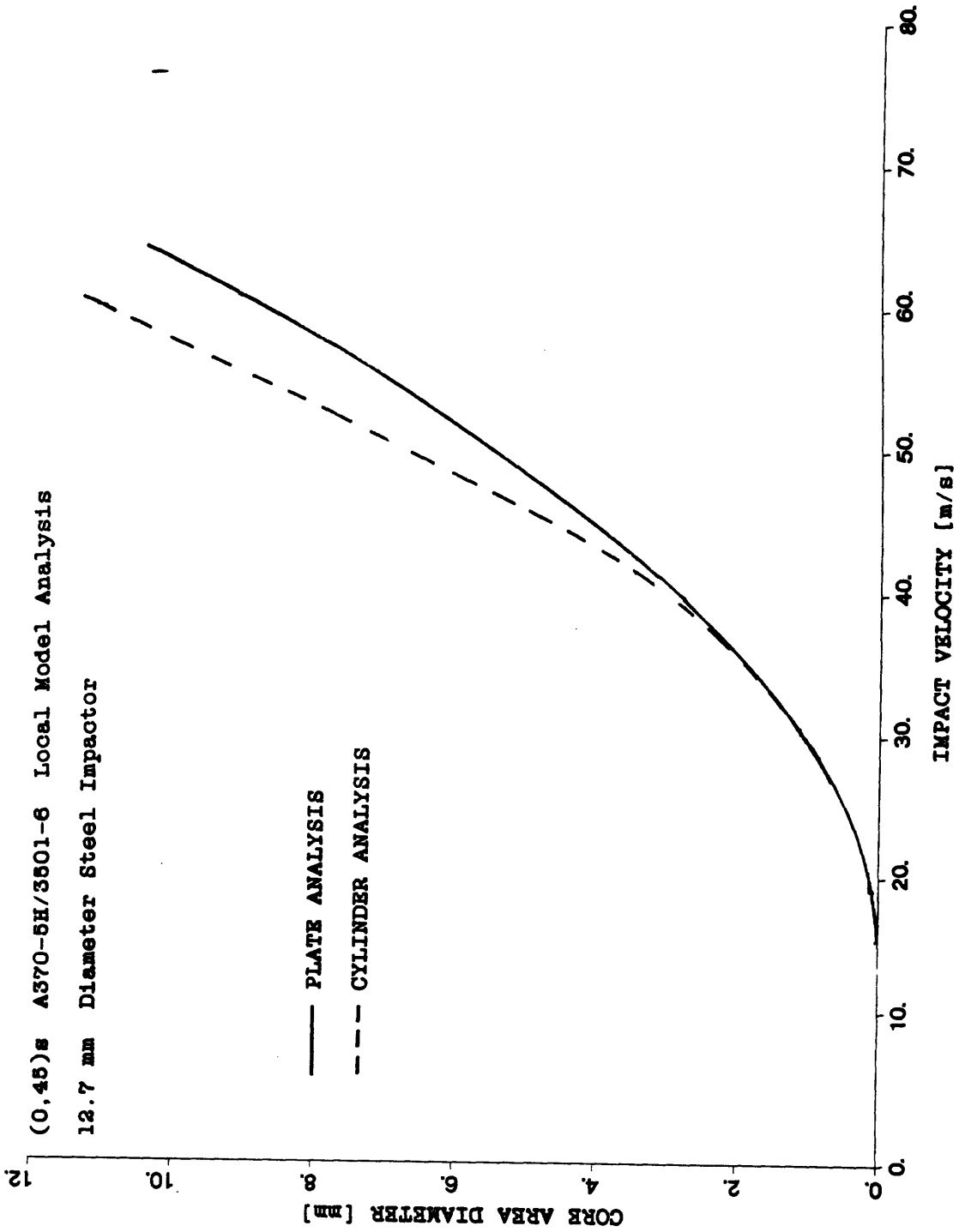

Figure 6.15 Comparison of Plate and Cylinder Geometry Damage Resistance

seen in Figures 6.8 and 6.11, the analysis predictions of fiber breakage provided a good approximation of the maximum radius of the experimentally determined core damage area. Note that the differences in the core area damage diameter are not extremely different between the two cases. This was a result of the peak loads of the plate and cylinder structures being fairly close for the same impact velocity. However, it was experimentally shown that the damage surrounding the core area was significantly different for the two geometries. The local model was unable to predict these differences.

Considering the damage resistance predictions for the plate geometry to be a baseline, the damage resistance of the cylinder was predicted reasonably well by using the adapted global model. Once again, the only difference between the two damage prediction analyses was the use of the orthotropic cylinder global model to generate the impact loading and acceleration histories. The local Fourier-Bessel model was implemented without modification. The resulting predictions for the inclusion area of the cylinder were as successful as the baseline plate analysis. Thus, the extension of the plate analysis to the cylinder geometry was successful, but only for prediction of the fiber damage.

6.4.2 Damage Tolerance

The use of the $(45)_s$ inclusion area yielded good results for the prediction of the damage tolerance of the plate

coupons loaded in tension. It was assumed for the cylinder analysis that if the failure modes of the two geometries were similar, a direct or corrected plate analysis could be used to determine the damage tolerance of an impacted cylinder.

For the $(0,45)_s$ A370-5H/3501-6 laminate, it appeared that both coupon and cylinder failure was governed by failure of the 0° plies. In both cases, the primary fracture path was perpendicular to the highest loaded direction. However, the strain field around the impact area was different for the two cases. The plate strain gage data showed no observable effect of the impact area when the coupon was loaded in tension. However, the pressurized cylinder strain gage data showed a considerable effect on the strain field around the impact area. This strain concentration indicated bending at the impact area because of the internal pressurization.

A correction factor for the bending stress at a notch has been used to relate the flat geometry to the pressure cylinder geometry where the failure modes and damage types of the two cases were similar [29]. However, the uncorrected direct application of the plate inclusion analysis shown in Figure 6.12 did not fit the cylinder data adequately. The analysis curve based on the unflawed cylinder failure pressures did not match the experimental data, but the reduced strength between threshold and punch-through impact was predicted well. A correction factor for the bending stress would move this prediction lower. If the analysis used the predicted failure pressure of the cylinders as the starting point, the curve

would be better matched, but the amount of strength reduction would not. Using the damage threshold level as a starting point provides an excellent fit. Currently, no analysis is capable of predicting where the damage threshold level occurs.

Another possible explanation for the discrepancy is that the bending at the impact damage area may have been a function of the level of impact damage. For small amounts of impact damage on the inside surface of the cylinder, the bending at the edge of the damage area is not as severe as the case for punch-through impact damage. As the damage to the cylinder increased, the effect of the localized bending became greater. In order to account for the changing localized bending because of the internal pressure load, a correction factor dependent on the amount of damage would have to be derived. Therefore, the plate inclusion analysis applied directly to the cylinder geometry to predict damage tolerance did not properly account for the structural effects associated with impact damage in pressurized cylinders. The use of a simple correction factor for bending at the impact damage edge could not be applied. A more complex behavior governed the damage tolerance of the cylinders that would have to be included in the analysis.

Saeger [41] developed a finite-difference model to determine the bending at a slit in a pressurized cylinder. A similar analysis may have to be performed with the degraded membrane of the predicted damage area to observe the

importance of the bending and the level of impact damage, which may require a local model that includes the cylinder curvature for determining the impact damage area. If this connection could be made and the correction factor determined, the uniaxially loaded inclusion model could be accurately applied to the pressure loaded cylinder condition.

CHAPTER SEVEN

CONCLUSIONS AND RECOMMENDATIONS

The experimental investigation of the impact damage resistance and damage tolerance provided an extensive amount of data on the type, extent, and influence of impact damage in fabric graphite/epoxy plate and cylinder structures. The experimental and analytical work provided a good first glimpse into the effects of curvature on the impact event. This chapter is a summary of the major conclusions drawn from this research. These conclusions are valid for the $(0,45)_s$ A370-5H/3501-6 fabric laminate and extension of the results may not be valid for other material systems. Recommendations for further study, based on the knowledge obtained in this work, are also given.

7.1 Conclusions

The major findings of the experimental investigation of the damage resistance of fabric plate and cylinder structures may be summarized as follows:

1. Impact damage in fabric laminates can be characterized by fiber bundle disbonding, matrix yielding and crushing, delamination, and fiber breakage. Damage occurs in the following order: (a) matrix yielding, (b) fiber bundle

disbonding, (c) fiber breakage, and (d) delamination.

2. The damage state in the fabric laminate for both the plate and cylinder structures is not symmetric through the thickness.

3. The core area diameter of the impacted plates was approximately the same as the core area diameter of the impacted cylinders for an identical impact event.

4. The damage state of a cylinder structure is characterized by a cleaner, more concentrated damage area than the plate structure exposed to the same impact event. The cylinder exhibits less delamination and fiber bundle disbonding around the core damage area than the plate.

5. The damage around the core area in the cylinder decreases after punch-through is achieved.

The damage tolerance investigation of plate/coupon structures under tensile uniaxial load and cylinders under pressurized load yielded the following results:

6. Both the plate and cylinder structures show a threshold level of impact damage before a reduction in the unflawed strength is observed. For the plate structures, the threshold is approximately 3 mm of core area damage as

measured from the Dib dye-penetrant enhanced x-ray photographs. The cylinders exhibit a threshold level of aproximately 5 mm of core area damage as visually determined from the footprint of the impactor on the cylinder surface.

7. The coupon specimens did not exhibit a measurable change in the strain field around the impact damage area. The pressurized cylinders, however, did typically show an increase in the strain field around the impact damage site. This indicated that bending at the impact area occured as the cylinder was pressurized.

The analytical approach considered the impact problem first at a global level to determine the force and acceleration time histories of the event and then at a local level to determine the damage and residual strength. The correction for the cylinder curvature was incorporated at the global level only. The results of the analysis may be summarized as follows:

8. The force-time histories of the plate and cylinder structures were significantly different. The cylinder loading history was much smoother and was accompanied by a short acceleration spike which died out within several microseconds. The plate loading history was much more erratic with significant acceleration of the plate

throughout the impact event.

9. The peak force versus impact velocity and acceleration versus impact velocity curves of the plate and cylinder structures were approximately linear for the impact velocities investigated. The magnitudes of the peak values for the plate and cylinder were approximately the same for the impact velocities studied.

10. The local Fourier-Bessel model and failure criterion could not duplicate the shape of the fiber damage found in the plate and cylinder structures. However, the model provided an accurate prediction of the maximum size of the fiber damage cross-hair found in the experimental epoxy burn-offs. This maximum size corresponded to the size of the core damage diameter measured from the x-ray photographs.

11. The local model could not predict a difference in the damage states around the core area for the two structural configurations considered.

12. The analysis implemented for this investigation correlated well to the experimental results for the plate damage tolerance. The inclusion model provided a conservative prediction for damage tolerance of the impacted plates.

13. The inclusion model for the plate, applied directly to the cylinder, did not correlate well the data for the pressurized cylinders. A simple correction factor for the bending at the inclusion edge could not improve the correlation. The use of the predicted unflawed failure pressure could provide better correlation to the failure pressure data for cylinders with high amounts of impact damage. However, the magnitude of the strength reduction could not be matched. These observations lead to the conclusion that the bending stress contribution at the impact damage edge could not be corrected by a simple method and that the stress intensification was dependent on the size and shape of the damage.

7.2 Recommendations for Further Research

As is true with most research, many questions remain unanswered after the investigation is done. An important concept highlighted by Cairns [1] is that the parts of the analysis used for this research are essentially independent of each other and may be substituted by other methods without altering the general approach to the problem. It is also important to provide more experimental correlation for the independent analyses. Thus it is recommended that the following be attempted:

1. The first model to address is the global model used to generate the force-time and acceleration-time impact event histories. The model should be tested against experimental data, especially to verify the difference between the loading patterns found for the plate and cylinder structures.

2. It has been shown in this research that the local Fourier-Bessel model cannot accurately duplicate the shape of the impact damage in the plane and through the thickness of the laminate, but it does provide an accurate assessment of the size of the damage. The peak load of the force-time impact history is currently used to predict damage. However, there is reason to believe that the shape of the loading history may effect the damage. A simple test to research this would be to utilize an instrumented tup. The tup could be used as a static indentor to examine the effects of impact velocity on a structure while the peak load remains a constant.

3. The Fourier-Bessel local model needs modification to more realistically deal with the impact problem. The local model uses a plate that is a plug removed from the structure used in the global analysis, therefore, shear and bending moments exist at the edges of the cut. The current model is a simply supported plate and some method of incorporating the actual boundary conditions should be

developed. The inertial loading on the plate is incorporated as a pressure load applied uniformly to the plate. The effects of this loading should be investigated experimentally by statically and dynamically loading the plate to the same peak load.

4. The inclusion model has not been tested experimentally for composite laminates. Better stated, the concept of using this model with the strain ratio in determining the residual strength of a laminate has not been tested. A test could be devised in which the inclusion could be manufactured into the laminate. The $(0,45)_s$ fabric laminate lends itself easily to this problem. By cutting circular holes in the outer 0° plies and shimming the bottom hole for the manufacturing cycle, an inclusion specimen could be easily obtained.

Essential to further progress in the impact of composite laminates is a broadening of the knowledge of the structural effects on the impact event. This investigation involved the study of two geometries without varying the dimensions of the problem. New research should involve the following:

5. The structural effects of increased curvature on impact damage resistance and impact damage tolerance should be researched through the use of pressurized cylinders of different radii.

6. In order to obtain the theoretical failure pressures for the cylinders, new specimens and manufacturing processes should be investigated. First, to avoid multiple seams a $(0)_4$ fabric layup in which the ply is continuously wrapped around the mandrel could be used. Second, to avoid ridges and other manufacturing anomalies different manufacturing procedures may need to be devised.

7. The cylinders should be tested using hydraulic equipment to allow a safer test in which the failure path may be more accurately determined.

8. Different material systems should be investigated. Particularly, material systems other than the A370-5H/3501-6 system should be investigated to determine the effects on damage resistance and damage tolerance.

These recommendations should be implemented and can serve to clear some unanswered questions, thus helping to obtain a greater understanding of the effects of impact on composite materials.

REFERENCES

1) Cairns, D.S., "Impact and Post-Impact Response of Graphite/Epoxy and Kevlar/Epoxy Structures," TELAC Report 87-13, Massachusetts Institute of Technology, Cambridge, MA, August 1987.

2) Takeda, N., Sierakowski, R.L., and Malvern, L.E., "Studies of Impacted Glass Fiber Reinforced Composite Laminates," SAMPE Quarterly, Vol. 12, No. 2, January 1981, pp9-17.

3) Malvern, L.E., Sierakowski, R.L., Ross, C.A., and Cristescu, N., "Impact Failure Mechanisms in Fiber-Reinforced Composite Plates," **High Velocity Deformation of Solids**, edited by Kawata, K. and Shiori, J., Springer-Verlag, Berlin 1978, pp120-130.

4) Takeda, N., "Experimental Studies of the Delamination Mechanisms in Impacted Fiber-Reinforced Composite Plates," Ph.D. Dissertation, University of Florida 1980.

5) Sierakowski, R.L., Ross, C.A., and Malvern, L.E., "Studies on the Fracture Mechanisms in Partially Penetrated Filament Reinforced Laminated Plates," Final Report on U.S. Army Research Office Grant DAAG 29-79-G-0007, University of Florida, Gainsville, FL, December 1981.

6) Sierakowski, R.L., Ross, C.A., Malvern, L.E., and Cristescu, N., "Studies on the Penetration Mechanics of Composite Plates," Final Report on U.S. Army Research Office Grant DAAG 29-76-G-0085, U.S. Army Research Office, N.C. December 1976.

7) Lagace, P.A., "Notch Sensitivity of Graphite/Epoxy fabric Laminates," Composites Science and Technology, Vol. 26, No. 2, 1986 pp95-117

8) Teti, R., Langella, F., Crivelli Visconti, I., and Caprino, G. "Impact Response of Carbon Cloth Reinforced Composites," 5th International Conference on Composite Materials ICCM-V, San Diego, CA pub. The Metallurgical Society, Warrendale, PA 1985 pp373-381

REFERENCES (continued)

9) Winkel, J.D. and Adams, D.F., "Instrumented Drop Weight Impact Testing of Cross-ply and Fabric Composites," Composites, Vol. 16, No. 4 October 1985 pp268-278

10) Whitney, J.M. and Pagano, N.J., "Shear Deformation in Heterogeneous Anistropic Plates," Journal of Applied Mechanics, Vol. 37, American Society of Mechanical Engineers, N.Y., N.Y. 1970 pp1031-1036.

11) Tan, T.M. and Sun, C.T., "Use of Statical Indentation Laws in the Impact Analysis of Laminated Composite Plates," Journal of Applied Mechanics, Vol. 52 March 1985 pp6-12

12) Sun, C.T. and Chen, J.K., "On the Impact of Initially Stressed Composite Laminates," Journal of Composite Materials, Vol. 19 November 1985 pp490-503

13) Wu, H.Y. and Springer, G.S., "Impact Damage of Composites," NASA-Ames Cooperative Agreement No. NCC 2-304, Interim Report, August 1985.

14) Cairns, D.S. and Lagace, P.A., "Transient Response of Graphite/Epoxy and Kevlar/Epoxy Laminates Subjected to Impact," presented at the AIAA/ASME/ASCE/AHS 29th Structures, Structural Dynamics, and Materials Conference, AIAA paper 88-2328, Williamsburg, VA, April 1988

15) Razi, Hamid and Lindsay, V.E.J., "Analysis of Simply-Supported Orthotropic Cylinder Subjected to Low Velocity Impact," presented at the AIAA/ASME/ASCE/AHS 28th Structures, Structural Dynamics, and Materials Conference, AIAA paper 87-0801,

16) Greszcuk, L.B., "Damage in Composite Materials Due to Low Velocity Impact," **Impact Dynamics**, John Wiley & Sons, New York, NY 1982.

17) Greszcuk, L.B., "Response of Isotropic and Composite Materials to Particle Impact," **Foreign Object Impact Damage to Composite Materials**, ASTM STP 568, American Society for Testing and Materials, Philadelphia, PA 1973, pp183-209

18) Cairns, D.S. and Lagace, P.A., "Thick Composite Plates Subjected to Lateral Loading," Journal of Applied Mechanics, Vol. 54 September 1987 pp611-616

REFERENCES (continued)

19) Gustafson, A.J., Ng, G.S., and Singley, G.T. "Impact Behavior of Fibrous Composites and Metal Substructures," Report no. USAAVRADCOM-TR-82-D-31, Applied Technology Laboratory, U.S. Army Research Laboratories, Fort Eustis, VA, October 1982

20) Click, H.F. Jr., "Application of Graphite and Aramid Composites on the YF-17 Prototype Fighter," Sixth National SAMPE Technical Conference, Dayton, OH, October 1974, pp352-360.

21) Williams, J.G. Anderson, M.S., Rhodes, M.D., Starnes, J.H. Jr., and Stroud, W.J., "Recent Developments in the Design, Testing, and Impact Damage Tolerance of Stiffened Composite Panels," NASA TM 80077, April 1979.

22) Starnes, J.H. Jr., and Rouse, M., "Postbuckling and Failure Characteristics of Selected Flat Rectangular Graphite/Epoxy Plates Loaded in Compression," AIAA/ASME/ASCE/AHS 22nd Structures, Structural Dynamics, and Materials Conference, Atlanta, GA, April 1981.

23) Starnes, J.H. Jr., Rhodes, M.D., and Williams, J.G., "The Effect of Impact Damage and Circular Holes on the Compressive Strength of a Graphite/Epoxy Laminate," NASA TM 78796, October 1978.

24) Caprino, G., "Residual Strength Prediction of Impacted CFRP Laminates," Journal of Composite Materials, Technomic Publishing Company, Westport, CT, Vol.18, 1984 pp508-518.

25) Dorey, G., Sidey, G.R., and Hutchings, "Impact Properties of Carbon Fibre/Kevlar 49 Fibre Hybrid Composites," Composites, January 1978, pp.26-32

26) Cairns, D.S. and Lagace, P.A., "Residual Strength of Graphite/Epoxy and Kevlar/Epoxy Laminates with Impact Damage," presented at the ASTM 9th Symposium on Composite Materials: Testing and Design, Reno, NV, April 1988, TELAC Report 88-3, Massachusetts Institute of Technology, Cambridge, MA, April 1988.

27) Lekhnitskii, S.G., **Theory of Elasticity of an Anisotropic Body**, Holden-Day, Inc., San Francisco, CA 1963.

REFERENCES (continued)

28) Lagace, P.A., and Cairns, D.S., "Tensile Response of Laminates to Implanted Delaminations," presented to the 32nd International SAMPE Symposium and Exhibition, Anaheim, CA, April 1987

29) Lagace, P.A. and Saeger, K.J., "Damage Tolerance Characteristics of Pressurized Graphite/Epoxy Cylinders," OMAE paper 87-607, presented at the Sixth ASME International Symposium on Offshore Mechanics and Arctic Engineering, March 1987.

30) Dugundgi, J., "Simple Expressions for Higher Vibration Modes of Uniform Euler Beams," AIAA Journal Technical Note - To be Published.

31) Jones, R.M., **Mechanics of Composite Materials**, Scripta Book Company, Wasington, D.C. 1975.

32) Whitney, J.M. and Nuismer, R.J., "Stress Fracture Criteria for Laminates Containing Stress Concentrations," Journal of Composite Materials, Technomic Publishing Company, Westport, CT, Vol. 8, 1974 pp253-265.

33) Kageyama, M., "The Effect of Delaminations on the Failure of Pressurized Graphite/Epoxy Cylinders," TELAC Report 86-18, Massachusetts Institute of Technology, February 1985.

34) Folias, E.S., "Asymtotic Approximations to Crack Problems in Shells," Mechanics of Fracture, Vol. 3, Noordhoff International, Leiden, the Netherlands, 1977 pp117-160.

35) Graves, M.J. and Lagace, P.A., "Damage Tolerance of Composite Cylinders," Composite Structures, Vol. 4, No. 1, 1985 pp75-91.

36) Robichaux, L.M., "Sensitivity of Graphite/Epoxy to Implanted Delaminations under Tensile Load: Initial Study," TELAC Report 86-4, Massachusetts Institute of Technology, Cambridge, MA, December 1985.

37) Salerno Tool Works Inc., 21034 Ryan Road, Warren, MI tel.(313)755-5000, contact: Jeff Michaeli

38) Freeman, S.M., "Characterization of Lamina and Interlaminar Damage in Graphite/Epoxy Composites by the Deply Technique," Proceedings of 6th Conference on Composite Materials: Testing and Design 1982, ASTM STP no. 787, pp50-62.

REFERENCES (continued)

39) Lagace, P.A., "Static Tensile Fracture of Graphite/Epoxy," TELAC Report 82-14, Massachusetts Institute of Technology, Cambridge, MA, June 1982 p223.

40) Unpublished Experimental Data for Hercules A370-5H/3501-6 fabric graphite/epoxy material system, Technology Laboratory for Advanced Composites, Massachusetts Institute of Technology, Cambridge, MA 1988.

41) Saeger, K.J., "Damage Tolerance of Composite Cylinders with a High Strain-to-Failure Matrix System," TELAC Report 86-11, Massachusetts Institute of Technology, Cambridge, MA 1986.

APPENDIX A

FORTRAN SOURCE CODES FOR ANALYSIS

This Appendix contains the FORTRAN source code listings for the global plate and cylinder impact event analyses, and the plate local contact problem analysis. The codes are compatible VAX FORTRAN Version 4.6. Codes that are not listed here are given in Cairns [1].

The steps involved in the impact event analysis are (a) compute the 3-D engineering properties for the laminate, (b) use the local Fourier-Bessel series model to fing the Hertzian spring constant, (c) use the global model to determine the force and acceleration time histories of the impact event, (d) extract the peak force and corresponding acceleration for the impact event and use this data in the local model to compute the stress and strain distribution in the impacted plate, (e) from the local model output determine the damage area based on the maximum strain criterion, (f) determine the size and type of the undamaged membrane for use in the inclusion model, (g) use the inclusion model to determine the far-field strain for the loading condition desired, (h) use the inclusion model to find the averaged strain at the inclusion border, and (i) take the ratio of these two values to determine the post-impact residual strength of the laminate.

In the codes that follow, all input data should be in compatible units, such as kilograms, meters, and seconds.

```
C*************************************************************************
C
C            THIS FILE CONTAINS A LISTING OF THE PROGRAMS REQUIRED
C                    FOR THE PLATE IMPACT ANALYSIS PACKAGE
C
C*************************************************************************
C
C       MAIN PROGRAM:     IMPACT              [GLOBAL1.FOR]
C
C         WRITTEN BY:     WILSON TSANG  19 APRIL 1988
C   MODIFICATIONS BY:     MICHAEL KRAFT
C
C        SUBROUTINES:     INPUT               [GLOBAL2.FOR]
C                         BCONS               [GLOBAL3.FOR]
C                         INTGL / INTGL1      [GLOBAL3.FOR]
C                         MATRIX              [GLOBAL4.FOR]
C                         ARRAN               [GLOBAL5.FOR]
C                         CONDENSE            [GLOBAL6.FOR]
C                         NEWMARK             [GLOBAL7.FOR]
C
C       [NAMES IN BRACKETS ARE THE STORAGE FILES]
C
C       LINPAK CALLS:     DSPFA
C                         DSPDI
C                         DCOPY
C                         DDOT
C                         DAXPY
C                         IDAMAX
C                         DSWAP
C
C       [ALL SUBROUTINES CALLED FROM THE LINPAK ROUTINE ARE CONTAINED
C        IN THE FILE LINPAK.FOR]
C
C
C       INCLUDE FILE:     IMPACT.INC
C           [INCLUDE FILE CONTAINS ARRAY DIMENSIONING PARAMETERS]
C
C*************************************************************************
```

```
C*************************************************************************
C
C  THIS IS THE INCLUDE FILE FOR THE PROGRAM IMPACT.FOR
C
C*************************************************************************
C
C   THE PARAMETERS USED IN DIMENSIONING THE ARRAYS ARE:
C
C       M1 = MAXIMUM NUMBER OF MODES IN X-DIRECTION
C       M2 = MAXIMUM NUMBER OF MODES IN Y-DIRECTION
C       M3 = (M1 * M2 * 3) + 1
C       M4 = (M3 * (M3 + 1)) / 2
C       M5 = (M1 * M2)*(M1 * M2 +1) / 2
C       M6 = (M1 * M2)
C
C-------------------------------------------------------------------------
C       23 MODES(X) BY 23 MODES(Y):
C
        PARAMETER(M1 = 23, M2 = 23,
     _           M3 = (M1 * M2 * 3) + 1. ,
     _           M4 = (M3 * (M3 + 1)) / 2. ,
     _           M5 = (M1 * M2)*(M1 * M2 + 1.) / 2. ,
     _           M6 = (M1 * M2) )
C*************************************************************************
```

```
      PROGRAM IMPACT
C*************************************************************************
C   THIS PROGRAM IS THE MAIN CONTROLLING PROGRAM FOR THE PLATE IMPACT
C         ANALYSIS OF THE TIME HISTORY OF AN IMPACT EVENT.
C
C   INFORMATION ON THE FILES AND SUBROUTINES USED BY THIS PACKAGE MAY
C               BE FOUND IN THE FILE 'IMPACT.DOC'
C
C   ORIGINAL PROGRAM WRITTEN BY:  WILSON TSANG  19 APRIL 1988
C            MODIFICATIONS BY:  MICHAEL KRAFT
C
C*************************************************************************
      IMPLICIT REAL*8 (A-H,O-Z)
      REAL*8 MASS
C
C    INCLUDE COMMON PARAMETER VALUES AND COMMON BLOCKS
C
      INCLUDE 'IMPACT.INC'
C
      DIMENSION XBETA(M1),XB(M1),YBETA(M2),YB(M2),
     _          PSI(3,3,M1,M1),PHI(3,3,M2,M2),WX(M1),WY(M2),
     _          MASS(M3),STIFF(M4),W(M3)
C
      COMMON /INVSE/ WORK(M3),KP(M3),DET(2),INERT(3)
C
C    OPEN ALL FILES USED FOR THIS ANALYSIS
C
C       UNIT        FILE            TYPE
C       10          IMPACT.DAT      INPUT
C       30          FORCE.RES       OUTPUT
C       40          ACCEL.RES       OUTPUT
C       70          IMPACT.RES      OUTPUT
C       80          DISP.RES        OUTPUT
C
      OPEN(UNIT=10,FILE='IMPACT.DAT',STATUS='OLD')
      OPEN(UNIT=30,FILE='FORCE.RES ',STATUS='NEW')
      OPEN(UNIT=40,FILE='ACCEL.RES ',STATUS='NEW')
      OPEN(UNIT=70,FILE='IMPACT.RES',STATUS='NEW')
      OPEN(UNIT=80,FILE='DISP.RES  ',STATUS='NEW')
C
      CALL INPUT(NX,NY,IX,IY,H,RHO,A,B,D11,D12,D16,D22,D26,D66,
     _           A44,A45,A55,S,HK,BM,DELT,NT,VI,PNX,PNY)
C
      CALL BCONS(XBETA,XTHETA,XA,XB,IX,NX)
C
      CALL BCONS(YBETA,YTHETA,YA,YB,IY,NY)
C
      IF (NX.EQ.4) THEN
         CALL INTGL1(XBETA,XTHETA,XA,XB,IX,PSI,WX)
      ELSE
         CALL INTGL(XBETA,XTHETA,XA,XB,IX,PSI,WX)
      ENDIF
C
      IF (NY.EQ.4) THEN
         CALL INTGL1(YBETA,YTHETA,YA,YB,IY,PHI,WY)
```

```
      ELSE
         CALL INTGL(YBETA,YTHETA,YA,YB,IY,PHI,WY)
      ENDIF
C
      CALL MATRIX(MASS,STIFF,W,IX,IY,PSI,PHI,WX,WY,
     -            H,RHO,A,B,D11,D12,D16,D22,D26,D66,
     -            A44,A45,A55,S,PNX,PNY)
      N=3*IX*IY
C
      IF(NX.EQ.4.OR.NY.EQ.4) CALL ARRAN(STIFF,MASS,W,N,NLIST)
C
      IF (IFC.EQ.1) CALL CONDENSE(MASS,STIFF,W,N,NLIST)
C
      CALL NEWMARK(MASS,STIFF,W,N,HK,BM,DELT,NT,VI)
C
      STOP
      END
C
C-----------------------------------------------------------------------
```

```
      SUBROUTINE INPUT(NX, NY, IX, IY, H, RHO, A, B,
     _                 D11, D12, D16, D22, D26, D66,
     _                 A44, A45, A55, S, HK, BM, DELT,
     _                 NT, VI, PNX, PNY)
C*****************************************************************************
C            THIS SUBROUTINE READS IN THE REQUIRED DATA FOR THE
C             PLATE IMPACT ANALYSIS PROGRAM FROM THE DATA FILE
C                          NAMED 'IMPACT.DAT'
C*****************************************************************************
       IMPLICIT REAL*8 (A-H,O-Z)
       CHARACTER*80 TITLE1,TITLE2,TITLE3
C
C  INCLUDE ALL COMMON PARAMETERS AND COMMON BLOCKS
C
       INCLUDE 'IMPACT.INC'
C
C*****************************************************************************
C    THE REQUIRED INPUT AND A DESCRIPTION OF THE UNITS REQUIRED:
C
C    DESCRIPTION            VARIABLE              UNITS
C
C    title  1               TITLE1              max 80 char
C    title  2               TITLE2
C    title  3               TITLE3
C
C    x-direction b.c.         NX                  integer
C    y-direction b.c.         NY                  integer
C
C    * where the index numbers for the boundary conditions are:
C          1 FOR SS-SS
C          2 FOR CL-FR
C          3 FOR CL-CL
C          4 FOR FR-FR
C          5 FOR SS-CL
C          6 FOR SS-FR
C
C    number of x-axis modes   IX                  integer
C    number of y-axis modes   IY                  integer
C    * note that IX = IY for this version
C
C    condense rotary inertia  IFC                 integer
C    * 1 = yes, 0 = no
C
C    plate thickness          H                   meters
C    plate density            RHO                 kg/m3
C
C    x-dimension              A                   meters
C    y-dimension              B                   meters
C
C    D11                      D11                 N*m
C    D12                      D12
C    D16                      D16
C    D22                      D22
C    D26                      D26
C    D66                      D66
```

```
C
C    A44                        A44                    N/m
C    A45                        A45
C    A55                        A55
C
C    shear correction factor    S                      real
C    * this must be the square root of the factor *
C
C    hertzian spring constant   HK                     N/m1.5
C    impactor mass              BM                     kg
C    time step length           DELT                   seconds
C    number of time steps       NT                     integer
C    impactor velocity          VI                     m/s
C
C    x-direction load           PNX                    N/m
C    y-direction load           PNY                    N/m
C
C*************************************************************************************
C
      READ(10,100) TITLE1
      READ(10,100) TITLE2
      READ(10,100) TITLE3
 100  FORMAT(A)
C
      READ(10,*) NX
      READ(10,*) NY
      READ(10,*) IX
      READ(10,*) IY
      READ(10,*) IFC
C
      READ(10,*) H, RHO, A, B
      READ(10,*) D11, D12, D16, D22, D26, D66
      READ(10,*) A44, A45, A55, S
      READ(10,*) HK, BM, DELT, NT, VI
C
      READ(10,*) PNX, PNY
C
      WRITE(6,110) TITLE1
      WRITE(6,110) TITLE2
      WRITE(6,110) TITLE3
 110  FORMAT(1X,A)
C
      WRITE(6,*)' '
      WRITE(6,*)'NUMBER OF X-DIRECTION MODES =',IX
      WRITE(6,*)'NUMBER OF Y-DIRECTION MODES =',IY
      WRITE(6,*)' '
      WRITE(6,*)'             TIME INCREMENT =',DELT
      WRITE(6,*)'       NUMBER OF TIME STEPS =',NT
      WRITE(6,*)' '
C
      CLOSE(UNIT=10)
      RETURN
      END
C
C-------------------------------------------------------------------------------------
```

```
      SUBROUTINE BCONS(BETA,THETA,A,B,I,N)
C*************************************************************************
C
C
C
C
C*************************************************************************
C
      IMPLICIT REAL*8 (A-H,O-Z)
C
C    INCLUDE ALL COMMON PARAMETERS AND COMMON BLOCKS
C
      INCLUDE 'IMPACT.INC'
C
      DIMENSION BETA(1), B(1)
C
      WRITE (6,*) 'SETTING UP BOUNDARY CONDITIONS'
C
      IF (N.EQ.1) THEN
         DO 10 J=1,I
           BETA(J)=J*3.141592654
           B(J)=0.
10       CONTINUE
         THETA=0.
         A=0.
         RETURN
      ENDIF
C
      IF (N.EQ.2) THEN
         DO 20 J=1,I
            BETA(J)=(J-.5)*3.141592654
            B(J)=2*MOD(J,2)-1
20       CONTINUE
         THETA=-.785398163
         A=1.
         RETURN
      ENDIF
C
      IF (N.EQ.3) THEN
         DO 30 J=1,I
            BETA(J)=(J+.5)*3.141592654
            B(J)=2*MOD(J,2)-1
30       CONTINUE
         THETA=-.785398163
         A=1.
         RETURN
      ENDIF
C
      IF (N.EQ.4) THEN
         BETA(1)=0.
         BETA(2)=0.
         B(1)=0.
         B(2)=0.
         DO 40 J=3,I
            BETA(J)=(J-2.+.5)*3.141592654
```

```
            B(J)=2*MOD(J-2,2)-1
 40       CONTINUE
          THETA=2.35619449
          A=1.
          RETURN
        ENDIF
C
        IF (N.EQ.5) THEN
          DO 50 J=1,I
            BETA(J)=(J+.25)*3.141592654
            B(J)=2*MOD(J,2)-1
 50       CONTINUE
          THETA=0.
          A=0.
          RETURN
        ENDIF
C
        IF (N.EQ.6) THEN
          DO 60 J=1,I
            BETA(J)=(J+.25)*3.141592654
            B(J)=2*MOD(J+1,2)-1
 60       CONTINUE
          THETA=0.
          A=0.
          RETURN
        ENDIF
C
        END
C
C
C
C-----------------------------------------------------------------------
C
C
C
      SUBROUTINE INTGL(BETA,THETA,A,B,II,F,W)
C*****************************************************************************
C
C
C
C*****************************************************************************
        IMPLICIT REAL*8 (A-H,O-Z)
        INTEGER P,Q
C
C   INCLUDE COMMON PARAMETER VALUES AND COMMON BLOCKS
C
        INCLUDE 'IMPACT.INC'
C
        DIMENSION BETA(1),B(1),F(3,3,M1,1),W(1)
C
        WRITE (6,*) 'CALCULATING INTEGRALS OF BEAM FUNCTIONS'
C
        PI=3.141592654
        DO 10 I=1,3
          DO 10 J=1,3
```

```
            DO 10 M=1,II
               DO 10 N=1,II
C
                  IF (I.GT.J) THEN
                     F(I,J,M,N)=F(J,I,N,M)
                     GOTO 10
                  ENDIF
C
                  P=I-1
                  Q=J-1
                  D1=BETA(M)-BETA(N)
                  D2=BETA(M)+BETA(N)
                  D3=BETA(M)*BETA(M)+BETA(N)*BETA(N)
                  D4=2*MOD(P+1,2)-1
                  D5=2*MOD(Q+1,2)-1
                  D6=THETA+P*PI/2.
                  D7=THETA+Q*PI/2.
C
                  IF (M.EQ.N) THEN
                     D8=COS(D6-D7)
                  ELSE
                     D8=(SIN(D1+D6-D7)-SIN(D6-D7))/D1
                  ENDIF
C
                     D9=(SIN(D6+D7)-SIN(D2+D6+D7))/D2
                     D10=D4*A*(BETA(N)*COS(D7)+BETA(M)*SIN(D7))
                     D11=B(M)*(BETA(M)*SIN(BETA(N)+D7)-
     -                        BETA(N)*COS(BETA(N)+D7))
                     D12=D5*A*(BETA(M)*COS(D6)+BETA(N)*SIN(D6))
                     D13=B(N)*(BETA(N)*SIN(BETA(M)+D6)-
     -                        BETA(M)*COS(BETA(M)+D6))
                     D14=(D4*D5*A*A+B(M)*B(N))/D2
C
                     F(I,J,M,N)=(BETA(M)**P)*(BETA(N)**Q)*
     -                          (D8+D9+D14+1.414213562*
     -                          (D10+D11+D12+D13)/D3)
 10      CONTINUE
C
         X=.5
         DO 20 I=1,II
            D15=BETA(I)*X+THETA
            D16=EXP(-BETA(I)*X)
            D17=EXP(-BETA(I)*(1.-X))
            W(I)=1.414213562*SIN(D15)+A*D16+B(I)*D17
 20      CONTINUE
         RETURN
         END
C
C
C
C-------------------------------------------------------------------------
C
C
C
      SUBROUTINE INTGL1(BETA,THETA,A,B,II,F,W)
```

```
C*******************************************************************************
C
C
C
C
C*******************************************************************************
      IMPLICIT REAL*8 (A-H,O-Z)
      INTEGER P,Q
C
C   INCLUDE COMMON PARAMETER VALUES AND COMMON BLOCKS
C
      INCLUDE 'IMPACT.INC'
C
      DIMENSION BETA(1),B(1),F(3,3,M1,1),W(1)
C
      WRITE (6,*) 'CALCULATING INTEGRALS OF BEAM FUNCTIONS'
C
      PI=3.141592654
      R2=1.414213562
      R3=1.732050808
      DO 10 I=1,3
         DO 10 J=1,3
            DO 20 M=1,2
               DO 20 N=1,II
                  F(I,J,M,N)=0.
 20         CONTINUE
            DO 30 M=1,II
               DO 30 N=1,2
                  F(I,J,M,N)=0.
 30         CONTINUE
            DO 10 M=3,II
               DO 10 N=3,II
C
                  IF (I.GT.J) THEN
                     F(I,J,M,N)=F(J,I,N,M)
                     GOTO 10
                  ENDIF
C
                  P=I-1
                  Q=J-1
                  D1=BETA(M)-BETA(N)
                  D2=BETA(M)+BETA(N)
                  D3=BETA(M)*BETA(M)+BETA(N)*BETA(N)
                  D4=2*MOD(P+1,2)-1
                  D5=2*MOD(Q+1,2)-1
                  D6=THETA+P*PI/2.
                  D7=THETA+Q*PI/2.
C
                  IF (M.EQ.N) THEN
                     D8=COS(D6-D7)
                  ELSE
                     D8=(SIN(D1+D6-D7)-SIN(D6-D7))/D1
                  ENDIF
C
                     D9=(SIN(D6+D7)-SIN(D2+D6+D7))/D2
```

```
                D10=D4*A*(BETA(N)*COS(D7)+BETA(M)*SIN(D7))
                D11=B(M)*(BETA(M)*SIN(BETA(N)+D7)-
     -                BETA(N)*COS(BETA(N)+D7))
                D12=D5*A*(BETA(M)*COS(D6)+BETA(N)*SIN(D6))
                D13=B(N)*(BETA(N)*SIN(BETA(M)+D6)-
     -                BETA(M)*COS(BETA(M)+D6))
                D14=(D4*D5*A*A+B(M)*B(N))/D2
                F(I,J,M,N)=(BETA(M)**P)*(BETA(N)**Q)*
     -                 (D8+D9+D14+R2*(D10+D11+D12+D13)/D3)
C
 10     CONTINUE
C
        DO 40 I=3,II
           D1=SIN(BETA(I)+THETA)+SIN(THETA)
           D2=SIN(BETA(I)+THETA)-SIN(THETA)
           D3=COS(BETA(I)+THETA)-COS(THETA)
           F(1,2,1,I)=R2*D2+B(I)-A
           F(2,1,I,1)=F(1,2,1,I)
           F(1,2,2,I)= R3*(-R2*D1-B(I)-A+2./BETA(I)*(-R2*D3+A+B(I)))
           F(2,1,I,2)=F(1,2,2,I)
           F(2,1,2,I)=2.*R3/BETA(I)*(R2*D3-A-B(I))
           F(1,2,I,2)=F(2,1,2,I)
           F(1,3,1,I)=BETA(I)*(R2*D3+A+B(I))
           F(3,1,I,1)=F(1,3,1,I)
           F(1,3,2,I)=R3*F(1,3,1,I)-2.*R3*(BETA(I)*(R2*COS(BETA(I)+
     -      THETA)+B(I))-R2*D2-B(I)+A)
           F(3,1,I,2)=F(1,3,2,I)
           F(2,3,2,I)=-2.*R3*BETA(I)*(R2*D3+A+B(I))
           F(3,2,I,2)=F(2,3,2,I)
           F(2,2,2,I)=2.*R3*(-R2*D2-B(I)+A)
           F(2,2,I,2)=F(2,2,2,I)
C
 40     CONTINUE
C
        F(1,1,1,1)=1.
        F(1,1,2,2)=1.
        F(1,2,1,2)=-2.*R3
        F(2,1,2,1)=-2.*R3
        F(2,2,2,2)=12.
C
        X=0.5
C
C  ASSIGN RIGID BODY MODE AMPLITUDES AT CENTER OF PLATE
C
        W(1)=1.
        W(2)=0.
        DO 50 I=3,II
           D15=BETA(I)*X+THETA
           D16=EXP(-BETA(I)*X)
           D17=EXP(-BETA(I)*(1.-X))
           W(I)=1.414213562*SIN(D15)+A*D16+B(I)*D17
 50     CONTINUE
        RETURN
        END
C
```

```
      SUBROUTINE MATRIX(MASS, STIFF, W, IX, IY, PSI, PHI, WX, WY,
     -                  H, RHO, A, B, D11, D12, D16, D22, D26, D66,
     -                  A44, A45, A55, S, PNX, PNY)
C
C*****************************************************************************
C
C
C
C
C*****************************************************************************
      IMPLICIT REAL*8 (A-H,O-Z)
      REAL*8 MASS
C
C   INCLUDE COMMON PARAMETER VALUES AND COMMON BLOCKS
C
      INCLUDE 'IMPACT.INC'
C
      DIMENSION PHI(3,3,M2,1), PSI(3,3,M1,1),
     -          MASS(1),STIFF(1),WX(1),WY(1),W(1)
C
      WRITE (6,*) 'SETTING UP STIFFNESS MATRIX'
      II=IX*IY
      DO 10 I=1,II
         DO 10 J=1,II
            M=(I-1)/IY+1
            N=I-IY*(M-1)
            K=(J-1)/IY+1
            L=J-IY*(K-1)
C
C  CALCULATE COMPONENTS OF STIFFNESS MATRIX AND STORE IMMEDIATELY
C                          IN VECTOR FORM
C
C       KAC(I,J)
C
      STIFF((J+2*II)*(J+2*II-1)/2+I) =
     -          S*S*(A55 * B * PSI(2,2,M,K) * PHI(1,1,N,L) +
     -               A45 * A * PSI(2,1,M,K) * PHI(1,2,N,L))
C
C       KAB(I,J)
C
      STIFF((J+II)*(J+II-1)/2+I) =
     -          D12 * PSI(3,1,M,K) * PHI(1,3,N,L) +
     -          D16 * B/A * PSI(3,2,M,K) * PHI(1,2,N,L) +
     -          D26 * A/B * PSI(2,1,M,K) * PHI(2,3,N,L) +
     -          D66 * PSI(2,2,M,K) * PHI(2,2,N,L) +
     -       S*S*A45 * A*B * PSI(1,1,M,K) * PHI(2,2,N,L)
C
C       KBC(I,J)
C
      STIFF((J+2*II)*(J+2*II-1)/2+I+II) =
     -       S*S*(A45 * B * PSI(1,2,M,K) * PHI(2,1,N,L) +
     -            A44 * A * PSI(1,1,M,K)*PHI(2,2,N,L))
C
      IF (I.GT.J) GOTO 10
C
```

```
C       KAA(I,J)
C
        STIFF(J*(J-1)/2+I) =
     _             D11 * B/A * PSI(3,3,M,K) * PHI(1,1,N,L) +
     _             D16 * PSI(3,2,M,K) * PHI(1,2,N,L) +
     _             D16 * PSI(2,3,M,K) * PHI(2,1,N,L) +
     _             D66 * A/B * PSI(2,2,M,K) * PHI(2,2,N,L) +
     _         S*S*A55 * B*A * PSI(2,2,M,K) * PHI(1,1,N,L)
C
C       KBB(I,J)
C
        STIFF((J+II)*(J+II-1)/2+I+II) =
     _             D22 * A/B * PSI(1,1,M,K) * PHI(3,3,N,L) +
     _             D26 * PSI(1,2,M,K) * PHI(3,2,N,L) +
     _             D26 * PSI(2,1,M,K) * PHI(2,3,N,L) +
     _             D66 / A*B * PSI(2,2,M,K) * PHI(2,2,N,L) +
     _         S*S*A44 * A*B * PSI(1,1,M,K) * PHI(2,2,N,L)
C
C       KCC(I,J)
C
        STIFF((J+2*II)*(J+2*II-1)/2+I+2*II) =
     _         S*S*(A55 * B/A * PSI(2,2,M,K) * PHI(1,1,N,L) +
     _              A44 * A/B * PSI(1,1,M,K) * PHI(2,2,N,L) +
     _              A45 * PSI(2,1,M,K) * PHI(1,2,N,L) +
     _              A45 * PSI(1,2,M,K) * PHI(2,1,N,L)) +
     _              PNX * B/A * PSI(2,2,M,K) * PHI(1,1,N,L) +
     _              PNY * A/B * PSI(1,1,M,K) * PHI(2,2,N,L)
C
 10     CONTINUE
C
        WRITE(6,*) 'SETTING UP MASS MATRIX'
        DO 30 I=1,II
           M=(I-1)/IY+1
           N=I-IY*(M-1)
C
C          MA(I)
C
           MASS(I) = RHO * H*H*H/12. * B*A * PSI(2,2,M,M)
C
C          MB(I)
C
           MASS(II+I) = RHO * H*H*H/12. * A*B * PHI(2,2,N,N)
C
C          MC(I)
C
           MASS(2*II+I) = RHO * H * A*B
C
 30     CONTINUE
C
        WRITE(6,*) 'WORKING OUT FORCE VECTOR'
        DO 40 I=1,II
           M=(I-1)/IY+1
           N=I-IY*(M-1)
           W(I)=0.
           W(I+II)=0.
```

```
            W(I+2*II)=WX(M)*WY(N)
 40       CONTINUE
C
          RETURN
          END
C
C-------------------------------------------------------------------------
```

```
      SUBROUTINE ARRAN(STIFF,MASS,W,N,NLIST)
C*****************************************************************************
C
C
C
C*****************************************************************************
      IMPLICIT REAL*8(A-H,O-Z)
      REAL*8 MASS
C
C   INCLUDE COMMON PARAMETER VALUES AND COMMON BLOCKS
C
      INCLUDE 'IMPACT.INC'
C
      DIMENSION STIFF(1), MASS(1), W(1), ILIST(M6)
C
      DO 5 I=1,N
         IF(MASS(I).EQ.0.) THEN
            NLIST=NLIST+1
            ILIST(NLIST)=I
         ENDIF
 5    CONTINUE
      WRITE(6,*) 'NLIST=',NLIST
      DO 7 I=1,NLIST
         WRITE(6,*) 'ILIST(',I,')=',ILIST(I)
 7    CONTINUE
C
      WRITE(6,*) 'REARRANGING MASS'
      IND1=1
      I=1
      IDUM=ILIST(IND1)
 10   CONTINUE
      IF(I.EQ.IDUM) THEN
         IND1=IND1+1
         DO 20 J=I,N+1-IND1
            MASS(J)=MASS(J+1)
 20      CONTINUE
         IDUM = ILIST(IND1)-IND1+1
         I=I-1
      ENDIF
C
      IF(IND1.EQ.NLIST+1) THEN
         GOTO 15
      ENDIF
C
      I=I+1
      GOTO 10
C
 15   WRITE(6,*) 'REARRANGING STIFF'
      IND1=1
      IND2=1
      IND3=1
      IND4=1
      DO 40 I=1,N
         IF (I.EQ.ILIST(IND3)) THEN
            IND3=IND3+1
```

```
            IND2=IND2+I
            GOTO 40
         ENDIF
         DO 50 J=1,I
            IF(J.EQ.ILIST(IND4)) THEN
               IND2=IND2+1
               IND4=IND4+1
               GOTO 50
            ENDIF
            STIFF(IND1)=STIFF(IND2)
            IND1=IND1+1
            IND2=IND2+1
 50       CONTINUE
          IND4 = 1
 40    CONTINUE
C
       WRITE(6,*) 'REARRANGING FORCE VECTOR'
       IND1=1
       I=1
       IDUM=ILIST(IND1)
 60    CONTINUE
       IF(I.EQ.IDUM) THEN
          IND1=IND1+1
          DO 120 J=I,N+1-IND1
             W(J)=W(J+1)
 120      CONTINUE
          IDUM = ILIST(IND1)-IND1+1
          I=I-1
       ENDIF
C
       IF(IND1.EQ.NLIST+1) THEN
         GOTO 25
       ENDIF
C
       I=I+1
       GOTO 60
C
 25    N=N-NLIST
       RETURN
       END
C
C-----------------------------------------------------------------------
```

```
      SUBROUTINE CONDENSE(MASS,STIFF,W,N,NLIST)
C*****************************************************************************
C
C
C
C*****************************************************************************
      IMPLICIT REAL*8(A-H,O-Z)
      REAL*8 MASS
C
C     INCLUDE COMMON PARAMETER VALUES AND COMMON BLOCKS
C
      INCLUDE 'IMPACT.INC'
C
      DIMENSION MASS(1),STIFF(1),W(1),WX(1),WY(1)
      DIMENSION H(M5)
C
      COMMON /INVSE/ WORK(M3),KP(M3),DET(2),INERT(3)
C
      N2=(N+NLIST)/3
      N1=N-N2
C
      WRITE(6,*) 'INVERTING K2'
      CALL DSPFA(STIFF,N1,KP,INFO)
      CALL DSPDI(STIFF,N1,KP,DET,INERT,WORK,001)
C
      WRITE(6,*)' '
      WRITE(6,*) 'K1T*K2-1*K1'
      WRITE(6,*)' '
      DO 10 J=1,N2
         WRITE(6,90) J
         DO 20 K=1,N1
            WORK(K)=0.
            DO 20 L=1,N1
            IF(K.LE.L) WORK(K)=WORK(K)+STIFF((L-1)*L/2+K)
     -        *STIFF((J+N1)*(J+N1-1)/2+L)
            IF(K.GT.L) WORK(K)=WORK(K)+STIFF((K-1)*K/2+L)
     -        *STIFF((J+N1)*(J+N1-1)/2+L)
 20      CONTINUE
         DO 30 I=J,N2
            DUM=0.
            DO 40 K=1,N1
               DUM=DUM+STIFF((I+N1)*(I+N1-1)/2+K)*WORK(K)
 40         CONTINUE
            H((I-1)*I/2+J)=DUM
 30      CONTINUE
 10   CONTINUE
C
      WRITE(6,*)
      WRITE(6,*) 'CONDENSING STIFF'
      DO 50 I=1,N2
         DO 50 J=I,N2
         STIFF((J-1)*J/2+I) =
     -        STIFF((J+N1-1)*(J+N1)/2+I+N1)-H((J-1)*J/2+I)
 50   CONTINUE
C
```

```
      WRITE(6,*) 'CONDENSING MASS _W'
      DO 60 I=1,N2
         MASS(I)=MASS(I+N1)
         W(I)=W(I+N1)
 60   CONTINUE
      N=N2
 90   FORMAT('+',I4)
      RETURN
      END
C
C-----------------------------------------------------------------------
```

```
      SUBROUTINE NEWMARK(MASS,STIFF,W,N,HK,BM,DELT,NT,VI)
C*****************************************************************************
C
C
C
C
C*****************************************************************************
      IMPLICIT REAL*8 (A-H,O-Z)
      REAL*8 MASS
C
C   INCLUDE COMMON PARAMETER VALUES AND COMMON BLOCKS
C
      INCLUDE 'IMPACT.INC'
C
      DIMENSION MASS(1),STIFF(1),W(1),A(M3),B(M3),F(M3)
      DIMENSION Z1(M3),Z2(M3),ZD1(M3),ZD2(M3),ZDD1(M3)
      DIMENSION ZDD2(M3)
C
      COMMON /INVSE/ WORK(M3),KP(M3),DET(2),INERT(3)
C
      WRITE(6,*) 'SETTING UP MASS* _STIFF*'
      II=N*(N+1)/2
      DO 5 I=II+1,II+1+N
         STIFF(I)=0.
 5    CONTINUE
      MASS(1+N)=BM
      W(N+1)=1.
C
      II=(N+1)*(N+2)/2
      N=N+1
C
      WRITE(6,*) 'INITIALIZING VARIABLES'
      R=0.
      DO 10 I=1,N
         Z1(I)=0.
         ZD1(I)=0.
         ZDD1(I)=0.
 10   CONTINUE
      ZD1(N)=VI
C
      DO 20 I=1,N
         STIFF(I*(I+1)/2)=4./DELT/DELT*MASS(I)+STIFF(I*(I+1)/2)
 20   CONTINUE
      WRITE(6,*) 'MATRIX INVERSION'
C
      CALL DSPFA(STIFF,N,KP,INFO)
C
      IF (INFO.EQ.1) THEN
         WRITE(6,*) 'PROBLEM IN MX INVERSION'
      ENDIF
C
      CALL DSPDI(STIFF,N,KP,DET,INERT,WORK,001)
C
      CALL MXMUL(N,STIFF,W,F)
C
```

```
      D1=0.
      DO 55 I=1,N
         D1=D1-W(I)*F(I)
 55   CONTINUE
      WRITE(6,*)' '
      WRITE(6,*) 'INTEGRATING BY NEWMARK'
C
      WRITE(6,*)' '
C
      ACCELMAX = 0.
      FORCEMAX = 0.
C
      DO 30 J=1,NT
         WRITE(6,80) J
C
         WC = 0.
         WD = 0.
         WDD = 0.
C
         DO 25 I=1,N-1
            WC = WC + W(I)*Z1(I)
            WD = WD + W(I)*ZD1(I)
            WDD= WDD + W(I)*ZDD1(I)
 25      CONTINUE
C
         WRITE(30,*) DELT*(J-1),R
         WRITE(40,*) DELT*(J-1),WDD
         WRITE(80,*) DELT*(J-1),-1.*WC
         WRITE(70,70) DELT*(J-1),R,WC,Z1(N),WD,ZD1(N),WDD
C
C  SAMPLE FOR MAXIMUM FORCE DURING HISTORY
C
         IF (R .GT. FORCEMAX) THEN
            FORCEMAX = R
            ACCELMAX = WDD
            INDEX = J
         ENDIF
C
         DO 50 I=1,N
            Z1(I)=4./DELT/DELT*(Z1(I)+ZD1(I)*DELT)
            ZDD1(I)=Z1(I)+ZDD1(I)
            A(I)=MASS(I)*ZDD1(I)
 50      CONTINUE
C
         CALL MXMUL(N,STIFF,A,B)
C
         D2=0.
         DO 40 I=1,N
            D2=D2+W(I)*B(I)
 40      CONTINUE
C
         CALL NEWRAP(D1,D2,HK,R,J)
C
         DO 60 I=1,N
            Z2(I)=-R*F(I)+B(I)
```

```
            ZD2(I)=ZD1(I)+2./DELT*Z2(I)-DELT/2.*Z1(I)
            ZDD2(I)=4./DELT/DELT*Z2(I)-ZDD1(I)
            Z1(I)=Z2(I)
            ZD1(I)=ZD2(I)
            ZDD1(I)=ZDD2(I)
 60       CONTINUE
 30     CONTINUE
C
       WRITE(6,*)' '
       WRITE(6,*)'        MAXIMUM FORCE = ',FORCEMAX
       WRITE(6,*)' MAXIMUM ACCELERATION = ',ACCELMAX
       WRITE(6,*)'OCCURING AT TIME STEP = ',INDEX
C
 70    FORMAT(1X,7E10.3)
 80    FORMAT('+',I4)
       RETURN
       END
C
C-----------------------------------------------------------------------
C
C
C
      SUBROUTINE MXMUL(N,DUM1,DUM2,DUM3)
C***********************************************************************
C
C
C
C***********************************************************************
       IMPLICIT REAL*8 (A-H,O-Z)
       DIMENSION DUM1(1),DUM2(1),DUM3(1)
       DO 10 I=1,N
          D1=0.
          DO 20 J=1,I
             D1=D1+DUM1((I-1)*I/2+J)*DUM2(J)
 20       CONTINUE
          D2=0.
          DO 30 J=I+1,N
             D2=D2+DUM1((J-1)*J/2+I)*DUM2(J)
 30       CONTINUE
          DUM3(I)=D1+D2
 10    CONTINUE
       RETURN
       END
C
C
C
C-----------------------------------------------------------------------
C
C
C
      SUBROUTINE NEWRAP(A,B,HK,R,J)
C***********************************************************************
C
C
C
```

```
C
C*******************************************************************************
      IMPLICIT REAL*8 (A-H,O-Z)
C
      IF ((A*R+B).LT.0.) THEN
         R=0.
         RETURN
      ENDIF
C
      DO 10 I=1,10
C
         IF (I.EQ.10) WRITE(6,*) 'CHECK J=',J
C
         FR=R-HK*(A*R+B)**1.5
         FDR=1.-1.5*HK*A*(A*R+B)**.5
C
         IF (ABS(FR/FDR).LT.1.E-10) RETURN
C
         R=R-FR/FDR
C
 10   CONTINUE
      RETURN
      END
C
C-------------------------------------------------------------------------------
```

```
C*************************************************************************
C          CYLINDER IMPACT RESPONSE
C*************************************************************************
C
      PARAMETER (NMAX=201,MAX=NMAX*NMAX)
      DIMENSION QI(MAX), QID(MAX), QIDD(MAX), WI2(MAX), CWI(MAX),
     _          SWI(MAX),
     _          WI(MAX), WEIGTH(MAX), WOFX(51,1), WOFY(51,1)
C
C     QI   : MODAL AMPLITUDE
C     QID  : MODAL VELOCITY
C     QIDD: MODAL ACCELERATION
C     WI2  : OMEGA SQUARED
C     CWI  : COS(OMEGA*DELTAT)
C     SWI  : SIN(OMEGA*DELTAT)
C     WI   : OMEGA
C     WEIGTH : VALUE OF MODE AT POINT OF IMPACT
C
      OPEN(UNIT=7,FILE='CYL.DAT',STATUS='OLD')
C
      READ(7,*) NX, NY
      READ(7,*) ACYL, RADIUS, RHO
      READ(7,*) D11, D22, D12, D66
      READ(7,*) A11, A22, A12, A66
      READ(7,*) BALLMASS, U, SPRINGK
      READ(7,*) DT, NSTEP, IFLAG, IOPT
C
      CLOSE(7)
C
      CYLMASS = ACYL*RADIUS*RHO*2.*3.14159
C
      NM = NX * NY
      DO 10 I = 1, NM*IOPT
         QI(I)  = 0.0
         QID(I) = 0.0
         QIDD(I)= 0.0
 10     CONTINUE
C
      WRITE(6,*) ' ---- CALCULATING FREQUENCIES ----'
C
      OPEN(UNIT=10,FILE='FORCE.RES',STATUS='NEW')
      OPEN(UNIT=11,FILE='W0.RES',STATUS='NEW')
      OPEN(UNIT=12,FILE='WB.RES',STATUS='NEW')
      OPEN(UNIT=13,FILE='W0D.RES',STATUS='NEW')
      OPEN(UNIT=14,FILE='WBD.RES',STATUS='NEW')
      OPEN(UNIT=17,FILE='ACCEL.RES',STATUS='NEW')
C
      CALL INITCONST(ACYL,RADIUS,RHO,D11,D22,D12,D66,
     _               A11,A22,A12,A66,DT,NX,NY,
     _               WI,WI2,CWI,SWI,WEIGTH,WOFX,WOFY,IFLAG,IOPT)
C
      WBALL  = U*DT/10.
      WDBALL = SQRT(U*U-4.*SPRINGK/5./BALLMASS*WBALL**2.5)
C
      WRITE(6,*) ' ---- TIME INTEGRATION ----'
```

```
C
      CALL TIMESTEP(CYLMASS,BALLMASS,QI,QID,QIDD,WI,WI2,CWI,SWI,
     _    WEIGTH,SPRINGK,WBALL,WDBALL,NM,DT,NSTEP,NX,NY,IFLAG,
     _    WOFX,WOFY,IOPT)
C
      CLOSE(10)
      CLOSE(11)
      CLOSE(12)
      CLOSE(13)
      CLOSE(14)
C
      STOP
      END
C-----------------------------------------------------------------------
C     INITIALIZE CONSTANTS SUCH OMEGA'S,....
C
      SUBROUTINE INITCONST(ACYL,RADIUS,RHO,D11,D22,D12,D66,
     _                     A11,A22,A12,A66,DT,NX,NY,
     _                     WI,WI2,CWI,SWI,WEIGTH,WOFX,WOFY,IFLAG,IOPT)
C
      IMPLICIT REAL*4 (A-H,O-Z)
      DIMENSION WI(1), WI2(1), CWI(1), SWI(1), WEIGTH(1),
     _         WOFX(51,1), WOFY(51,1), OMEGA2(3), WMN(3)
C
      PI  = 3.14159
C
C --- MODE SHAPES ARE SIN(M*PI*X/A) COS(N*Y/R)
C     M = 1, 3, 5,...    N = 0, 1, 2, 3, ...
C
C      OPEN(UNIT=16,FILE='FREQ.DAT',STATUS='UNKNOWN')
      I = 0
      DO 10 M = 1, 2*NX-1, 2
      DO 10 N = 0, NY-1
        CORRECTION = 1.
        IF (N.EQ.0) CORRECTION = 0.5
C
C --- DEFINE NATURAL FREQUENCIES FOR SIMPLY-SUPPORTED CYLINDER
C
        CALL OMEGA(A11,A22,A12,A66,D11,D22,D12,D66,ACYL,RADIUS,RHO,
     _                 M,N,OMEGA2,WMN)
        DO 10 K = 1, IOPT
          I = I+1
          WI2(I) = OMEGA2(K)
          WI(I)  = SQRT(WI2(I))
          CWI(I) = COS(WI(I)*DT)
          SWI(I) = SIN(WI(I)*DT)
C          FREQ = WI(I)/2./PI
C          WRITE(16,*) M, N, FREQ, WMN(K)
C
C --- WEIGHT = W AT X = A/2, Y =0
C
          WEIGTH(I) = WMN(K)*SIN(0.5*M*PI) / CORRECTION
C
C --- SHAPE FUNCTION VALUES
C
```

```
          IF (IFLAG.EQ.0) GO TO 10
C
          DO 80 J = 1, 51
            X = (J-1.)/50.
            WOFX(J,I) = SIN(M*PI*X)
 80         CONTINUE
C
          DO 90 J = -25, 25
            Y = PI*J/25.
            WOFY(J+26,I) = SIN(M*PI*0.5)*COS(N*Y)
 90         CONTINUE
C
 10     CONTINUE
C
C       CLOSE(16)
       RETURN
       END
C-----------------------------------------------------------------------
C      TIME INTEGRATION
C
       SUBROUTINE TIMESTEP(CYLMASS,BALLMASS,QI,QID,QIDD,WI,WI2,CWI,
     _       SWI,WEIGTH,SPRINGK,WBALL,WDBALL,NM,DT,NSTEP,NX,NY,
     _       IFLAG,WOFX,WOFY,IOPT)
       IMPLICIT REAL*4 (A-H,O-Z)
       DIMENSION QI(1), QID(1), QIDD(1), WI(1), WI2(1), SWI(1), CWI(1),
     _         WEIGTH(1), WOFX(51,1), WOFY(51,1)
C
       IT = 1
       U0 = WDBALL
       REDMASS = CYLMASS/4.
C
C --- CHECK STATIC DEFLECTION UNDER UNIT POINT LOAD
C
       I = 0
       CI = 0.
       DO 2 M = 1, NX
       DO 2 N = 1, NY
       DO 2 K = 1, IOPT
         I = I + 1
         WI2(I) = WI2(I)*REDMASS
         CI = CI + 1.0 / WI2(I) * WEIGTH(I)
 2     CONTINUE
       WRITE(6,*) ' STATIC DEFLECTION =', CI
C
C       WRITE(6,*) 'ETA='
C       READ(5,*) ETA
       ETA = 0.
C
C --- BEGINNING OF LOOP
C
 10    CONTINUE
C
C --- CALCULATE CENTER DISPLACEMENT, VELOCITY
C
       W0  = 0.
```

```
      W0D = 0.
      W0DD= 0.
      DO 20 I = 1, IOPT*NM
        W0  = W0  + QI(I)*WEIGTH(I)
        W0D = W0D + QID(I)*WEIGTH(I)
        W0DD= W0DD+ QIDD(I)*WEIGTH(I)
 20     CONTINUE
C
C --- CALCULATE FORCE (F0) AND FORCE TIME DERIVATIVE (F1)
C
      IF ((WBALL-W0).GT.0.) THEN
        F0 = SPRINGK*(WBALL-W0)**1.5
        F1 = 1.5*SPRINGK*(WBALL-W0)**0.5*(WDBALL-W0D)
        ELSE
        F0 = 0.
        F1 = 0.
        ENDIF
C       F0 = 1.
C       F1 = 0.
C
      TIME = IT * DT
      WRITE(10,*) TIME, F0
      WRITE(11,*) TIME, W0
      WRITE(12,*) TIME, WBALL
      WRITE(13,*) TIME, W0D
      WRITE(14,*) TIME, WDBALL
      WRITE(17,*) TIME, W0DD
C
C --- EVERY 10 STEPS, WRITE W(X,0) AND W(0.5,Y)  TO FILE
C
      IF ((IFLAG.EQ.1).AND.(MOD(IT,10).EQ.0)) THEN
        OPEN(UNIT=15,FILE='WOFX.DAT',STATUS='NEW')
        DO 80 J = 1, 51
          X = (J-1.)/50.
          W = 0.0
          DO 85 I = 1, NM*IOPT
            W = W + QI(I)*WOFX(J,I)
 85         CONTINUE
          WRITE(15,*) X, W
 80       CONTINUE
        CLOSE(15)
C
        OPEN(UNIT=15,FILE='WOFY.DAT',STATUS='NEW')
        DO 90 J = -25, 25
          Y = PI*J/25.
          W = 0.0
          DO 95 I = 1, NM*IOPT
            W = W + QI(I)*WOFY(J+26,I)
 95         CONTINUE
          WRITE(15,*) Y, W
 90       CONTINUE
        CLOSE(15)
        ENDIF
C
C --- UPDATE Q(I)'S
```

```
C
      I = 0
      DO 100 M = 1, NX
      DO 100 N = 1, NY
      DO 100 K = 1, IOPT
        I = I + 1
        CI = F0 / WI2(I) * WEIGTH(I)
        DI = F1 / WI2(I) * WEIGTH(I)
        AI = QI(I) - CI
        BI = (QID(I)-DI) / WI(I)
        QI(I)  = AI*CWI(I) + BI*SWI(I) + CI + DI*DT
        QID(I) =-AI*WI(I)*SWI(I) + BI*WI(I)*CWI(I) + DI
        QIDD(I)= -WI(I) * WI(I) * ( AI*CWI(I) + BI*SWI(I) )
 100    CONTINUE
C
C ---- UPDATE BALL POSITION
C
      WBALL = WBALL + WDBALL*DT - (F0*DT**2/2.+F1*DT**3/6.)/BALLMASS
      WDBALL = WDBALL - (F0*DT+F1*DT**2/2.)/BALLMASS
      WORK = WORK + F0*WDBALL*DT
C
      IT = IT + 1
      IF (MOD(IT,50).EQ.0) WRITE(6,*) IT
      IF (IT.LT.NSTEP) GO TO 10
C
      ENER0 = 0.5*BALLMASS*(U0)**2
      ENER  = 0.5*BALLMASS*(WDBALL)**2
      WRITE(6,*) ' INITIAL ENERGY =',ENER0
      WRITE(6,*) ' TOTAL WORK DONE =',WORK
      WRITE(6,*) ' BALL KINETIC ENERGY =',ENER
C
      RETURN
      END
C-----------------------------------------------------------------------
C
      SUBROUTINE OMEGA(A11,A22,A12,A66,D11,D22,D12,D66,A,RAD,RHO,
     _                 M,N,OMEGA2,WMN)
      IMPLICIT REAL*4 (A-H,O-Z)
      DIMENSION  AA(10),R(10), OMEGA2(3), WMN(3)
C
      PI  = 3.141592654
C
      AA(1) = A11*(M*PI/A)**2 + A66*(N/RAD)**2
      AA(2) = (-A12-A66)*(M*PI/A)*(N/RAD)
      AA(3) = A22*(N/RAD)**2 + A66*(M*PI/A)**2 + D22*(N/RAD/RAD)**2
      AA(4) = -A12*(M*PI/A)*(1./RAD)
      AA(5) = A22*(N/RAD/RAD) + D22*(N**3/RAD**4)
     _     + D12*(M*PI/A)**2*(N/RAD/RAD)
      AA(6) = D11*(M*PI/A)**4 + (2.*D12+4.*D66)*(M*PI/A*N/RAD)**2
     _     + D22*(N/RAD)**4  + A22/RAD**2
C
      IF (N.EQ.0) AA(2) = 0.
C
      DO 10 I = 1, 6
 10     AA(I) = AA(I)/RHO
```

```
C
      MV = 0
      NN = 3
C
      CALL EIGEN(AA,R,NN,MV)
C
C ---- LOWEST EIGENVALUE CORRESPONDING TO TRANSVERSE MOTION
C
      OMEGA2(1) = AA(6)
      WMN(1)    = R(9)
      OMEGA2(2) = AA(3)
      WMN(2)    = R(6)
      OMEGA2(3) = AA(1)
      WMN(3)    = R(3)
C
      DO 20 I = 1, 3
        IF (OMEGA2(I).EQ.0) THEN
          OMEGA2(I) = 1.
          WMN(I)    = 0.
          ENDIF
 20     CONTINUE
C
 99   RETURN
      END
C-----------------------------------------------------------------------
      SUBROUTINE EIGEN(A,R,N,MV)
C
C     PURPOSE:
C     COMPUTE EIGENVALUES AND EIGENVECTORS OF A REAL SYMMETRIC MATRIX
C
C     A - ORIGINAL MATRIX (SYMMETRIC), DESTROYED IN COMPUTATION.
C         RESULTANT EIGENVALUES ARE DEVELOPED IN DIAGONAL OF
C         MATRIX A IN DESCENDING ORDER.
C     R - RESULTANT MATRIX OF EIGENVECTORS (STORED COLUMNWISE,
C         IN SAME SEQUENCE AS EIGENVALUES)
C     N - ORDER OF MATRICES A AND R
C     MV- INPUT CODE
C         0  COMPUTE EIGENVALUES AND EIGENVECTORS
C         1 COMPUTE EIGENVALUES ONLY (R NEED NOT BE
C           DIMENSIONED BUT MUST STILL APPEAR IN CALLING SEQUENCE)
C
C     REMARKS
C     ORIGINAL MATRIX A MUST BE REAL SYMMETRIC (STORAGE MODE=1)
C     MATRIX A CANNOT BE IN THE SAME LOCATION AS MATRIX R
C
C     METHOD
C     DIAGONALIZATION METHOD ORIGINATED BY JACOBI AND ADAPTED
C     BY VON NEUMANN FOR LARGE COMPUTERS AS FOUND IN 'MATHEMATICAL
C     METHODS FOR DIGITAL COMPUTERS', EDITED BY A. RALSTON AND
C     H.S. WILF, JOHN WILEY AND SONS, NEW YORK, 1962, CHAPTER 7
C
C     .....................................................................
C
      DIMENSION A(1),R(1)
C
```

```
C
      MV = 0
      NN = 3
C
      CALL EIGEN(AA,R,NN,MV)
C
C ---- LOWEST EIGENVALUE CORRESPONDING TO TRANSVERSE MOTION
C
      OMEGA2(1) = AA(6)
      WMN(1)    = R(9)
      OMEGA2(2) = AA(3)
      WMN(2)    = R(6)
      OMEGA2(3) = AA(1)
      WMN(3)    = R(3)
C
      DO 20 I = 1, 3
        IF (OMEGA2(I).EQ.0) THEN
          OMEGA2(I) = 1.
          WMN(I)    = 0.
          ENDIF
 20     CONTINUE
C
 99   RETURN
      END
C-----------------------------------------------------------------------
      SUBROUTINE EIGEN(A,R,N,MV)
C
C     PURPOSE:
C     COMPUTE EIGENVALUES AND EIGENVECTORS OF A REAL SYMMETRIC MATRIX
C
C     A - ORIGINAL MATRIX (SYMMETRIC), DESTROYED IN COMPUTATION.
C         RESULTANT EIGENVALUES ARE DEVELOPED IN DIAGONAL OF
C         MATRIX A IN DESCENDING ORDER.
C     R - RESULTANT MATRIX OF EIGENVECTORS (STORED COLUMNWISE,
C         IN SAME SEQUENCE AS EIGENVALUES)
C     N - ORDER OF MATRICES A AND R
C     MV- INPUT CODE
C         0  COMPUTE EIGENVALUES AND EIGENVECTORS
C         1 COMPUTE EIGENVALUES ONLY (R NEED NOT BE
C           DIMENSIONED BUT MUST STILL APPEAR IN CALLING SEQUENCE)
C
C     REMARKS
C     ORIGINAL MATRIX A MUST BE REAL SYMMETRIC (STORAGE MODE=1)
C     MATRIX A CANNOT BE IN THE SAME LOCATION AS MATRIX R
C
C     METHOD
C     DIAGONALIZATION METHOD ORIGINATED BY JACOBI AND ADAPTED
C     BY VON NEUMANN FOR LARGE COMPUTERS AS FOUND IN 'MATHEMATICAL
C     METHODS FOR DIGITAL COMPUTERS', EDITED BY A. RALSTON AND
C     H.S. WILF, JOHN WILEY AND SONS, NEW YORK, 1962, CHAPTER 7
C
C     ..................................................................
C
      DIMENSION A(1),R(1)
C
```

```
      REAL*4   A,R,ANORM,ANRMX,THR,X,Y,SINX,SINX2,COSX,
     1         COSX2,SINCS,RANGE
C
C        GENERATE IDENTITY MATRIX
C
    5 RANGE=1.0E-12
      IF(MV-1) 10,25,10
   10 IQ=-N
      DO 20 J=1,N
      IQ=IQ+N
      DO 20 I=1,N
      IJ=IQ+I
      R(IJ)=0.0
      IF(I-J) 20,15,20
   15 R(IJ)=1.0
   20 CONTINUE
C
C        COMPUTE INITIAL AND FINAL NORMS (ANORM AND ANORMX)
C
   25 ANORM=0.0
      DO 35 I=1,N
      DO 35 J=I,N
      IF(I-J) 30,35,30
   30 IA=I+(J*J-J)/2
      ANORM=ANORM+A(IA)*A(IA)
   35 CONTINUE
      IF(ANORM) 165,165,40
   40 ANORM=1.4142136*SQRT(ANORM)
      ANRMX=ANORM*RANGE/FLOAT(N)
C
C        INITIALIZE INDICATORS AND COMPUTE THRESHOLD, THR
C
      IND=0
      THR=ANORM
   45 THR=THR/FLOAT(N)
   50 L=1
   55 M=L+1
C
C        COMPUTE SIN AND COS
C
   60 MQ=(M*M-M)/2
      LQ=(L*L-L)/2
      LM=L+MQ
   62 IF(ABS(A(LM))-THR) 130,65,65
   65 IND=1
      LL=L+LQ
      MM=M+MQ
      X=0.5*(A(LL)-A(MM))
   68 Y=-A(LM)/SQRT(A(LM)*A(LM)+X*X)
      IF(X) 70,75,75
   70 Y=-Y
   75 SINX=Y/SQRT(2.0*(1.0+(SQRT(1.0-Y*Y))))
      SINX2=SINX*SINX
   78 COSX=SQRT(1.0-SINX2)
      COSX2=COSX*COSX
```

```
      SINCS =SINX*COSX
C
C        ROTATE L AND M COLUMNS
C
      ILQ=N*(L-1)
      IMQ=N*(M-1)
      DO 125 I=1,N
      IQ=(I*I-I)/2
      IF(I-L) 80,115,80
   80 IF(I-M) 85,115,90
   85 IM=I+MQ
      GO TO 95
   90 IM=M+IQ
   95 IF(I-L) 100,105,105
  100 IL=I+LQ
      GO TO 110
  105 IL=L+IQ
  110 X=A(IL)*COSX-A(IM)*SINX
      A(IM)=A(IL)*SINX+A(IM)*COSX
      A(IL)=X
  115 IF(MV-1) 120,125,120
  120 ILR=ILQ+I
      IMR=IMQ+I
      X=R(ILR)*COSX-R(IMR)*SINX
      R(IMR)=R(ILR)*SINX+R(IMR)*COSX
      R(ILR)=X
  125 CONTINUE
      X=2.0*A(LM)*SINCS
      Y=A(LL)*COSX2+A(MM)*SINX2-X
      X=A(LL)*SINX2+A(MM)*COSX2+X
      A(LM)=(A(LL)-A(MM))*SINCS+A(LM)*(COSX2-SINX2)
      A(LL)=Y
      A(MM)=X
C
C     TESTS FOR COMPLETION
C
C     TEST FOR M = LAST COLUMN
C
  130 IF(M-N) 135,140,135
  135 M=M+1
      GO TO 60
C
C        TEST FOR L = SECOND FROM LAST COLUMN
C
  140 IF(L-(N-1)) 145,150,145
  145 L=L+1
      GO TO 55
  150 IF(IND-1) 160,155,160
  155 IND=0
      GO TO 50
C
C        COMPARE THRESHOLD WITH FINAL NORM
C
  160 IF(THR-ANRMX) 165,165,45
C
```

```
C        SORT EIGENVALUES AND EIGENVECTORS
C
  165 IQ=-N
      DO 185 I=1,N
      IQ=IQ+N
      LL=I+(I*I-I)/2
      JQ=N*(I-2)
      DO 185 J=I,N
      JQ=JQ+N
      MM=J+(J*J-J)/2
      IF(A(LL)-A(MM)) 170,185,185
  170 X=A(LL)
      A(LL)=A(MM)
      A(MM)=X
      IF(MV-1) 175,185,175
  175 DO 180 K=1,N
      ILR=IQ+K
      IMR=JQ+K
      X=R(ILR)
      R(ILR)=R(IMR)
  180 R(IMR)=X
  185 CONTINUE
      RETURN
      END
```

```
C ********************************************************************************
C
C              THIS PROGRAM CALCULATES THE STRESSES AND
C          STRAINS IN A RADIALLY ORTHOTROPIC PLATE DUE TO A
C                              CONTACT LOAD
C
C********************************************************************************
C    THIS IS THE SECOND GENERATION PROGRAM FOR THE LOCAL MODEL OF THE IMPACT
C    ANALYSIS PACKAGE ORIGINALLY WRITTEN BY D.S. CAIRNS.  THIS REVISION WAS
C    WRITTEN BY M.J. KRAFT AND MANY CHANGES HAVE BEEN INCORPORATED.
C
C        ++++      DO NOT USE THIS PROGRAM BLINDLY, IT WILL       ++++
C        ++++ GIVE YOU STUPID ANSWERS FOR STUPID INPUT PARAMETERS ++++
C ********************************************************************************
C
      PROGRAM BESSEL
      IMPLICIT REAL*8 (A-H,O-Z)
      PARAMETER (N1=60,N2=300,N3=40,N4=100)
C
C  PARAMETERS FOR ARRAYS
C
C       N1 = MAXIMUM NUMBER OF LAMINATE PLIES
C       N2 = MAXIMUM NUMBER OF HARMONICS
C       N3 = MAXIMUM NUMBER OF RADIUS DIVISIONS
C       N4 = BETAM INTEGRATION STEPS
C
      REAL*8
     _ EPL(3,3),EP(3,3),EPI(3,3),THET(0:N2),XT(3,3),TT(3,3),
     _ ETT(0:N3,0:N1),ERR(0:N3,0:N1),EZZ(0:N3,0:N1),
     _ EPTMAX(3,3), EPCMAX(3,3),
     _ GA(0:N3,0:N1),STT(0:N3,0:N1),SZZ(0:N3,0:N1),
     _ SRR(0:N3,0:N1),SRZ(0:N3,0:N1),SIP(0:N1),DI(0:N4),A(4,4),B(4),
     _ NU1, NU2, LDD, K, J0, J1, JO, JP, JD, JT
C
      CHARACTER*20 OFILE,IFILE
      CHARACTER*3 LD$, TEST(3,3)
      CHARACTER*1 OUTYP
      INTEGER V
C
      PI = 3.141592654
C
C PROGRAM INTRODUCTION
C
      WRITE(6,*)'-------------------------------------------------------'
      WRITE(6,*)'   PROGRAM BESSEL- COMPUTES STRESSES AND STRAINS'
      WRITE(6,*)'                   IN A RADIALLY ORTHOTROPIC PLATE  '
      WRITE(6,*)'                   DUE TO A CONTACT LOAD'
      WRITE(6,*)'-------------------------------------------------------'
      WRITE(6,*)
C
C INPUT THE LOADING TYPE
C
      WRITE(6,*)'THE AVAILABLE LOADING TYPES FOR THIS ANALYSIS:'
      WRITE(6,*)' '
      WRITE(6,*)'   TYPE PT  -  POINT LOAD'
```

```
      WRITE(6,*)'   TYPE HZ  -  HERTZIAN DISTRIBUTION'
      WRITE(6,*)'   TYPE HZS -  HERTZIAN, FORCE FINDING OPTION'
      WRITE(6,*)'   TYPE HT  -  HAT LOAD'
      WRITE(6,*)
      WRITE(6,*)'PLEASE INPUT THE LOADING TYPE PT, HZ, HZS, OR HT'
      READ(5,1)LD$
    1 FORMAT (A)
      WRITE(6,*)'WHAT IS THE COMPLETE NAME OF THE OUTPUT FILE?'
      READ(5,1)OFILE
      OPEN(UNIT=12,FILE=OFILE,STATUS='NEW')
      OPEN(UNIT=13,FILE='FORCE.RES',STATUS='NEW')
      OPEN(UNIT=14,FILE='DISP.RES',STATUS='NEW')
C
C INPUT THE PROBLEM PARAMETERS
C
      WRITE(6,*)'PLATE THICKNESS[m], RADIUS[m] AND   OF HARMONICS'
      READ(5,*)T,R,M
C
      WRITE(6,*)'INPUT Etheta[Pa], Ez[Pa], nu r-theta, nu r-z, Gr-z[Pa]'
      READ(5,*)XET,XEZ,NU1,NU2,G
C
      IF (LD$.EQ.'PT') THEN
         WRITE(6,*)'-------------------------------------------------'
         WRITE(6,*)'     LOAD TYPE PT  -  DESCRIPTION              '
         WRITE(6,*)'-------------------------------------------------'
         WRITE(6,*)'INPUT TOTAL IMPACT LOAD, DENSITY, ACCELERATION'
         WRITE(6,*)'   ( LOAD[kN], DENSITY[kg/m3], ACC[m/s2] )  '
         WRITE(6,*)' '
         READ(5,*) LDD,RHO,ACC
         GAM = -RHO*ACC
      ENDIF
C
      IF(LD$.EQ.'HZ') THEN
         WRITE(6,*)'-------------------------------------------------'
         WRITE(6,*)'          LOAD TYPE HZ  -  DESCRIPTION           '
         WRITE(6,*)'-------------------------------------------------'
         WRITE(6,*)'INPUT APPROACH, PROJ. RADIUS, DENSITY, ACCEL.'
         WRITE(6,*)'     (RADII[mm], DENSITY[kg/m3], ACC[m/s2])     '
         WRITE(6,*)' '
         READ(5,*) ALPHA,RI,RHO,ACC
         GAM = -RHO*ACC
C
         WRITE(6,*)'INPUT TOTAL LOAD [N]'
         READ(5,*) TQ
C
C COMPUTE FOOTPRINT SIZE FROM GEOMETRIC RELATIONSHIP
C
         XEP = SQRT(RI**2-(RI-ALPHA)**2)
         PZ = 3.*TQ/(2.*PI*XEP**2)
C
      ENDIF
C
      IF(LD$ .EQ. 'HZS') THEN
         WRITE(6,*)'-------------------------------------------------'
         WRITE(6,*)'  LOAD TYPE HZS - FIND FORCE GIVEN ALPHA OPTION'
```

```
      WRITE(6,*)'-------------------------------------------------'
      WRITE(6,*)'INPUT APPROACH ALPHA[m], PROJ. RADIUS[m]'
      WRITE(6,*)' '
      READ(5,*)ALPHA,RI
      GAM = 0.0
      ACC = 0.0
C
      WRITE(6,*)'INPUT TOTAL LOAD TARGET VALUE[N]'
      READ(5,*) TQ
C
C COMPUTE FOOTPRINT SIZE FROM GEOMETRIC RELATIONSHIP
C
      XEP = SQRT(RI**2-(RI-ALPHA)**2)
      PZ = 3.*TQ/(2.*PI*XEP**2)
C
      ENDIF
C
      IF (LD$.EQ.'HT') THEN
        WRITE(6,*)'-------------------------------------------------'
        WRITE(6,*)'     LOAD TYPE HT  -  DESCRIPTION          '
        WRITE(6,*)'-------------------------------------------------'
        WRITE(6,*)' '
        WRITE(6,*)'PLEASE INPUT THE LOADING RADIUS[mm]'
        READ(5,*) XEP
      ENDIF
C
C  END OF LOADING INPUT INFORMATION SECTION
C
      IF (LD$ .NE. 'HZS') THEN
        WRITE(6,*)'INPUT THE NO. OF RADIUS DIVISIONS AND NO. OF PLIES'
        READ(5,*) NRS, NZT
C
        WRITE(6,*)'DO YOU WANT ALL OF THE PLY INFORMATION? [Y/N]'
        READ(5,1)OUTYP
C
        IF (OUTYP.EQ.'N') GOTO 30
          DO 25 I=1,NZT
            WRITE(6,*)'INPUT THETA OF PLY',I
            READ(5,*)THET(I)
   25     CONTINUE
C
        WRITE(6,*)'INPUT THE THETA DIVISIONS (UP TO 90 DEGREES)'
        READ (5,*)NTH
C
C  INPUT THE STRAIN FAILURE CRITERIA
C
        WRITE(6,*)' '
        WRITE(6,*)'PLY TENSILE STRAIN TO FAILURE CRITERIA [STRAIN]'
        WRITE(6,*)' '
        WRITE(6,*)'EPTMAX(1,1), EPTMAX(1,2), EPTMAX(1,3)'
        READ(5,*)  EPTMAX(1,1), EPTMAX(1,2), EPTMAX(1,3)
C
        WRITE(6,*)'EPTMAX(2,2), EPTMAX(2,3)'
        READ(5,*)  EPTMAX(2,2), EPTMAX(2,3)
C
```

```
      WRITE(6,*)'EPTMAX(3,3)'
      READ(5,*)  EPTMAX(3,3)
      WRITE(6,*)' '
C
      WRITE(6,*)'PLY COMPRESSIVE STRAIN TO FAILURE CRITERIA [STRAIN]'
      WRITE(6,*)' '
      WRITE(6,*)'EPCMAX(1,1), EPCMAX(1,2), EPCMAX(1,3)'
      READ(5,*)  EPCMAX(1,1), EPCMAX(1,2), EPCMAX(1,3)
C
      WRITE(6,*)'EPCMAX(2,2), EPCMAX(2,3)'
      READ(5,*)  EPCMAX(2,2), EPCMAX(2,3)
C
      WRITE(6,*)'EPCMAX(3,3)'
      READ(5,*)  EPCMAX(3,3)
C
      DO II= 1, 3
         DO JJ=1, II
            EPTMAX(II,JJ) = EPTMAX(JJ,II)
            EPCMAX(II,JJ) = EPCMAX(JJ,II)
         ENDDO
      ENDDO
C
   ELSE
      OUTYP='N'
      NRS=0
      NZT=2
   ENDIF
C
 30   CLOSE(UNIT=5)
C
C INITIALIZING THE MATRICIES
C
      DO 50 I=0,N3-1
         DO 40 J=0,N1-1
            ETT(I,J) = 0.0
            ERR(I,J) = 0.0
            EZZ(I,J) = 0.0
            SRR(I,J) = 0.0
            STT(I,J) = 0.0
            SZZ(I,J) = 0.0
            SRZ(I,J) = 0.0
  40     CONTINUE
  50  CONTINUE
C
      A1 = 1./XET
      A2 = -NU1/XET
      A3 = -NU2/XET
      A4 = 1./XEZ
      A5 = 1./G
C
C DETERMINING THE COEFFICIENTS
C
      AA = A3*(A1-A2)/(A1*A4-A3**2)
      BB = (A3*(A3+A5)-A2*A4)/(A1*A4-A3**2)
      CC = (A3*(A1-A2)+A1*A5)/(A1*A4-A3**2)
```

```
      DD = (A1**2-A2**2)/(A1*A4-A3**2)
C
C DETERMINING THE EIGENVALUES
C
      S1 = ((AA+CC+((AA+CC)**2-4.*DD)**.5)/(2.*DD))**.5
      S2 = ((AA+CC-((AA+CC)**2-4.*DD)**.5)/(2.*DD))**.5
C
C INITIALIZE DISPLACEMENT AND SUM MODES
C
      DISP = 0.0
      FORCE = 0.0
C
      WRITE(6,*)' '
      WRITE(6,*)'     MODE       APPROACH ALPHA'
      WRITE(6,*)' '
C
      DO 1000 V = 1,M
         WM = ZEROJ0(V)/R
C
C DETERMINING THE NON-HOMOGENEOUS PORTION
C
         IF (LD$.EQ.'PT') THEN
            BETAM = LDD / (PI * J1(ZEROJ0(V))**2 * R**2)
            FORCE = BETAM + FORCE
         ENDIF
C
         IF (LD$.EQ.'PA') THEN
            U = WM*XEP
            C0 = -2./(R**2*ZEROJ1(V)**2)*(1./WM**2*U*J0(X)-
     _     1./(U**2*WM**2)*(U*(U**2-4)*J1(X)+2.*U**2*J0(X)))
         ENDIF
C
         IF (LD$.EQ.'HT') THEN
            C0 = -2.*J1(X)*10.*X/(XEP**2*R**2*PI*ZEROJ1(V)**2*WM**5
     _     *XEP**2*PI)
         ENDIF
C
C   NUMERICAL INTEGRATION FOR A HERTZIAN LOADING DISTRIBUTION
C      USING SIMPSON'S RULE TO DETERMINE COEFFICIENT BETAm
C
         IF ((LD$.EQ.'HZ') .OR. (LD$.EQ.'HZS')) THEN
            INTN = N4
            STEP = XEP / INTN
            HI = STEP / 3.0
            DI(0) = 1.0
            DO 90 L=1, (INTN-1), 2
               DI(L) = 4.0
               DI(L+1) = 2.0
 90         CONTINUE
            DI(INTN)=1.0
C
C   INTEGRATE THAT HEINOUS BABY
C
            BETAM = 0.0
            RINT = 0.0
```

```
            DO 100 LINT = 0, INTN
C
               IF (RINT .GT. XEP) GOTO 100
               FACT = 2.0 / (J1(ZEROJ0(V))**2*R**2)
               RINTEGRAL = PZ * (1 - (RINT / XEP)**2)**0.5 *
     _                     RINT * J0(WM*RINT)
               BETAM = BETAM + DI(LINT) * FACT * RINTEGRAL
               RINT = RINT + STEP
 100        CONTINUE
            BETAM = BETAM * HI
C
C COMPUTE RECOVERED FORCE ON PLATE
C
            FORCE = FORCE + BETAM*J0(0)
C
         ENDIF
C
C         NUMERICAL INTEGRATION FOR INERTIAL LOADING BODY FORCE
C   DISTRIBUTION USING SIMPSON'S RULE TO DETERMINE COEFFICIENT GAMMAm
C
            INTN = N4
            STEP = XEP / INTN
            HI = STEP / 3.0
            DI(0) = 1.0
            DO L=1, (INTN-1), 2
               DI(L) = 4.0
               DI(L+1) = 2.0
            ENDDO
            DI(INTN)=1.0
C
C   INTEGRATE THAT HEINOUS BABY
C
            GAMMAM = 0.0
            RINT = 0.0
            DO 150 LINT = 0, INTN
C
               IF (RINT .GT. XEP) GOTO 150
               FACT = - 2.0 * GAM / (J1(ZEROJ0(V))**2*R**2)
               RINTEGRAL = J0(WM*RINT) * RINT
               GAMMAM = GAMMAM + DI(LINT) * FACT * RINTEGRAL
               RINT = RINT + STEP
 150        CONTINUE
            GAMMAM = GAMMAM * HI
C
C SOLVE FOR MODAL AMPLITUDES AM, BM, CM, AND DM FOR FZ SOLUTION
C
C    SET UP MATRIX FOR Ax = B SOLUTION FOR MODAL AMPLITUDES
C
         A(1,1) = (-CC*S1 + DD*S1**3) * COSH(-WM*S1*T/2)
         A(1,2) = (-CC*S1 + DD*S1**3) * SINH(-WM*S1*T/2)
         A(1,3) = (-CC*S2 + DD*S2**3) * COSH(-WM*S2*T/2)
         A(1,4) = (-CC*S2 + DD*S2**3) * SINH(-WM*S2*T/2)
C
         A(2,1) = (-CC*S1 + DD*S1**3) * COSH( WM*S1*T/2)
         A(2,2) = (-CC*S1 + DD*S1**3) * SINH( WM*S1*T/2)
```

```
      A(2,3) = (-CC*S2 + DD*S2**3) * COSH( WM*S2*T/2)
      A(2,4) = (-CC*S2 + DD*S2**3) * SINH( WM*S2*T/2)
C
      A(3,1) = ( 1. - AA*S1**2) * SINH( WM*S1*T/2)
      A(3,2) = ( 1. - AA*S1**2) * COSH( WM*S1*T/2)
      A(3,3) = ( 1. - AA*S2**2) * SINH( WM*S2*T/2)
      A(3,4) = ( 1. - AA*S2**2) * COSH( WM*S2*T/2)
C
      A(4,1) = ( 1. - AA*S1**2) * SINH(-WM*S1*T/2)
      A(4,2) = ( 1. - AA*S1**2) * COSH(-WM*S1*T/2)
      A(4,3) = ( 1. - AA*S2**2) * SINH(-WM*S2*T/2)
      A(4,4) = ( 1. - AA*S2**2) * COSH(-WM*S2*T/2)
C
      B(1) = ( -BETAM + GAMMAM*T/2 ) / WM**3
      B(2) =  -GAMMAM*T/2 / WM**3
      B(3) = 0.0
      B(4) = 0.0
C
C  CALL GAUSS-JORDON ELIMINATION SUBROUTINE TO FIND AMPLITUDES
C
      CALL GAUSSJ(A,4,4,B,1,1)
C
      AM = B(1)
      BM = B(2)
      CM = B(3)
      DM = B(4)
C
      DO 300 NRA = 0, NRS
         DO 200 NZE = 1, NZT
C
C     CALCULATE FUNCTION VALUES AT PLY MIDPLANE, UNLESS RUNNING
C  ANALYSIS FOR FORCE GIVEN ALPHA, WHERE FUNCTIONS ARE CALCULATED
C                   ONLY AT +H/2 AND -H/2
C
            IF (LD$ .NE. 'HZS') THEN
               Z = -T/2.+T/(2.*NZT)+T*(NZE-1)/NZT
            ELSE
               Z = -T/2. + (NZE-1)*T
            ENDIF
C
C CALCULATE THE VALUES OF F, F', F'', F'''
C
            FZ = AM * SINH( S1*WM*Z) + BM * COSH( S1*WM*Z) +
     _           CM * SINH( S2*WM*Z) + DM * COSH( S2*WM*Z)
C
            FP = AM * ( S1*WM) * COSH( S1*WM*Z) +
     _           BM * ( S1*WM) * SINH( S1*WM*Z) +
     _           CM * ( S2*WM) * COSH( S2*WM*Z) +
     _           DM * ( S2*WM) * SINH( S2*WM*Z)
C
            FD = AM * ( S1*WM)**2 * SINH( S1*WM*Z) +
     _           BM * ( S1*WM)**2 * COSH( S1*WM*Z) +
     _           CM * ( S2*WM)**2 * SINH( S2*WM*Z) +
     _           DM * ( S2*WM)**2 * COSH( S2*WM*Z)
C
```

```
            FT = AM * ( S1*WM)**3 * COSH( S1*WM*Z) +
     _           BM * ( S1*WM)**3 * SINH( S1*WM*Z) +
     _           CM * ( S2*WM)**3 * COSH( S2*WM*Z) +
     _           DM * ( S2*WM)**3 * SINH( S2*WM*Z)
C
C  DEFINE BESSEL FUNCTION AND DERIVATIVES JP, JD, JT
C
            IF (NRA .NE. 0) THEN
               RD = (R / NRS) * NRA
C
               JO = J0(WM*RD)
               JP =   -WM  * J1(WM*RD)
               JD = WM**2 * (-JO + J1(WM*RD)/(WM*RD))
               JT = WM**3 * ( JO/(WM*RD) +
     _                ( 1. - 2./(WM*RD)**2 ) * J1(WM*RD) )
            ELSE
C
C  LIMIT VALUES OF JO, JP, JD, AND JT AT RD=0
C
               JO =  1.
               JP =  0.
               JD = -0.5 * WM**2
               JT =  0.
            ENDIF
C
C-----------------------------------------------------------------
C   RECOVER DISPLACEMENTS AND ALPHA FOR NONLINEAR CONTACT PROBLEM
C-----------------------------------------------------------------
C
C   COMPUTE DISPLACEMENTS AT THE ZERO RADIUS POSITION ONLY
C
          IF (NRA .EQ. 0) THEN
C
            IF ((NZE .EQ. 1) .OR. (NZE .EQ. NZT)) THEN
             IF  (NZE .EQ. 1)  THEN
               DISPTOP =
     _             -A3 * ((BB+1)*( 2.*JD*FZ ) + 2.*AA*FD ) +
     _              A4 * ( 2.*CC*JD*FZ + DD*FD )
             ENDIF
             IF (NZE .EQ. NZT) THEN
               DISPBOT =
     _             -A3 * ((BB+1)*( 2.*JD*FZ ) + 2.*AA*FD ) +
     _              A4 * ( 2.*CC*JD*FZ + DD*FD )
C
               DISP = DISP + (DISPTOP-DISPBOT)
             ENDIF
C
            ENDIF
          ENDIF
C
          IF (LD$ .EQ. 'HZS') GOTO 200
C-----------------------------------------------------------------
C  COMPUTE THE STRESSES IN THE PLATE AXES
C-----------------------------------------------------------------
C
```

```
C
            IF (NRA .EQ. 0) THEN
C
C  LIMIT VALUES OF STRESSES AT RD=0
C
              STT(NRA,NZE) = STT(NRA,NZE) +
                           (-( BB*JD*FP ) - ( JD*FP ) -
     -                       ( AA*JO*FT ))
C
              SZZ(NRA,NZE) = SZZ(NRA,NZE) +
                           ( CC*JD*FP ) + (CC*JD*FP) +
     -                     ( DD*JO*FT )
C
              SRR(NRA,NZE) = SRR(NRA,NZE) +
                           (-( JD*FP ) - ( BB*JD*FP ) -
     -                       ( AA*JO*FT ))
C
              SRZ(NRA,NZE) = SRZ(NRA,NZE) +
                             FZ*JT + 0.5*JT*FZ +
     -                       JT*FZ + AA*JP*FD
            ELSE
C
              STT(NRA,NZE) = STT(NRA,NZE) - (
                           ( BB*JD*FP ) + ( 1./RD*JP*FP ) +
     -                     ( AA*JO*FT ) )
C
              SZZ(NRA,NZE) = SZZ(NRA,NZE) + (
                           ( CC*JD*FP ) + ( CC/RD*JP*FP ) +
     -                     ( DD*JO*FT ) )
C
              SRR(NRA,NZE) = SRR(NRA,NZE) - (
                           (    JD*FP ) + ( BB/RD*JP*FP ) -
     -                     ( AA*JO*FT ) )
C
              SRZ(NRA,NZE) = SRZ(NRA,NZE) + (
                           (    JT*FZ ) - ( 1./RD**2*JP*FZ ) +
     -                     ( 1.0/RD*JD*FZ ) + ( AA*JP*FD ) )
C
            ENDIF
C
C-------------------------------------------------------------------
C
  200         CONTINUE
  300       CONTINUE
C
C  WRITE DISPLACEMENT AND FORCE TO OUTPUT SOURCES FOR CONVERGENCE CHECK
C
            WRITE(6,900) V,DISP
            WRITE(14,*) V,DISP
            WRITE(13,*) V,FORCE
  900       FORMAT('+',5X,I4,8X,E12.5)
C
 1000 CONTINUE
C
C-------------------------------------------------------------------
```

```
C  WRITING INPUT INFORMATION TO THE OUTPUT FILE
C-------------------------------------------------------------------
C
      WRITE(12,*)'FOURIER - BESSEL IMPACT ANALYSIS'
      WRITE(12,*)' '
      WRITE(12,*)'ANALYSIS FOR LOADING INPUT TYPE'
      WRITE(12,2)LD$
    2 FORMAT(1X,A)
    3 FORMAT(A23,E12.5)
    4 FORMAT(A23,I4)
    5 FORMAT(A23,E12.5)
      WRITE(12,*)' '
      WRITE(12,3)'THICKNESS      [mm] =',T
      WRITE(12,3)'RADIUS         [mm] =',R
      WRITE(12,4)'NUMBER OF HARMONICS =',M
      WRITE(12,*)' '
      WRITE(12,3)'       Etheta [GPa] =',XET
      WRITE(12,3)'       Ez     [GPa] =',XEZ
      WRITE(12,3)'       Grz    [GPa] =',G
      WRITE(12,3)'       nu r-theta   =',NU1
      WRITE(12,3)'       nu r-z       =',NU2
      WRITE(12,*)' '
C
      IF (LD$.EQ.'PT') THEN
         WRITE(12,3)'TOTAL LOAD =',LDD
         WRITE(12,3)'DENSITY =',RHO
         WRITE(12,3)'CENTER ACCELERATION =',ACC
         WRITE(12,*)' '
      ENDIF
C
      IF ((LD$.EQ.'HZ').OR.(LD$.EQ.'HZS')) THEN
         WRITE(12,3)'TOTAL LOAD =',TQ
         WRITE(12,3)'DENSITY =',RHO
         WRITE(12,3)'CENTER ACCELERATION =',ACC
         WRITE(12,3)'IMPACT RADIUS =',XEP,'PROJECTILE RADIUS =',RI
         WRITE(12,*)' '
      ENDIF
C
C CALCULATE THE GEOMETRIC INDENTATION
C
      ALPHAI = RI-SQRT(RI**2-XEP**2)
C
      WRITE(6,*)' '
      WRITE(6,*)' '
      WRITE(6,*)'DISPLACEMENT APPROACH = ',DISP
      WRITE(6,*)'   GEOMETRIC APPROACH = ',ALPHAI
      WRITE(6,*)'       INPUT PRESSURE = ',PZ
      WRITE(6,*)'   RECOVERED PRESSURE = ',FORCE
      WRITE(6,*)'              INPUT LOAD = ',TQ
      WRITE(6,*)' LOAD FOR GIVEN ALPHA = ',TQ*(ALPHAI/DISP)
      WRITE(12,*)' '
      WRITE(12,*)'DISPLACEMENT APPROACH = ',DISP
      WRITE(12,*)'   GEOMETRIC APPROACH = ',ALPHAI
      WRITE(12,*)'       INPUT PRESSURE = ',PZ
      WRITE(12,*)'   RECOVERED PRESSURE = ',FORCE
```

```
      WRITE(12,*)'           INPUT LOAD = ',TQ
      WRITE(12,*)' LOAD FOR GIVEN ALPHA = ',TQ*(ALPHAI/DISP)
      WRITE(12,*)' '
C
C STOP PROGRAM IF IT WAS A STATIC ANALYSIS
C
      IF (LD$ .EQ. 'HZS') STOP
C
      WRITE(12,450)
  450 FORMAT(1X,'RAD. ',1X,'PLY',5X,'SIGMA R',8X,'SIGMA T',9X
     _'SIGMA Z',9X,'TAU RZ')
C
      DO 500 I=0,NRS
         DO 400 J = 1,NZT
            WRITE(12,550)I,J,SRR(I,J),STT(I,J),SZZ(I,J),SRZ(I,J)
  550       FORMAT(1X,I2,4X,I2,5X,E10.4,5X,E10.4,5X,E10.4,5X,E10.4)
  400    CONTINUE
  500 CONTINUE
C
C CALCULATING THE STRAINS FROM THE STRESSES
C
      WRITE(12,*)' '
      WRITE(12,*)' '
      WRITE(12,455)
  455 FORMAT(1X,'RAD',1X,'PLY',2X,'EPS. R',8X,'EPS. T',
     _5X,'EPS. Z',5X,'GAMMA RZ')
C
      DO 700 I=0,NRS
         DO 600 J=1,NZT
            ERR(I,J) = A1*SRR(I,J)+A2*STT(I,J)+A3*SZZ(I,J)
            ETT(I,J) = A2*SRR(I,J)+A1*STT(I,J)+A3*SZZ(I,J)
            EZZ(I,J) = A3*(SRR(I,J)+STT(I,J))+A4*SZZ(I,J)
            GA(I,J) = A5*SRZ(I,J)
            WRITE(12,555)I,J,ERR(I,J),ETT(I,J),EZZ(I,J),GA(I,J)
  555       FORMAT(1X,I2,2X,I2,2X,E10.4,2X,E10.4,2X,E10.4,2X,E10.4)
  600    CONTINUE
  700 CONTINUE
C
      WRITE(12,*)' '
      WRITE(12,*)' '
C
      IF (OUTYP.EQ.'N') GOTO 1100
      DO 830 I=0,NTH
        DO 820 J=0,NRS
          DO 810 K=1,NZT
             EPL(1,1) = ERR(J,K)
             EPL(2,2) = ETT(J,K)
             EPL(3,3) = EZZ(J,K)
             EPL(1,3) = GA(J,K)*0.5
             EPL(3,1) = EPL(1,3)
             THT = 90./FLOAT(NTH) * FLOAT(I)
             THP = -(THT - THET(K))
             THP = THP * PI/180.
             XT(1,1) = COS(THP)
             TT(1,1) = XT(1,1)
```

```
            XT(2,2) = XT(1,1)
            TT(2,2) = XT(2,2)
            XT(1,2) = -SIN(THP)
            TT(2,1) = XT(1,2)
            XT(2,1) = +XT(1,2)
            TT(1,2) = XT(2,1)
            XT(3,3) = 1.0
            XT(1,3) = 0.0
            XT(2,3) = 0.0
            TT(1,3) = 0.0
            TT(2,3) = 0.0
C
C  TENSOR TRANSFORMATIONS
C
            DO 875 L=1,3
              DO 865 M=1,3
                EP(L,M)=(XT(1,L)*XT(1,M)*EPL(1,1)+
     _          XT(1,L)*XT(2,M)*EPL(1,2)+XT(1,L)*
     _          XT(3,M)*EPL(1,3))+(XT(2,L)*XT(1,M)*
     _          EPL(2,1)+XT(2,L)*XT(2,M)*EPL(2,2)+
     _          XT(3,L)*XT(3,M)*EPL(2,3))+(XT(3,L)*
     _          XT(1,M)*EPL(3,1)+XT(3,L)*XT(2,M)*
     _          EPL(3,2)+XT(3,L)*XT(3,M)*EPL(3,3))
  865         CONTINUE
  875       CONTINUE
C
            RTHP = 90./FLOAT(NTH)*FLOAT(I)
C
            WRITE(12,*)'THETA              =',RTHP
            WRITE(12,*)'RADIUS STEP        =',J
            WRITE(12,*)'PLY                =',K
            WRITE(12,*)
            WRITE(12,*)'EPSILON(I,J) IN PRINCIPAL AXES'
C
C  TEST FOR STRAINS GREATER THAN MAXIMUM VALUES AND MARK WITH ****
C
            DO II= 1, 3
               DO JJ= 1, 3
                  IF ((EP(II,JJ) .LT. EPTMAX(II,JJ)) .AND.
     _               (EP(II,JJ) .GT. EPCMAX(II,JJ))) THEN
                     TEST(II,JJ)='   '
                  ELSE
                     TEST(II,JJ)='***'
                  ENDIF
               ENDDO
            ENDDO
C
            DO II= 1, 3
               WRITE(12,805) EP(II,1),TEST(II,1),
     _                       EP(II,2),TEST(II,2),
     _                       EP(II,3),TEST(II,3)
            ENDDO
  805          FORMAT(1X,E12.5,A,1X,E12.5,A,1X,E12.5,A)
C
            WRITE(12,*)' '
```

```
  810      CONTINUE
  820    CONTINUE
  830 CONTINUE
 1100 STOP
      END
```

```
C*********************************************************************
C
C       FUNCTION J0:  USED FOR DEFINING BESSEL FUNCTIONS
C                TAKEN FROM 'NUMERICAL RECIPES'
C
C*********************************************************************
C
      REAL*8 FUNCTION J0(X)
      IMPLICIT REAL*8 (A-H,O-Z)
C
      DATA P1,P2,P3,P4,P5 /
     _    1.D0,    -.1098628627D-2,  .2734510407D-4, -.2073370639D-5,
     _     .2093887211D-6 /,
     _    Q1,Q2,Q3,Q4,Q5 /
     _    -.1562499995D-1,  .1430488765D-3, -.6911147651D-5,
     _     .7621095161D-6, -.934945152D-7 /
      DATA R1,R2,R3,R4,R5,R6 /
     _    57568490574.D0, -13362590354.D0,  651619640.7D0,
     _    -11214424.18D0,   77392.3317D0,  -184.905245600 /,
     _    S1,S2,S3,S4,S5,S6 /
     _    57568490411.D0,  1029532985.D0,  9494680.718D0,
     _     59272.64853D0,  267.8532712D0,  1.D0 /
C
      IF (ABS(X) .LT. 8.) THEN
         Y = X**2
             J0 = (R1+Y*(R2+Y*(R3+Y*(R4+Y*(R5+Y*R6)))))
     _          /(S1+Y*(S2+Y*(S3+Y*(S4+Y*(S5+Y*S6)))))
      ELSE
         AX = ABS(X)
         Z = 8./AX
         Y = Z**2
         XX = AX-0.785398164
             J0 = SQRT(0.636619772/AX)*
     _          (COS(XX)*(P1+Y*(P2+Y*(P3+Y*(P4+Y*P5))))-
     _          Z*SIN(XX)*(Q1+Y*(Q2+Y*(Q3+Y*(Q4+Y*Q5)))))
         ENDIF
         RETURN
         END
C
C*********************************************************************
C
C       FUNCTION J1:  USED FOR DEFINING BESSEL FUNCTIONS
C                TAKEN FROM 'NUMERICAL RECIPES'
C
C*********************************************************************
C
      REAL*8 FUNCTION J1(X)
      IMPLICIT REAL*8 (A-H,O-Z)
C
      DATA R1,R2,R3,R4,R5,R6 /
     _    72362614232.D0, -7895059235.D0, 242396853.1D0,
     _    -2972611.439D0,  15704.48260D0, -30.16036606D0 /,
     _    S1,S2,S3,S4,S5,S6 /
     _    144725228442.D0, 2300535178.D0, 18583304.74D0,
     _      99447.43394D0, 376.9991397D0, 1.D0 /
```

```
      DATA P1,P2,P3,P4,P5 /
     _             1.D0,  .183105D-2,  -.3516396496D-4,
     _    .2457520174D-5,  .240337019D-6 /,
     _    Q1,Q2,Q3,Q4,Q5 /
     _    .0468749999950,  -.2002690873D-3, .8449199096D-5,
     _     -.88228987D-6,   .105787412D-6 /
C
      IF (ABS(X) .LT. 8.) THEN
         Y = X**2
            J1 = X*(R1+Y*(R2+Y*(R3+Y*(R4+Y*(R5+Y*R6)))))
     _           /(S1+Y*(S2+Y*(S3+Y*(S4+Y*(S5+Y*S6)))))
      ELSE
         AX = ABS(X)
         Z = 8./AX
         Y = Z**2
         XX = AX-2.356194491
            J1 = SQRT(.636619772/AX)*
     _           (COS(XX)*(P1+Y*(P2+Y*(P3+Y*(P4+Y*P5))))-
     _          Z*SIN(XX)*(Q1+Y*(Q2+Y*(Q3+Y*(Q4+Y*Q5)))))
         ENDIF
         RETURN
         END
C
C*****************************************************************
C
C  FUNCTION TO DEFINE ITH ZERO OF J0
C
C*****************************************************************
C
      REAL*8 FUNCTION ZEROJ0(I)
      IMPLICIT REAL*8 (A-H,O-Z)
      REAL*8 XM(20)
C
      PI = 3.141592654
C
      IF (I .LT. 21) THEN
C
C  ZEROS FOR J0 BESSEL FUNCTION
C
        DATA (XM(I),I=1,20) /
     _       2.40483,  5.52008,  8.65373, 11.79153, 14.93092,
     _      18.07106, 21.21164, 24.35247, 27.49348, 30.63461,
     _      33.77582, 36.91709, 40.05842, 43.19979, 46.34119,
     _      49.48261, 52.62405, 55.76551, 58.90698, 62.04847 /
C
        ZEROJ0 = XM(I)
C
      ELSE
        S = FLOAT(I)
        A = 4.*S-1.
        AX = A*PI
C
        ZEROJ0 = 0.25*AX*
     _          ( 1.D0+ 2.D0/AX**2 - 62.D0/(3.D0*AX**4) +
     _          15116.D0/(15.*AX**6) - 12554474.D0/(105.D0*AX**8) +
```

```
     _          8368654292.D0/(315.D0*AX**10) )
C
      ENDIF
      RETURN
      END
C
C*****************************************************************
C
C  FUNCTION TO DEFINE ITH ZERO OF J1
C
C*****************************************************************
C
      REAL*8 FUNCTION ZEROJ1(I)
      IMPLICIT REAL*8 (A-H,O-Z)
C
      PI = 3.141592654
C
      S = FLOAT(I)
      B = 4.*S+1
      BX = B*PI
C
      ZEROJ1 = 0.25*BX*
     _        ( 1.D0 - 6.D0/BX**2 + 6.D0/BX**4 -
     _        4716.D0/(5.D0*BX**6) + 3902418.D0/(35.D0*BX**8) -
     _        895167324.D0/(35.D0*BX**10) )
C
      RETURN
      END
C
      SUBROUTINE GAUSSJ(A,N,NP,B,M,MP)
C*****************************************************************
C
C  THIS IS A GENERAL ROUTINE FOR GAUSS-JORDAN ELIMINATION WITH
C     WITH FULL PIVOTING - TAKEN FROM 'NUMERICAL RECIPES'
C
C*****************************************************************
C
      IMPLICIT REAL*8 (A-H,O-Z)
      PARAMETER (NMAX = 50)
      DIMENSION A(NP,NP), B(NP,MP), IPIV(NMAX),
     _          INDXR(NMAX), INDXC(NMAX)
C
      DO 11 J=1, N
         IPIV(J) = 0.0
 11   CONTINUE
C
      DO 22 I=1, N
         BIG = 0.
         DO 13 J=1, N
            IF (IPIV(J) .NE. 1) THEN
               DO 12 K=1, N
                  IF (IPIV(K) .EQ. 0) THEN
                      IF (ABS(A(J,K)) .GE. BIG) THEN
                         BIG = ABS(A(J,K))
                         IROW = J
```

```
                        ICOL = K
                     ENDIF
                  ELSE IF (IPIV(K) .GT. 1) THEN
                     PAUSE 'SINGULAR MATRIX'
                  ENDIF
 12            CONTINUE
               ENDIF
 13         CONTINUE
C
           IPIV(ICOL) = IPIV(ICOL)+1
C
           IF (IROW .NE. ICOL) THEN
              DO 14 L=1, N
                 DUM = A(IROW,L)
                 A(IROW,L) = A(ICOL,L)
                 A(ICOL,L) = DUM
 14           CONTINUE
C
              DO 15 L=1,M
                 DUM = B(IROW,L)
                 B(IROW,L) = B(ICOL,L)
                 B(ICOL,L) = DUM
 15           CONTINUE
           ENDIF
           INDXR(I) = IROW
           INDXC(I) = ICOL
           IF (A(ICOL,ICOL) .EQ. 0.) PAUSE 'SINGULAR MATRIX'
           PIVINV = 1./A(ICOL,ICOL)
           A(ICOL,ICOL) = 1.
           DO 16 L=1, N
              A(ICOL,L) = A(ICOL,L)*PIVINV
 16        CONTINUE
           DO 17 L=1, M
              B(ICOL,L) = B(ICOL,L)*PIVINV
 17        CONTINUE
           DO 21 LL=1, N
              IF (LL .NE. ICOL) THEN
                 DUM = A(LL,ICOL)
                 A(LL,ICOL) = 0.
                 DO 18 L=1, N
                    A(LL,L) = A(LL,L) - A(ICOL,L)*DUM
 18              CONTINUE
                 DO 19 L=1, M
                    B(LL,L) = B(LL,L) - B(ICOL,L)*DUM
 19              CONTINUE
              ENDIF
 21        CONTINUE
 22     CONTINUE
C
        DO 24 L=N,1,-1
           IF (INDXR(L) .NE. INDXC(L)) THEN
              DO 23 K=1,N
                 DUM = A(K,INDXR(L))
                 A(K,INDXR(L)) = A(K,INDXC(L))
                 A(K,INDXC(L)) = DUM
```

```
23          CONTINUE
          ENDIF
24    CONTINUE
      RETURN
      END
```

APPENDIX B

DATA TABLES FOR PLATE SPECIMENS

This appendix contains data obtained for the flat plate specimens. The plate damage characterization specimen data is given, followed by a listing of the data for the residual strength specimens. Pertinent measurements, impact velocities, and damage measurements are given. Unless otherwise noted, specimens with incomplete listings were not suitable for the research, the cause largely being errant impacts.

TABLE B.1 - PLATE DAMAGE CHARACTERIZATION DATA

Specimen ID	Thickness (mm)	Impact Velocity (m/s)	Core Diameter (mm)	Delamination Length long. (mm)	Delamination Length tran. (mm)
1-1	1.32				
1-2	1.32				
1-3	1.32				
1-4	1.31	**** used for gun calibration and ****			
1-5	1.28	**** Dib x-ray refinement ****			
1-6	1.32				
1-7	1.32				
1-8	1.27				
2-1	1.27	17.5	--	--	--
2-2	1.29	28.2	--	--	--
2-3	1.29	33.2		9	13
2-4	1.29	39.3		14	22
2-5	1.29	48.5		24	30
2-6	1.29	51.3		15	36
2-7	1.27	56.7	14	25	55
2-8	1.27	62.2	13	25	58
3-1	1.27	44.4		15	28
3-2	1.28	33.6	--	24	25
3-3	1.28	39.6		11	19
3-4	1.26				
3-5	1.26	49.3		10	17
3-6	1.29	43.0		14	25
3-7	1.28	55.4	14	27	42
3-8	1.26				

TABLE B.1 - PLATE DAMAGE CHARACTERIZATION DATA (continued)

Specimen ID	Thickness (mm)	Impact Velocity (m/s)	Core Diameter (mm)	Delamination Length long. (mm)	Delamination Length tran. (mm)
4-1	1.28	48.3			
4-2	1.32	40.2			
4-3	1.29	32.6			
4-4	1.27	63.9			
4-5	1.28				
4-6	1.31				
4-7	1.31				
4-8	1.30				
5-1	1.29	30.8		8	14
5-2	1.30	38.2		10	20
5-3	1.30	41.8		11	20
5-4	1.29	42.5	10	19	58
5-5	1.28	42.2		11	19
5-6	1.28	51.9		17	26
5-7	1.31	55.4		22	36
5-8	1.27	52.2	--	22	30
6-1	1.30				
6-2	1.31	66.4	15	31	55
6-3	1.31	79.5	15	25	55
6-4	1.30	85.9	14	26	76
6-5	1.30	91.3	13	30	79
6-6	1.32				
6-7	1.31	9.5			
6-8	1.30	24.0			

TABLE B.1 - PLATE DAMAGE CHARACTERIZATION DATA (continued)

Specimen ID	Thickness (mm)	Impact Velocity (m/s)	Core Diameter (mm)	Delamination Length long. (mm)	Delamination Length tran. (mm)
7-1	1.28	30.0			
7-2	1.31	29.0	4	10	12
7-3	1.31	30.0			
7-4	1.30	38.0	2	17	20
7-5	1.27	50.0	--	25	35
7-6	1.30	54.0	19	20	38
7-7	1.33	68.0	16	30	47
7-8	1.30	47.0	3	15	30
8-1	1.28				
8-2	1.30				
8-3	1.28	**** used for design concept tests ****			
8-4	1.28	**** in cylinder test ****			
8-5	1.29	**** fixture development ****			
8-6	1.30				
8-7	1.30				
8-8	1.27				
9-1	1.28				
9-2	1.29				
9-3	1.30	**** used for design concept tests ****			
9-4	1.27	**** in cylinder test ****			
9-5	1.30	**** fixture development ****			
9-6	1.29				
9-7	1.31				
9-8	1.28				

TABLE B.2 - RESIDUAL STRENGTH SPECIMEN MEASUREMENTS

Specimen ID	Specimen Width (mm)		Specimen Thickness (mm)
11-1	69.56		1.33
11-2	69.66		1.32
11-3	69.60		1.33
11-4	69.67		1.31
		Average:	1.32
		C.V. %:	0.79
12-1	69.71		1.32
12-2	69.64		1.32
12-3	69.65		1.32
12-4	69.73		1.30
		Average:	1.31
		C.V. %:	0.79
13-1	69.69		1.30
13-2	69.59		1.31
13-3	69.64		1.31
13-4	69.74		1.30
		Average:	1.31
		C.V. %:	0.90
14-1	69.72		1.31
14-2	69.68		1.32
14-3	69.67		1.32
14-4	69.45		1.30
		Average:	1.31
		C.V. %:	0.89

TABLE B.2 - RESIDUAL STRENGTH SPECIMEN MEASUREMENTS (continued)

Specimen ID	Specimen Width (mm)		Specimen Thickness (mm)
15-1	70.17		1.33
15-2	70.03		1.36
15-3	70.16		1.36
15-4	70.13		1.35
		Average:	1.35
		C.V. %:	1.06
16-1	70.12		1.33
16-2	69.94		1.37
16-3	69.76		1.37
16-4	70.32		1.36
		Average:	1.36
		C.V. %:	1.38
17-1	69.96		1.34
17-2	70.27		1.36
17-3	70.21		1.36
17-4	70.34		1.35
		Average:	1.35
		C.V. %:	1.46
18-1	69.96		1.34
18-2	70.00		1.35
18-3	70.17		1.37
18-4	70.36		1.34
		Average:	1.35
		C.V. %:	1.45

TABLE B.3 - RESIDUAL STRENGTH SPECIMEN DATA

Specimen ID	Impact Speed (m/s)	Modulus (GPa)	Ultimate Stress (MPa)	Core Diameter (mm)	Failure Mode
11-1	31.7	53.5	606	0.0	f,y
11-2	40.1	52.8	575	3.0	f,y
11-3	70.0	54.3	367	14.5	f,x
11-4	62.0	58.4	307	8.5	f,x
12-1	45.9	50.4	598	2.5	f,d
12-2	-	49.7	587	-	f
12-3	-	51.0	596	-	f
12-4	-	51.2	586	-	f
13-1	-	53.7	620	-	f
13-2	-	55.5	594	-	f
13-3	41.1	56.9	578	7.0	f
13-4	49.4	55.8	440	5.5	f,x
14-1	64.4	53.1	388	12.0	f,x
14-2	63.8	56.2	369	11.0	f,x
14-3	84.7	51.9	358	14.0	f,x
14-4	35.6	49.3	578	2.0	f,y

Key to Failure Mode:

d - delamination
f - in-plane fracture
x - failure at impact site
y - failure away from impact site

Note: The failure mode code f,d symbolizes a fracture failure with a large amount of delamination present near the failure location.

TABLE B.3 - RESIDUAL STRENGTH SPECIMEN DATA (continued)

Specimen ID	Impact Speed (m/s)	Modulus (GPa)	Ultimate Stress (MPa)	Core Diameter (mm)	Failure Mode
15-1p	39.9	56.3	572	2.0	f,x
15-2	46.1	52.4	503	3.0	f,d
15-3p	57.2	55.6	417	11.0	f,x
15-4	46.5	48.3	518	3.0	f,d
16-1	50.4	60.9	556	3.0	f,d
16-2	48.8	60.4	454	3.0	f,x
16-3	45.2	59.3	545	-	f,d
16-4	48.2	51.2	403	3.0	f,d
17-1	56.0	52.4	437	8.0	f,x
17-2	68.2	61.8	543	14.0	f,x
17-3	65.6	58.6	373	15.0	f,x
17-4h	-	47.1	332	12.7	f
18-1h	-	46.8	358	12.7	f
18-2h	-	44.7	313	12.7	f
18-3h	-	43.8	317	12.7	f
18-4h	-	49.2	324	12.7	f

Key to Failure Mode:

d - delamination
f - in-plane failure
x - failure at impact site
y - failure away from impact site

Note: The failure mode code f,d symbolizes a fracture failure with a large amount of delamination present near the failure location.

h - denotes drilled hole specimen
p - denotes photoelastic specimen

APPENDIX C

DATA TABLES FOR CYLINDER SPECIMENS

This appendix contains the pertinent information gathered for the damage resistance and damage tolerance study of cylindrical pressure vessels. The data on the cylinder damage characterization specimens is given, followed by the data obtained for the pressurized cylinder tests.

TABLE C.1 - CYLINDER DAMAGE CHARACTERIZATION DATA

Specimen[a] ID	Impact Velocity (m/s)	Core Diameter (mm)
1B	38.6	3.6
2B	-	
3B	-	
4B	68.5	15.0
5B	62.6	14.3
6B	59.0	15.5
7B	52.0	12.7
8B	46.0	2.0
1M	70.5	15.0
2M	63.1	13.5
3M	60.4	15.0
4M	51.5	8.0
5M	55.3	11.0
6M	38.5	1.0
7M	-	
8M	-	
1T	-	
2T	52.4	7.9
3T	41.9	4.0
4T	-	
5T	66.8	14.3
6T	63.1	13.1
7T	57.8	9.0
8T	54.8	12.7

a - these specimens were sectioned from Tube 1,

TABLE C.2 - PRESSURE CYLINDER RESIDUAL STRENGTH DATA

Specimen ID	Impact Speed (m/s)	Footprint Diameter (mm)	Failure Pressure (MPa)	Failure Mode
Tube 1	sectioned			
Tube 2	sectioned			
Tube 3	unflawed		2.76	s
Tube 4	unflawed		2.45	s
Tube 5	61.0	12.5p	2.96	i
Tube 6	44.9	5.0	3.79	i
Tube 7	59.9	12.5+	2.41	i
Tube 8	55.6	12.5p	2.93	i
Tube 9	48.8	9.0	3.74	i
Tube 10	53.5	4.0	4.77	i
Tube 11	45.1	5.0	2.24	s
Tube 12	51.2	6.0	4.13	i
Tube 13	** unable to test **			
Tube 14	unflawed		3.79	
Tube 15	unflawed		4.69	

Key to Failure Mode:

i - failure path through impact site
s - failure at tube seam

Key to Damage Size:

p - punch through
+ - bundle damage occurs outside footprint

APPENDIX D

DELAMINATION STUDY DATA

This appendix contains the specimen data for the delamination implant study. Specimen measurements, delamination sizes, failure strengths, and longitudinal modulus data is included. All implants were circular.

TABLE D.1 - DELAMINATION SPECIMEN MEASUREMENTS

Specimen ID	Specimen Width (mm)		Specimen Thickness (mm)
A	71.21		1.40
B	72.20		1.41
C	73.27		1.43
D	70.99		1.42
		Average:	1.42
		C.V. %:	0.98
E	71.78		1.39
F	72.15		1.42
G	71.96		1.41
H	71.86		1.41
		Average:	1.41
		C.V. %:	0.89
I	72.27		1.43
J	71.79		1.43
K	71.57		1.42
L	71.80		1.39
		Average:	1.42
		C.V. %:	1.34

TABLE D.1 - DELAMINATION SPECIMEN MEASUREMENTS (continued)

Specimen ID	Specimen Width (mm)		Specimen Thickness (mm)
M1	72.93		1.40
M2	71.67		1.41
M3	71.81		1.41
N1	72.33		1.37
		Average:	1.40
		C.V. %:	1.35
N2	71.62		1.37
O1	70.98		1.37
O2	71.65		1.41
O3	71.62		1.40
		Average:	1.39
		C.V. %:	1.49
P	72.33		1.38
Q1	72.38		1.38
Q2	72.55		1.38
Q3	72.36		1.38
		Average:	1.38
		C.V. %:	0.00

APPENDIX TABLE D.2 - DELAMINATION SPECIMEN DATA

Specimen ID	Ultimate Stress (MPa)	Modulus (GPa)	Delamination[a] Diameter (mm)	Failure Mode
A	537	49	0, 20, 0	y
B	542	55	0, 30, 0	y
C	526	48	0, 40, 0	y
D	550	51	0, 50, 0	y
E	500	49	50, 40, 30	y
F	496	53	40, 30, 20	y
G	508	48	30, 20, 0	y
H	550	57	20, 0, 0	x
I	529	47	30, 0, 0	x
J	523	48	40, 0, 0	x
K	512	45	50, 0, 0	x
L	514	47	-	y,f
M1	484	54	50, 50, 50	x
M2	486	50	50, 50, 50	x
M3	516	49	50, 50, 50	x
N1	593	58	10, 0, 0	y
N2	605	47	10, 0, 0	y
O1	563	56	30, 30, 30	y,f
O2	561	49	30, 30, 30	y
O3	540	50	30, 30, 30	x
P	597	50	0, 10, 0	y
Q1	596	55	10, 10, 10	y
Q2	562	54	10, 10, 10	y
Q3	561	59	10, 10, 10	y

a - denoted as 0/45 interface, 45/45 interface, 45/0 interface

Key to Failure Mode:

d - delamination
f - in-plane fracture
x - failure at implant location
y - failure away from implant location

APPENDIX E

EQUATIONS FOR LOCAL MODEL BOUNDARY CONDITIONS

The equations presented in this appendix are the result of applying the boundary conditions at the top and bottom surfaces of the local plate model as shown in Figure 3.3 and stated again here:

$$\sigma_{zz}\,(\,r\,,\,-h/2\,) = -p(r) \qquad \sigma_{rz}\,(\,r\,,\,-h/2\,) = 0$$

$$\sigma_{zz}\,(\,r\,,\,+h/2\,) = 0 \qquad \sigma_{rz}\,(\,r\,,\,+h/2\,) = 0 \tag{E.1}$$

Application of the boundary conditions yield the system of equations:

$$\begin{bmatrix} A_{11} & A_{12} & A_{13} & A_{14} \\ A_{21} & A_{22} & A_{23} & A_{24} \\ A_{31} & A_{32} & A_{33} & A_{34} \\ A_{41} & A_{42} & A_{43} & A_{44} \end{bmatrix} \begin{Bmatrix} A_m \\ B_m \\ C_m \\ D_m \end{Bmatrix} = \begin{Bmatrix} -p(r) \\ 0 \\ 0 \\ 0 \end{Bmatrix} \tag{E.2}$$

The components of the A matrix are given by:

$$A_{11} = \left(- c\, s_1 + d\, s_1^{\,3} \right) \cosh \left(-\omega_m s_1 \, t/2 \right)$$

$$A_{12} = \left(- c\, s_1 + d\, s_1^{\,3} \right) \sinh \left(-\omega_m s_1 \, t/2 \right)$$

$$A_{13} = \left(- c\, s_2 + d\, s_2^{\,3} \right) \cosh \left(-\omega_m s_2 \, t/2 \right)$$

$$A_{14} = \left(- c\, s_2 + d\, s_2^{\,3} \right) \sinh \left(-\omega_m s_2 \, t/2 \right)$$

$$A_{21} = \left(- c\, s_1 + d\, s_2^{\,3} \right) \cosh \left(\omega_m s_1 \, t/2 \right)$$

$$A_{22} = \left(- c\, s_1 + d\, s_1^{\,3} \right) \sinh \left(\omega_m s_1 \, t/2 \right)$$

$$A_{23} = \left(- c\, s_2 + d\, s_2^{\,3} \right) \cosh \left(\omega_m s_2 \, t/2 \right)$$

$$A_{24} = \left(- c\, s_2 + d\, s_2^{\,3} \right) \sinh \left(\omega_m s_2 \, t/2 \right)$$

$$A_{31} = \left(1.0 - a\, s_1^{\,2} \right) \sinh \left(\omega_m s_1 \, t/2 \right)$$

$$A_{32} = \left(1.0 - a\, s_1^{\,2} \right) \cosh \left(\omega_m s_1 \, t/2 \right)$$

$$A_{33} = \left(1.0 - a\, s_2^{\,2} \right) \sinh \left(\omega_m s_2 \, t/2 \right) \qquad \text{(E.3)}$$

$$A_{34} = \left(1.0 - a\, s_2^{\,2} \right) \cosh \left(\omega_m s_2 \, t/2 \right)$$

$$A_{41} = \left(1.0 - a\, s_1^{\,2} \right) \sinh \left(-\omega_m s_1 \, t/2 \right)$$

$$A_{42} = \left(1.0 - a\, s_1^{\,2} \right) \cosh \left(-\omega_m s_1 \, t/2 \right)$$

$$A_{43} = \left(1.0 - a\, s_2^{\,2} \right) \sinh \left(-\omega_m s_2 \, t/2 \right)$$

$$A_{44} = \left(1.0 - a\, s_2^{\,2} \right) \cosh \left(-\omega_m s_2 \, t/2 \right)$$

The constants in these equations are given by:

$$a = \frac{a_{13}\,(a_{11} - a_{12})}{\Delta}$$

$$b = \frac{a_{13}\,(a_{13} + a_{44}) - a_{12}a_{33}}{\Delta}$$

$$c = \frac{a_{13}\,(a_{11} - a_{12}) + a_{11}a_{44}}{\Delta} \qquad \text{(E.4)}$$

$$d = \frac{a_{11}^{\,2} - a_{12}^{\,2}}{\Delta}$$

$$\Delta = a_{11}a_{33} - a_{13}^{\,2}$$

The a_{ij} terms are the components of the engineering compliance matrix for a transversely isotropic material. The s_i are the roots of the characteristic equation and are given by:

$$s_i = \left[\frac{a + c \pm [(a + c)^2 - 4d]^{1/2}}{2d} \right] \qquad \text{(E.5)}$$

On the top of the plate the loading is known and may be expanded as the Fourier-Bessel series of the form:

$$p(r) = \sum_{m=1}^{\infty} \beta_m J_o(\omega_m r) \qquad (E.6)$$

where β_m is given by:

$$\beta_m = \frac{2}{J_1^2(\mu_m) R_p^2} \int_0^{R_p} p(r) r J_o(\omega_m r) dr$$

The natural freguencies of the plate are represented as:

$$\omega_m = \frac{\mu_m}{R_d} \qquad J_o(\mu_m) = 0 \qquad (E.7)$$

Solving the set of equations yields the required modal amplitudes for the solution of the problem. This development is based entirely on that by Cairns and Lagace [18]. A full explanation of the constants may be found in their work.